

DEFORMATION OF MULTILAYERS  
COMPRESSED NORMAL TO THE LAYERING

by

Tewolde Woldekidan

A thesis submitted for the degree of Doctor of Philosophy  
of the University of London

Department of Geology  
Royal School of Mines  
Imperial College  
London SW7

March 1982

A B S T R A C T

There are three main sections in this thesis. Section one contains a detailed literature review of boudins and related structures which are formed by compression normal or at high angle to a mechanical layering or fabric. Section one also contains a summary of the theoretical, experimental and finite element studies of the formation of boudins and related structures.

In section two selected experiments using paraffin wax and plasticine models which were performed to investigate the initiation and development of the structures which are formed when a multilayer is compressed at a high angle to the layering are presented. The structures formed in these experiments have been classified into four main groups, A, B, C and D, based on their mechanism of initiation. These groups are A - interlocking pinch-and-swell structures, B - lenticular 'boudins' formed in thinly layered media, C - classical boudins in which competent layers are broken by tensile fracture and D - boudins generated by shear fractures.

Experiments were also performed in which single layers containing pinch-and-swell structures were compressed parallel or sub-parallel to the layer. These experiments show how the wavelength and symmetry of the folds that develop are governed by the pinch-and-swell structures.

In section three the structures, developed in the experiments described in section two, are discussed and an attempt is made to relate these structures to those predicted by the various theories discussed in section one.

It is concluded that although the deformation of geological multilayers when compressed at high angle to the layering is often complex, the structures that form can generally be explained by the existing theories for the deformation of single layers, multilayers and anisotropic media.

### ACKNOWLEDGEMENTS

I would like to thank Dr. John Cosgrove for his most valuable discussions, support and supervision during the course of study and for his vital help in the improvement of the final draft of the manuscript.

I am very grateful to my colleague John-Paul Latham for his valuable suggestions and discussions and for reading part of the manuscript.

My gratitude is also extended to Dr. Neville Price for suggesting the topic of research and for his general support.

My thanks are due to Grace Lou, Nick Morton and Adolfo Cash for their help in photographic techniques.

Carolyne Holloway is also thanked for typing the thesis.

The research was carried out under the award of the World University Service which is gratefully acknowledged.

Finally my deepest gratitude is due to my wife, Dahab, for her understanding and encouragement during the last four years when our two daughters Mahta and Showit were born.

C O N T E N T S

	<u>Page</u>
Abstract	ii
Acknowledgements	iii
Chapter 1 Review of Previous work on Boudinage and related structures	1
1.1 Introduction	1
1.11 Nomenclature	1
1.12 Sizes, shapes and classification of boudins	7
1.13 Natural occurrence	9
1.2 Previous Experimental work on the formation of boudins	25
1.21 Single-layer boudinage	25
1.211 Rock analogue	25
1.212 Real rock analogue	52
1.22 Multilayer Boudinage	58
1.3 Theoretical (work on single-layer boudinage)	61
1.4 Finite element method	95
1.5 Multilayer boudinage (theoretical work)	101
1.6 Pinch-and-swell structures	114
1.61 Deformation of pinch-and-swell structures	118
Chapter 2 Experiments	120
2.1 Introduction	120
2.11 Apparatus	120
2.12 Modelling materials	122
2.13 Number of experiments	124
2.2 Type A structures - Interlocking pinch-and-swell structures	131
2.3 Type B-I structures	143
2.4 Type B-II structures	147
2.5 Type C structures	153
2.6 Type D structures	165



	<u>Page</u>
2.61 Singl-layer models	166
2.62 Inclined single-layer models	169
2.63 Double-layer models	172
2.7 Deformation of pinch-and-swell structures	176
2.8 Experimental problems	186
Chapter 3 Discussion	189
Introduction	189
3.1 Type A structures	189
3.2 Type B-I structures	197
3.3 Type B-II structures	202
3.4 Type C structures	203
3.41 Effect of temperature on fracture spacing	203
3.42 The effect of thickness on fracture spacing	204
3.43 The breaking of boudins during progressive deformation	214
3.5 Type D structures	218
3.6 Deformed pinch-and-swell structures	224
Chapter 4 Conclusions	226
4.1 Experimental	226
4.2 Theoretical	228
4.3 Future work on boudinage and related structres	230
Appendix	233
Appendix A Apparatus	233
A.1 Pure Shear Deformation Rig	233
A.2 Wooden Deformation Box	235
Appendix B Modelling materials	235
B.1 Paraffin waxes	235

	<u>Page</u>
B.11 Physical and chemical constitution of paraffin wax	237
B.12 Frictional properties of wax surfaces	238
B.2 Plasticine and putty	238
B.21 Composition of putty and plasticine	239
B.22 Mechanism of deformation and rheology of plasticine	239
Appendix C Model Construction	241
C.1 Wax models	241
C.11 Layered models	241
C.12 Single-layered models	241
C.13 Construction of pinch-and-swell models	242
C.2 Plasticine models	243
Bibliography	246

## CHAPTER 1

### REVIEW OF PREVIOUS WORK ON BOUDINAGE AND RELATED STRUCTURES

#### 1. Introduction

##### 1.1 Nomenclature

The term 'boudinage' was first introduced by Lohest (1909) for a peculiar structure in sandstone beds in the Bastogne in Belgium, when he observed "the sandstone beds were segmented and the segments separated from each other by quartz veins. Each part is thickened in the centre and appears in cross-section almost like a barrel. The tops and bottoms of these barrels are formed by the quartz veins. Looking at the bedding plane one sees enormous cylinders or boudins side by side" (fig. 1.1).

Literally 'boudin' means sausage in French and therefore boudinage is the process of boudin formation.

According to Rast (1956) ever since the term boudinage was introduced by Lohest (1909), there had been a tendency to apply the term 'boudin' to any isolated body which had been held to be formed by the tectonic disruption of any originally more or less extensive layer (McIntyre, 1951). Rast warns that such a wide use is undesirable because it may obscure the different modes of origin of such bodies and he proposed that all such bodies be called 'tectonic inclusion.'

Fig. 1.2 shows the current descriptive terminology for boudins (Wilson, 1961; A.G. Jones, 1959).

Figure 1.1 The original boudinage structures described from the Lower Devonian quartzites and schists, Bastogne, Belgium. A, C, E, and H: Shale with foliation clearly independent of stratification and without quartz veins. B: Slightly boudinaged grit (sandstone) with numerous veins. D and G: Boudinaged grit (sandstone) with numerous quartz veins. F: Stratified schistose sandstone without foliation but with thin quartz veins. I: Folded grit cut by numerous large veins. (After Lohest, 1910, Fig. 1).

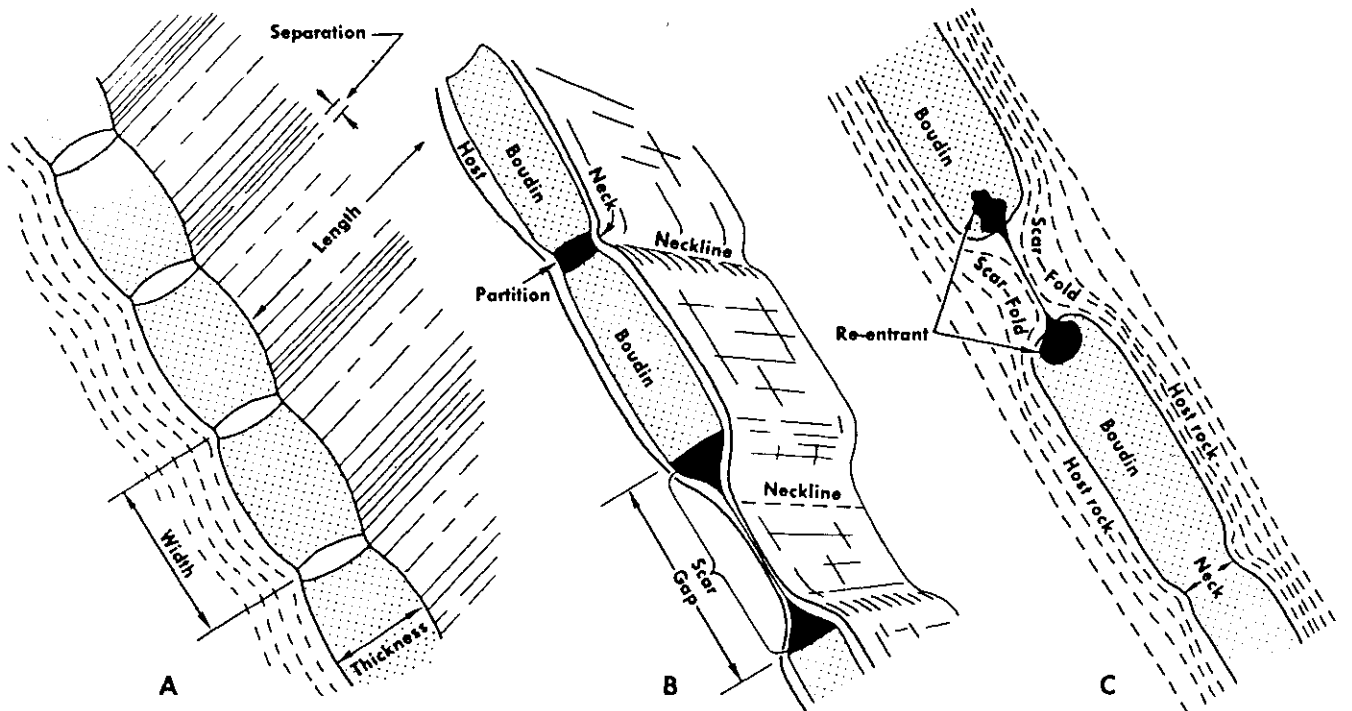
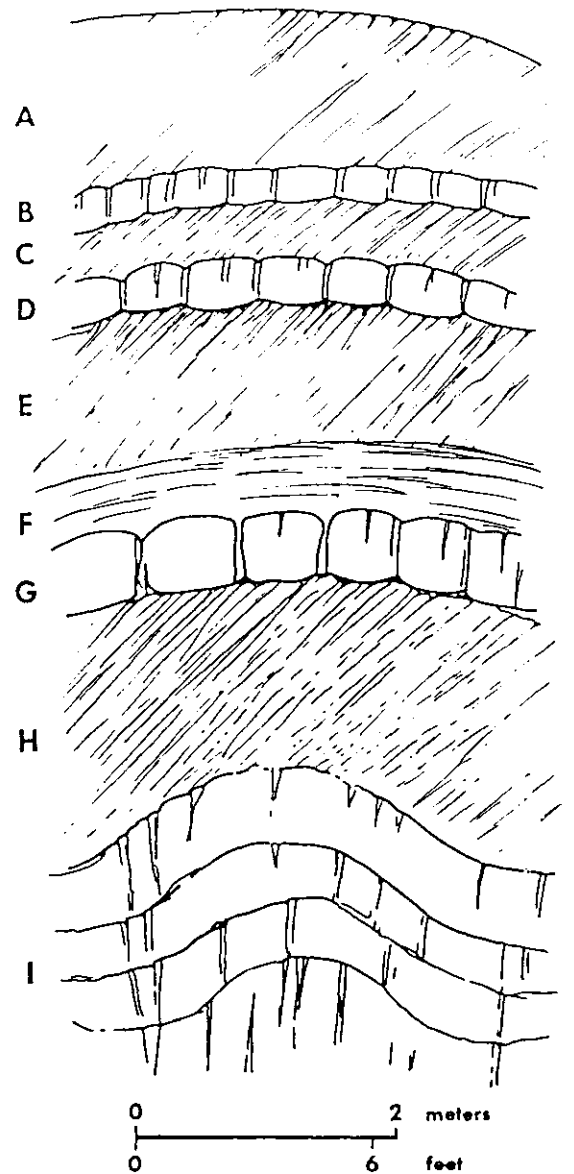


Figure 1.2 Descriptive terminology in current use for boudins. A after Wilson, 1961, Fig. 34A; B and C after A. G. Jones, 1959, Figs. 23 and 24).

Fig. 1.3

- A. Tension joints in amphibolite layer in quartz-feldspar gneiss from West Greenland.
- B. Boudins of amphibolite in heterogeneous gneiss from West Greenland (thickness of boudins  $\approx 40\text{cm}$ ).
- C. Boudins of calcareous sandstone in shale from Trøndelag, Norway (thickness of boudins  $\approx 20\text{cm}$ ).
- D. Pinch-and-swell pegmatites in gneiss from West Greenland (after Ramberg, 1955).

Fig. 1.4

- A. Ruptured and separated amphibolite layers in gneiss.
  - B. Rectangular boudins of amphibolite in granitic gneiss (thickness of layers  $\approx 30\text{cm}$ ).
  - C. Lenticular boudins of amphibolite (altered diabase dykes) in gneiss.
  - D. Boudins of amphibolitized diabase dykes, about 20 metres thick, in granodioritic gneiss.
- All examples come from West Greenland. (after Ramberg, 1955).

Fig. 1.5

- A. The ends of two boudins of quartz-feldspar pegmatite in mica schist from Wind River Mountain, Wyoming, U.S.A. (thickness of pegmatite about 25cm.)
  - B. 'Rotated' amphibolite boudins in mica schist from West Greenland.
  - C. Barrel-shaped amphibolite boudins in gneiss from West Greenland.
  - D. 'Rotated' amphibolite boudins in granitic gneiss from W.Greenland.
  - E. Pegmatite boudin in micaceous quartzite from Wind River Mountain, Wyoming, U.S.A. (scale in cm.)
- (after Ramberg, 1955).

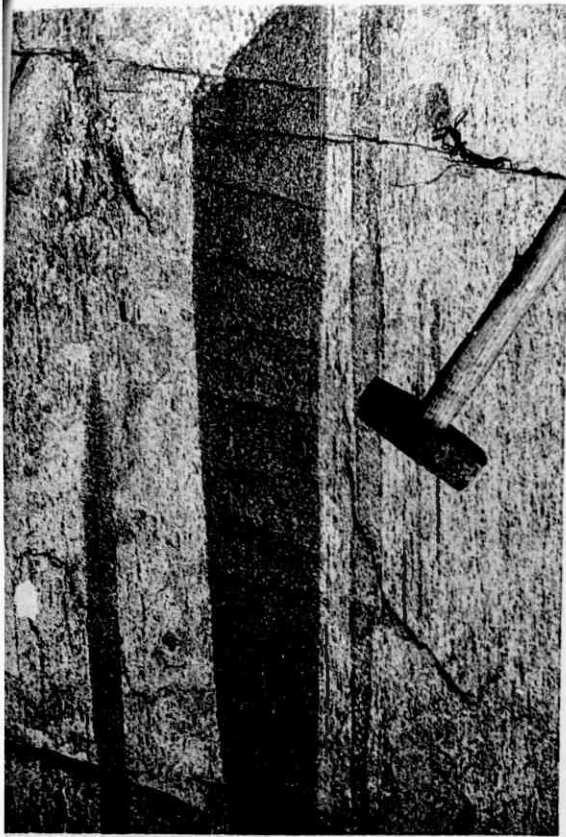
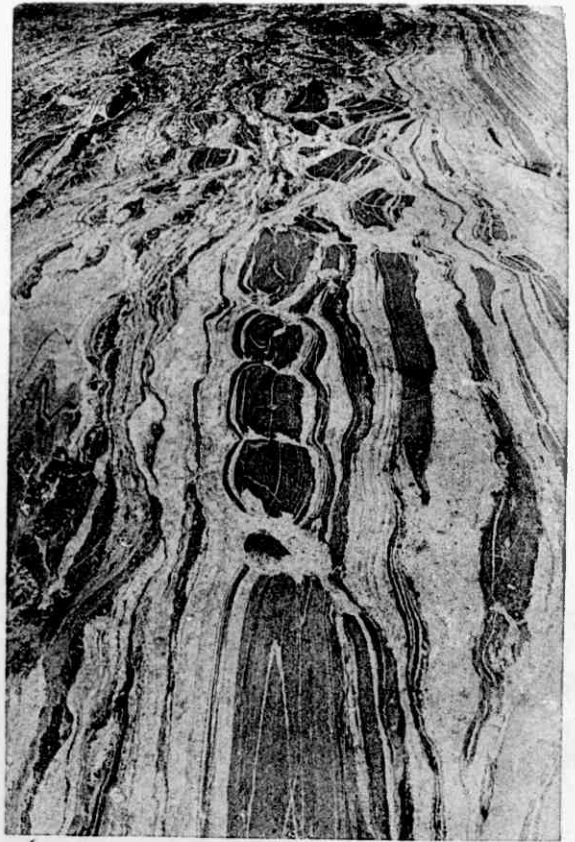
**A****B****C****D**

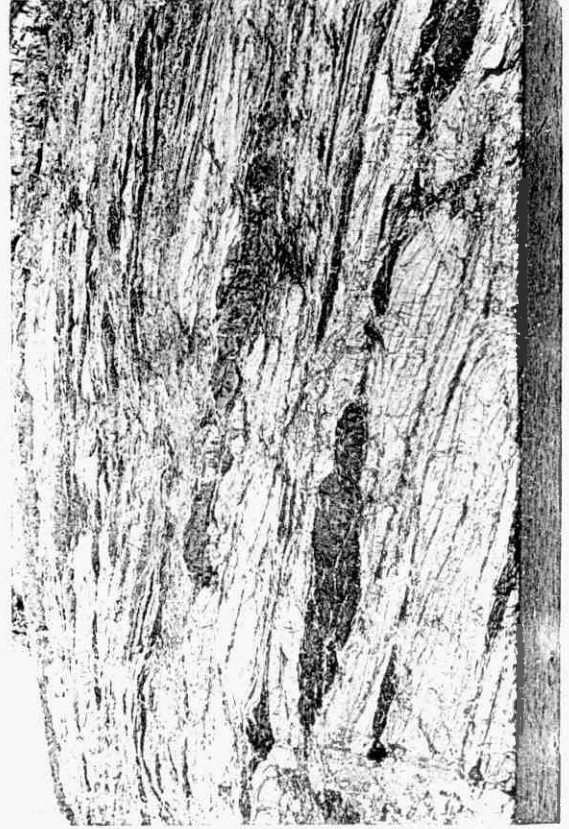
Fig. 1.3. Features of natural boudins and pinch-and-swell pegmatites



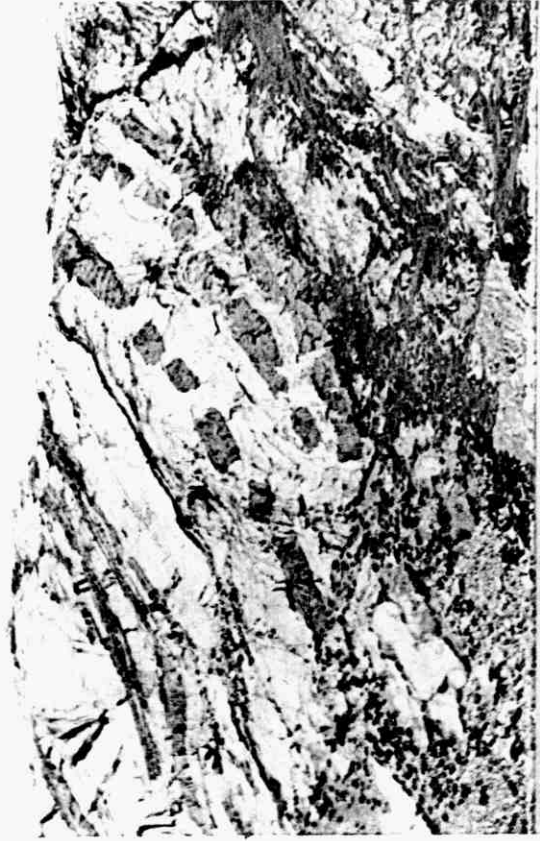
A



B



C



D

Fig. 1.4. Features of natural boudins





A



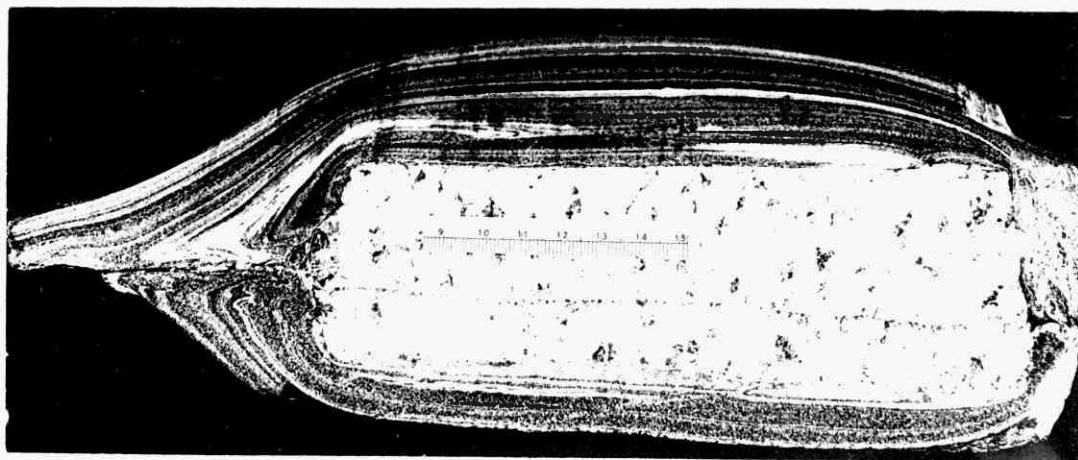
B



C



D



E

Fig. 1.5. Features of natural boudins



## 1.2 Sizes, Shapes and Classification of Boudins

Ramberg (1955) points out that most boudins are only exposed in two-dimensions. Accordingly his description of sizes and shapes refers chiefly to the sizes and shapes of boudins as exposed in the two-dimensional erosion surfaces of rocks.

He concluded that boudins are usually oblong bodies with the shortest dimension perpendicular to the schistosity in the enclosing rocks and the longest dimension parallel to schistosity. When a schistosity is developed in the incompetent beds, however, the cleavage is generally curved towards the gaps between the boudins (fig. 1.3. B,C).

Ramberg (1955) comments that according to his observation the range of thickness of boudins is between 1 cm and 20 metres. Today it is well known that the range is much greater.

Often originally rectangular boudins suffer some heterogeneous ductile deformation as the matrix flows into the neck regions between the boudins. The local shear stresses developed at the boudin corners causes the boudins to become barrel shaped. Various amounts of barreling are shown in fig. 1.6(i), extreme barreling produces boudins with a lenticular geometry.

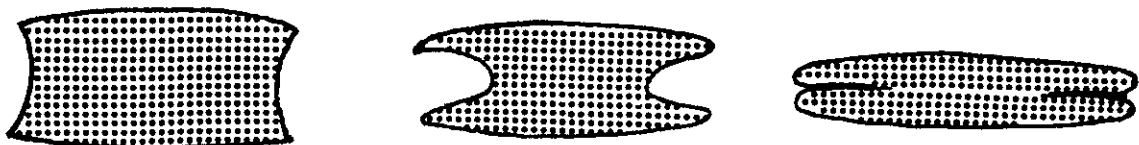


Fig. 1.6(i)

Lenticular boudins are also formed by the necking down of the boudins before separation (fig. 1.3-B, D).

Sometimes the boudins are formed by shear failure of the relatively competent layer and not by tensile failure. When this occurs the failure planes are not normal to the competent layer but make an angle of  $\approx 60^\circ$  to it. Such boudins have been termed 'rhombodhedral' by Stromgard (1973).

Most geologists classify boudinage structures according to their shapes in profile section normal to their length. Some of the commonly found shapes are shown below (fig. 1.6(ii)).

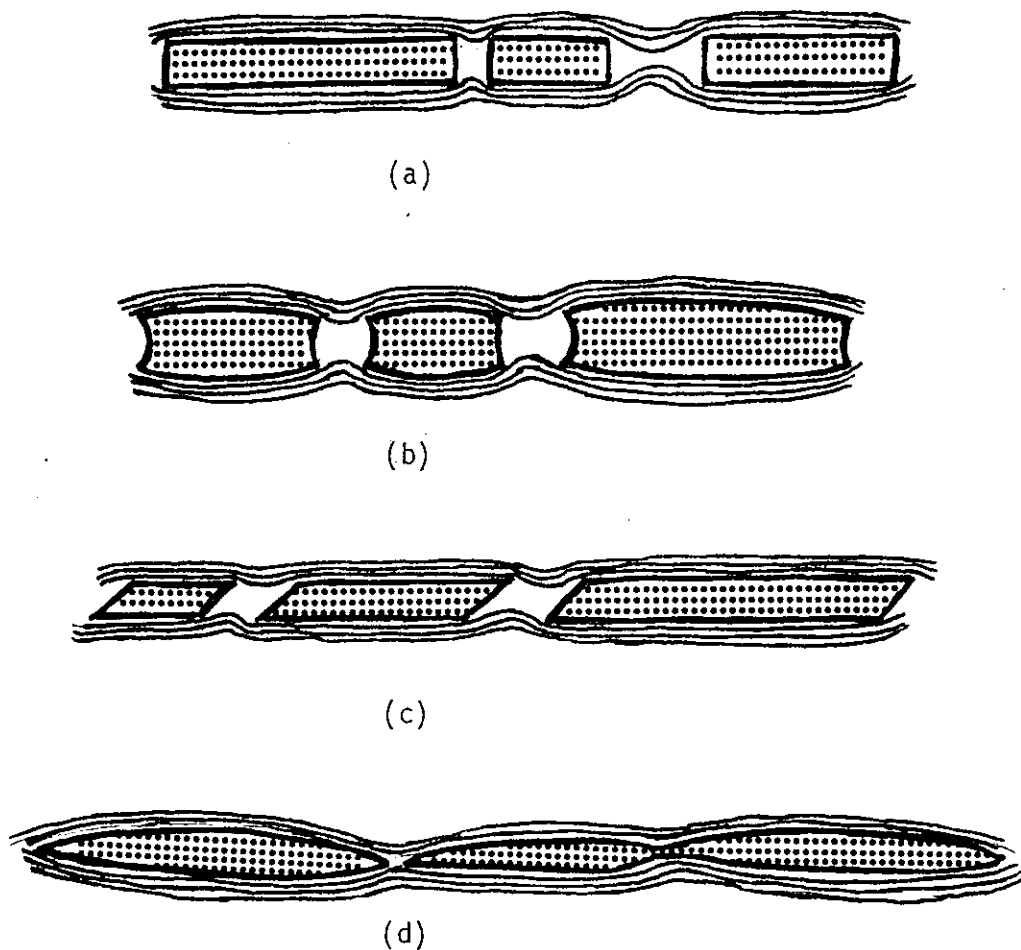


Fig. 1.6(ii)

### 1.3 Natural Occurrence

The structure called boudinage by Lohest was observed as long ago as 1866 by Ramsay and 1889 by Harker. Ramsay may have observed the structure described by Walls (1937), who notes that "in the great quarry of the Ffestiniog and Trawsfynydd fault the cleavage dips from  $45^{\circ}$  to  $50^{\circ}$  northwest, the inclination of the beds being about  $34^{\circ}$  in the same direction and a greenstone dyke runs through them between the cleavage planes ... bulging and thinning off in a rapid succession of oval-shaped masses three or four feet in length. Associated with it are quartz veins occurring principally at points between the separate bulgings of greenstone".

Reyner (1892) describes boudinage in the limbs of the anticlines due to elongation in a down-dip direction. He does not use any special term for the phenomenon. Lohest shows that the quartz veins of the Bastogne locality in Belgium contains tourmaline and garnet implying that they are not of primary origin but of later origin (fig. 1.1, 1.7b)

In his geological description of the Tammersfons quadrangle, Finland (fig. 1.7), Sederholm (1911) shows boudinage but does not use the term. A granite dyke is broken and pulled apart, the fracture is filled with quartz which does not penetrate the schist. On the other hand the schist has a tendency to move into the fracture. Balk (1927) shows similar structures where a norite dyke has been stretched. The fractures are, however, not filled with quartz veins but by the flow of gneiss (fig. 1.7g).

As shown by Holmquist (1931) veins and dykes frequently form boudinage structures during subsequent deformation. In Fig. (1.7e) a skarn layer has been pulled apart and the gaps between the segments are partially filled with quartz. The surrounding leptites are also

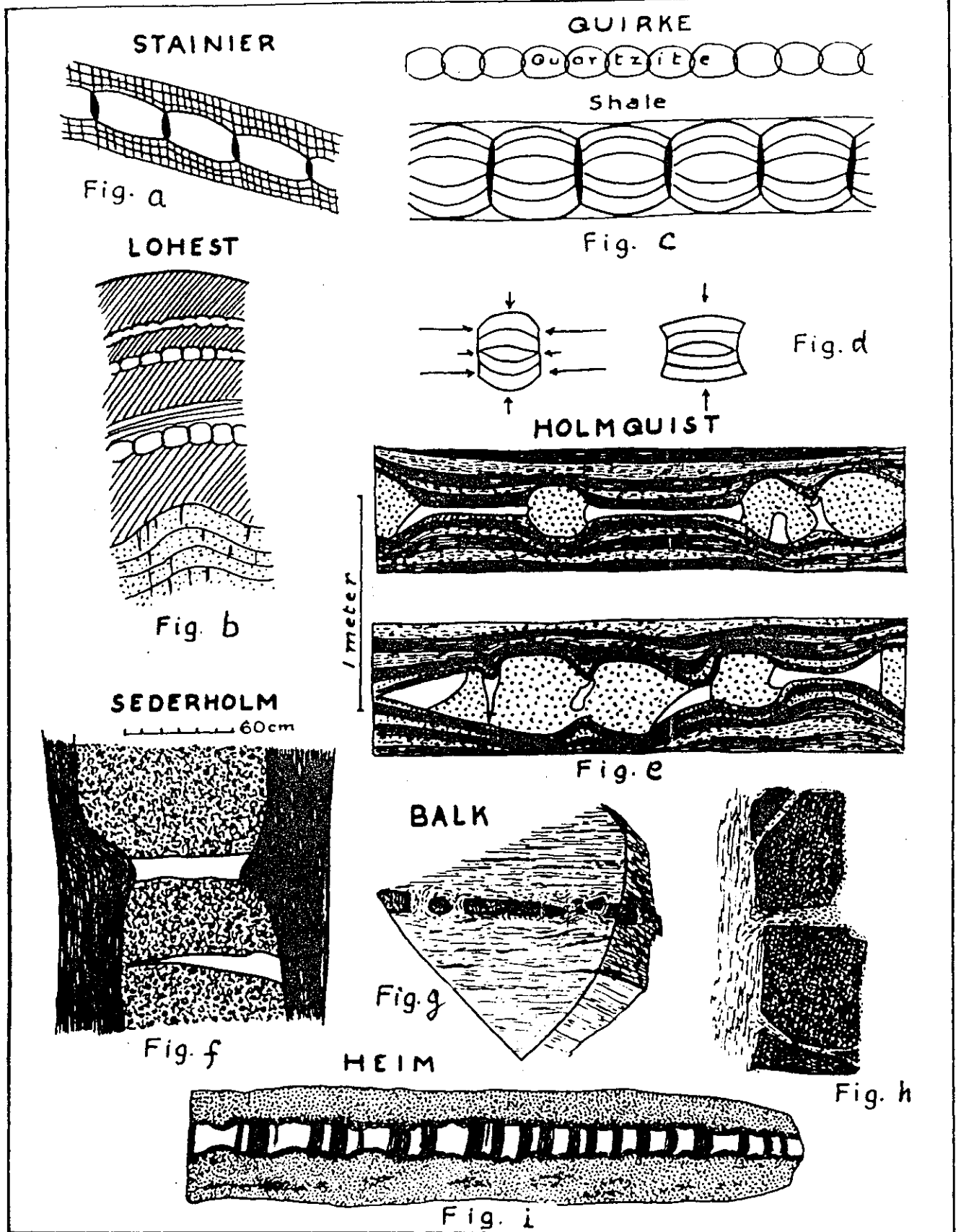


Fig. 1.7a-Boudinage after Stainier (1907); Fig. b - Boudinage in quartzite (white) in a fold, cleavage in shale beds is at an angle to bedding, after Lohest (1909); Fig. c - Schematic drawing of boudinage after Quirke (1923), black vein of quartz; Fig. d - Explanation of thickening of boudins by lateral compression and release of elastic deformation, after Quirke (1923); Fig. e - Ladder vein in leptite, dotted areas are skarn rocks, white are quartz veins, dark are banded leptite, after Holmquist (1931); Fig. f - Porphyry dyke is fractured and the schist drawn into the gap which is filled with quartz, after Sederholm (1911); Fig. g - Norite dyke in gneiss, extended in the direction of stretching, gaps are filled by gneiss, after Balk (1927); Fig. h - norite dyke extended and traversed by several apophyses of gneiss, after Balk (1927); Fig. i - stretched belemnite in shale with white partitions filled with calcite, after A. Heim (1921).

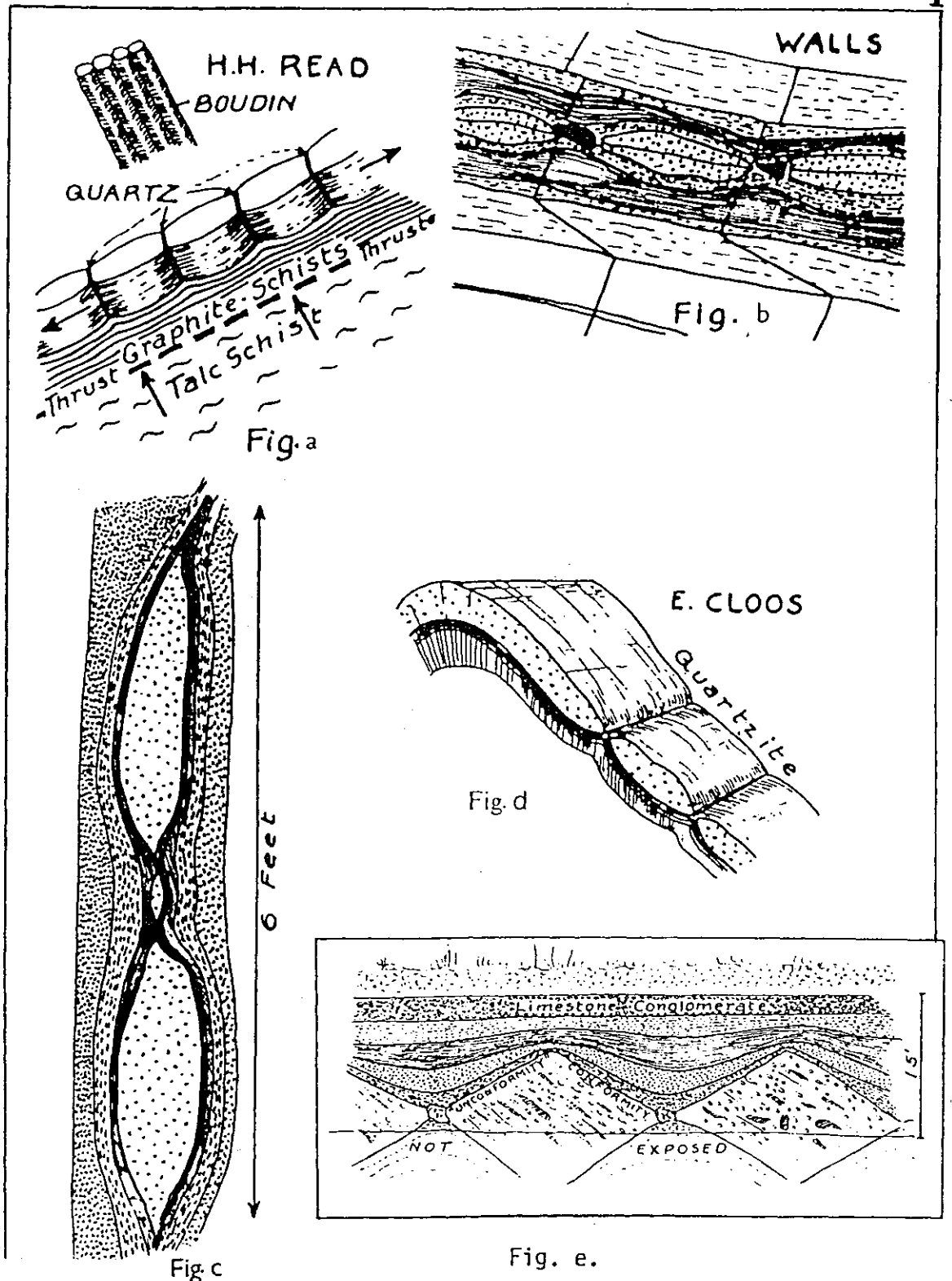


Fig. 1.8

"Schematic representation of the boudinage structure at the Taig, Nor Wick, Unst", after H.H. Read (1934); Fig. b - Quartzite boudins (dotted) separated by quartz veins in matrix of fine siltstone after Walls (1937); Fig. c - Quartzite bed in Wissahickon schist is partitioned into boudins on the limb of a fold, after E. Cloos (1946); Fig. d - Dolomite bed is drawn out in the direction of elongation in limestone, Howellville quarry, N.E. of Paoli, Pennsylvania. Fig. e - Boudinage in edgewise conglomerate bed from Martic area, Lancaster County, Pennsylvania, U.S.A. (after Cloos, 1941).

drawn in and help fill the gaps.

Both Corin (1932) and Wegmann (1932) did further studies on the classical localities of boudinage in Belgium. Wegmann also studied boudins in granite terrains. They confirm that the quartzite segments or boudins had general continuity and had no doubt that they were originally portions of an entire bed of quartzite probably of uniform thickness.

Read (1934) produced a summary of the structure with an excellent illustration of steeply dipping boudins (fig. 1.8a). Walls (1937) writes a descriptive record of boudinage structure in Scotland (fig. 1.8b).

Waters and Krauskopf (1941) working in Colville simply list boudinage as one of the structures present without any particular description or illustration. Gault (1948) however does illustrate boudinage in granodiorite, where inclusions are pulled apart as in the dyke described by Balk (1927) (fig. 1.7h).

A rather special type of boudinage structure was noted by Cloos (1941) in the Martic area, Lancaster County, Pennsylvania. A thick bed of edgewise conglomerate has been broken into almost square blocks. These were then rotated clockwise so that the longest diagonal is now in the direction of bedding. There are pegmatites, calcite, or quartz veins between the blocks and the shale above and below has flowed into the area between the blocks (fig. 1.8e).

Cloos (1946) further called attention to boudinage with illustrations (fig. 1.8c) and made an extensive review of early literature on boudinage in 1947.

In his review Cloos (1947) writes that boudins appear to form independent of composition or kind of materials as long as there

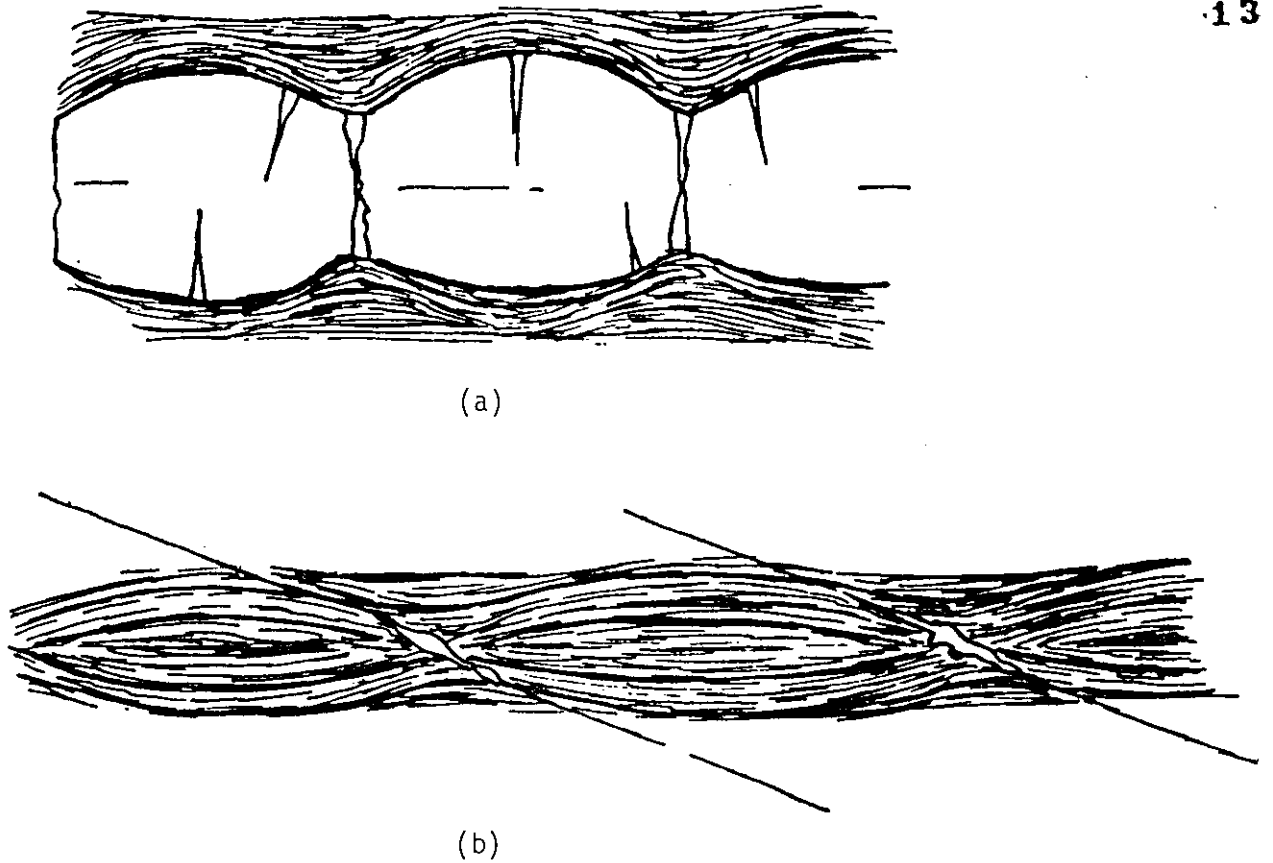


Fig. 1.9 Two types of boudinage structures observed  
by Coe, 1959.

is a difference between competency of beds involved and a definite layering. A dyke in granite, quartzite between shale beds, dolomite layers between shale or limestone, or greenstone between volcanic ash, all may produce similar structures. (He gives examples for each). One of his examples, shown in Fig. 1.8c, is boudinage formed in a quartzite in schist beds. The quartzite which is between Wissahickon schist (Cloos 1946) beds is cut by tension fractures which are perpendicular to bedding and parallel to the fold axis. These fractures are also normal to the dip of the beds and to elongation down dip. The edges of the bed at the fractures were rounded off and the bed appears lenticular in cross section. Cleavage is at a large angle to bedding and the schist layers have filled the gaps. There is no doubt that boudinage is here caused by elongation down dip of the limb of the fold.

Cloos (1947) notes that a rather peculiar but excellent example of boudinage occurs below Great Falls in the Potomac river gorge near Washington, D.C. Here shaly beds are metamorphosed and have become more competent than the sandy layers. The beds are completely disrupted and sandy layers fill the gaps. From Ramberg's and Cloos' discussion of the occurrence of boudinage it appears that the structure occurs in all the three types of rocks - sedimentary, igneous and metamorphic.

In parts of the Monashee Group, Shuswap, British Columbia, Canada, A.G. Jones (1959) found that there were two sets of approximately perpendicular necklines one parallel and one perpendicular to the linear structures and fold axes. Carbonate partitions or gaps only occur in those necklines approximately perpendicular to the regional linear structures.

Coe (1959) also found two perpendicular sets of barrel shaped boudins. Fig. 1.9 shows a 45cm thick lithified slumped siltstone sheet lying between flaggy siltstones. The slumped siltstone has boudinaged in two directions, lithification must have transformed the slumped silts into a competent unit. The well-formed and smaller boudins are elongated normal to the fold axis. The less well-formed boudins are parallel to the fold axis and exposed on two-dimensional sections.

Fyson (1962) described similar geometrical relationships in South Devon, England.



Rast (1956) suggested that the evolution of the barrel-shaped boudins involved the following stages:-

- (a) The extension of the competent layer accompanied by plastic deformation or 'necking.'
- (b) Ultimate fracture when extension surpasses the plastic limit.
- (c) Separation of the individual segments and formation of tectonic inclusions of lozenge-shaped cross section.

Necking is the process of local thinning (or pinching) when a layer or a rod undergoes extension as the result of either compression perpendicular to the layer (or long axis of the rod) or tension parallel to the layer. Nadai (1950) studied necking in metals (by reviewing a number of tension tests) and concluded that as soon as necking starts, the stress field becomes nonuniform. The reduced cross-sectional area of the rod at the neck means that the tensile stress increases locally. Deformation therefore continues at this point and becomes more and more localised as the cross sectional area of the neck decreases. Necking, initially a ductile deformation, often leads to brittle failure as the strain rate (associated with the rapid increase in stress value at the neck) increases.

In metallurgy necking is observed to occur both at right angles and oblique to the direction of extension. It is found to be dependent on the ratios of thickness of the bar to the width of the bar. If  $t/w < 1/7$  the necking is at right angles to the direction of extension, whereas if  $t/w > 1/7$  it results in oblique necking, the necks make an angle of  $53^\circ$  -

Fig.1.10 Necking along an oblique plane in flat steel bar tested in tension. (The steel sheet was reduced in thickness by 20% by cold rolling before the tensile test was made.) (After F. Koerber and E. Siebel, see Nadai, 1950)



$-55^{\circ}$  to the axis of extension (fig. 1.10) (Nadai, 1950). The development of these types of necks indicates that the distribution of stresses and strains within a rigid material depends on its geometric properties as well as on the type and direction of the external force.

Wunderlich (1962) showed that even after allowing for compaction effects, a considerable volume of material must be squeezed from a fold core during continued compression and flexural-slip folding. He believed that expulsion of the less competent rocks from a fold core can stretch the competent units in both the fold flanks and the closures. On the basis of theoretical and experimental studies Ramberg (1959, p.108) concluded that boudins normal to the fold-axis can result from pure shear (fig.1.11-B).

On the separation of boudins Coe (1959) suggested that two distinct types of boudinage can be defined: 1. boudins produced during folding with their length parallel to the fold axis, and 2. perpendicular sets of boudins arranged perpendicular and parallel to the fold axis.

Ramsay (1967) has shown that strain ellipses can be classified as one of three main types according to the values of their principal extensions and that these types fall into three main fields when plotted on a graph of  $\lambda_1$  against  $\lambda_2$  (fig.1.12-a). Considering strain in the plane of a competent layer, different types of minor structures will develop in the layer according to the deformation field in which the strain ellipse is situated. As shown on the diagram (fig.1.12-a) if the strain state falls in field 1 ( $\lambda_1 > \lambda_2 > 1$ ), the structures that develop will be entirely of boudinage as all directions have suffered extension. Wegmann's

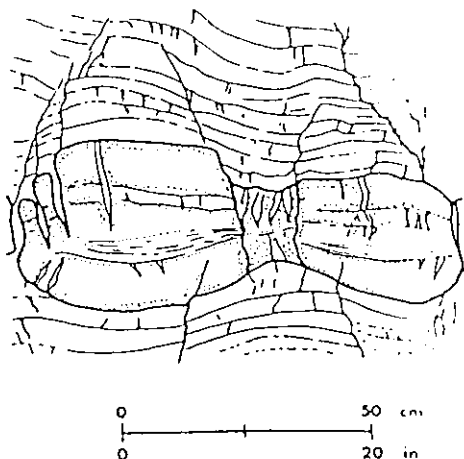


Fig.1.11-a. 'incipient' boudinage structure (after Wundelich, 1962).

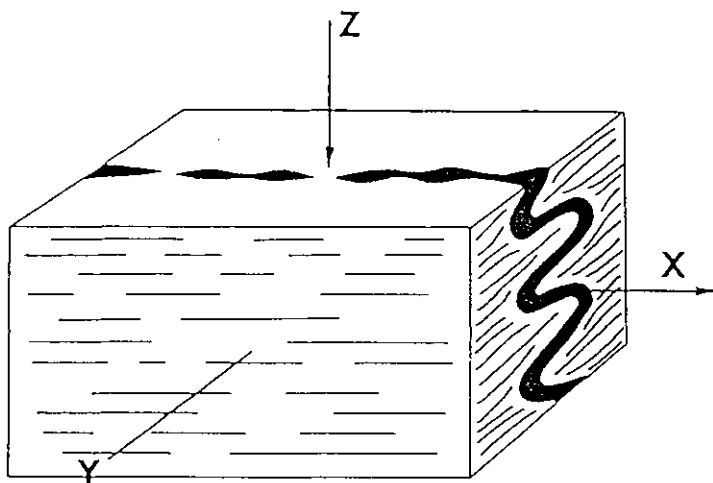


Figure 1.11-b Minor folds and boudinage-like attenuations in a crosscutting vein produced simultaneously by pure shear under experimental conditions.  $X$  = maximum extension strain;  $Y$  = zero strain;  $Z$  = maximum compression. Axes of principal stress coincide with axes of principal strain (no rotation of coordinate axes during strain) (After Ramberg, 1959, Fig. 3).

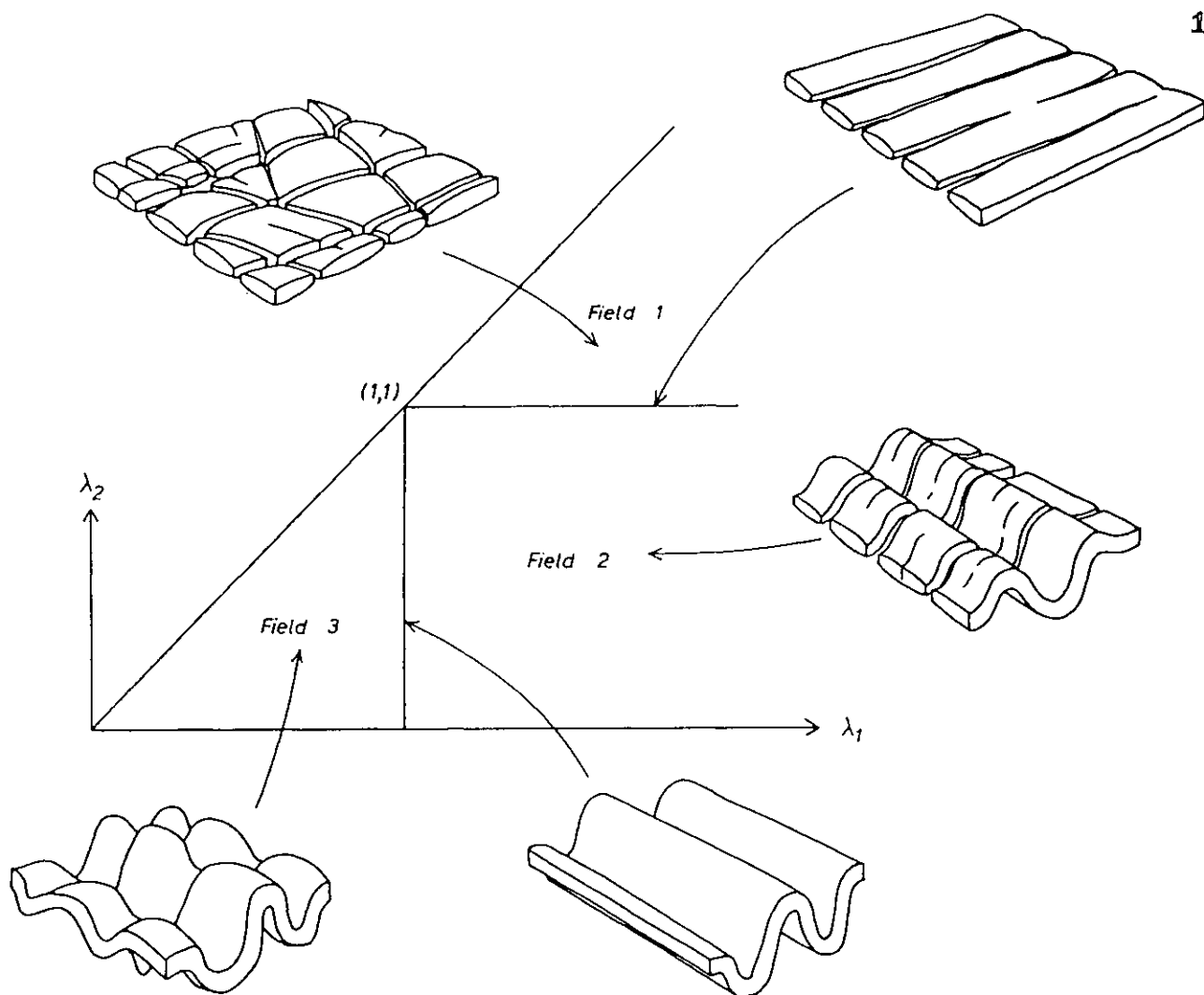


Fig. 1.12-a The geological structure that may be developed in the three fields of strain ellipse (after Ramsay, 1967)

chocolate tablet structure will occur in this field. If the strain ellipse falls on the line  $\lambda_2 = 1$  one set of boudins is developed in the layer, and the lengths of the boudins will be normal to principal axis  $\lambda_1$ , although this may not be so if fractures or joints were present before the deformation.

Folding in one direction and boudinage or cross jointing normal to the fold axis, will be produced by strain states that fall in field 2 ( $\lambda_1 > 1 > \lambda_2$ ) because the ellipses in this field will have an extension along one principal strain direction and contraction along the other principal strain direction. Strain states which plot along  $\lambda_1 = 1$  produce a single set of folds and those that plot in field 3 ( $1 > \lambda_1 > \lambda_2$ ) produce folding in more than one direction because all

directions are contracted.

Ramsay (1967) extended this two dimensional strain presentation to three dimensions and following Ramberg (1959) and Flinn (1962) considered five main constant volume ellipsoids described by the parameter  $k$ . (fig.1.12-b). He summarized this relation as follows. Layers in which structures will develop will cut this ellipsoid. The state of strain on this layer will correspond to the ellipse defined by the intersection of the layer and the strain ellipsoid.

For the ellipsoids with  $\infty > k > 1$  (constriction type) ellipse sections will fall into fields 1 or 2, that is either complex crossing boudinage or other extension structures, or alternatively, ptigmatic folding in one direction with boudinage at right angles to the fold axes.

For the ellipsoids with  $k = 1$ , ellipse sections all fall into field 2 or on boundary lines of this field. The dominant structures are folds with structures indicating extension subperpendicular to the fold axes. In some special section folds only ( $\lambda_1 = 1$ ) or boudinage only ( $\lambda_2 = 1$ ) will develop.

For the ellipsoids with  $1 > k > 0$  (flattening types) ellipse sections will fall in fields 2 or 3, i.e. competent layers will show folding and boudinage if in field 2, or complex folding in several directions if in field 3.

Following Flinn (1962) and Ramsay (1967), Sanderson (1974) considers extensional structures during folding, with fold axis parallel to  $Y$  in the five constant volume ellipsoids (fig. 1.12b,c). He points out that they need not be developed in a unique direction within a deformed body, and their location is determined by the relation of the extended layer to the finite and/or infinitesimal strain ellipsoids. He

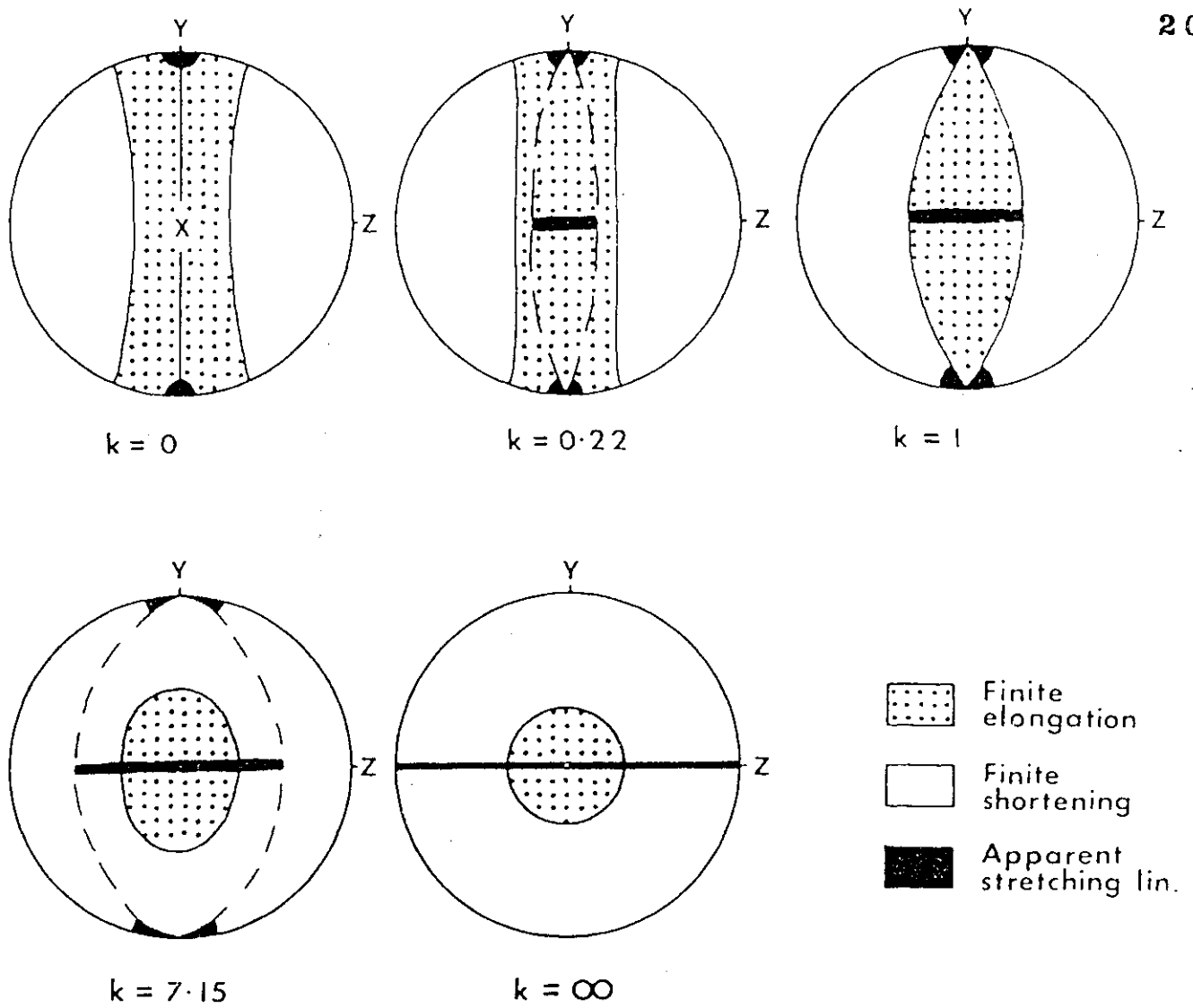


Fig. 1.12b—Equal-area projection of zones of elongation and shortening for five volume standardized finite strain ellipsoids; showing location of apparent stretching lineations for planes through  $Y$ . Dashed lines are circular sections of strain ellipsoid. (after Sanderson, 1974)

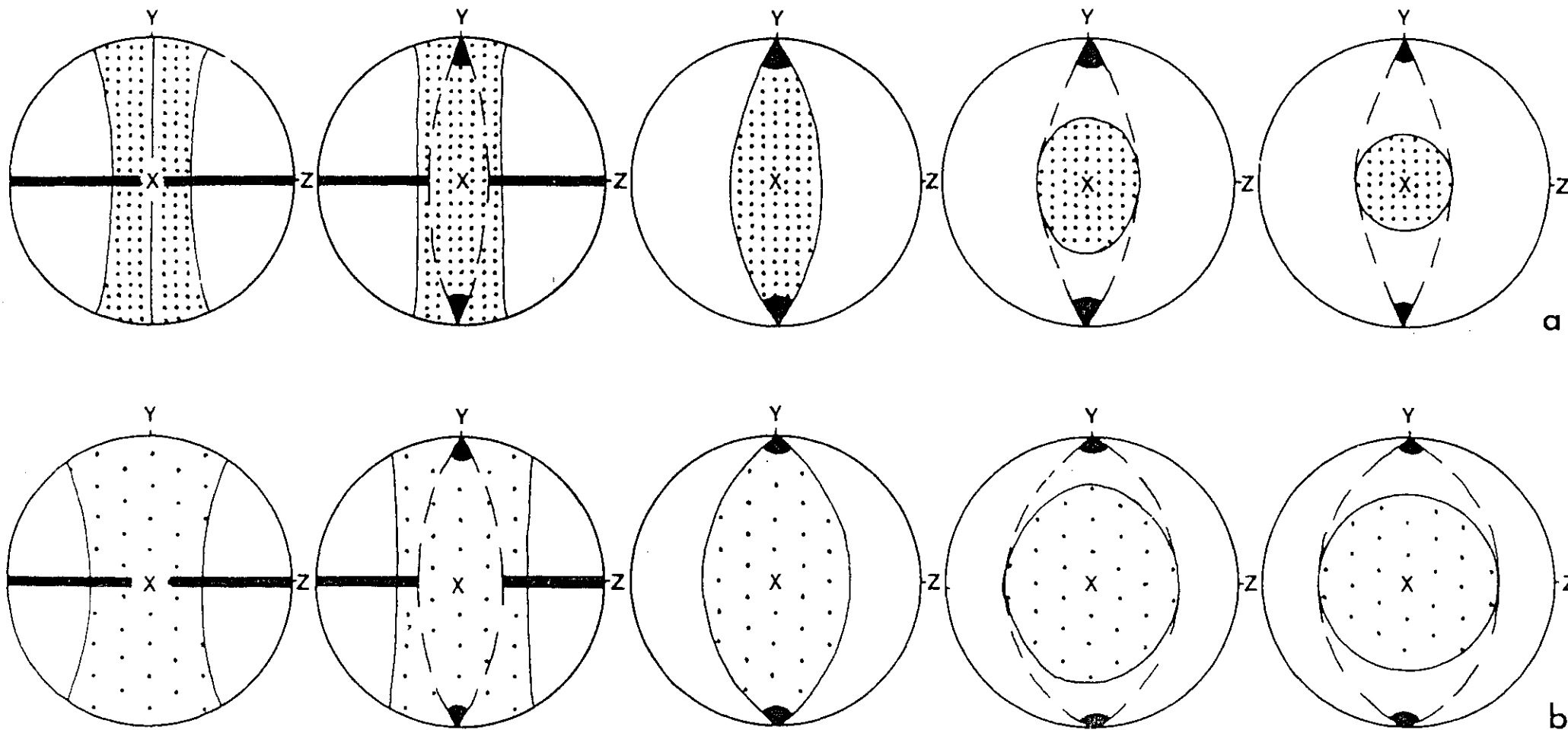


Fig. 1.12-C --Equal-area projection showing the location of boudin long axes for five different strain states, as fig.1.12b(a) based on finite strain model, (b) based on infinitesimal strain model. Elongation shown by stippled areas and dashed lines are circular sections of strain ellipsoid.

(after Sanderson, 1974)

recognises the following features.

1. Boudin long axis parallel to fold axis can occur in any strain state, except  $k = 0$ .

2. Boudin long axes normal to fold axis implies flattening-type deformation  $k' < k < 1$ , that is, field 3 (fig. 1.12-a).

3. Double boudinage may result from boudinage with long axes normal to fold axis followed by boudinage with long axes parallel to fold axis. Hence double boudinage also implies  $k < 1$  as in 2.

4. Irregular boudinage may develop by: (a) the layer being parallel to XY during strain with  $k = 0$  (unlikely to be common during progressive deformation), or (b) fold axis oblique to Y, in which case there will be a progressive rotation of active boudin axes (fig. 1.12e, f).

Examples of the relationship of boudin long axis and fold axes are shown in fig. 1.12-d.



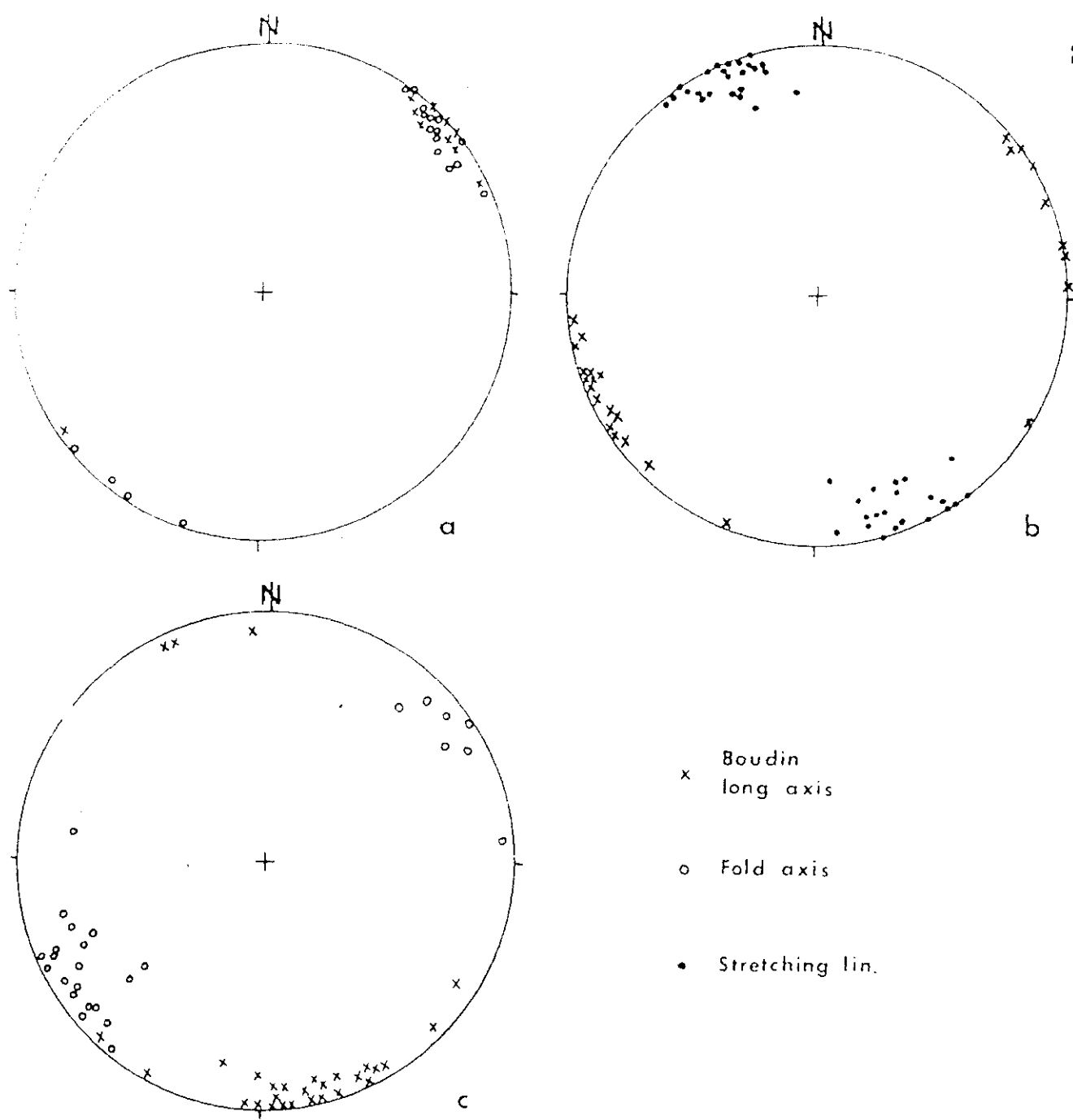


Fig.1.12-d--Examples of the relationship of boudin long axes from Devonian slates in Cornwall, England. (a) Boudin long axes parallel to  $F_3$  fold axes, Porthleven; (b) Boudin long axes normal to stretching lineations, Tintagel; (c) Boudin long axes normal to fold axes ( $F_1$ ), Watergate Bay, Newquay. (after Sanderson, 1974)

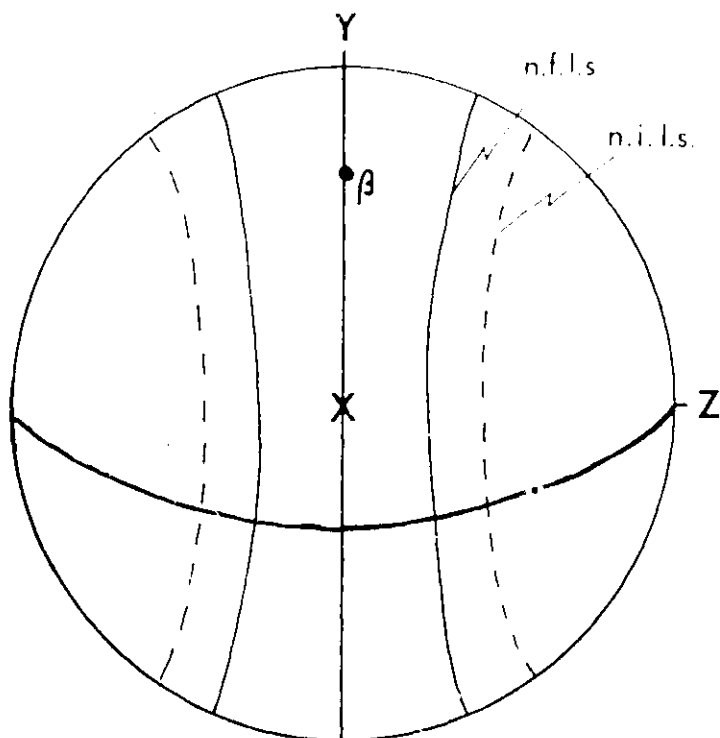


Fig. 1.12-e --Equal area projection of locus of boudin long axes (heavy continuous line) for planes passing through  $\beta$ , which is at  $30^\circ$  to  $Y$ . Right side of diagram based on finite strain model, left side on infinitesimal strain model, but both produce similar results. Lines of no finite longitudinal strain (n.f.l.s.) based on  $a = 1.00$ ,  $b = 2.82$ , and lines of no infinitesimal strain (n.i.l.s.) based on  $k' = 0$ . Apparent stretching lineations are parallel to  $\beta$  for all planes passing through  $\beta$ .

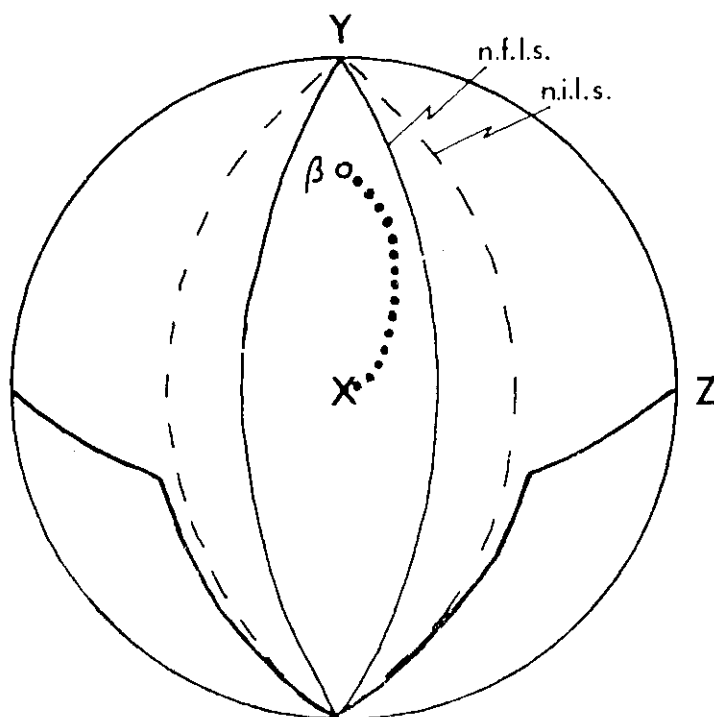


Fig. 1.12-f As fig.1.12-d, but for plane strain with  $a = b = 2$  and  $K' = 1$ . Heavy dotted line shows position of apparent stretching lineations. (after Sanderson, 1974)

## 1.2 Previous Experimental Work on the formation of Boudinage

### 1.21 Single-Layer Boudinage

#### 1.211 Rock Analogues

Ramberg (1955) was the first to produce boudins experimentally. He used putty to simulate the incompetent layer and various kinds of modelling clay, plasticine and cheese to simulate the competent layer.

Competent sheets with uniform thickness from 2 to 5 mm were used in each experiment, one competent sheet was placed between incompetent putty layers, 1 - 5 cm thick. These layered stacks were compressed between two stiff plates. In most of the experiments, the models were allowed to expand in two directions. In a few, however, the expansion was restricted to one direction by performing the experiments in an oblong box. The models were cut with a razor blade after compression (which lasted a few minutes), and the cross sections were examined and photographed. In all the models, the competent layers were either ruptured and formed boudins, or were locally necked down to form pinch-and-swell structures. In the most competent types of layers (cheese and some types of plasticine) relatively sharp-edged boudins were formed, whereas in the less competent layers smooth, lenticular (lozenge-shaped) boudins and pinch-and-swell structures were formed. Some runs were made with layers of differently coloured putty, to study details of the flowage pattern in the incompetent putty. It was found that the putty layer in direct contact with the competent cheese or plasticine sheets was always thicker adjacent to the boudins than in the regions between the boudins (Fig. 1.14 B-F). Putty layers further away from the competent sheets were thinner just outside the boudins than in the regions between them (Fig. 1.15F). This is because of friction along the boudin surface; the lateral flowage was small in the layer close to the boudins and greater in layers further away. This effect is shown even if the layer in contact with boudins is more

ductile than the putty layers further away. However, when the contact putty layer was a little less ductile than the outer putty layers, the flowage in the contact layer was very small along the boudins; consequently, the contact layer would neck-down and break completely at the terminations of the boudins, forming a concentric outer zone or it would thin out to an almost invisible thickness in regions between the boudins (Fig. 1.14, C, D, E, F). This happened in spite of the fact that the contact layer (putty) was too ductile to form boudins on its own. In some runs drag folds formed close to the ends of the boudins (Fig. 1.15E, F); very similar to folds found near the ends of natural boudins (Fig. 1.5 E).

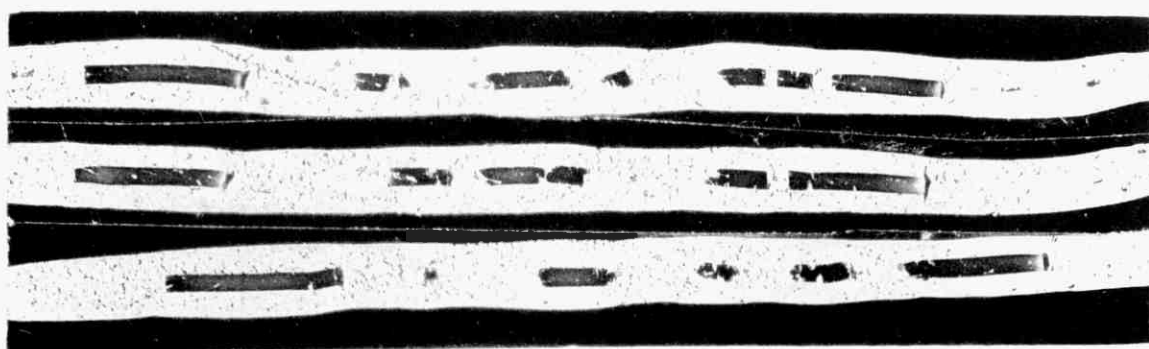
The barrel-shape, so characteristic of many natural boudins, was formed in the more competent plasticine (Fig. 1.13-D). In the less competent plasticine layers lens-shaped structures formed due to a local necking down before rupture took place.

Models made of petrolatum and 'gun grease' which was 'shot' into or between compressed layers were built by Bogadov (1947), Kirillova (1949) and Chertkova (1950) in association with Belousov (1952). Compression varied in different parts of the model and allowed the less 'viscous' layers to flow from places of high to low pressure. Viscous flow in the ductile layers produced local tensile stresses of sufficient magnitude to break the brittle layers. Shorter boudins occurred where the compression across the layer was the larger.

Fig. 1.13. Sections of compressed 'cakes' of putty and plasticine (scales in cm.). A, B and C represent a sequence of decreasing competency of the boudin layer. In A, the boudin layer is cheese, in B, somewhat 'brittle' plasticine and in C, less competent plasticine. In D, the putty has been mixed with a little coloured plasticine to bring out the flowage in the putty during the compression experiment. (after Ramberg, 1955).

Fig. 1.14. Sections of compressed layered 'cakes' of putty with different colours simulating bonded incompetent rocks, and plasticine (A,B,C) or cheese (D,E and F) simulating the competent rock (scale in cm.) In A, the light grey putty layer in contact with the boudin layer is less viscous than the outer dark grey putty layer. In B, the contact putty layer (dark grey) has the same viscosity as the outer putty layers. In C, the contact putty layer (dark grey) is more competent than the outer putty layers. D, E and F same as C with the exception that cheese was used as the competent layer. (after Ramberg, 1955).

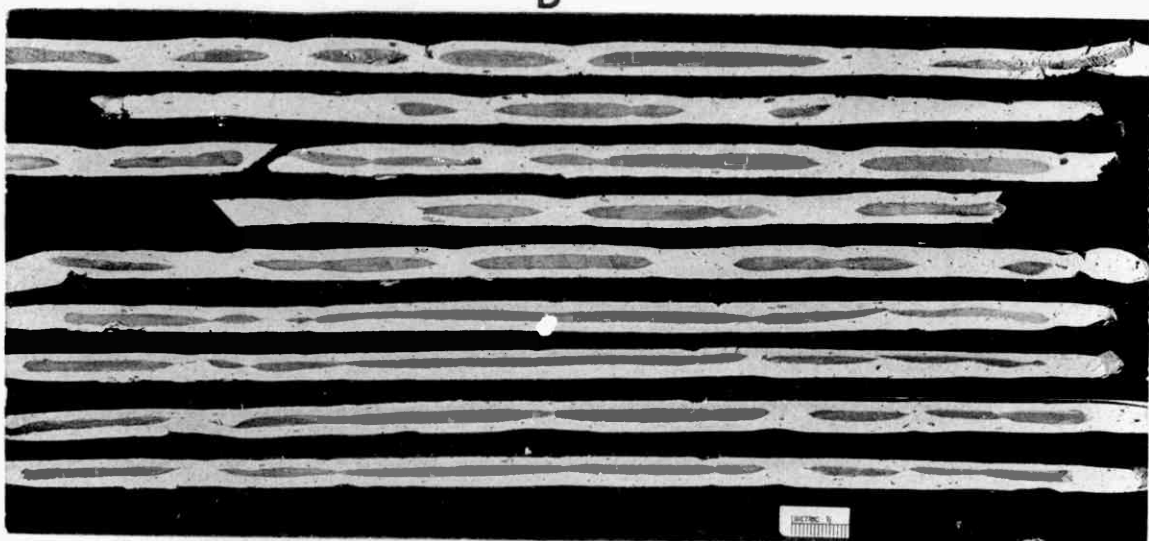
Fig. 1.15. A. Cataclastically deformed corner of boudin of pegmatite in mica schist from Wind River Mountain (see fig. 1.5A,E).  
 B. Quartz fillings between 'unsymmetric' boudins in banded gneiss from Fosen, Norway.  
 C. Plane view of putty-plasticine layered 'cake' sometime after deformation. The straight horizontal lines are cut through the 'cake.'  
 D and E enlarged details of fig. 1.14D.  
 F. Cross-section of 3-colour putty - plasticine cake (compare fig. 1.5E) showing the drag-fold-like structures in the contact layer at the ends of the boudins. (after Ramberg, 1955).



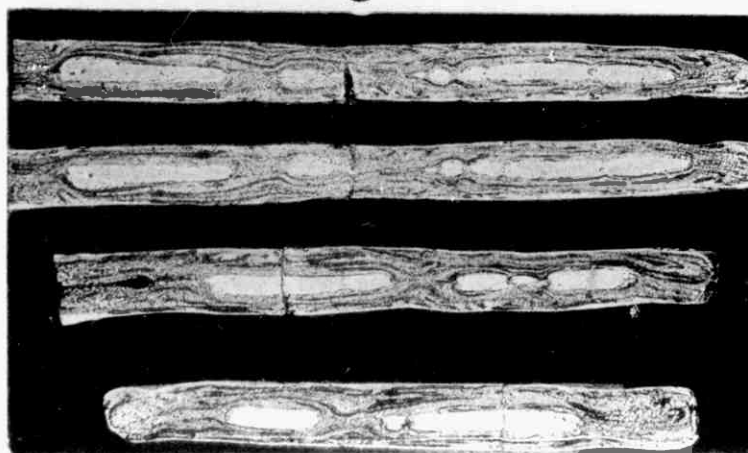
A



B



C



D

Fig. 1.13. Features of experimental boudins

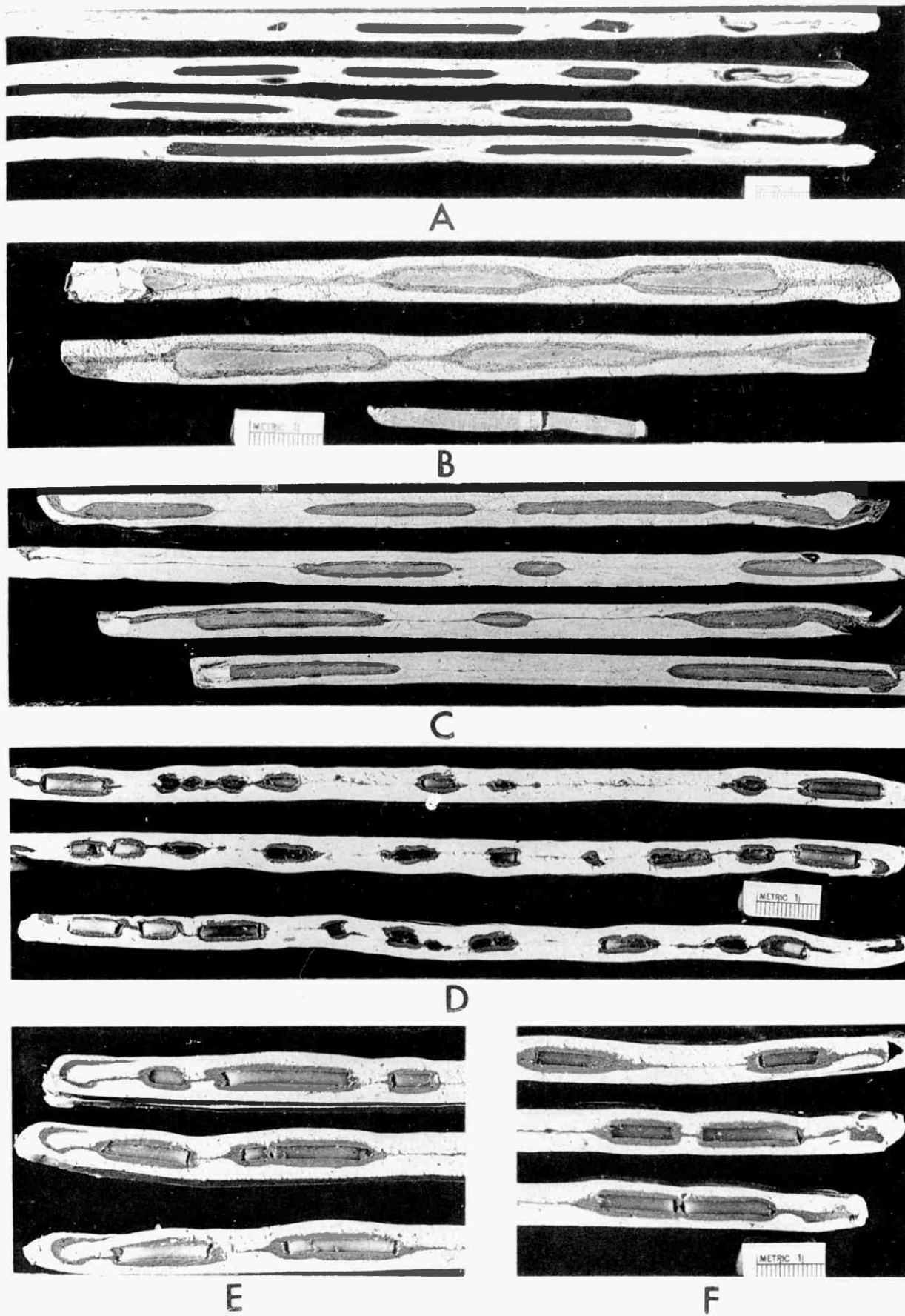


Fig. 1.14. Features of experimental boudins

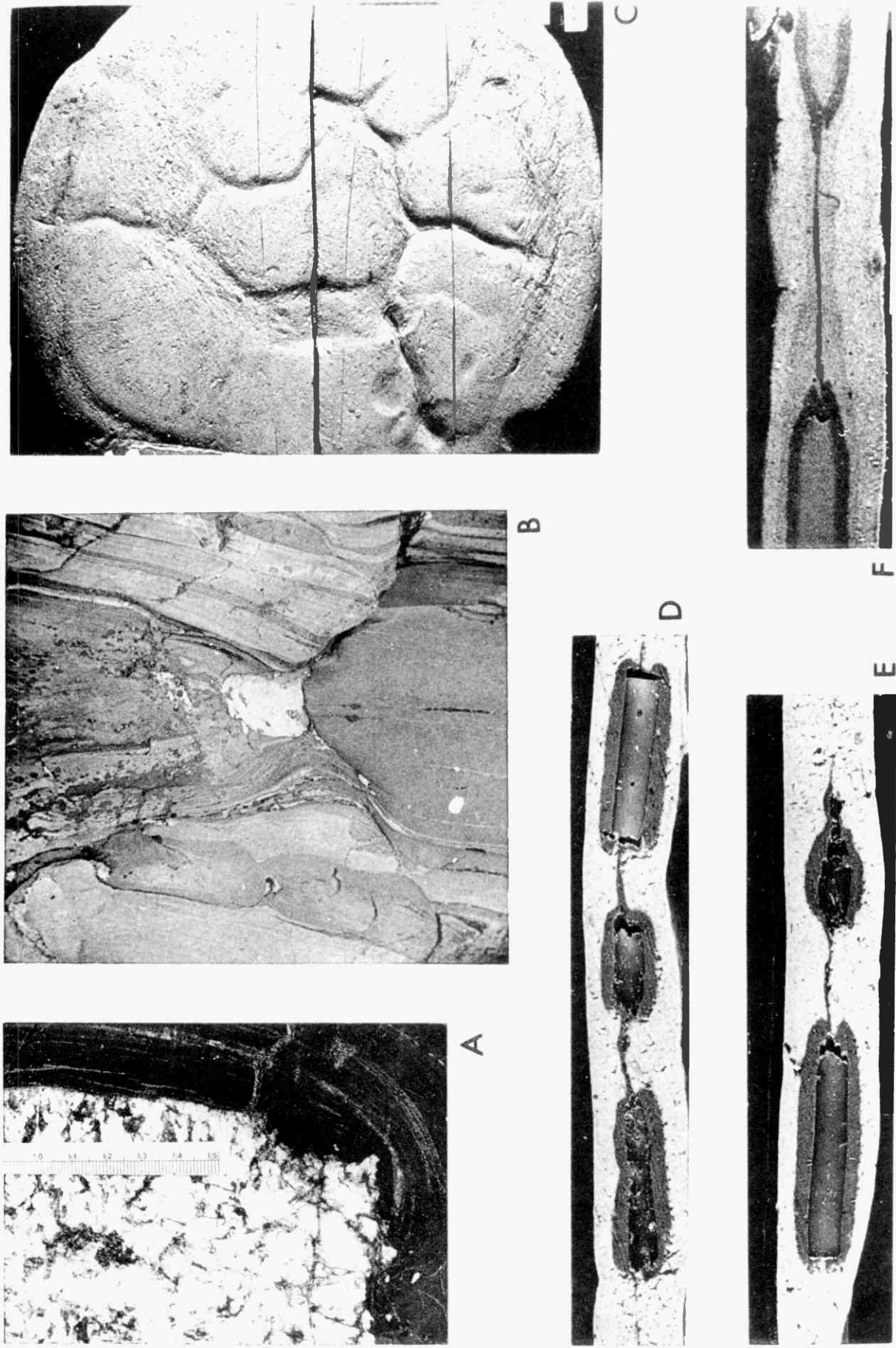


Fig. 1.15. Features of natural and experimental toothfish.



Ramsay (1967) used wooden blocks to simulate a competent layer. A sheet of wood was cut into a number of strips with rectangular cross sections, and these were placed side by side in a ductile material (plasticine or putty) (Fig. 1.16-a). The model was deformed and the blocks became separated into boudins. The results of Ramsay's experiments show how the length of the minor axis of the strain ellipse in the boudin profile section influences the structure around boudins. Where the length of the minor axis of the strain ellipse is short ( $\lambda_1 = 4.9$ ,  $\lambda_3 = 0.2$ ) the surrounding ductile material flowed into the necks between the boudins (Fig. 1.16-b), but where the length of the minor axis is long ( $\lambda_1 = 4.4$ ,  $\lambda_3 = 0.7$ ) open voids were developed between the boudins, although the blocks were separated by the same amount (Fig. 1.16-c). In naturally deformed boudins solutions would be drawn into such voids and any material carried in solution would crystallize.

Ramsay (1967) performed another experiment to investigate the rotation of boudins. He arranged the layer of wooden blocks within the ductile material oblique to principal compression direction. It was observed that although the marker bands in the ductile material rotated, the markers in the boudins changed very little in orientation. The angle of rotation of the boudin was always less than that of the matrix but varied according to the ratio of thickness to length of the cross section of the boudins.

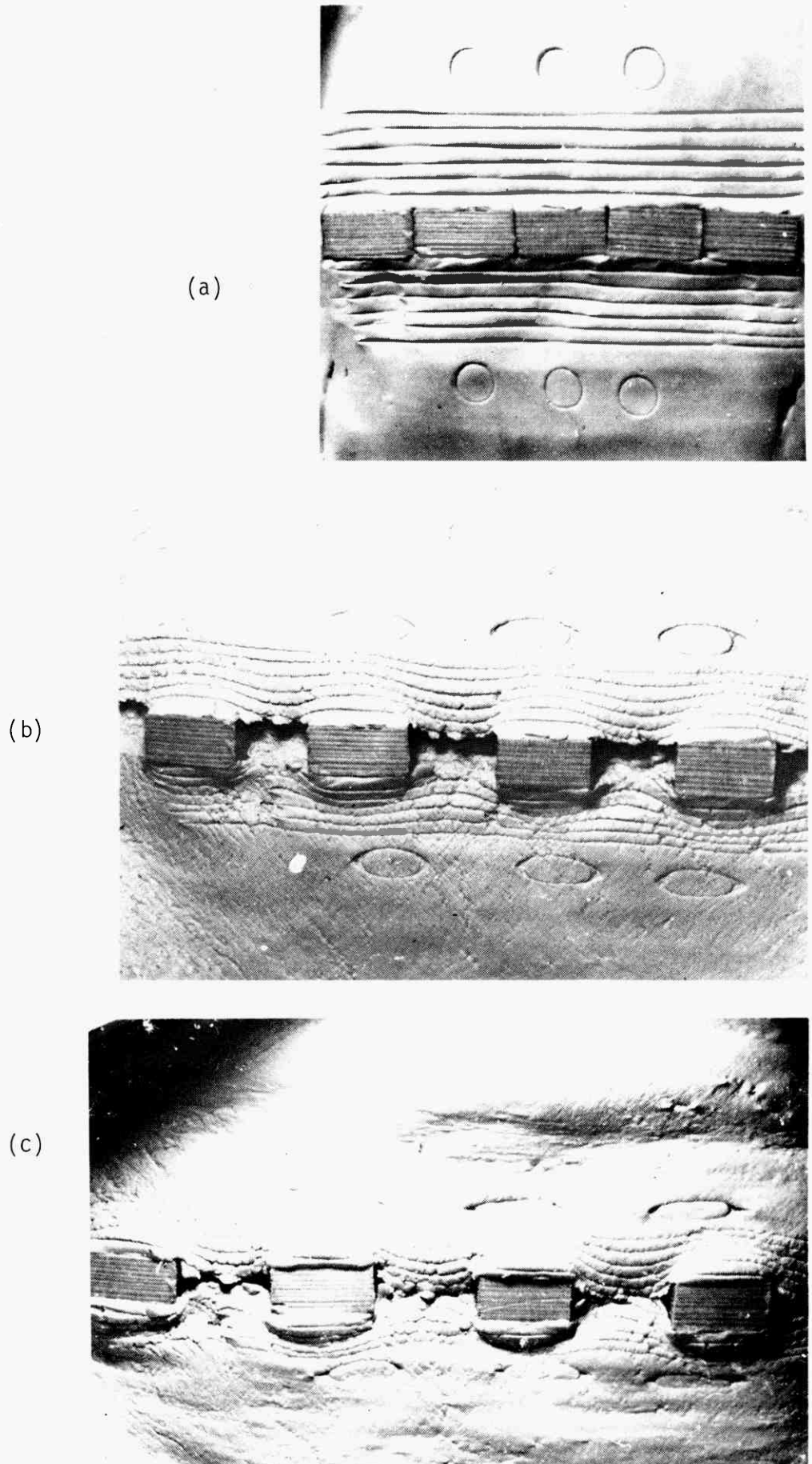


Fig. 1.16 A series of experiments to show the type of structure which develops at boudin necks; (a) undeformed; (b) deformed with little contraction perpendicular to the markers ; (c) deformed with considerable contraction perpendicular to the markers. (after Ramsay, 1967)

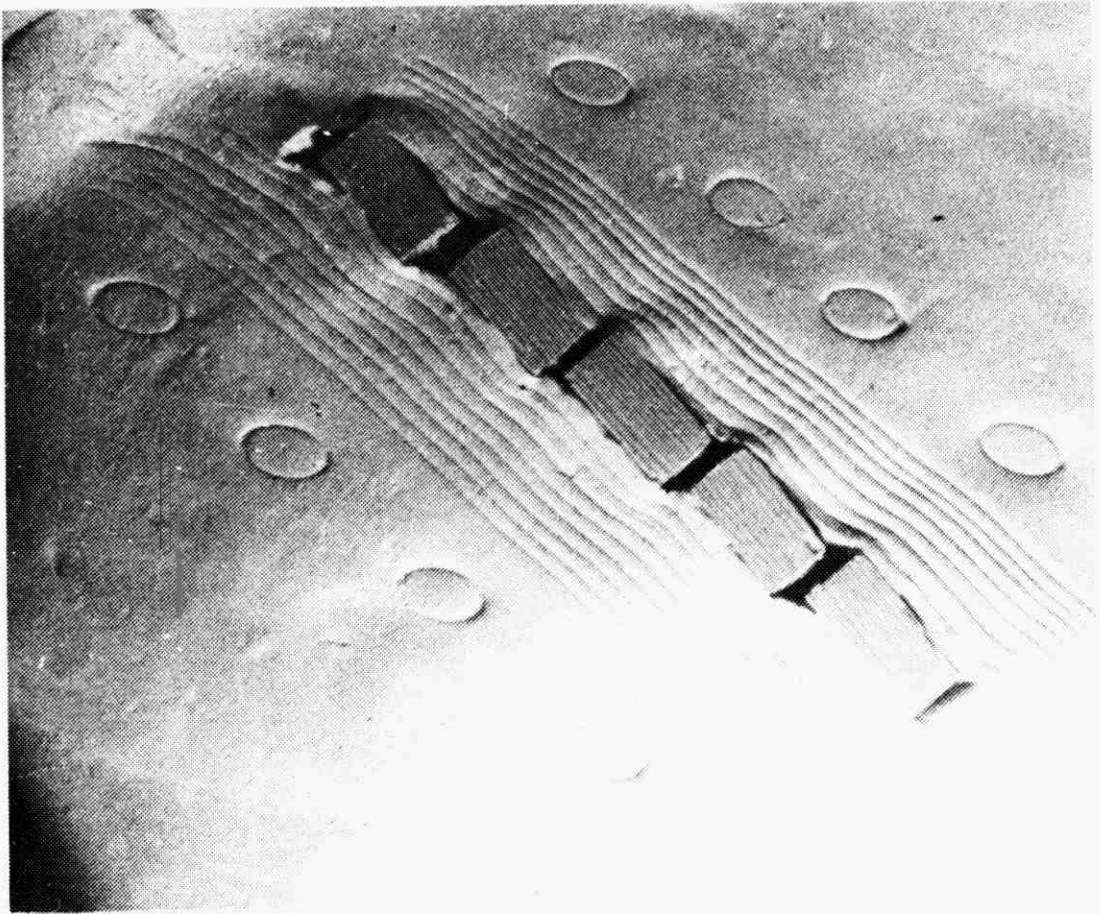


Fig. 1.16-d Experimental 'rotated' boudinage. The competent layer was initially arranged obliquely to the principal axis of strain and the markers in the boudinaged layer rotated less than that in the surrounding ductile material (after Ramsay, 1967).

Hossain (1979) also used wooden blocks to model the formation of 'en-echelon' structure in stretched belemnites. With progressive deformation the layer made up of wooden blocks started to rotate towards the extension direction. However the rate of rotation of the individual segments was found to be slower than that of the composite layer.

Sowers (1973) performed three types of experiments to verify his theoretical work on fracture spacing. The first type involved work on photoelastic gel models. Several 'three layer' sandwich models were flattened in plane strain between appressed 'rigid' platens. The centre layer was thinner and more competent than the embedding layers. In some models the interfacial contacts were welded while in others they were free. The ends of the layers were free of constraint. It was possible to visually monitor the stress field during the experiment.

The other two types of models were (1) multiple layers of alternating clay and putty. These were compressed to produce fractures and boudins, and (2) rock layers. These were stretched in high pressure testing machines. The experiments using rock layers were abortive because of technical failures in their jackets.

The photoelastic model experiments were performed under a 15 in. (38 cm.) clear field Chapman research polariscope which had been equipped with a motor drive which rotated analyser and polariser simultaneously. Special laboratory equipment was made (1) to measure the Young's moduli of gelatin and (2) to cast weak gels.

Homogeneity and optical properties were greatly improved by homogenising the gel and water in a blender before heating; then the mixture was heated for two hours at 90°C to improve dispersion of colloidal particles.

Gelatin gels used were usually composed of 16% gelatin, 16% glycerin and 68% distilled water by weight. The standard gelatin gel has a Poisson's ratio of about 0.5 and a Young's modulus of about  $2 \times 10^6$  dynes/cm<sup>2</sup>. The agar gel was varied from 1.4% to 2.9% (Young's modulus for a 2% agar gel is about  $3 \times 10^6$  dynes/cm<sup>2</sup>). The ratio of modulus of hard to soft layers was about 3:1 but was varied to as much as 6:1. The models were loaded so that a displacement was applied normal to the layering at two strain rates, one 15% strain in 5 min. and the other 15% strain in 30 min. (displaced 2 cm in both cases).

Experimental errors caused by friction are appreciably large in models made from weak gels. They cannot be measured because they occur on front and rear glass walls and are of opposite signs, so their optical effects are self-cancelling in this set up.

#### Description of Model Deformation

Before deformation starts the stress pattern in the model is more or less uniform. But as the elastic instability occurs, at a critical stress, the stress pattern becomes non-uniform. It is very hard to detect the small stress pattern changes in the agar gel but as the load is increased the agar gel develops periodic changes in the internal pattern that correlate directly with fractures which form almost immediately afterwards. One can observe the nearly simultaneous (fig. 1.18) formation of a set of stress concentrations and see that they form before fracture starts in photoelastic models.

Stress concentrations are larger and more closely spaced in those models with welded contacts than in those with either

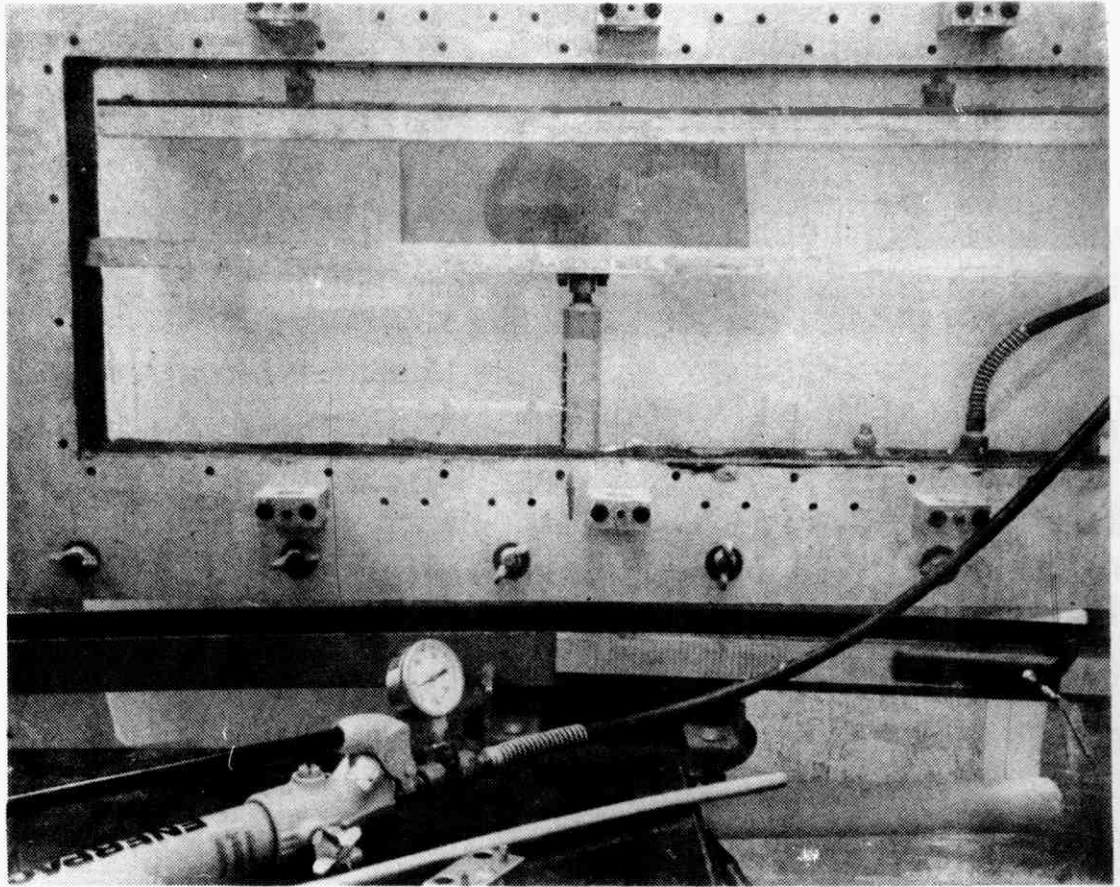


Fig. 1.17-A **Strain frame and polariscope showing model set up.**  
**Frame is about 90 cm by 50 cm.**

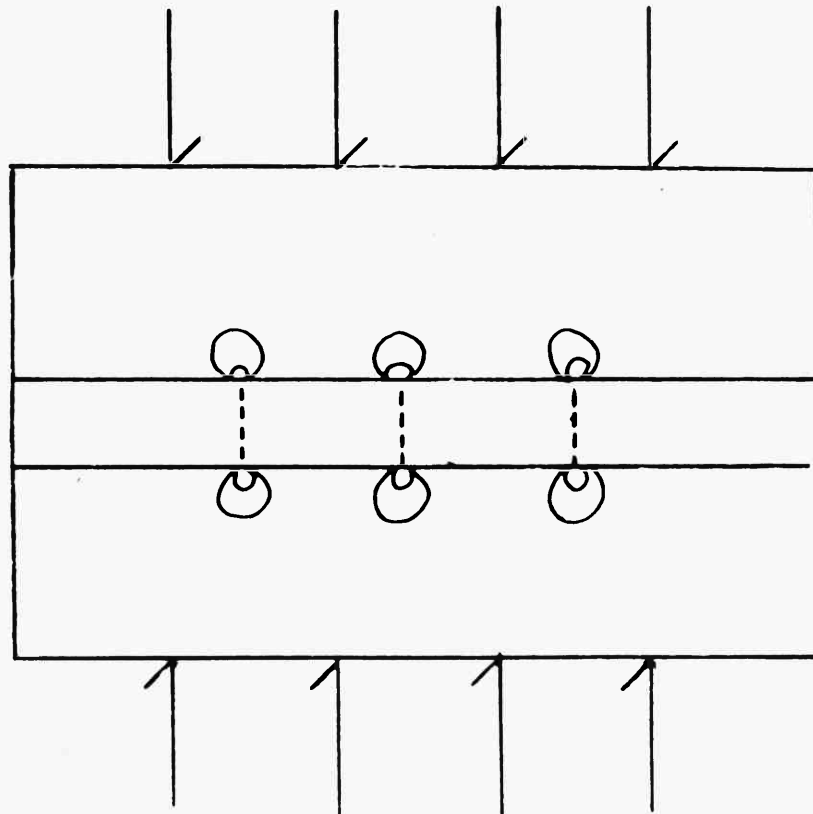


Fig. 1.17-B **Early indication of instability.** Small concentric circles are isochromatic fringes that appear in the gelatin adjacent to agar layer. These indicators of high stress concentration appear before the fractures occur. Fractures will appear along dashed lines.

(after Sowers, 1973).

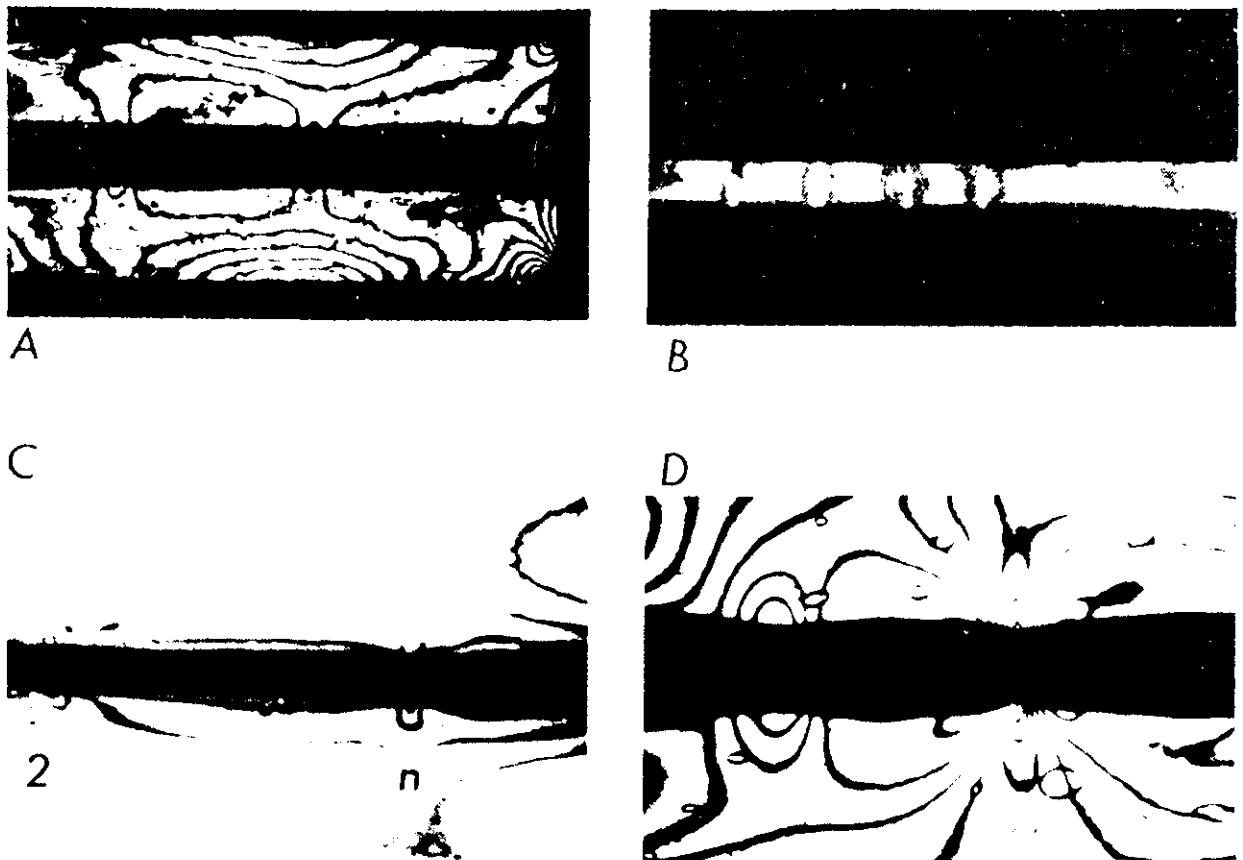


Fig. 1.18 Photoelastic patterns. A. Expt III isochromatics in gelatin gel prior to failure. Agar layer covered. B. Expt III fracture in agar layer and weak isochromatic pattern associated with fracture. Pattern appears before fracture, gelatin layers covered. C. Expt X pattern in gelatin shows two stages. At left (2), fracture exists in covered agar layer; at right (n), no visible fracture. D. Expt XI isochromatic pattern in gelatin in which necking has occurred. Flaws at the surface and in either layer between necks are stable. Necking is a perturbation of the *entire* brittle rod, not unstable growth of randomly located thin places. (after Sowers, 1972)

unwelded or freely lubricated interfaces. In some of these lubricated interface models instabilities did not seem to develop and failure occurred on a single fracture in the middle of the model.

Sowers (1972) noted that "in most models several modes of fracture occur. Other fracture modes form beside the predicted ones related to elastic instabilities. Some develop when loads are increased beyond the load at which the first-formed fractures initiate. These fractures seem to form without disrupting the stress field geometry until

they migrate into the surrounding gelatin gel. This second fracture set consists of short fractures and probably forms as the layer is crushed by compressive stress that exceeds the strength of material.

A third mode of fracturing occurs in a few of the gel experiments and nearly all the putty experiments. Very small, closely spaced fractures form on the interface (usually in the outer few millimetres) of the brittle layer. Fractures are usually less than 1 cm in length and are separated by only 2 to 3 mm. These tension fractures may be arranged in an en-echelon pattern along a line of potential failure. In a gel model, small fractures of this sort formed along the line of potential shear fracture well within the layer. Fractures close to the surface are probably controlled by interfacial instability." Because of this multiple modes of fractures, spacing of fracture at the end of an experiment is variable.

Of the 63 photoelastic tests listed in table 1, 53 were made on models with welded contacts. Fast deformation (larger loads) produced more fractures in about half of the tests. Thicknesses of competent layers varied from 13 to 41 mm. It was found that the spacing interval (or width of segment) is directly proportional to the thickness of the competent layer for fast strain rate experiments (fig. 1.18-E).

The influence of interfacial shear stress on the formation of the instability is clearly demonstrated by the fact that tests with free interfaces or with low frictional contact have few or no fractures.

Results of 10 tests on a 3mm thick clay layer in a matrix of putty (Table 2) indicates that the fracture spacing to thickness relationships for clay is different to that for gelatin. For the same thickness of layer the fracture spacing in gelatin is about 10 times greater than in clay. Clay-putty models differ from gelatin models in that 1. the clay-putty layers have much higher Young's moduli, 2. they have a larger



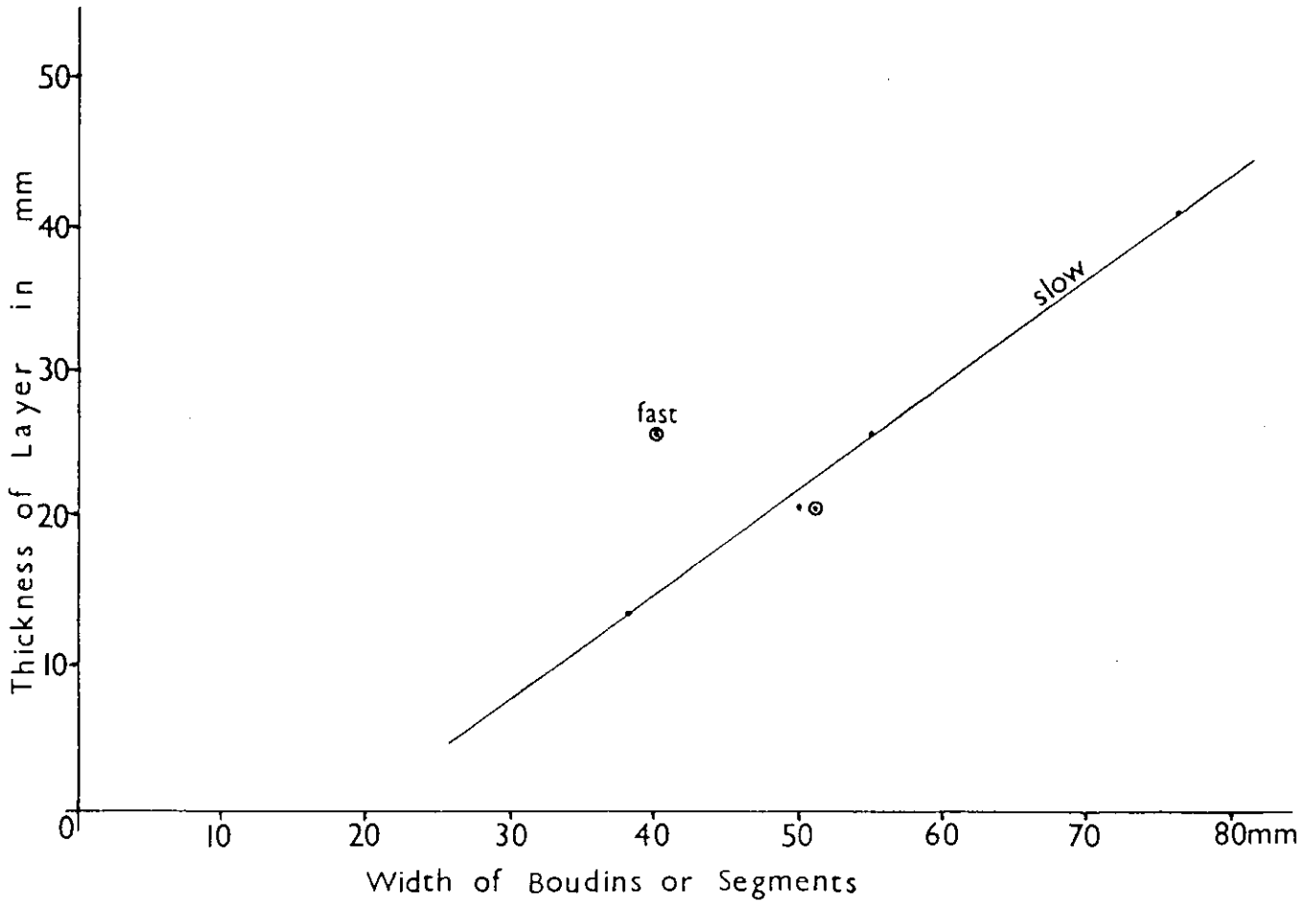


Fig. 1.18-E. Plot of thickness of competent layer against the average width of the boudins or segments. Note the linear relationship between thickness and width of boudins which were formed in slow strain rate experiments (see Table 1.1).

competence contrast between layers and, 3. relative to their Young's moduli they have very low yield strength.

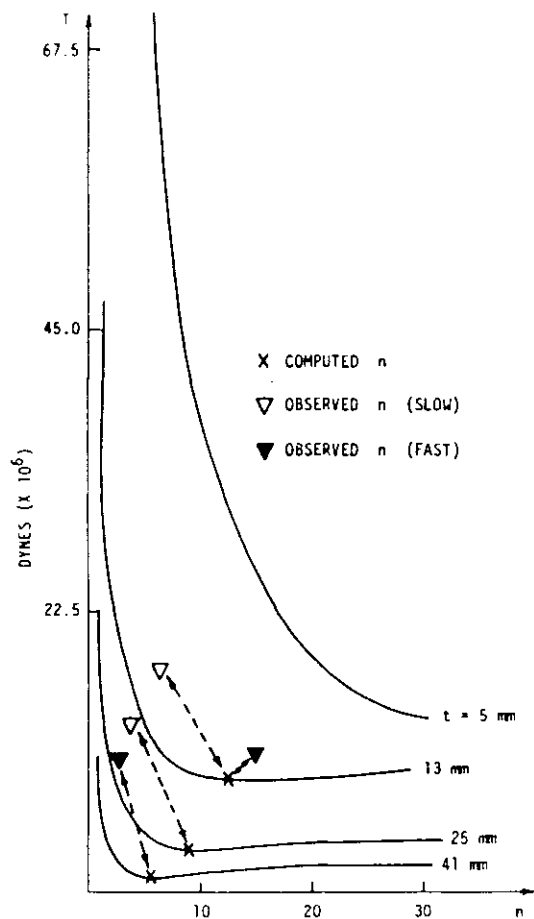
Sowers graphic representation of his experimental results are shown in figs. 1.19 to 1.21 and these are compared to his theoretically predicted results which are discussed in section 1.3.

TABLE 1. EXPERIMENTAL RESULTS, GEL MODELS

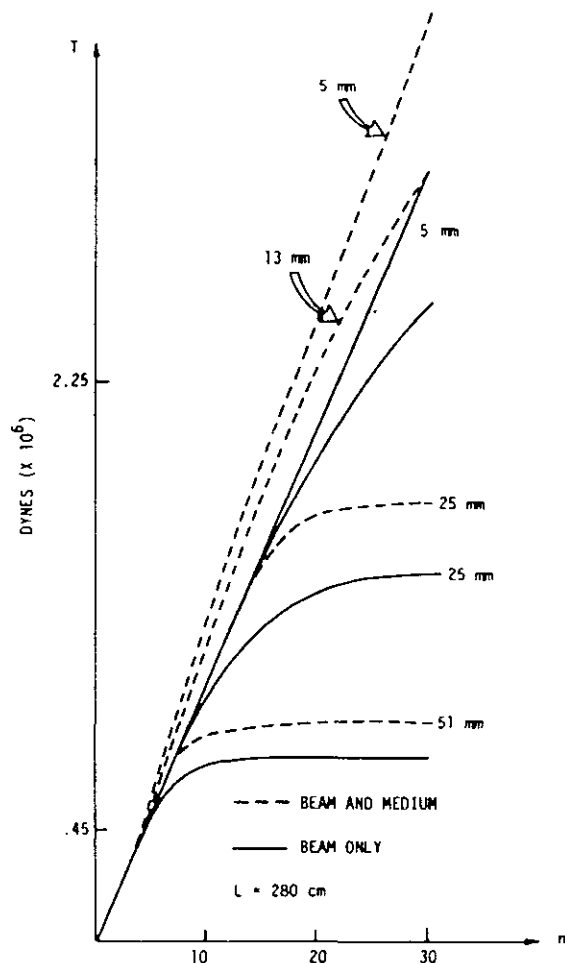
Layer	Thickness		Young's modulus		Average number of fractures	Spacing interval	Number of tests	Applied load
	Medium X 2	Layer	Medium	(X 10 <sup>6</sup> dynes)				
A. Welded contacts								
40.8 mm	121.8 mm	slow	0.42	0.21	2.1	76 mm	2	1.7 X 10 <sup>6</sup> dynes
25.4 mm	125.7 mm	slow	0.42-0.28	0.25-0.21	3.8	55 mm	16	2.2 X 10 <sup>6</sup> dynes
20.6 mm	128.5 mm	slow	0.42	0.25	4.2	50 mm	6	2.4 X 10 <sup>6</sup> dynes
13.0 mm	135.0 mm	slow	0.42	0.25	7.1	38 mm	6	2.9 X 10 <sup>6</sup> dynes
25.4 mm	125.7 mm	fast loading	0.36-0.42	0.21-0.25	15.5	40 mm	11	1.9 X 10 <sup>6</sup> dynes
20.6 mm	128.5 mm	fast loading	0.32-0.36	0.21	5.1	51 mm	12	
B. Frictional contacts								
21 mm	128 mm		0.4	0.2	5.0	50 mm	1	Fractures appear in second stage; 2 then 3 fractures
25 mm	125 mm		0.4	0.2	1.0		2	Second test; rapidly overloaded layer shattered
C. Free interfaces—very low friction								
13 mm	135 mm		0.4	0.2	0		3	Water lubricant
7 mm	142 mm		0.4	0.2	0		2	
60 mm	120 mm		0.4	0.2	1.0		1	
25 mm	120 mm		0.4	0.2	100s			Foam lubricant, shatter
20 mm	120 mm		0.4	0.2	0-100s		1	Shattered

TABLE 2. EXPERIMENTAL RESULTS, CLAY MODELS

Clay layer length		Number of fractures		Fracture interval	Number of tests
Initial	Final	Major	Secondary		
A. Clay layers—3 mm thick, clay plasticine embedded in putty					
203 mm	254 mm	4.1	20-25/in.	65 mm	3
280 mm	240 mm	4.0	20-25/in.	70 mm	1
175 mm	240 mm	3.0	20-25/in.	70 mm	3
B. Clay layers—3 mm thick					
203 mm	245 mm	2.0		90 mm	3



A



B

Fig. 1.19.A Graph of tension versus number of nodes (fracture sites) at various layer thickness. Critical tension and fracture spacing indicated for observed values in gelatin-agar model (gelatin  $E = 0.42 \times 10^6$  dynes/cm<sup>2</sup>; agar  $E = 0.21 \times 10^6$  dynes/cm<sup>2</sup>), length 28cm. Note linear arrangement of three critical tensions from slow tests at three-layer thickness. Slope differs from slope of three corresponding computed values. Combined action shear and normal forces on interface produces minima (critical values).

Fig. 1.19.B Graph of tension versus number of nodes at various thickness for only normal forces on interfacial surface; otherwise as in Figure 1.19.A. (after Sowers, 1973).

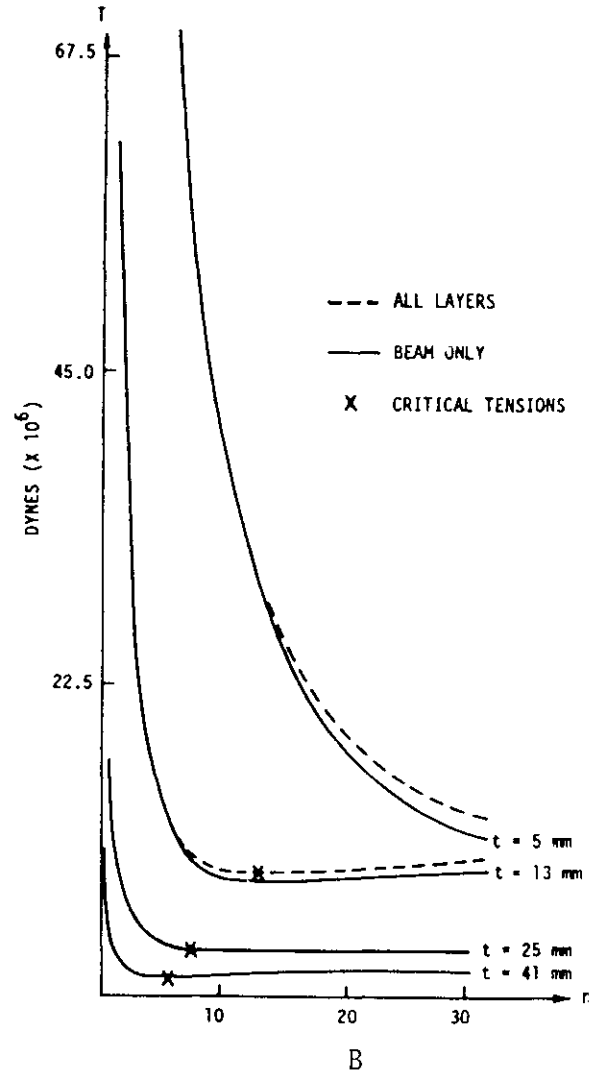
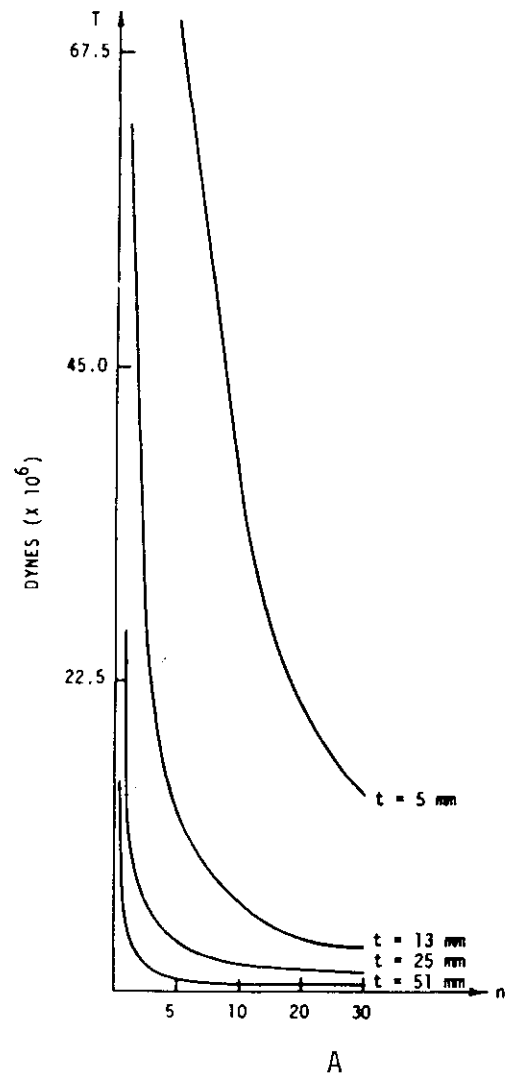


Figure 1.20.A. Graph of tension versus number of nodes at various thickness, for only shear forces act on interfacial surface. Other conditions as in Figure 1.19.A.

Figure 1.20.B. Comparison of critical values computed for three layer model with those obtained for the stiff layer alone. Conditions as in Figure 1.19.A. (after Sowers, 1973).

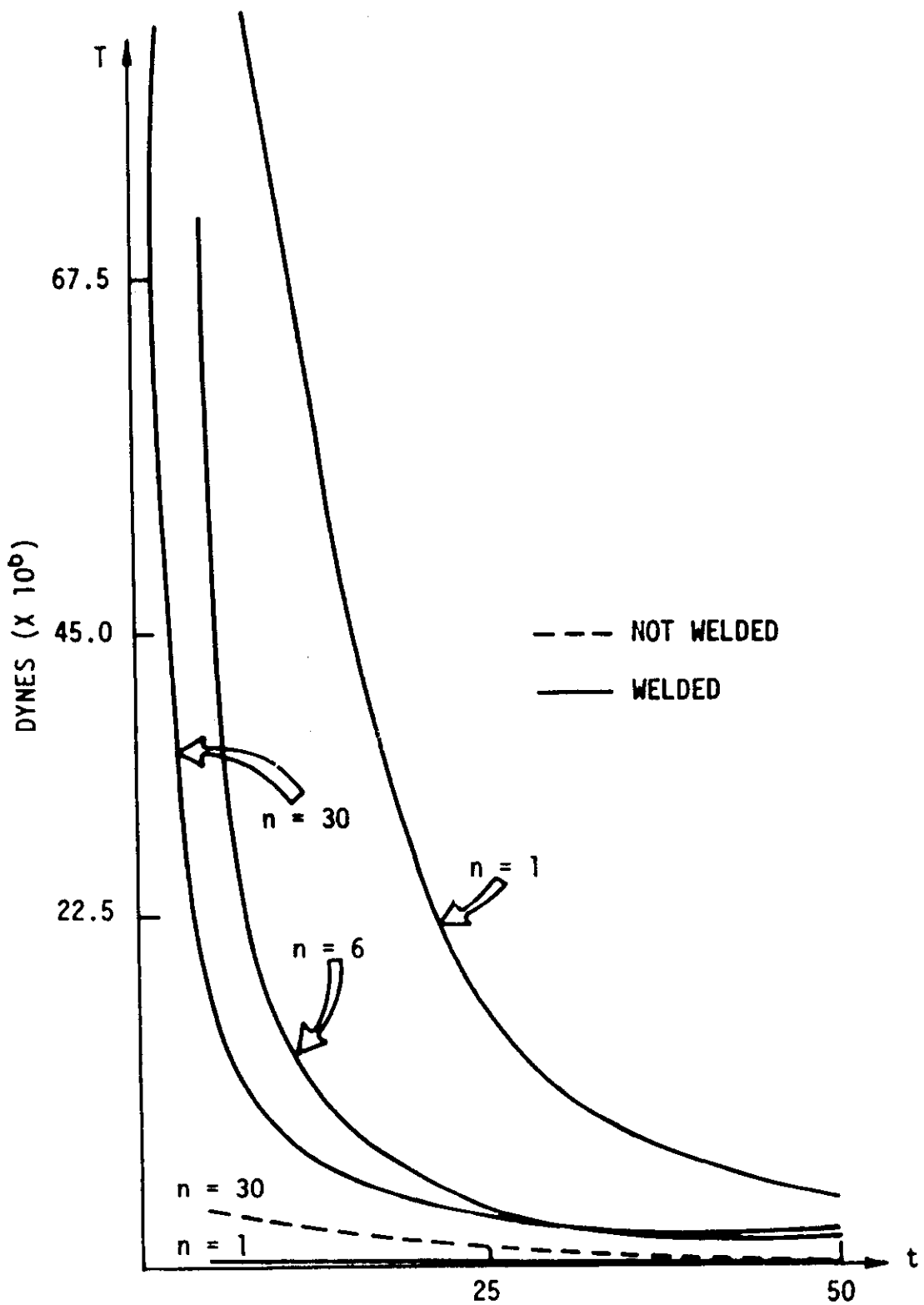


Fig. 1.21-A Graph of tension versus thickness at various constant number of nodes (fracture sites). No critical tensions occur in unwelded case. (after Sowers, 1973).

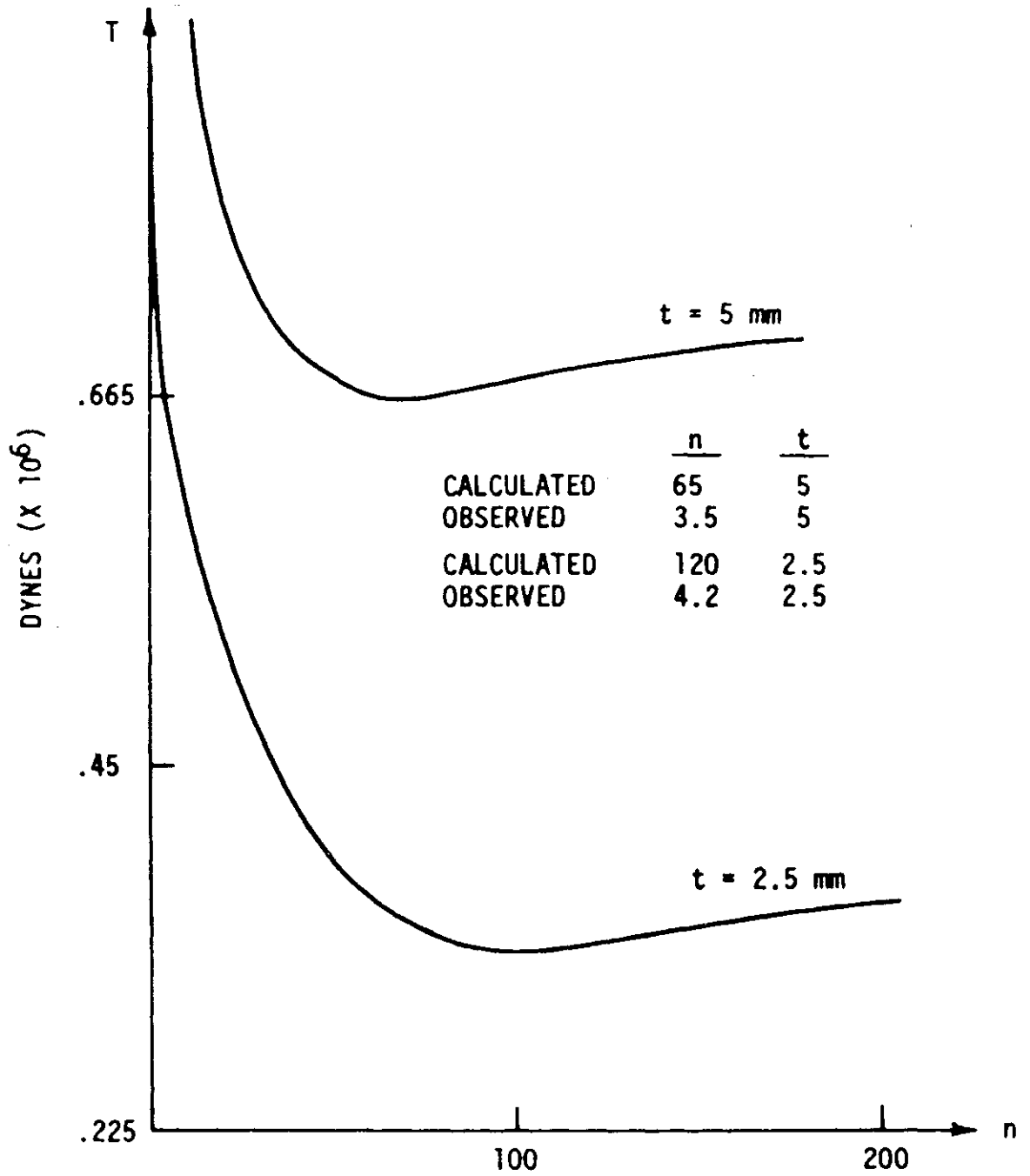


Fig. 1.21-B Graph of tension versus number of nodes for clay-putty model. Length 25.0 cm. Assumed values: clay  $E = 4.9 \times 10^6$  dynes/cm<sup>2</sup>; putty  $E$  assumed to be negligible (after Sowers 1973).

Stromgard (1973) used cellulose acetate and benzylalcohol as competent layers and in another model he used the photoelastic properties of gelatin to study the change in the stress distribution caused by the development of tension fractures in the competent layers (fig. 1.22-a&b) respectively.

Because of the relatively high tensile strength of the competent layer material the 'fracture' had to be produced by cutting, before deformation started, in both models. Before fracturing, the maximum tensile stress,  $\sigma_1$ , along the x-axis has its maximum value in the middle of the competent layer A (point P in fig. 1.22-b). After fracturing, tension is maximum a certain distance from the fracture (i.e. at point Q fig. 1.22-b-B). A comparison of the isochromatic and isoclinic patterns before and after fracturing showed that the fracture only measurably influences the stress distribution within a limited area. The fracture caused the value of  $\sigma_1$  to decrease along the line R-R (fig. 1.22-b-B).

Variations in Young's modulus ratio did not significantly change the size of domains of reduced tensile stress in the models (highest modulus ratio approximately 4).

The gelatin model consists of a competent gelatin inclusion in an incompetent gelatin surrounding. First the isochromatics and isoclinics of the loaded model in the unfractured state were studied, and then a central tension fracture was cut at E (fig. 1.23-A) and the new stress distribution examined.

The orientation of the principal compressive stress in the model deviated at most  $10^0$  from the x- and y-directions. A simplified picture of the calculated shear-stress distribution inside the competent layer or boudin after fracturing is shown in fig. 1.23B.



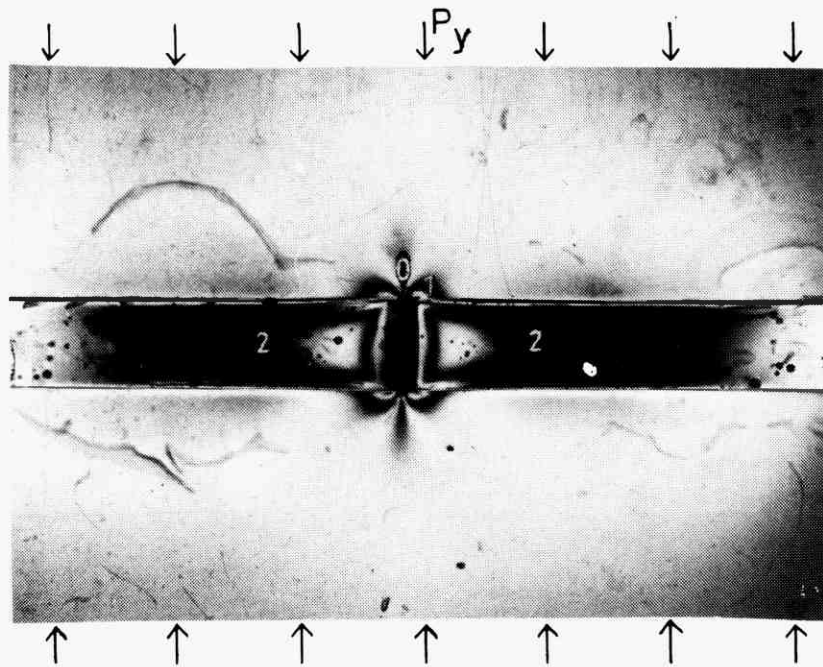


Fig. 1.22.a. Stress distribution at boudinage initiation; isochromatics; cellulose acetate + benzylalcohol model; Young's modulus ratio  $k \approx 3$ . (after Stromgard, 1973)

Fig. 1.23.C shows the approximate variations in the magnitude of the principal stresses  $\sigma_1$  and  $\sigma_3$  along the horizontal axis of symmetry in the model (CDE fig. 1.23.a). After fracturing, points of maximum value of  $\sigma_1$  are located approximately in the middle of the segments (H). The maximum value of  $\sigma_1$  is slightly lower than before fracturing (fig. 1.23.C). The values of  $\sigma_1$  in the competent layer were found to be higher along the horizontal contacts than along the horizontal line of symmetry. At mid-width in a segment, however, this difference in the value of  $\sigma_1$  is high if width/thickness ratio of segment is small.

#### Stage after the boudins have separated

For models with small differences in competency, the directions of  $\sigma_1$  and  $\sigma_3$  in both the boudins and the surrounding deviate little from the directions of applied stresses. The maximum shear stress is concentrated at the ends of the boudins. Fig. 1.24 shows the distribution of maximum

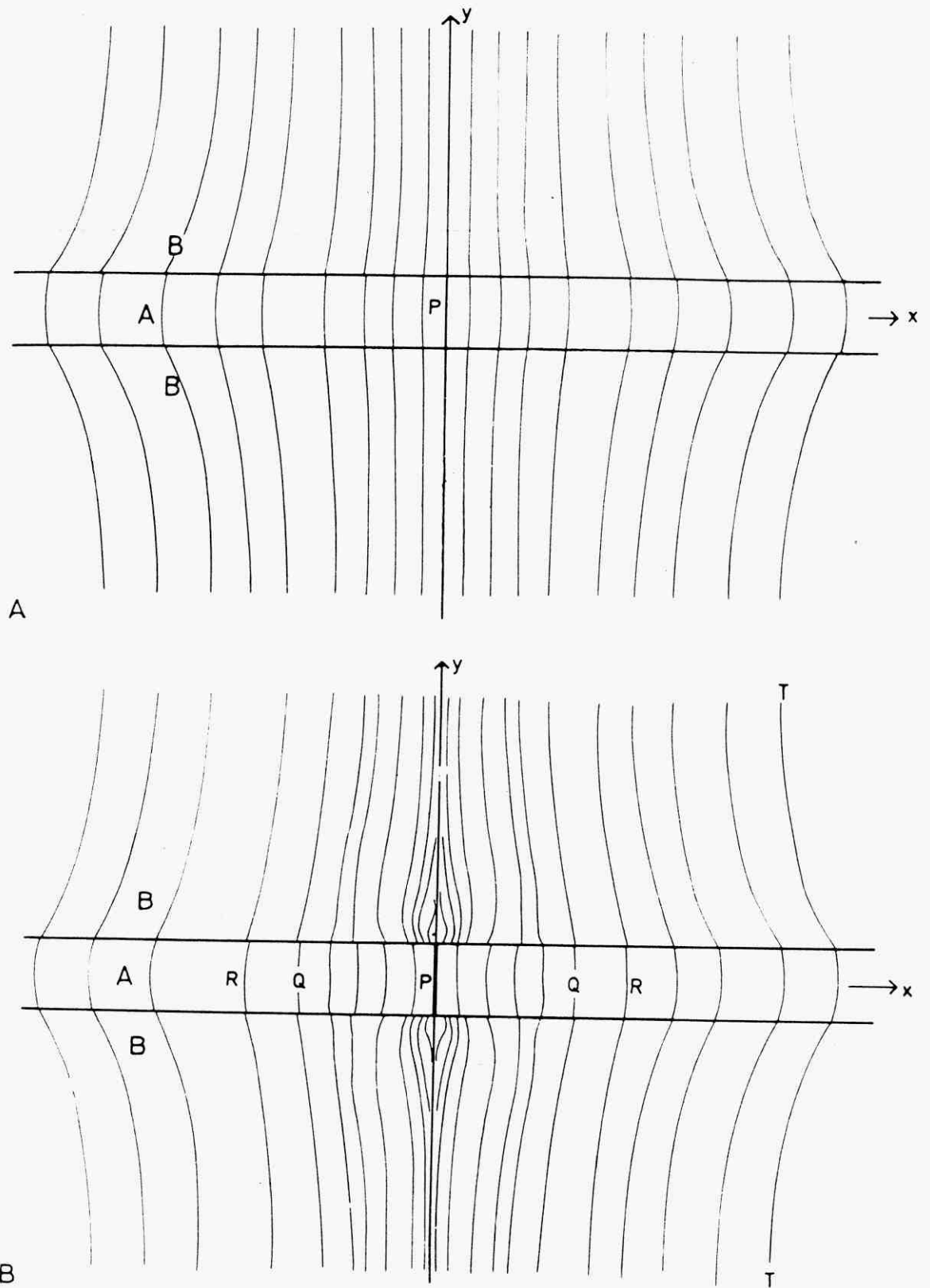


Fig. 1.22-b Trajectories of maximum compressive stress in a photoelastic model; A = competent layer of cellulose acetate + benzylalcohol; B = incompetent layers of the same material. A. Before formation of a fracture in the competent layer. B. After formation of fracture; the isochromatic pattern is shown in fig. 1.22a.

(after Stromgard, 1973).

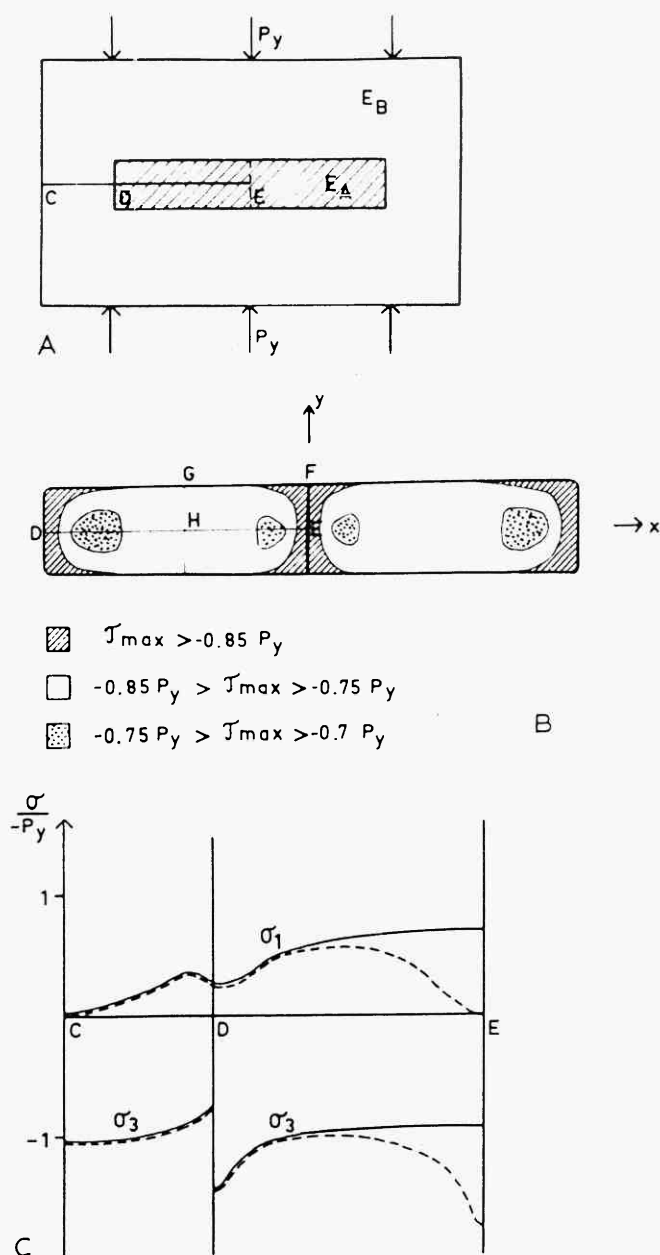


Fig. 1.23 Boudinage in gelatine model. A. Loading of model,  $k=E_A/E_B=2.3$ . B. Simplified representation of the distribution of maximum shear stress after fracturing. C. Principal stress along section CDE before fracturing (solid line) and after fracturing (broken line). (after Stromgard, 1973).

shear stress calculated from the model in fig. 1.23.D. The  $\tau_{\max}$  is maximum between the boudins. The value of  $\frac{\tau_{\max}}{P_y}$  at this point was found to increase with increasing modulus ratio  $k$ . The value of  $\sigma_3 = \sigma_y$  at the same point presumably increases with  $k$ , because of a supporting effect of the boudins, which reduces the vertical compression in the area between the boudins. The stiffer the boudins the stronger is the supporting effect. The fact that the values of  $\sigma_3$  and  $\tau_{\max}$

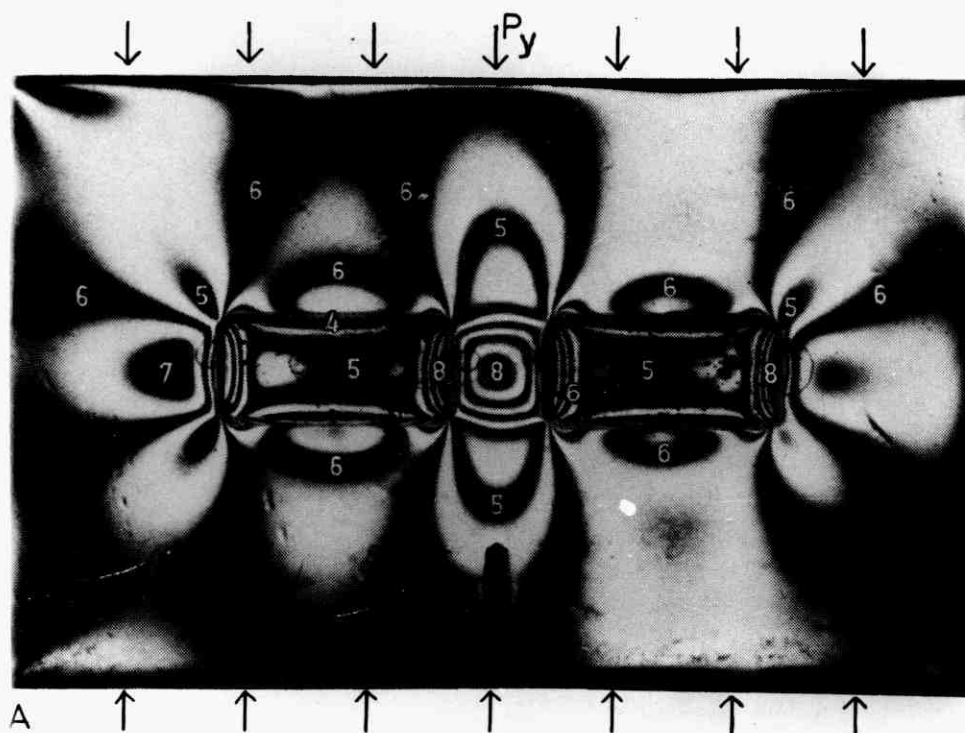


Fig. 1.23-D Stress distribution for two separated boudins; isochromatics; gelatin model;  $k=2.3$ ,  $P_y=-0.15$  bar,  $E_A=1.9$  bar,  $E_B=0.8$  bar,  $F_A=0.025$  bar/fringe and  $F_B=0.013$  bar/fringe. An  $n$ -th order fringe corresponds to  $\tau_{\max}=-n \cdot 0.17P_y$  in the surrounding material (A), and to  $\tau_{\max}=-n \cdot 0.09P_y$  in the boudin material (B). Fig. 24a gives the distribution of  $\tau_{\max}$  after correction for the initial thermal stresses. (after Stromgard, 1973)

both increase with  $k$  implies that  $\sigma_1$  must increase more rapidly with  $k$  than  $\sigma_3$ . From this relationship it can be inferred, that values of  $\sigma_1$  and mean stress  $\bar{\sigma} = \frac{(\sigma_1 + \sigma_2 + \sigma_3)}{3} \approx \frac{(\sigma_1 + \sigma_3)}{3}$  will both be algebraically high at high  $k$ -value. (Magnitudes of  $\sigma_1$  and  $\sigma_3$  could not be determined accurately for the models because of the errors involved in subtraction of initial thermal stresses and errors of graphical integration process. The main feature of the distribution of principal stresses are shown, however in fig. 1.24-a).

Models with different distances between boudins revealed that the values of  $\tau_{\max}$  and  $\sigma_1$  in the central part of a boudin decrease with increasing separation of the boudins if loading is constant.

Following Frochts (1966) work of photo-elastic methods, Sen and Mukherjee (1975) calculated the strain distribution inside an elliptical shaped boudin under normal progressive stress. (see Sen and Mukherjee (1975) fig, 1, Plates 1 and 2, pages 192-96).

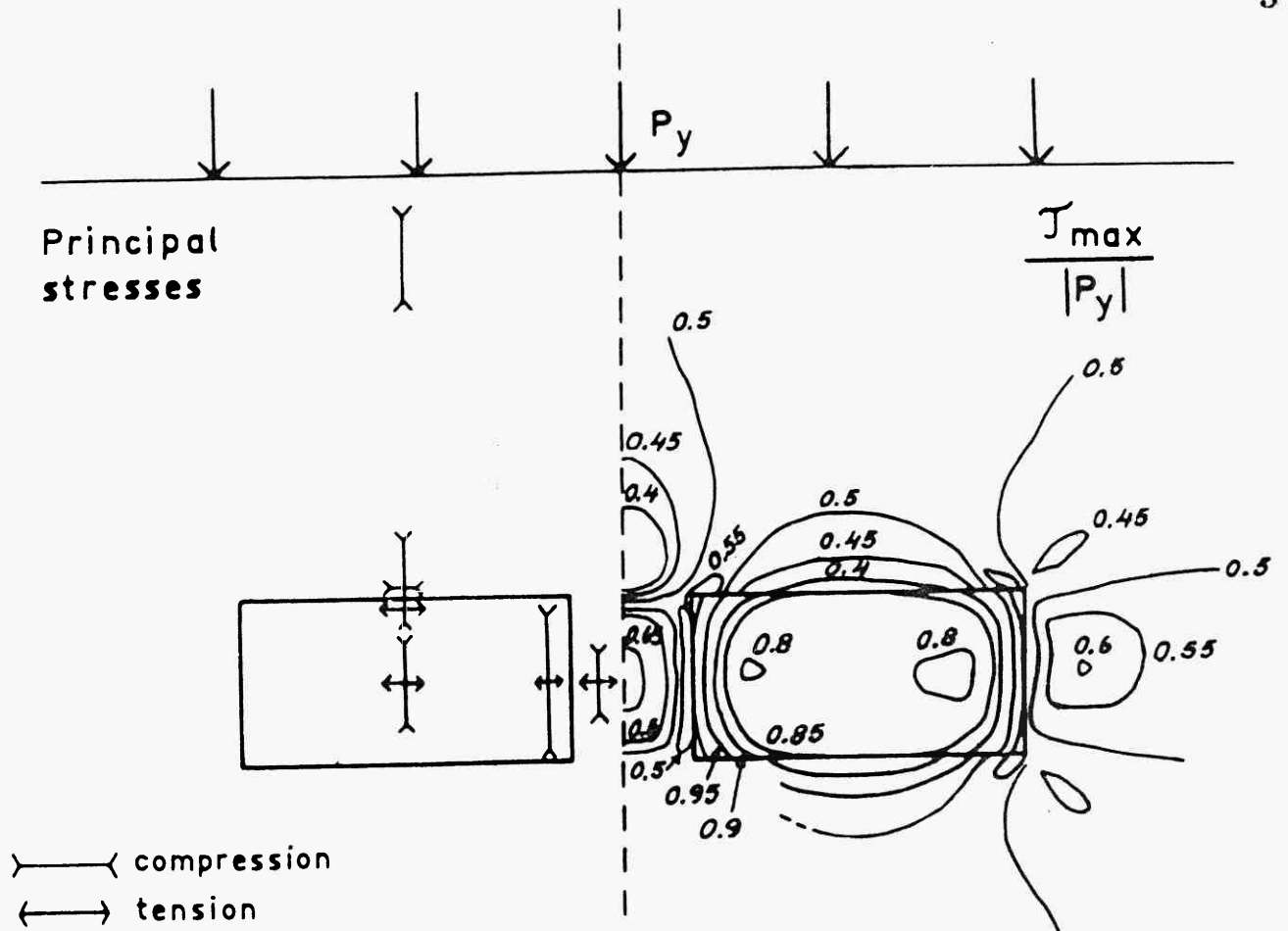


Fig. 1.24-a Stress distribution in a gelatin model of boudinage. Young's modulus ratio  $k=2.3$ .

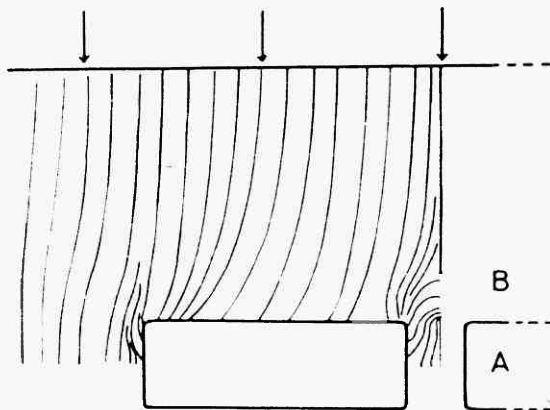


Fig. 1.24-b Trajectories of maximum compressive stress around two rigid boudins

(after Stromgard, 1973).

### 1.212 Real Rock Analogues

Griggs and Handin (1960) extended concentric rock cylinders under high pressure to simulate boudinage. In these tests the inner core was relatively more brittle (dolomite, for example) than the enclosing rock (e.g. limestone). The ends of the composite specimen were restrained so that total extension of both cylinders was the same, although the longitudinal strain varied widely in different parts of the specimen. The inner core was ruptured in one or more places, and individual pieces were engulfed by the influx of the ductile matrix into the cracks. Sometimes the inner core fractured into several more or less equant blocks along either shear or extension fractures that usually terminated against the outer cylinder without crossing it. Fractures often opened and the ductile material penetrated the openings. As the tests were done on dry rocks, fracture formation could not involve hydraulic mechanisms. Where deformation was brittle, more or less triangular and rhombohedral blocks were formed, within which permanent deformation was negligible and lengthening took place by separations of these blocks (fig. 1.26).

Paterson and Weiss (1968) used Nelligan phyllite which has an average grain size of about 0.01 mm and consists essentially of chlorite and sericite with variable but minor amounts of disseminated quartz, commonly in tabular grains. The grains of all these minerals have their long dimensions in almost perfectly parallel preferred orientation, defining a regular and strongly platy foliation. Additional quartz occurs locally in variable amounts and in various ways, e.g. as

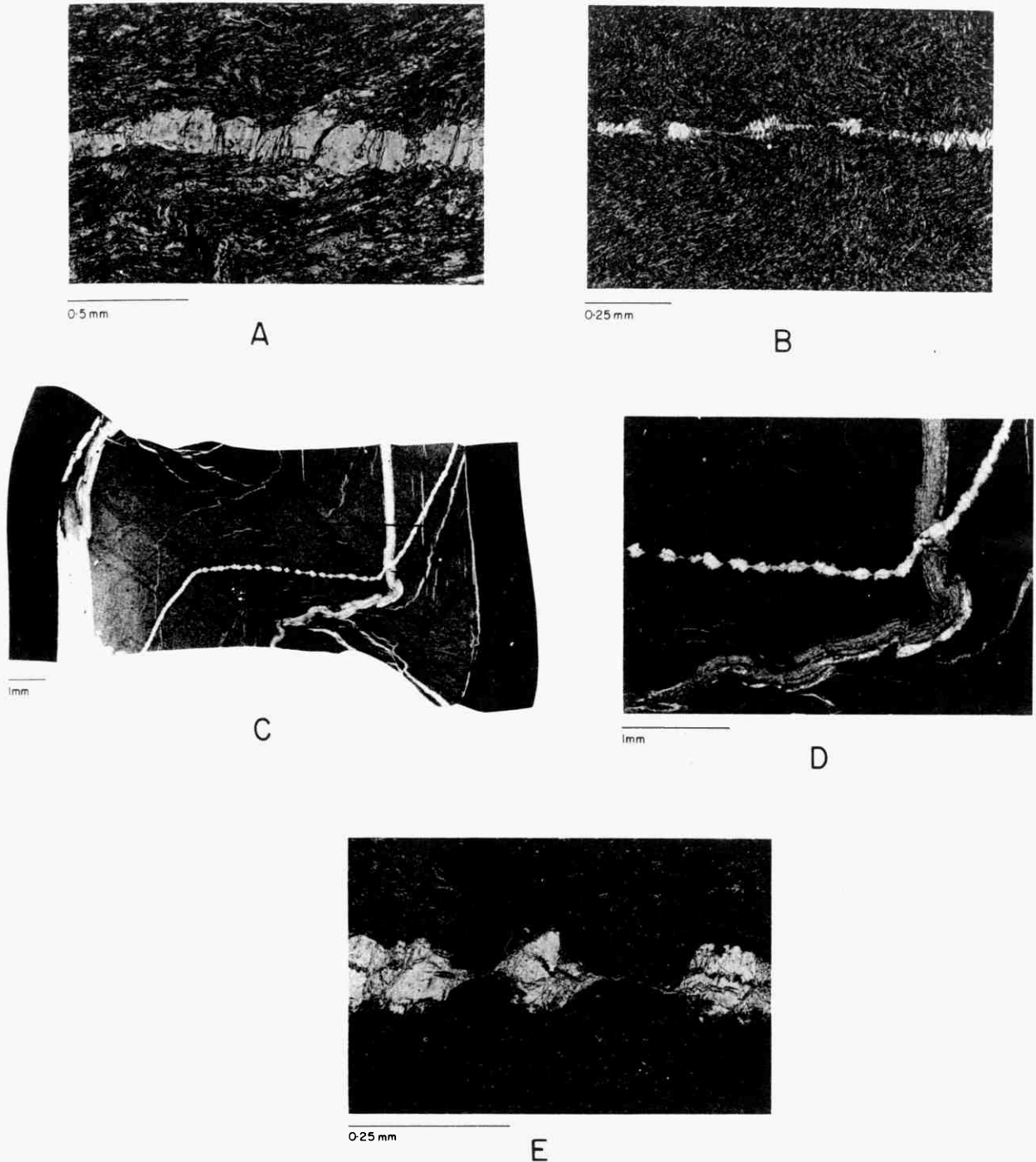


Fig. 1.27-a

A. Tensile fractures perpendicular to unfoliated polycrystalline quartz vein extended in large kink. B. Tensile fractures, pinch and swell structure, and incipient boudinage in partly foliated polycrystalline quartz layer. C. Specimen in steel jacket (shown black), shortened 40 percent parallel to foliation, showing boudinage of quartz layer extended in large kink. D. Detail of area outlined in C. E. Detail of boudins in C.

#### EXTENSION FRACTURES, NECKING, AND BOUDINAGE OF QUARTZ LAYERS

(after Patterson and Weiss, 1968)

In one particular experiment in which compression was parallel to the foliation a massive quartz vein (oblique to the foliation) developed extension fracture subperpendicular to the vein. Prior to this fracturing the vein was locally rotated into a position approximately normal to the principal compression by the development of a kink band, fig. 1.27a. When this occurred pinch-and-swell structure formed in the vein and these then separated into discrete rhombic or lens-shaped boudins.

Gay and Jaeger (1975) compressed relatively long cylinders of rock (25 - 27mm length and 5 - 7mm diameter) in a matrix of crushed rock to loads of 4.5 MN. Composite cylindrical specimens (diameter 75 - 85mm and 25mm in height) were prepared by pouring crushed marble to make a layer of matrix into a thick-walled rubber jacket, placing the cylinder to be boudinaged in the centre of the jacket and then pouring an equal amount of matrix on top (fig. 1.27-b).

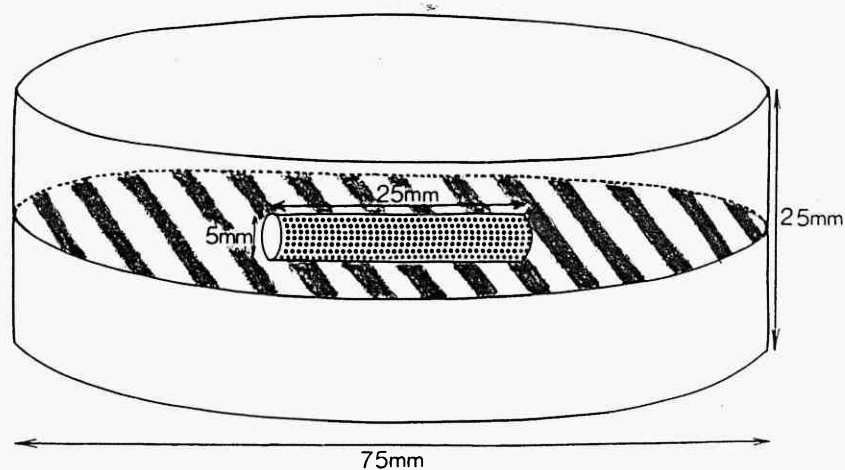


Fig. 1.27-b. Diagrammatic representation of the composite cylindrical specimen.

The material used for the matrix was crushed Wombeyan marble but in one test adamellite was used. The rock types used for the preparation of the competent cylinders (in order of increasing strength) were: Woodline shale, Carrara marble, Solenhofen limestone and Rangar oolitic



limestone. The specimens were placed between steel plates and compressed uniaxially at a standard controlled rate in a large testing machine.

During the deformation the unconsolidated matrix was compacted and the central competent cylinders thinned and boudinaged. From their experiments Gay and Jaeger (1975) found the response of cylinders to the deforming forces was very strongly controlled by their ductility. The very ductile Woodline shale flattened and elongated. The intermediate cylinders thinned and formed boudins of one type or another. The least ductile specimen, Rangari oolitic limestone underwent significant necking by collapse along  $60^{\circ}$  to  $70^{\circ}$  normal faults but hardly deformed internally.

From their experimental results they drew the following conclusions on the mechanisms of boudinage formation

(1) Initial effect of the axial compression is to flatten and elongate the specimen homogeneously. (2) A region of necking develops normally in the centre of the specimen where the applied pressure is greatest and barrelling at the ends of the specimen develop. The mechanism of necking, in all specimens, is due to collapse of material along a pair of conjugate normal faults to form a small graben-like structure. These shear faults then either cut through the specimen or coalesce with extension fractures or shear fractures initiated from the opposite side to form a curved fracture. In this way the cylinder is separated into boudins. The final stage is the physical separations of the boudins. In all specimens the matrix flowed into the opening low-pressure area between boudins.

Gay and Jaeger pointed out that the result of their work is different from those of previous writers (namely Ramberg, 1955; Ramsay, 1967; and Stromgard, 1973). These writers have considered extension

fracturing to be the main mechanism for boudin initiation. Gay and Jaeger's result, however, does not support this idea; instead, it shows that necking by collapse along shear fractures occurs first. Griggs and Handin (1960) and Paterson and Weiss (1968) who also used rocks as the model materials in their experiments also emphasized the importance of shear fracturing.

Gay and Jaeger (1975) warn that their experimental results should not be used to re-interpret all occurrences of natural boudinage because they are only directly applicable to specialized geological situations in which boudinage takes place under cataclastic conditions.

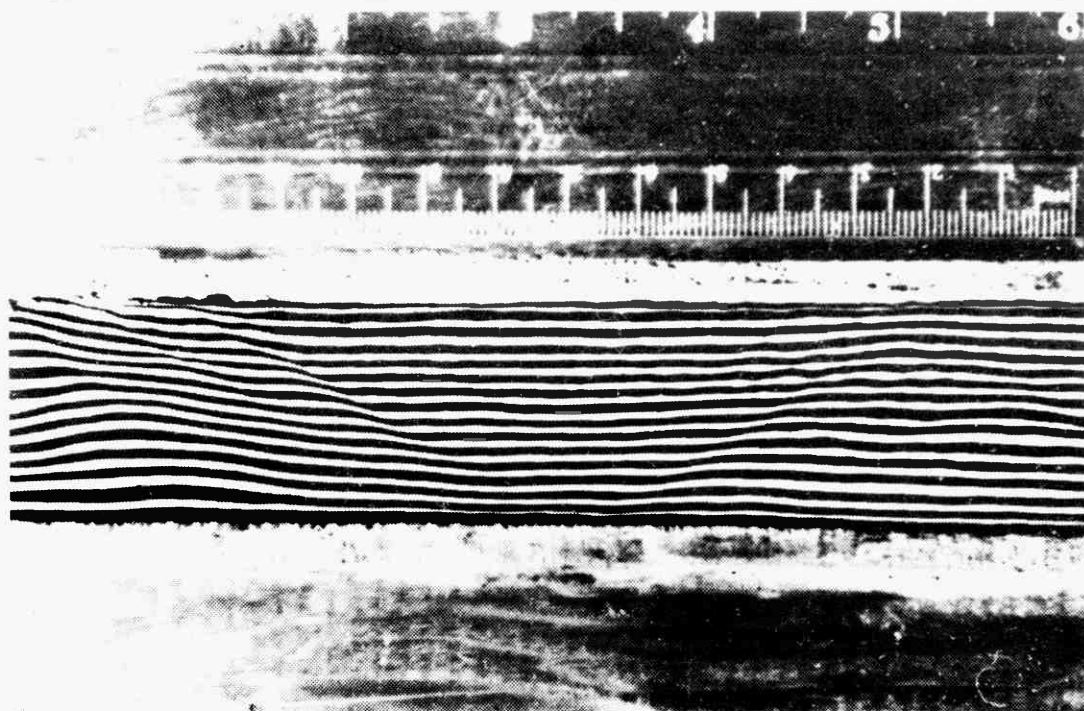


Fig.1.28-a . Interlocking pinch-and-swell structures (internal boudins) and normal kink-bands developed in a model , as a result of compression normal to the layering.

### 1.22 Multilayer Boudinage (Experimental)

Cobbold et al. (1971) compressed a lubricated plasticine multilayer to investigate the combined effect of degree of anisotropy and orientation of compression direction on the structures that form when compression normal to layering occurs. A stack of lubricated plasticine layers were compressed normal to the layering in a box with hand-operated pistons. They produced interlocking pinch-and-swell structures and normal kink bands (fig.1.28-a).

From their experimental results and theoretical analysis, which will be discussed in section 1.51, Cobbold et al. (1971) concluded that in an anisotropic continuum compressed normal or at high angle to the layering the degree of anisotropy plays an important role in determining the types of structure that may form. Low degree of anisotropy produces interlocking pinch-and-swell structures (internal boudins) and in a high degree of anisotropy normal kink bands are formed.

Following Cobbold et al. (1971), Woldekidan (1975) produced similar structures by compressing a stack of lubricated layers of plasticine (models with and without competence contrast) normal to the layering. In most of the models with a competence contrast (fig. 1.28-c) tension fractures appeared first in the competent individual layers, followed by high angled ( $2\theta \ll 90^\circ$ ) shear fractures which cut across many of the layers. The few interlocking pinch-and-swell structures that formed were destroyed as the shear fractures propagated and became 'shear zones.' Similar structures were formed in the models without competence contrast between adjacent layers (fig. 1.28-b). In these models, however, only a few isolated individual layers (fig. 1.28-b(i)) were ruptured (after necking) by tension fracture. This occurred as the discrete shear fracture appeared. Many of the major shear fractures which cut across many of the layers became 'shear zones' after about 25-30% shortening.

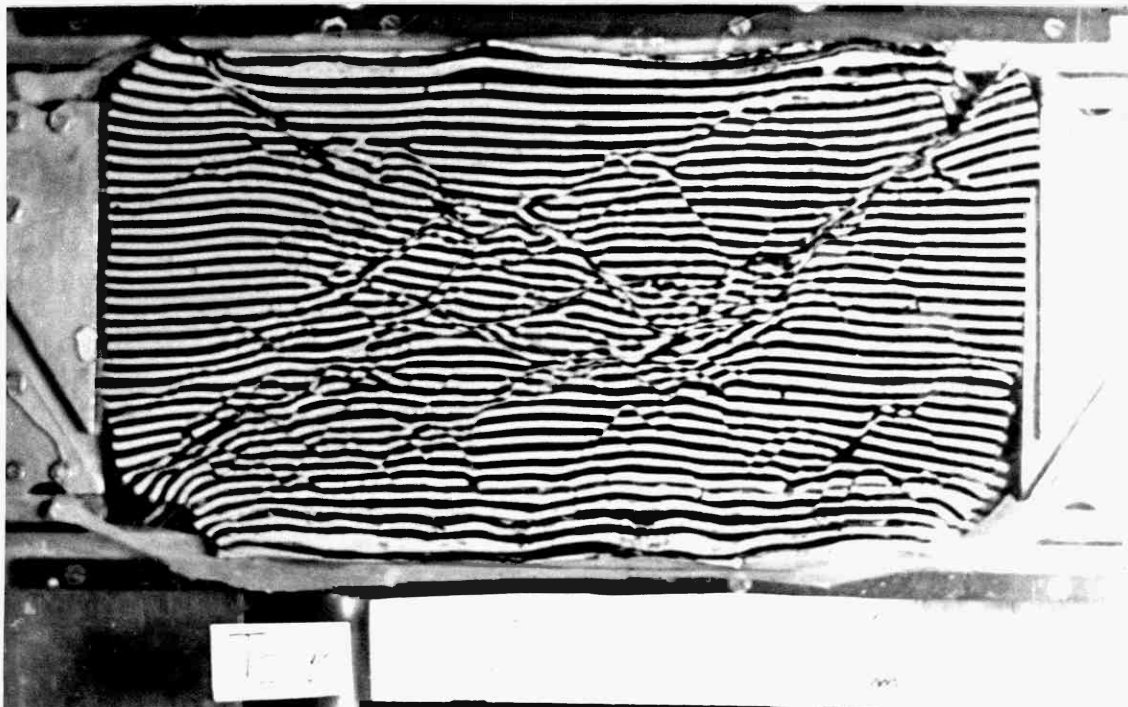
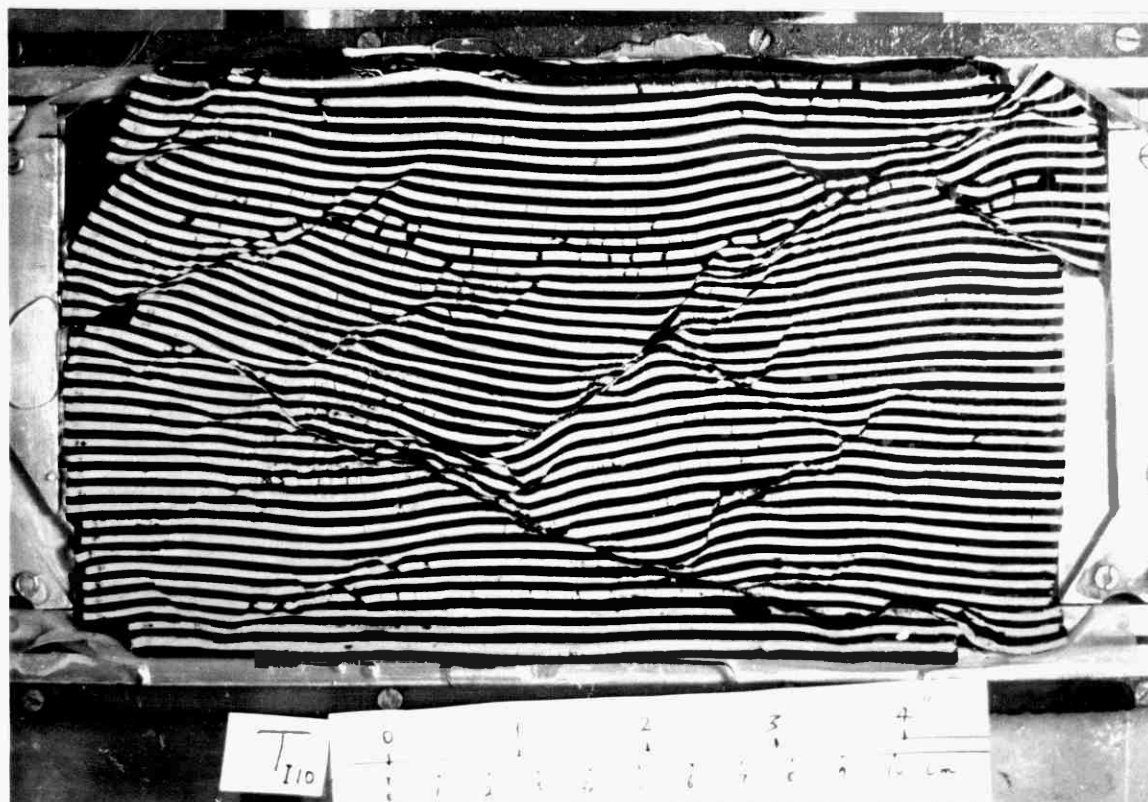


Fig. 1.28-b Shear fractures, shear zones and normal kink bands developed in a model consisting of identical layers compressed normal to the layering.

Fig. 1.28-c Similar structures develop in a model made up of relatively competent (light) and incompetent (dark) layers. Note in this case the competent layers have ruptured by tension fractures. Note also the conjugate sets of shear zones and kink bands give the appearance of interlocking pinch-and-swell.



### 1.3 THEORETICAL ( WORK ON SINGLE LAYER BOUDINAGE)

Ever since Lohest (1909) introduced the term 'boudin' many authors have tried to give an adequate explanation or theory for the development of boudinaged structures. Lohest established that the segments or boudins were originally portions of the entire quartzite bed. He also confirmed that the quartz veins that filled the gaps between the boudins were of secondary origin not primarily diagenetic structures as had been suggested by Renard (1909).

Quirk (1923) ascribed the barrel-shaped boudins to compression parallel to the bedding plane and the modification of their form by elastic reaction to release of load. Quirk's idea was rejected by Wegmann (1932) and Corin (1932). Wegmann shows how the barrel-shaped boudins may be deformed into entirely disconnected lenticular 'pebbles' in extremely mobile areas (fig. 1.29-a). They agree that the formation of boudinage is due to stretching or elongation of a competent between incompetent beds. Cloos (1947) elaborates on the ideas of Wegmann and Corin but basically agrees with them.

Most geologists now agree that boudinage structures are produced during compression normal or at a high angle to rock layering. Furthermore, according to Stromgard (1973) most geologists agree with Ramberg (1955), that compensating elongation parallel to layering causes competent layers to break into segments or boudins and that boudins gradually separate during progressive deformation (fig. 1.29-b).

Goguel (1946) first applied mechanical principles to the problem of boudinage. From geological observation he decided that the 'plastic' flow of weaker members of a geological sequence controlled the deformation of the whole sequence, including markedly stronger layers. He used Prandtl's solution for the 'plastic' flow between two appressed rigid

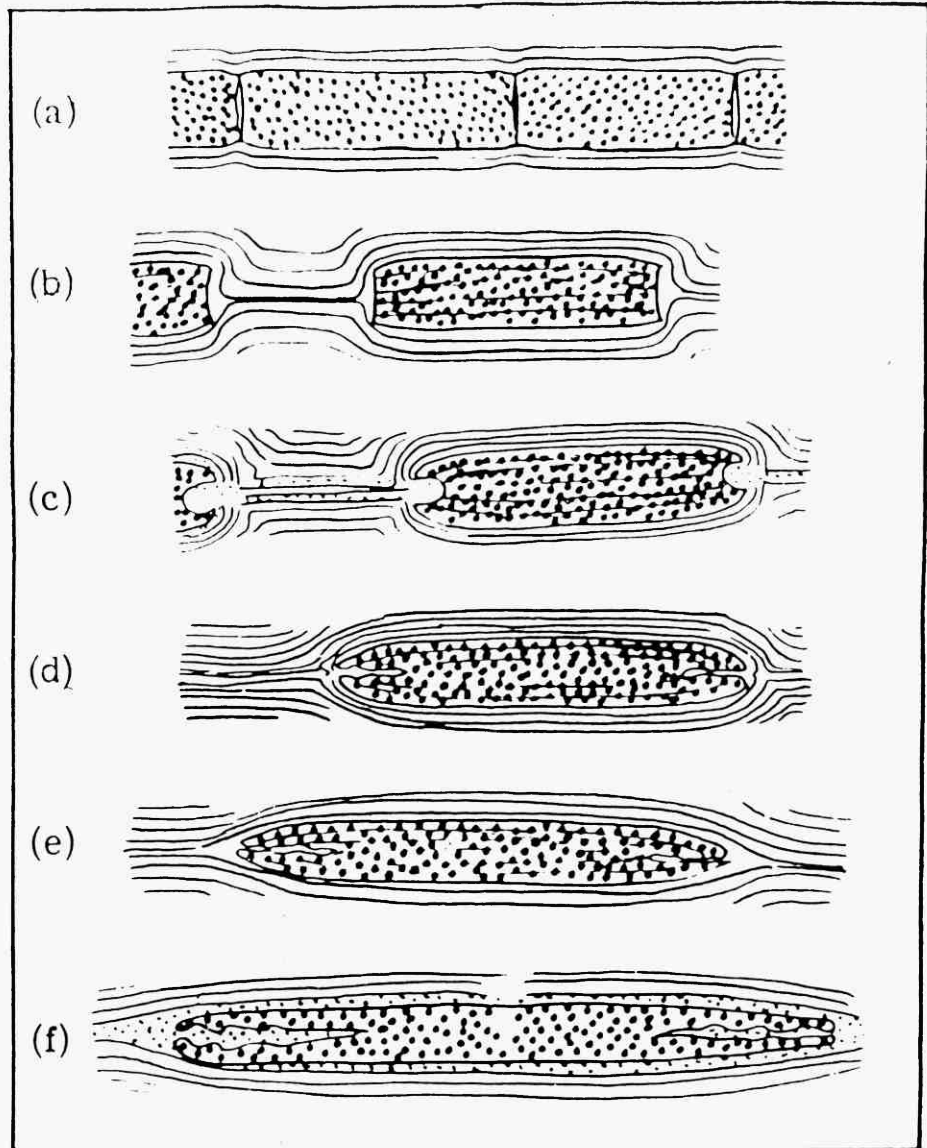


Fig. 1.29-a Boudinage after WEGMANN [1932]: (a) Classical stage (Lohest, Read); (b) Beds of differing resistance; (c) Boudinage in granitized terranes; (d) The ends of (c) are almost entirely turned in; (e) Final stage withoung pegmatization; (f) Far advanced stage from highly mobilized terrane

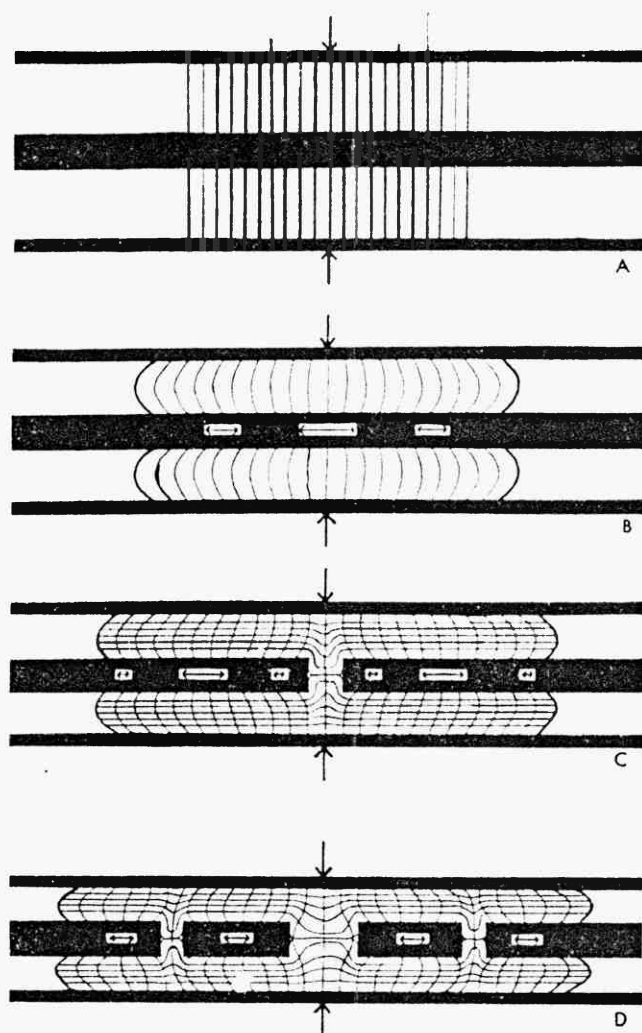


Fig. 1.29-b—Successive steps during formation of boudinage structures. *A*, state prior to compression. The black layer in the middle is the competent body on either side of which incompetent bodies exist (*vertically lined regions*). Compressive stress is transmitted by means of two stiff sheets (*black*). *B*, compression has started, the plastic flowage in the incompetent layers is indicated by the distortion of the originally vertical lines. Arrows in the competent black layer indicate tensile stress. *C*, a more advanced step than *B*. Competent layer is now ruptured in the middle where tension was greatest. The network in the incompetent layer indicates pattern of flowage. This network is not a further evolution of the deformed network in *B*, but rather the evolution of an imaginary rectangular network not shown in *B*. Horizontal arrows show tensile stresses in the competent layer. *D*, a stage more advanced than *C*. Competent layer has ruptured at two new places. The pattern of the network indicates plastic flowage in the incompetent layers during evolution from *C* to *D*. Again, the deformed network in *D* is supposed to have developed from a rectangular imaginary network not shown in *C*. (after Ramberg, 1955, and reviewed by Sowers, 1973).



platens to obtain the displacement and flow velocity fields that might develop in the 'plastic' layers. The large blocks of adjacent layers were supposed to assume the role of the rigid platens of Prandtl's model that were displaced towards one another in a direction normal to bedding with uniform velocity and displacement. The stronger layer was acted on by tensile stress produced by the shear forces at the interfaces. These interfacial forces were supposed to be caused by viscous flow of the weak material, and were calculated from well-known formulas for viscous drag. By calculating strain energy Goguel was able to calculate the lengths of boudins that would form.

In Ramberg's (1955) mathematical study of boudinage he assumed (1) the deformation of the incompetent rock layers occurred by viscous flow and (2) the competent layer deformed elastically before rupture. Based on these assumptions Ramberg derived the following equation for extension parallel to the layer in one direction. The tensile stress in the centre of the competent layer is given by

$$S_o = - \frac{Z_i}{Z_c} (P_o - P_1) \quad (1.1)$$

where  $S_o$  = tensile stress at centre

$Z_i$  and  $Z_c$  = thickness of incompetent and competent layers respectively.

$(P_o - P_1)$  → pressure difference ( $P_o$  at centre of the block and  $P_1$  at the end).

The pressure difference during the formation of boudins can be limited by the condition

$$\frac{Z_c}{Z_i} S_s > (P_o - P_1) > \frac{1}{2} \frac{Z_c}{Z_i} S_s \text{ Kg/cm}^2 \quad (1.2)$$

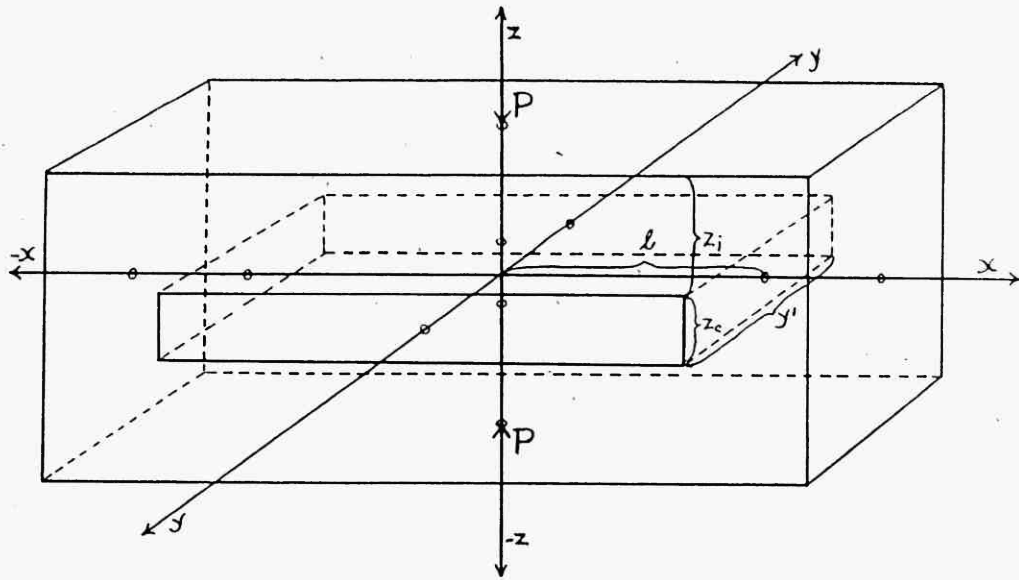


Fig. 1.29-c. A competent layer enclosed in a matrix of incompetent rock (after Ramberg, 1955).

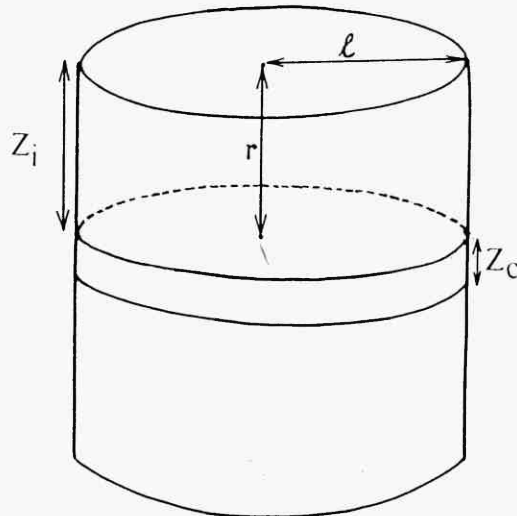


Fig. 1. 29-d. Ramberg's boudinage model with extension in more than one direction.

and the rate of compression

$$\frac{\partial Z}{\partial t} = \frac{Z_i^3}{\ell^2 6\mu} (P_0 - P_1) \quad (1.3)$$

where  $S_s$  = tensile stress

$\mu$  = viscosity coefficient of incompetent layer

$\ell$  = width of competent layer (see fig. 1.29-c)

From these three equations one can find the tensile stress in the boudin layer and rate of compression provided the pressure difference and thicknesses of layers are known. In order to determine the rate of compression it is essential to know the viscosity of the materials.

Sowers (1973), however, is critical of the assumptions made by Ramberg. He suggests that the ductile flow in Ramberg's experiments and in his own experiments is plastic rather than viscous. He points out that in the experiments of Griggs and Handin (1960) little or no viscous flow occurred, yet fractures and boudins were formed. In their specimens neither the amount of flow nor the flow field matches that required by Ramberg's viscous flow model. Ramberg's assumption that the 'platens' remain straight and rigid up to the moment of necking is not always valid in natural rock deformation. Sowers accepts the quantitative relations developed by Ramberg but considers that the simple viscous model leads to large errors when calculating the viscous drag forces. If natural flow is indeed viscous it is very slow and the coefficient of viscosity is very large. Therefore, the drag forces, calculated by Ramberg become unrealistic for thick viscous layers.

Ramberg arrives at the following stress equations applicable to a boudinage model with extension in more than one direction (fig. 1.27-d).

$$\sigma_n = \frac{1}{8} (3 + m)^2 \frac{Z_i (P_0 - P_1)}{Z_c \ell^2} (\ell^2 - r^2) \quad (1.4)$$

and

$$\tau = \frac{1}{4} \frac{Z_i}{Z_c} \frac{(P_0 - P_1)}{\ell^2} |(3 + m)\ell^2 - (1 + 3m)r^2| \quad (1.5)$$

where  $r$  = distance from centre (of cylinder)

$\ell$  = radius of circular disc

$m$  = Poisson's ratio of competent layer

$Z_c$  = thickness of competent layer

$Z_i$  = thickness of incompetent layer

$\sigma_n$  and  $\tau$  = radial and tangential tensile stresses respectively.

According to equations (1.4) and (1.5) one would expect radial fissures to form first, originating in the centre and spreading to the circumference. This did not generally occur in Ramberg's experiments, probably because the analysis is based on the assumption that the materials are perfectly homogeneous and elastic and are unable to yield plastically. Release of stress by plastic yielding of the competent sheet during the deformation would inhibit the formation of the radial fissures.

Sowers (1973) reviewed the quantitative theoretical work on fracture spacing and boudinage of both metallurgical work done on rods and experiments performed on rocks.

Based on the theory of incremental deformation of Biot (1965) he

developed a theory that explains fracture spacing without requiring large viscous flow. His theory provides a simple way of understanding the role of initial tension and anisotropy in the physics of the deformation of layers. Sowers' approach in developing an explanation to fracture spacing differs from previous theories of Ramberg (1955) and Belousov (1964) in the following ways.

(1) A variation is made in the shape of the entire competent layer (as opposed to the variation of a diameter of a rod.)

(2) Instability is introduced by means of a sinusoidal perturbation of the interfacial forces. Such perturbances may result in various unstable configurations similar to those which Biot (1965) has described in buckling (both single layer and internal) where the shape of the 'brittle' layer changes while the outer margins of thick embedding ductile layers do not change. Under other conditions the outer layers may change into shapes that are concentric to the inner ones. Another possibility which Biot points out is that the interfaces become unstable and wrinkle into folds that die out exponentially away from the interface.

In adopting Biot's (1965) theory of internal instability Sowers assumed that if the layers are thin relative to their length the layered material may be considered to approximate to a continuous anisotropic material. The basic theory is greatly simplified by using this assumption, but as shown by Biot (1965, p. 216), it is not a necessary one. The other assumption is that the material has orthotropic or orthorhombic symmetry, one axis of symmetry is normal to 'bedding' and the others lie in the bedding plane.

Biot (1965, pp. 182-259) has discussed buckling of layered media. The general theory of tensional instability that was developed by Sowers (1973) is substantially the same although the difference in sign of the

axial pre-stress alters the effect of moduli in some important relationships which determine stability. Internal instability occurs in either anisotropic or layered media, in the latter case layers must be alternatively elastically hard and soft but not of too large contrast.

The case considered by Sowers is that of plane strain deformation in which the ends of the layers are subjected to uniform tensile stress. The upper and lower surfaces are confined between effectively rigid walls but are in perfectly free contact with them (Fig. 1.30A,B). For further simplification Biot assumes homogeneity and incompressibility of the entire domain. Individual layers may be either isotropic or orthotropic. Instability develops if the material is anisotropic to incremental stresses even if it is isotropic to prestress.

Based on the above assumptions and considerations Sowers arrived at the following equations:-

$$\left(Q + \frac{T}{2}\right) \frac{\partial^4 \phi}{\partial x^4} + 2(2N - Q) \frac{\partial^4 \phi}{\partial x^2 \partial y^2} + \left(Q - \frac{T}{2}\right) \frac{\partial^4 \phi}{\partial y^4} = 0 \quad (1.6)$$

where  $N$  and  $Q$  are the normal & shear elastic moduli for anisotropic materials;  $T$  is the tensile stress and  $\phi$  is the displacement function that describes permitted deformation. It is defined as follows:-

$$u = \frac{\partial \phi}{\partial y}, \quad v = \frac{\partial \phi}{\partial x}$$

This equation can be solved for  $\phi$  to get a complete elastic solution, as Biot notes, the characteristic equation then becomes

$$\xi^4 + 2m\xi^2 + k^2 = 0 \quad (1.7)$$

where  $\xi$  is the ratio of wave length in the  $x$  and  $y$  direction respectively.

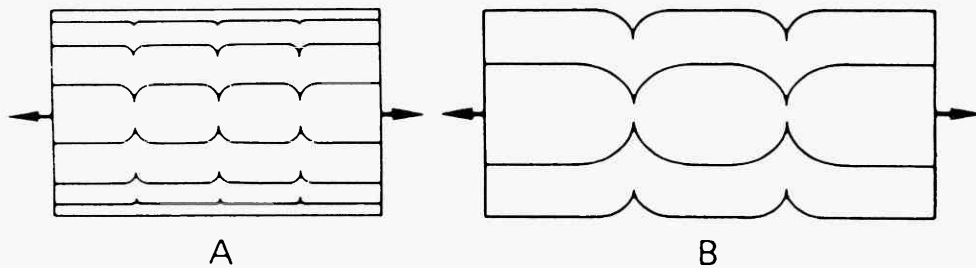


Fig. 1.30 A. Internal instability of layered media. Under action of external tension outer margins of rectangular domain are deformed to produce longer, narrower rectangular body shown. Inside the body the central stiff layer has deformed into a pinch and swell structure because of the growth of a sinusoidal perturbation. B. Necking instability of entire domain. Top and bottom soft layer as well as inner stiff layers are deformed. (after Sowers, 1973).

$$m = \frac{2N - Q}{Q - \frac{T}{2}}, \quad k^2 = \frac{Q + \frac{T}{2}}{Q - \frac{T}{2}}$$

Roots of this equation are:

$$\xi = -m \pm \sqrt{m^2 - k^2}$$

Real roots of  $\xi$  occur when

(case 1)  $m > 0$ ,  $k < 0$  or equivalently  $T > 2Q$ ,  $Q > 2N$

(case 2)  $m < 0$ ,  $m^2 > k^2 > 0$  or equivalently  $T < 2Q$ ,  $Q > 2N$  and  $|2N - Q| > |Q - \frac{T}{2}|$ .

Case 1 occurs only if the brittle, higher modulus layer is much thinner than the embedding medium, otherwise the applied tension would exceed the strength of the material before onset of instability.

Case 2 may give rise to 'shear instability', related probably to the development of ductile fracture in necked rods.

Unstable solutions occur in a stretched anisotropic domain when tension along layers exceeds a certain critical value. For this condition to occur in nature the material must have the strength to support the required critical applied stress; otherwise unstable stress conditions will never come into existence before fracture occurs.

Biot (1965) considered another solution to equation (1.6)

$$\phi = \frac{f(y)}{\ell^2} \sin \ell x \quad \text{for what he called surface instability.}$$

$$\frac{\partial^4 f}{\partial y^4} - 2m \frac{\partial^2 f}{\partial y^2} + k^2 f = 0 \quad (1.8a)$$

where  $\ell$  = wave number.

This equation has solutions of the type

$$f = \exp^{\beta \ell y} \quad \text{where } \beta \text{ is the solution of the characteristic equation}$$

$$\beta^4 - 2m\beta^2 + k^2 = 0 \quad (1.8b)$$

If  $\beta$  were equal to  $i\xi$  equation (1.8b) would be equal to equation (1.7) except for the sign of the second term.

With  $f = C_1 e^{\beta i \ell y}$  and for the condition  $f = 0$  when  $y = -\infty$ , unstable solutions occur if

$$\text{(case 1) } T < 2Q \text{ or } m > 0;$$

$$Q < 2N \text{ or } K^2 > 0$$

$$\text{(case 2) } T > 2Q \text{ or } m < 0$$

$$m^2 < k^2 < 0 \text{ or } Q < 2N$$

$$|2N - Q| < |Q - \frac{T}{2}|$$

These are exactly the conditions excluded from internal instability. Case 1 should occur easily and frequently in nature but would not affect thick layers because the stress dies out exponentially away from the interface. Surface instability is favoured by low ratios of  $N:Q$  or in deformations where large normal strains occur relative to shear strain.



$$\text{Assume } f = C_1 \cosh \beta_1 \lambda_y + C_2 \cosh \beta_2 \lambda_y \sin \lambda x \quad (1.8c)$$

where  $\beta$  is a solution for the characteristic equation (1.8b).

If different boundary conditions are chosen from those for internal instability then different structures may result. For example, if deflection of the layer boundaries are permitted layer instability (fig. 1.30-B) may develop. Layer instability occurs for the same conditions of  $T$ ,  $Q$  and  $N$  as for surface instability. In this case the solution does not contain the exponential decay term in  $y$ , and the entire layered sequence becomes unstable, the rectangular outer form changing to pinch-and-swell shape.

As yet  $N$ ,  $Q$  and other moduli have not been measured for rocks under tension. This difficulty limits the use of these theoretical methods and precludes the likelihood of obtaining a closed form solution in this way, hence Sowers (1973) turns to strain energy methods.

### Strain Energy Methods

Sowers (1973) reviewed Biot's (1965) general strain energy methods of incremental deformations and applied it to the problem of fracture spacing. Biot equation for the total incremental strain energy per unit area,  $\Delta V$ , within the domain is

$$\Delta V = 2Me_{xx}^2 + 2Le_{xy}^2 + \frac{T}{2} \left( \frac{\partial v}{\partial x} \right)^2 \quad (1.9a)$$

where  $T$  is the tension ( $S_{11} - S_{22}$ ),  $M$  and  $L$  are moduli ( $M = \frac{N-T}{4}$ ,  $L$ , the slide modulus, is  $\frac{Q-T}{2}$ ) and  $e$  is strain. Equation (1.9a) states that the incremental strain energy (related to incremental stresses) and the work done by the tension in lengthening the body equal the total incremental strain energy.

According to Sowers the total incremental strain energy potential for the entire body is obtained by integrating  $\Delta V$  over the entire area (which is of unit thickness). Because this general equation (1.9a) for potential energy expresses the instability condition, its solutions provide the stress field needed to locate the high stress concentrations believed to localize fracture.

Using sinusoidal displacement fields in  $\Delta V$ , following Biot (1965, p.204) the characteristic equation for internal instability can be obtained

$$L\xi^4 + 2(2M-L)\xi^2 + L + T = 0 \quad (1.9b)$$

which is identical to equation (1.7).

According to Sowers equation (1.9b) identifies the variational principle with the internal instability condition.

After Sowers had analysed the possible development of fracture in an anisotropic material using Biot's (1965) general strain energy methods, he turned to the classical strain energy methods to test this hypothesis and developed a fracture spacing theory independent of the more exact theory of

Biot. This is outlined below.

The incremental strain energy stored in a system ( $\Delta V$ ) is equal to the work done by the external forces for the incremental deformation ( $\Delta W$ ) (Timoshenko and Goodier, 1970).

$$\Delta V - \Delta W = 0 \quad (1.10a)$$

Both  $\Delta V$  and  $\Delta W$  must be calculated to use this principle (1.10a). This equation can be used to find the critical tension,  $T$ , for elastic instability.

Sowers (1972) considered a three-layer sandwich in which the stiffer layer is embedded between two less competent layers (fig.1.30-c).

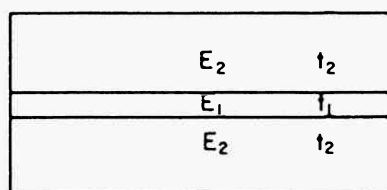


Fig.1.30c. Layered domain for which theory has been developed.  $E_1 > E_2$ ,  $t_1 \ll t_2$ . The central layer is the stiffer one.

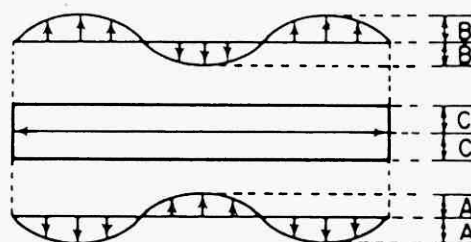


Fig.1.30d. Load distribution on stiffer layer.

(after Sowers, 1973)

He calculated the strain energy associated with deformations caused by assuming sinusoidally distributed stresses on the surface of the stiffer layer (fig. 1.30d). The second order part of the incremental strain energy for an element of the beam (stiffer layer) is given by Timoshenko and Goodier (1970) as

$$\Delta V = \frac{1}{2E} (\sigma_x^2 + \sigma_y^2) - \left( \frac{\mu}{E} \sigma_x \sigma_y + \frac{1}{2G} \tau_{xy}^2 \right) \quad (1.10b)$$

and the total incremental strain energy for the domain as a whole is

$$V = \int_0^l \int_0^c \left\{ \frac{1}{2E} (\sigma_x^2 + \sigma_y^2) - \frac{\mu}{E} \sigma_x \sigma_y + \frac{1}{2G} \tau_{xy}^2 \right\} d_x d_y \quad (1.10c)$$

where  $\ell$  is the length of the layer,  $c$  is constant.

The layer is loaded on top and bottom surfaces sinusoidally (fig.1.30d) so that the boundary conditions are:-

$$y = +c; \tau_{xy} = 0; \sigma_y = -B\sin\alpha x$$

$$y = -c; \tau_{xy} = 0; \sigma_y = -A\sin\alpha x$$

The maximum amplitude of the applied forces are  $A$  and  $B$ , and  $\alpha = \frac{n\pi}{\ell}$  where  $n$  is an integer equal to the number of half waves and  $\ell$  is the length of the layer.

Stresses can be determined by using the Airy stress function  $\phi$  in the biharmonic equation

$$\phi = \sin\alpha x (c_1 \cosh\alpha y + c_2 \sinh\alpha y + c_3 y \cosh\alpha y + c_4 y \sinh\alpha y) \quad (1.10d)$$

For the embedding incompetent medium (matrix) the stored strain energy can be calculated using elastic solution obtained by Biot (1937)

$$\phi = \frac{B}{\alpha^2} \sin\alpha x e^{-\alpha y} (1 + \alpha y) \quad (1.10e)$$

Once the stress components have been determined the strain energy can be calculated using equation (1.10c).

Consider now the work done by the external forces during incremental deformation. In order to calculate the work done by the external forces Sowers assumed that the surface forces cause a sinusoidal deflection of amplitude,  $\frac{B}{E}$ , where  $E$  is the Young's modulus of the stiffer layer. By finding the change in length,  $\Delta\ell$ , of the stiffer layer by the sinusoidal surface loading and multiplying by the tension,  $T$ , work,  $W$  can be obtained

$$W = T\Delta\ell \quad (1.11a)$$

Sowers (1973, p.41) discussed various ways of computing  $\Delta l$  and considers, after introducing several approximations that the external work,  $W$ , can be written as

$$W = \frac{\beta^2 n^2 \pi^2}{2l} T \quad (1.11b)$$

where  $n$  is the wave number and  $\beta^1$  is the amplitude of the sinusoidal perturbation.

Using equation (1.11b) to calculate the work means that all terms in the equation of virtual work depend on the square of the amplitude; therefore the equation (1.10a) becomes independent of the deflection and a critical  $T$  can be found. By varying the wave number,  $n$ , of the sinusoidal perturbation, the least value of the tension,  $T$ , for each perturbation can be computed.

#### Comparison of Theoretical and Experimental Results

Sowers calculated the fracture spacing using the strain energy methods described above and compared the calculated spacings of areas of high stress concentration (i.e. nodal points) with the spacing observed in the experiments. These comparisons are represented graphically (fig. 1.19 - 1.21). To find the number of nodes which occur at the lowest possible tension ( $T$ ), called the critical tension, he plotted  $T$  against nodal points ( $n$ ) for various layer thicknesses (fig. 1.19-A). The curve for each thickness represents the boundary for the stability of the rectangular form of the competent layer at that thickness.

By plotting tension against number of nodes (fracture sites) at various layer thickness for only normal surface forces (fig. 1.19-B) and for only shear forces on interfacial surface (fig. 1.20-A), the physical nature of the instability is brought out. In the first graph (fig. 1.19B) the number of nodes increases nearly linearly with tension, but in the latter ones (fig. 1.19-A) the nodes are inversely related to the tension.

These results show generally that nodal points (fracture sites) are

more frequent in thin layers than in thick ones, other things being equal. This relationship is not linear in models. In calculated tensions shown on Figs. 1.19-A and 1.20-B, critical tension in thin layers are higher than in thick. Fig. 1.20-B shows comparison of critical values of tension calculated from the theory and those measured in the experiments. Although off-set from one another the theoretical curve and the experiment derived curve are parallel and the difference between theoretical and experimental results is not large.

The critical tension values calculated from the three-layer model and those obtained for the stiff layer alone is shown in fig. 1.20-B. The figure shows the effect of interfacial slip on the development of instability. It is clear that shear stress plays an important role in the formation of the instability. As shown on Fig. 1.21-A, which is a plot of tension against thickness for various constant number of nodes ( $n$ ) for both welded and frictionless contacts, the tension on the unwelded interfaces is nearly uniform for all 'nodal points', which contrasts sharply with the variation in tension on welded interfaces. This compares well with experimental results. In experiments with lubricated interfaces, that is, experiments in which negligible shear stress can develop along the interface either one fracture occurs at the centre of the layer or none form. It is concluded that a single centrally located stress concentration develops and remains stable as the load increases.

From his computation Sowers (1973) found that the effects of the variation of thickness of the embedding layers are most important in thin layers. For example, the critical tension for a 5mm layer sandwiched between two 5mm layers is about half the value of that for two 50mm layers. This is because as the stress dies out exponentially away from the interface in the embedding medium, effects of thickness are most important in thin layers.

As shown in fig. 1.21-B the elastic strain energy fracture spacing

theory does not seem to describe fracture spacing developed experimentally in clay. This is because clay is not an elastic material.

From the study of the dependence of critical stress and fracture spacing on the ratio of moduli of the two materials, Sowers (1973) concluded fractures are more widely spaced for large competence contrast in material.

Smith (1975) pointed out the disadvantages of the Euler beam buckling theory in the analytical study of folding in layered rocks; (1) it is limited to long wavelengths and hence a large viscosity ratio; (2) it obscures the driving mechanism of the instability; (3) it fails to describe structures such as boudinage. Smith turned to the methods of linear hydrodynamic stability theory. The approach is as follows:- (a) A basic flow is found that is a possible state of motion for the mechanical system. This basic flow is represented by an exact solution to the governing equations and boundary conditions. (b) It is then determined whether the basic flow is a stable or unstable state of motion. If small disturbance (which are always present in practice) grow, the basic state becomes unstable. A flow is stable if all disturbances decay, leaving the system in its basic state of flow. In the case of amplifying disturbances the basic flow cannot exist for long and will not be found in nature. The flow associated with the disturbance will eventually dominate.

In his mathematical study of folding, boudinage and mullion formation, Smith (1975) made the following physical assumptions:

- (1) The materials are assumed to be Newtonian, incompressible, homogeneous, and isotropic, that is, shear dependent viscosity, normal stress effects, and elasticity are not considered.
- (2) The geometry analysed is the simplest that retains the phenomena of folding and boudinage.
- (3) The background applied stress must be planar, with principal directions either perpendicular to or parallel to the bed.
- (4) The perturbation velocities and interface deflections are assumed to be small. The analysis is meant to describe only the early stages of growth of an instability.



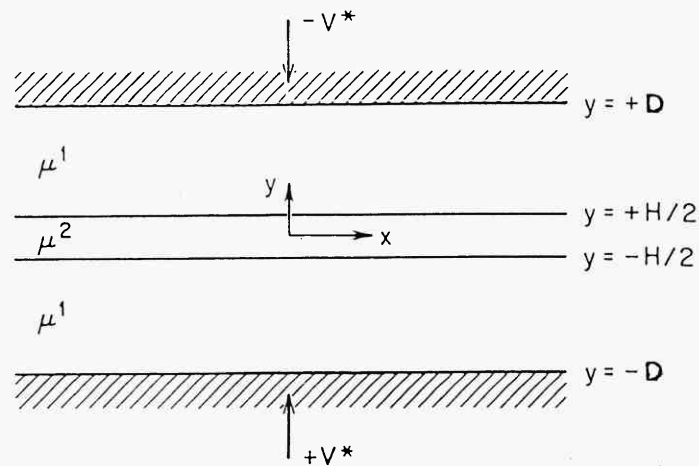


Fig. 1.31-A. Diagram of model problem, showing a thin layer between two thick layers of different material, all squeezing out from between two smooth rigid plates slowly moving together.

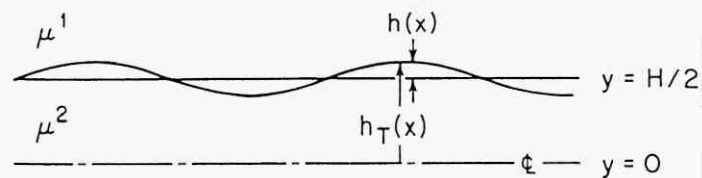


Fig. 1.31-B. Diagram illustrating nomenclature used for describing interface position.  $H/2$  is distance from middle of layer to mean interface position;  $h(x)$  is local displacement of interface from its mean position.

Referring to Fig. 1.31-B, the interface position  $h_T$  can be represented as  $h_T = H/2 + h(x)$  (1.12)

The rate of change of the interface position can be written in terms of the velocity field:-

$$\frac{\partial h_T}{\partial t} = \left[ -u \frac{\partial h_T}{\partial x} + v \right]_{y=h_T} \quad (1.13)$$

Now if the velocity field is represented as the sum of the basic flow plus a small disturbance  $\tilde{u}$  and  $\tilde{v}$ ,

$$\begin{aligned} u &= U + \tilde{u} \\ v &= V + \tilde{v} \end{aligned} \quad (1.14)$$

where  $u$  is the velocity parallel to  $x$

$v$  is the velocity parallel to  $y$

The strain in the  $x$  and  $y$  direction is obtained by differentiating  $u$  and  $v$ ,  $x$  and  $y$

$$\begin{aligned} U' &= \frac{dU}{dx} = \frac{V^*}{D} \\ V' &= \frac{dV}{dy} = \frac{V^*}{D} \end{aligned} \quad (1.15)$$

where  $U = U'x$  and  $V = V'y$

Substituting equation (1.12), (1.14) and (1.15) into (1.13)

Using the above assumptions Smith arrived at the following equation:-

$$\frac{\partial H/2}{\partial t} + \frac{\partial h}{\partial t} = V'H/2 - \underbrace{U'x \frac{\partial h}{\partial x} + V'h}_{\text{kinematic distortion}} - \underbrace{\left[ \tilde{u} \frac{\partial h}{\partial x} + \tilde{v} \right]}_{\text{dynamic distortion}} \Big|_{H/2+h(x)} \quad (1.16)$$

Considering only the dynamic distortion Smith arrived at the following equation:-

$$E = \frac{1}{R} \frac{\partial U}{\partial x} (m - 1) \quad (1.17)$$

where  $E = \frac{1}{a} \cdot \frac{da}{dt}$  i.e. the growing rate of the amplitude ( $a$ ) for a particular sinusoidal disturbance on the interface.

$$R = + \frac{1}{4} (\Delta T_{11} / \mu' E) \quad T_{11} = \text{stress difference (tension)}$$

$$m = \mu_2 / \mu_1$$

When the thin layer has a larger viscosity than the surroundings (i.e.  $m > 1$ ), and the compression is perpendicular to the bed ( $\partial U / \partial x > 0$ ); the conditions are those normally associated with boudinage.

The growth rate of the disturbances can be simplified by defining the normalized growth rate as

$$\epsilon(\beta, m) \equiv E(\beta, m) / \frac{\partial U}{\partial x} = \frac{1}{R(\beta, m)} |m - 1| \quad (1.18)$$

where  $\beta =$  wave number,  $m = \frac{\mu_2}{\mu_1}$

This function (1.18) has an extremum(maximum)  $\epsilon_m$  at  $\beta_m$  for each  $m$ , (fig. 1.31-C). It is the disturbance of this wave number,  $\beta_m$ , that will grow most rapidly and eventually dominate the flow. The value  $m$  is directly related to the dominant wavelength  $\lambda_m = \frac{H\pi}{\beta_m}$

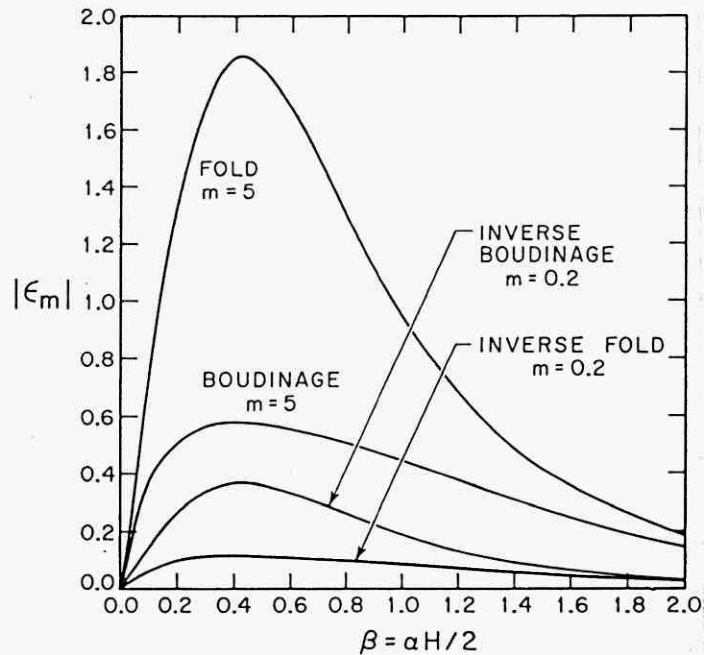


Fig. 1.31-C. Plot of normalized dynamic growth rate (see equation 1.18) versus nondimensional disturbance wavenumber. Curves shown are those for which one material is five times as viscous as the other. These growth rates are result of secondary flow only, not basic flow. (after Smith, 1975).

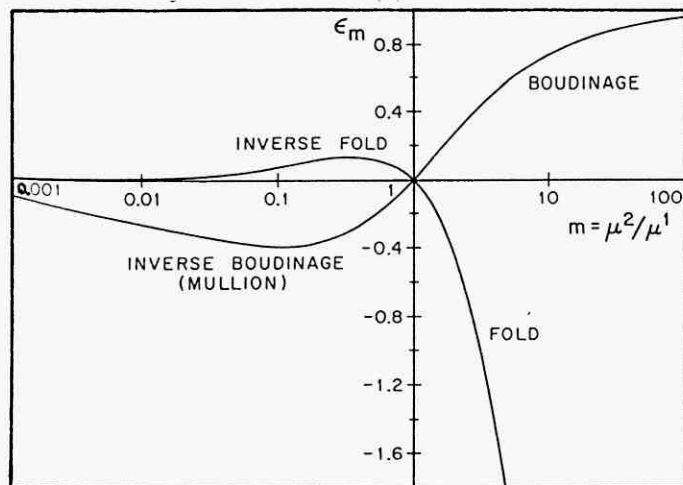


Figure 1.31-D. Plot of maximum normalized dynamic growth rate versus viscosity ratio. These growth rates are result of secondary flow only. (after Smith, 1975).

The maximum growth rate at each  $m$  is plotted in Fig. 1.31-D.

According to Smith (1975) the sign of  $\Delta T_{11}$  is the crucial factor which determines whether a pinch-and-swell or foldlike disturbance grows.

The secondary flows produced by  $\Delta T_{11}$  and a wavy interface are shown in fig. 1.31-E. Note in the diagrams that the vertical velocity at the interface amplifies the existing interface shape.

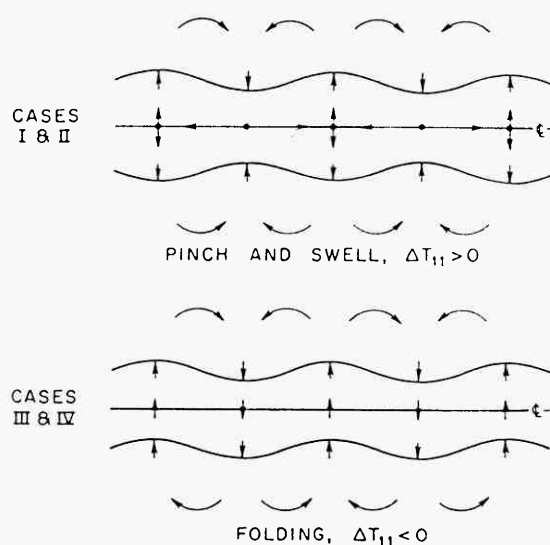


Fig. 1.31-E. Qualitative sketch of secondary flow associated with growing disturbance. Vertical velocities near interfaces are such as to further deform interface, which in turn will produce even stronger secondary flow (after Smith, 1975).

From his theoretical analysis, Smith (1975) arrived at the following conclusions. The kinematic and dynamic effects co-operate in the formation of regular folding and mullion formation, but they compete in the formation of inverse folding and pinch-and-swell structure. Therefore, for boudinage the dynamic growth rate  $\gamma_d$  is less than 1 regardless of the viscosity ratio,  $m$ . The theory predicts that the kinematic flattening of the background compression ( $\gamma_k$ ) will be  $-1$  and that the stress-induced secondary flow produces a positive normalized growth rate where  $\gamma_d < 1$ . Thus the total growth rate

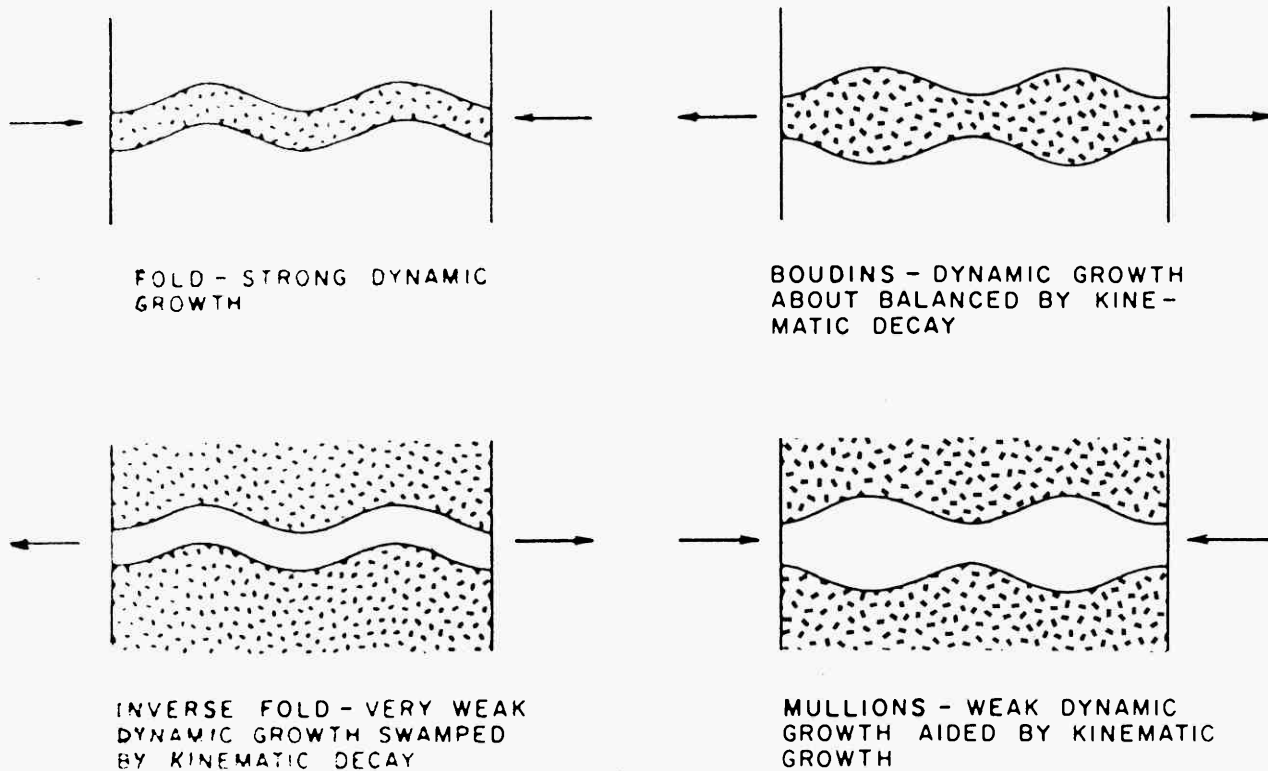


Fig. 1.32 - a. **Four cases of dynamic instability on single layer** for linear viscous materials. (after Smith, 1975)

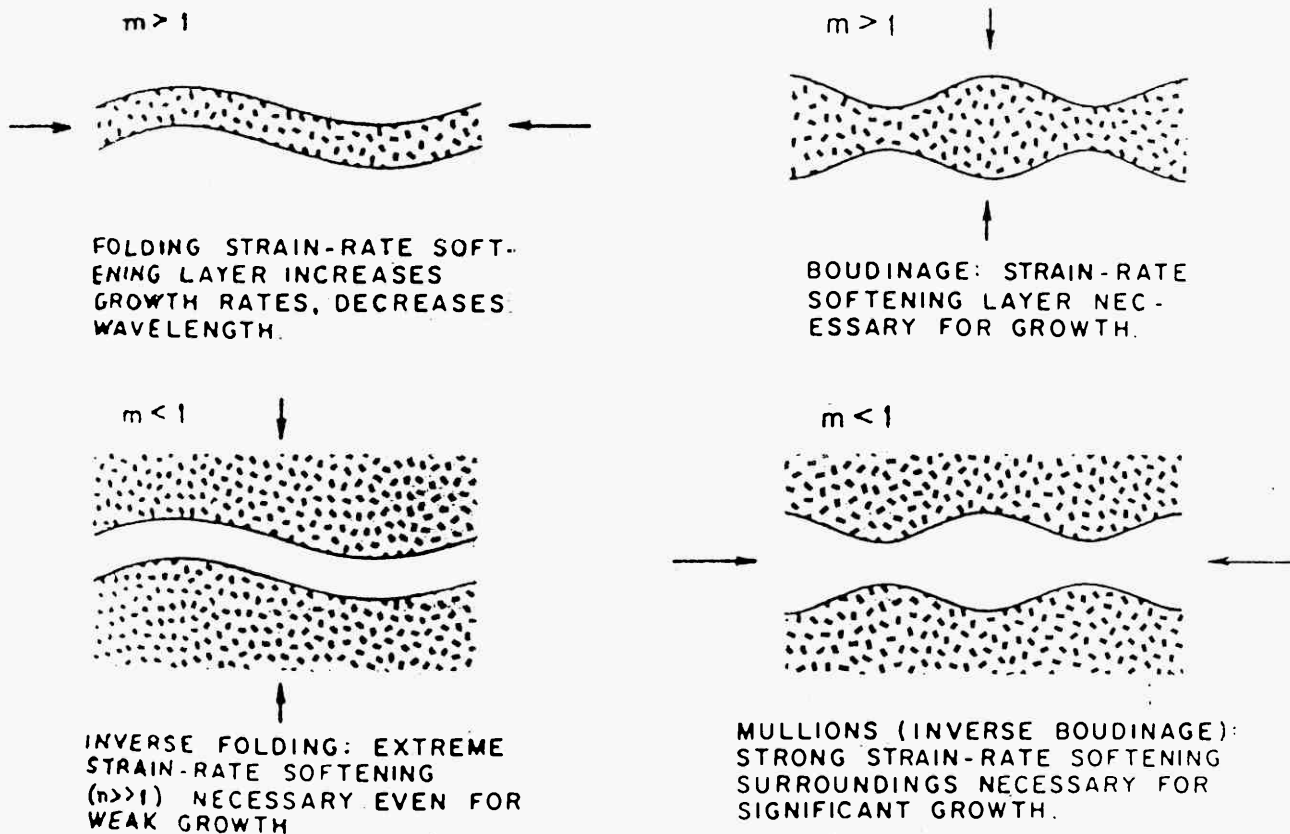


Fig. 1.32-b. Diagram summarizing the four single-layer shearing instabilities and the effect on each of the non-linear viscous (specifically strain-rate softening) behaviours.

$\gamma = \gamma_k + \gamma_d$  is always negative. This means that although the disturbance amplitude may grow relative to the layer thickness (which is decreasing), it will decay in absolute terms. It follows then that pinch-and-swell structure will not grow in absolute terms in a linear viscous (Newtonian) material. Although the theory may have the correct qualitative description of the growth mechanism (fig. 1.32-a) it does not provide adequate explanation for the observed pinch-and-swell structures.

As mentioned above Smith's (1975) analysis of pinch-and-swell structures formation leads to the conclusion that the growth rate of boudins in linear viscous materials will be very slow. He subsequently (1977) extended the analysis to incorporate non-linear viscous materials (fig. 1.33-a).

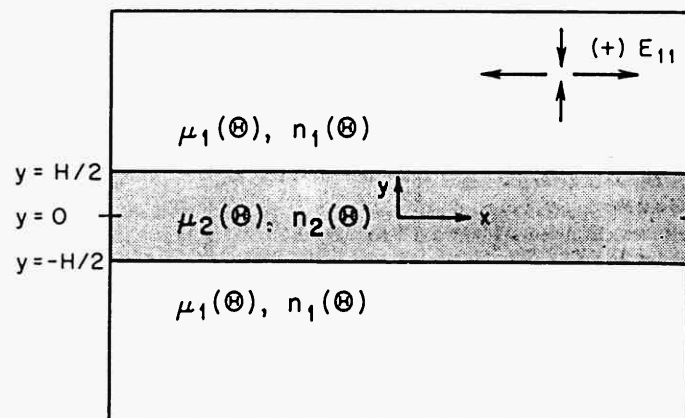


Fig. 1.33-a. Geometry and dimensions of the single layer non-linear viscous system. Also shown the positive sense for the basic strain rate ( $E_{11}$ ). (drawn from Smith, 1977).

One type of non-linear viscous material Smith (1977) considered was a power law material. The exponent  $n$  is found to be the ratio of two viscosities  $\mu$  and  $\eta$ .

$$n = \frac{\mu}{\eta} \quad (1.19)$$

where  $\mu$  is the viscosity appropriate for basic strain rate  $E_{11}$  and perturbation simple shear and  $\eta$  is the effective viscosity for perturbation normal shear (see fig. 1.33-c). If the fluid is not a power law material,  $n$  is simply the ratio  $S_2/S_3$  at the point  $E_{11}$  in fig. 1.33-b. In this latter case,  $n$  will depend on the basic rate of strain  $E_{11}$ .

Smith obtained the following results. The dynamic growth rates of the instability  $G$  (calculated from the eigen value problem, Smith 1977, page 320) can be normalized defining the normalized growth rate  $\gamma_d$  as

$$\gamma_d \equiv \frac{G}{(\frac{1}{2})E_{11}} \quad (1.20)$$

The normalized growth rate  $\gamma_d$  is associated physically with the deformation of the interfaces by the secondary (i.e. perturbation) flow.

The normalized growth rate  $\gamma$  is obtained by adding the normalized dynamic ( $\gamma_d$ ) and kinematic ( $\gamma_k$ ) growth rates.

The total normalized growth rate is

$$\gamma = \gamma_d + \gamma_k \quad (1.21)$$

and as  $\gamma_k = -1$ ,  $\gamma = \gamma_d - 1$ .

It is found (except for strongly strain softening materials) that the family of instabilities that develops falls readily into four (see fig. 1.32) on the basis of whether the perturbation is symmetric or anti-symmetric and on whether viscosity ratio,  $m$  is greater or less than 1. That is,

$$\begin{array}{ll} m > 1 \rightarrow \gamma_d < 0 & \text{for foldlike instability} \\ m < 1 \rightarrow \gamma_d > 0 & \\ m > 1 \rightarrow \gamma_d > 0 & \text{for pinch-and-swell instability} \\ m < 1 \rightarrow \gamma_d < 0 & \text{(fig. 1.32-b).} \end{array}$$

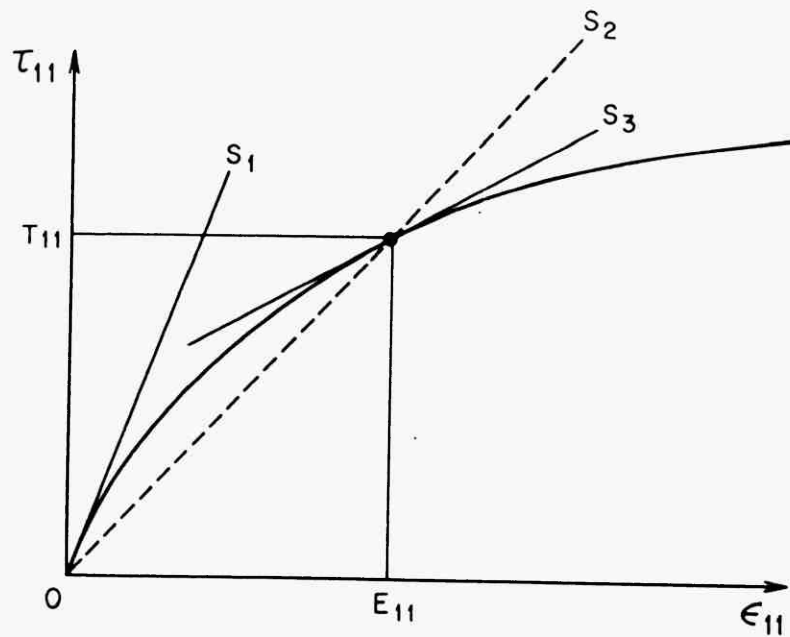


Fig. 1.33-b. Plot of normal stress versus normal strain rate for a typical strain rate softening material. The values of stress  $T_{11}$  and strain rate  $E_{11}$  that characterize the basic state are shown. Slopes  $S_1$ ,  $S_2$  and  $S_3$  represent the effective viscosity for (1) small perturbations about a state of rest, (2) small tangential strain rates about the basic state, and (3) small normal strain rates about the basic state, (drawn from Smith, 1977).

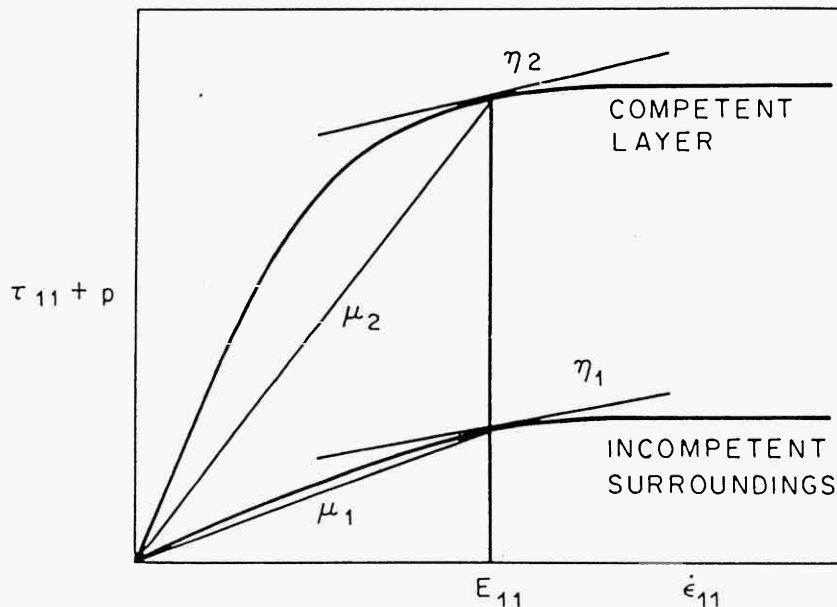


Fig. 1.33-c. Flow laws for the layer and surroundings. At the basic strain rate  $E_{11}$  two slopes (for each material) are relevant to fold initiation:  $\mu$  - the viscosity appropriate for the basic state  $E_{11}$  and perturbation simple shear, and  $\eta$  - the effective viscosity for perturbation normal shear. The ratio  $\mu/\eta \equiv n$ , is the effective power law for the material (after Smith, 1979).



Smith's (1977) theory indicates that symmetric pinch-and-swallow instability occurs when the compression is perpendicular to the bedding ( $\lambda_d > 1$ ). The growth rate has a maximum, for a particular combination of material properties (i.e.  $m$ ,  $n_1$ ,  $n_2$ ) at the dominant wavelength  $\lambda_m$  of the pinch-and-swallow structure.  $\lambda_m$  normalized relative to the layer thickness is shown in fig. 1.34-a and the corresponding maximum normalized dynamic growth rates  $\gamma_d(\lambda_m; m, n_1, n_2)$  are shown in fig. 1.34-b. Useful asymptotic expressions for the dominant wavelength ( $\lambda_m$ ) and  $\gamma_d$  ( $\lambda_m$ ) valid for large  $m$  values are

$$\frac{\lambda_m}{H} = 3.46 \frac{n_1^{1/6}}{n_2^{1/3}} m^{1/3} \quad (1.22)$$

$$\text{and } \gamma_d(\lambda_m) = n_2 \quad (1.23)$$

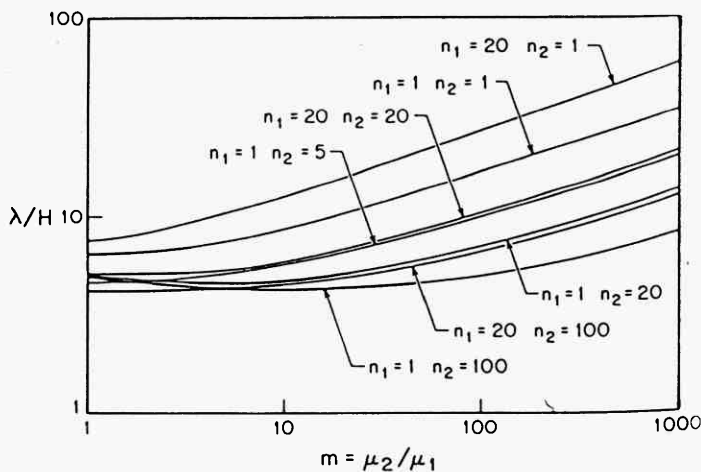


Fig. 1.34-a. Dominant normalised wavelength ( $\lambda_m/H$ ) for folding and boudinage is plotted against viscosity ratio ( $m$ ) for various values of the effective power-law exponents  $n_1$  and  $n_2$ . Only strain-rate softening materials ( $n > 1$ ) are shown (after Smith, 1977).

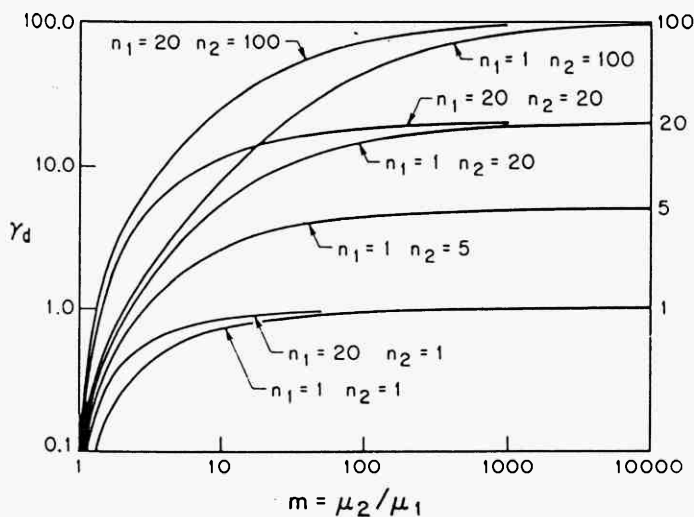


Fig. 1.34-b. Normalized dynamic growth rate ( $\gamma_d$ ) for boudinage is plotted versus viscosity ratio ( $m$ ) for various values of the exponents  $n_1$  and  $n_2$ . Only strain-rate softening materials ( $n > 1$ ) are shown. To obtain the total growth rate ( $\gamma$ ), 1.0 must

be subtracted from these  $\gamma_d$  (after Smith, 1977).

From equations (1.22) and (1.23) and figures 1.34-a and 1.34-b Smith (1977) noted the following:

1. Strain-rate softening behaviour in the layer ( $n_2 > 1$ ) decreases the dominant wavelength, whereas similar behaviour in the surroundings ( $n_1 > 1$ ) increases it. When the quantity  $n_1^{1/6}/n_2^{1/3}$  is small, the dominant wavelength is nearly independent of  $m$  ( $\lambda/H \approx 4$ ) until  $m$  is large.

2. The maximum growth rate is increased by strain-rate softening behaviour of either the layer or the surroundings or both. At large viscosity ratios, however, only  $n_2$  matters. For example, if the competent layer has an effective power-law exponent ( $n_2$ ) of 20 and  $m$  is greater than 100 or so, then  $\gamma_d \approx 20$  and  $\gamma = \gamma_d - 1 \approx 19$ . Thus every 1% extension of the layer is accompanied by 19% growth in the disturbance amplitude. Using the logarithmic relationship, eqn. (1.24) shows that

$$\ln \frac{a}{a_0} = \gamma \ln \frac{D}{D_0} \quad \text{where } a = \text{amplitude} \quad (1.24)$$

$D = \text{marker line}$

A thousandfold increase in disturbance amplitude could be caused by a  $\frac{D}{D_0} = 1.44$ , that is, a 44% stretching of the layer and its surrounding.

This example shows for a moderately non-linear viscous layer  $\gamma_d$  is large enough to overcome the kinematic decay and still provide for strong growth. In other words, the very existence of flow boudinage is evidence that the rock has behaved in a non-linear viscous way.

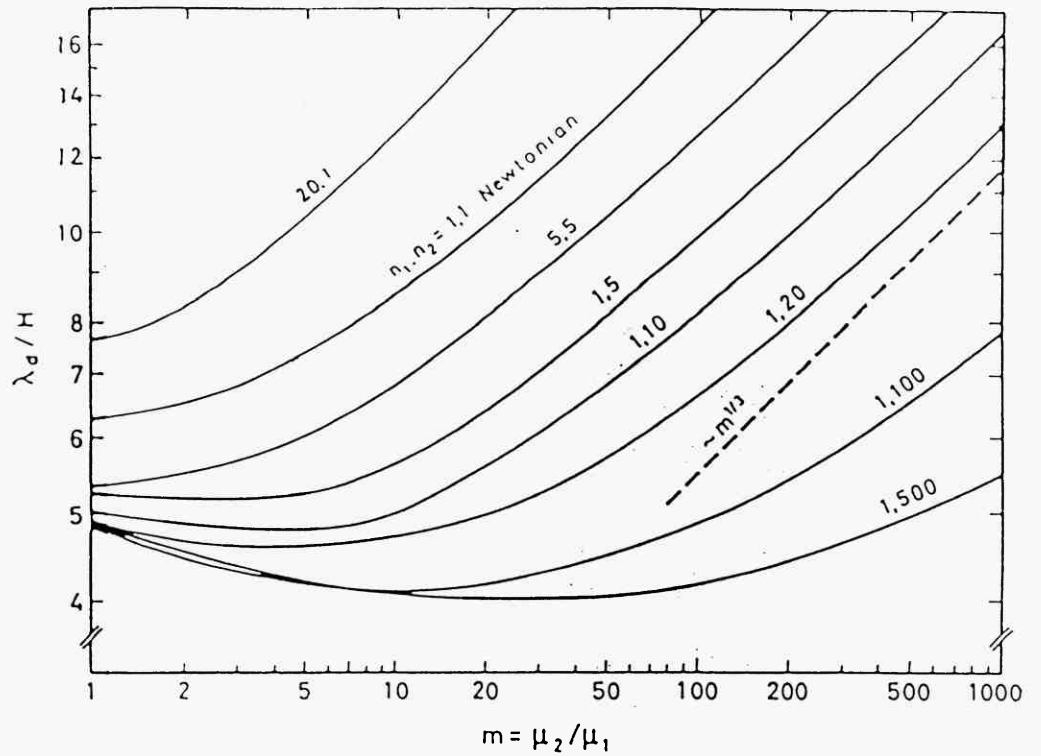


Fig. 1.34-c

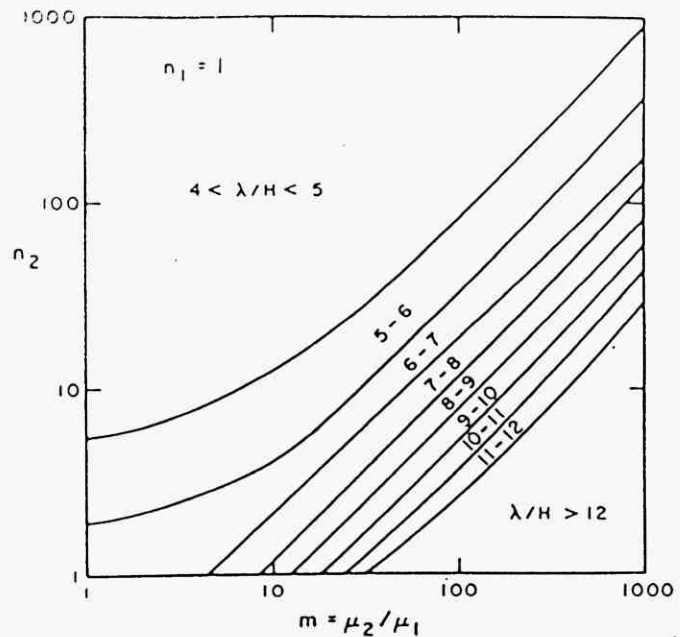


Fig. 1.34-d.

Fig. 1.34-c. The ratio of the dominant wavelength ( $\lambda_d$ ) to the layer thickness ( $H$ ) is plotted against the viscosity ratio  $m$ , for various values of  $n_1$  and  $n_2$ . At large  $m$ ,  $\lambda_d/H$  increases as  $m^{1/3}$  in agreement with classical buckling theory. When  $n_2$  is large the curves cluster between  $\lambda_d/H = 4$  and 6.

Fig. 1.34-d. The dominant wavelength data of figure 1.34-c replotted as a parameter map with  $n_1 = 1$ . The ratio  $\lambda_d/H$  resulting from any particular combination of  $m$  and  $n_2$  is indicated. When  $m > n_2$  (low and to the right)  $\lambda_d/H$  depends on the material properties in agreement with classical buckling theory while when  $n_2 > m$ ,  $\lambda_d/H$  approaches four and is nearly independent of the material properties. (after Smith, 1979).

In the strongly non-linear viscous limit the dominant wavelength ( $\lambda_d$ ) and associated growth rate for pinch-and-swell (which Smith calls boudinage) become (Smith, 1979) -

$$\frac{\lambda_d}{H} = 4; \quad \gamma = m\sqrt{n_1} \quad (1.25)$$

where  $n_1$  is the power law for the matrix. He predicts that the dominant wavelength (but not the growth rate) of folding and pinch-and-swell in strongly non-linear viscous layer units are equal. One important difference is that pinch-and-swell requires non-linear viscous behaviour for growth. A large fraction of the observed cases of flow pinch-and-swell structures should have  $4 < \frac{\lambda}{H} < 6$  (fig. 1.34, C, D).

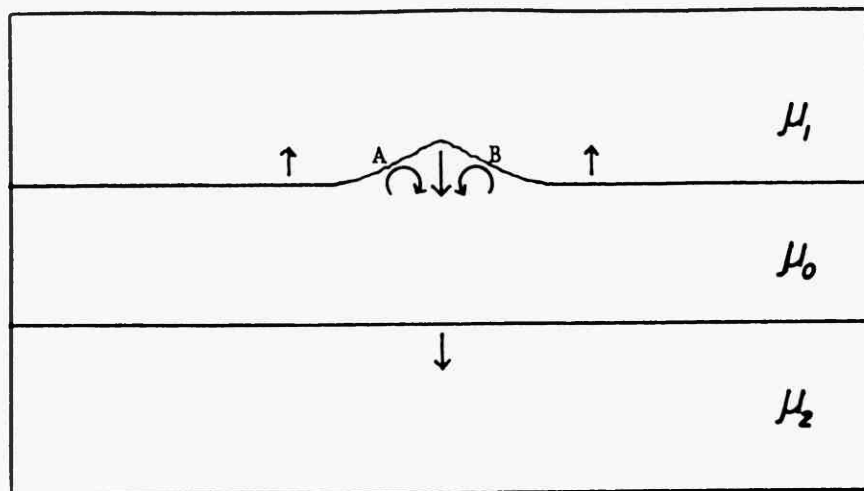


Fig.1.35-a Vorticity and velocity distributions near a small deflection on the upper interface of a more-viscous layer during extension. The vorticity in the layer is dominant. The original deflection is attenuated, and deflection geometry tends towards symmetry about the layer midplane. (after Fullagar, 1980)

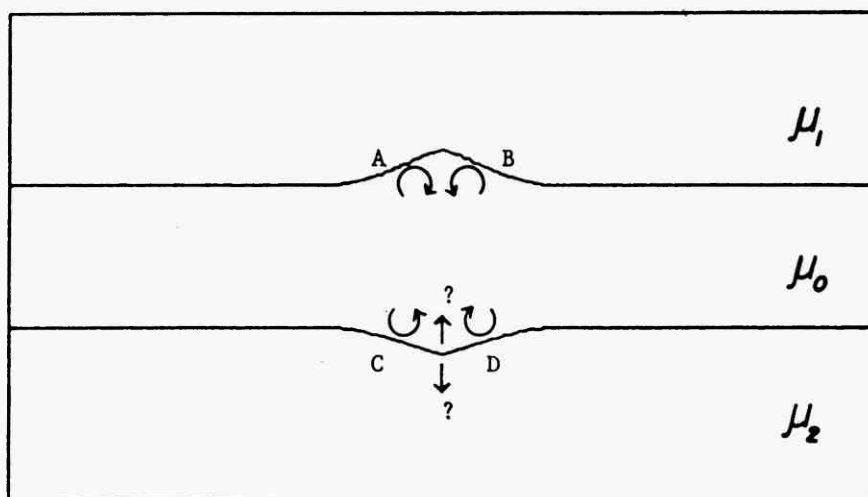


Fig.1.35-b "Cross-over" during extension of a more viscous layer; as deflection geometry tends towards symmetry, a point is reached at which vorticity in the layer no longer dominates the flow. (after Fullagar, 1980)

Fullagar (1980) suggests that for slow plane flow of an infinite two-dimensional layer of incompressible Newtonian fluid sandwiched between infinite viscous media of the same density, vorticity (the curl of velocity) is a potentially valuable interpretational aid, being simply related both to velocity (via the Biot-Savart law) and to pressure (via the equations of motion). It provides a link between dynamics and kinematics.

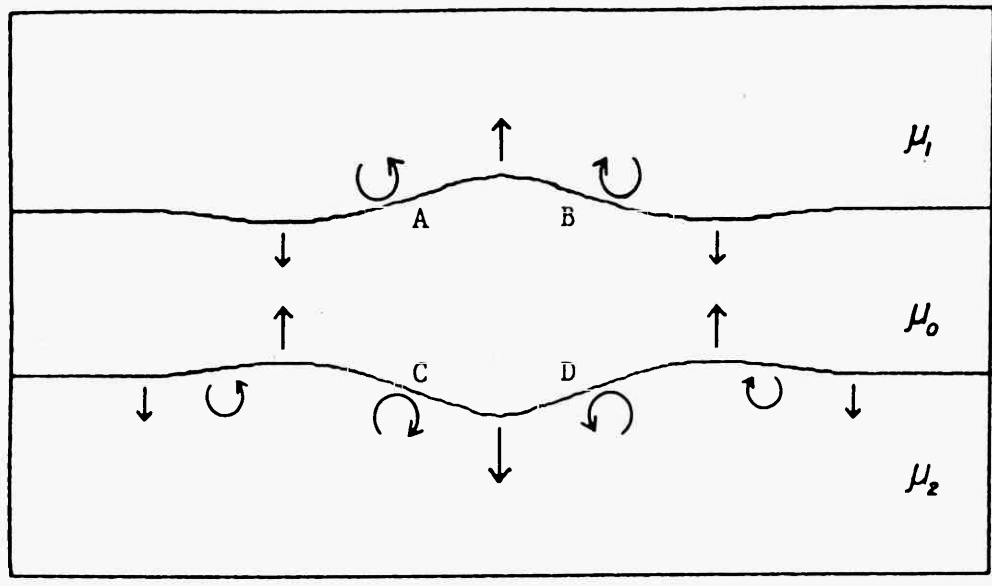


Fig.1.35-c. Vorticity and velocity distributions characteristic of amplification and nucleation of pinch-and-swell during extension of a more-viscous layer. The vorticity in the media is dominant, as per (1.28). Vorticity at each interface is conducive to local amplification and nucleation, but there is destructive interference between vorticity at the upper and lower interfaces. (after Fullagar, 1980).

During extension the flow is driven by relatively weak pressure gradients, although pinch-and-swell structure does nucleate, destructive interference between the vorticity in the two media precludes the development of classical boudins.

Fullagar (1980) arrived at the following conclusions:-

For long-wavelength asymmetrical deflections (fig. 1.35-a), the magnitude of the vorticity at the interface is always greater in the layer than in the matrix, as long as  $\mu_0 > \mu_1$  or  $\mu_2$ .

$$|W_0| \gg |W_1| \tag{1.26}$$

where  $W$  is the vorticity defined by  $W = V^x - U^y$ ,  $W_0$  in the layer and  $W_1$  in the matrix superscripts  $x$  and  $y$  are used to denote partial derivations.

Near a small symmetrical deflection of long wavelength, the magnitude of the vorticity is greater in the matrix than the layer, as long as  $\mu_0 > \mu_1$  or  $\mu_2$  (fig. 1.35-b)

$$|W_1| > |W_0| \tag{1.27-a}$$

or

$$|W_2| > |W_0| \tag{1.27-b}$$

Continuity of tangential (sgn) traction is expressed by:-

$$\text{sgn}(W_0 - W_1) = \text{sgn}[(1-r_1)T] \quad (1.28-a)$$

$$\text{sgn}(W_0 - W_2) = \text{sgn}[(1-r_2)T] \quad (1.28-b)$$

$$\text{where } r_1 = \frac{\mu_1}{\mu_0} \quad r_2 = \frac{\mu_2}{\mu_0}$$

$$T = 2\gamma \sin 2\theta$$

$\gamma$  = an externally imposed strain rate

$\theta$  = inclination of the surface of the layer (fig. 1.35-a).

Considering the layer in fig. 1.35-a, the primary tangential tractions ( $T$ ) at A and B must be negative and positive respectively and from 1.26 and 1.28-a, it follows that  $W_0(A)$  is negative and  $W_0(B)$  is positive. Application of the Biot-Savart Law shows downward motion at the crest of the deflection and at all points directly beneath. At this stage the perturbation flow is controlled by the vorticity at the upper interface. Very soon the vorticity at the lower interface counteracts the effect of that at the upper, vorticity being positive at C and negative at D (fig. 1.35-b). This is considered to mark a transition or 'cross-over.'

After the cross-over the magnitude of the vorticity is greater in the matrices than in the layer (1.28).  $W_1(A)$  and  $W_1(B)$  are positive and negative respectively while  $W_2(C)$  and  $W_2(D)$  are negative & positive respectively (fig. 1.35-c). The equivalent perturbation velocity distribution (arrows in fig. 1.35-c) causes amplification and nucleation of pinch-and-swell eventually.

#### 1.4 Finite Element Method

Stephansson and Berner (1971) were the first geologists to use the finite-element method to produce boudinage structure. Because of symmetry, they considered one-fourth of the boudin concerned. An analysis of deformation of an elastic boudin shows the development of the barrel shape so characteristic of many natural boudins (fig. 1.37-A, B). The precipitation of minerals observed in nature in the gaps between boudins can be accounted for by the mean stress disturbance deduced from the analysis (fig. 1.36, 1.37, C, D). It can be seen that at both ends of the boudin an area of low pressure forms. Consequently the most mobile constituents in the rock ( $\text{CO}_2$ ,  $\text{SiO}_2$ ) will migrate from the surroundings towards these low pressure areas. The chemical analysis made by Berglund and Ekstrom (1974), using sphalerite as a geobarometer (based on the varying content of FeS in sphalerite) from different parts of a boudin on a specimen from the Udden mine, North Sweden, confirms the mean stress variation shown on fig. 1.37-D. The natural boudin they analysed is of amphibolite in a matrix dominated by pyrite (fig. 1.38-A). The content of FeS in sphalerite from different parts of the boudin is shown in fig. 1.38-B.

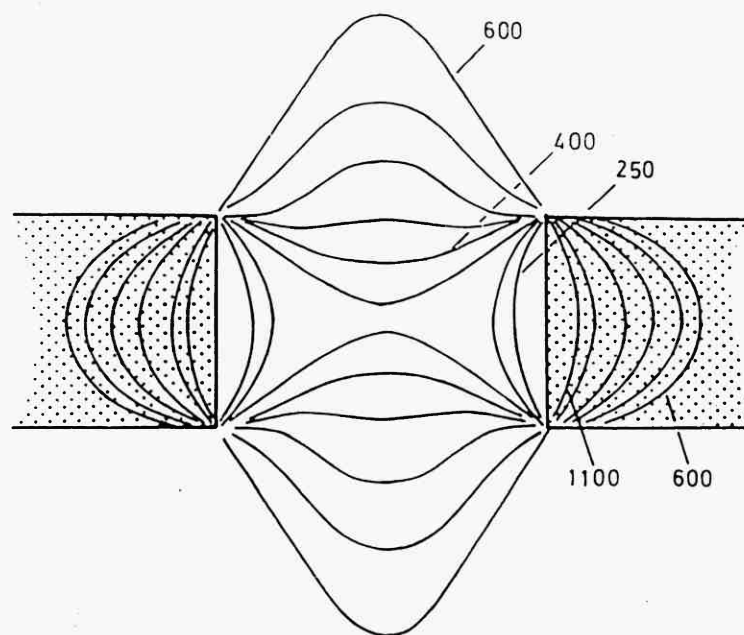


Fig. 1.36 The mean stress distribution in a theoretical boudinage after Stephansson & Berner (1971). The pressure is recalculated to  $\text{kg/cm}^2$ . (after Berglund and Ekstrom, 1974).



They argue that the different content of FeS in different parts of the boudin corresponds to differences in stress values and that the variations match well the variations in the mean stress in a theoretical boudinage structure (fig. 1.38-C).

Following Wilson (1963) and Stephansson and Berner (1971), and Selkman (1978) investigated the relationship of stress distribution and mineral distribution of boudinage from the Udine Mine, using the finite-element method. A boudinage from the Udine Mine area has been examined in detail (fig. 1.38-a) with regard to its mineral distribution, chemical variations (Berglund and Ekstrom, 1974) and grain-size distribution (fig. 1.39-b compare with 1.38-B). In his programmes, Selkman assumed elastic or plastic material properties. During one iterative step, each nodal point is displaced and this displacement provides the basis for calculation of normal stress, principal stress and shear stress at the centre of each element. At a later stage, plain strain is maintained, which creates a possibility of calculating the mean stress  $\sigma = \left( \frac{\sigma_1 + \sigma_2 + \sigma_3}{3} \right)$ . The models can be carried through several iterations, in such a way that the nodal points, after one iteration, set up new points for the next iteration.

This programme indicates that the stress distribution around the boudin is compatible with the mineral distribution around the boudin from the Udine Mine. His investigation also shows that there is a direct relationship between grain size and stress distribution (compare fig. 1.39-b and 1.40).

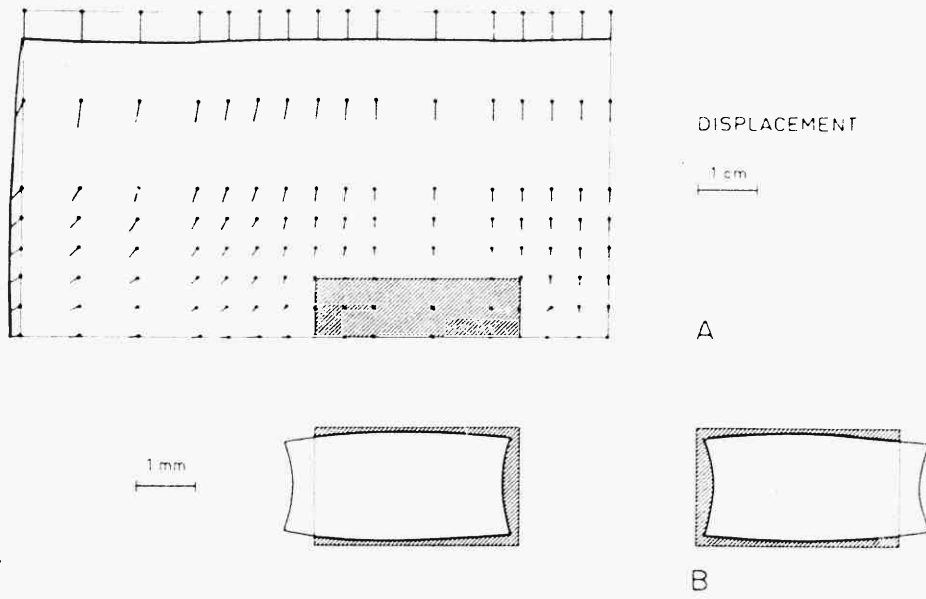


Fig. 1.37

Deformation of the boudinage structure. A. Displacements of nodal points, dots indicating their original positions. B. Enlargement of deformed boudin; notice the barrel shape and the slight separation of the boudins.

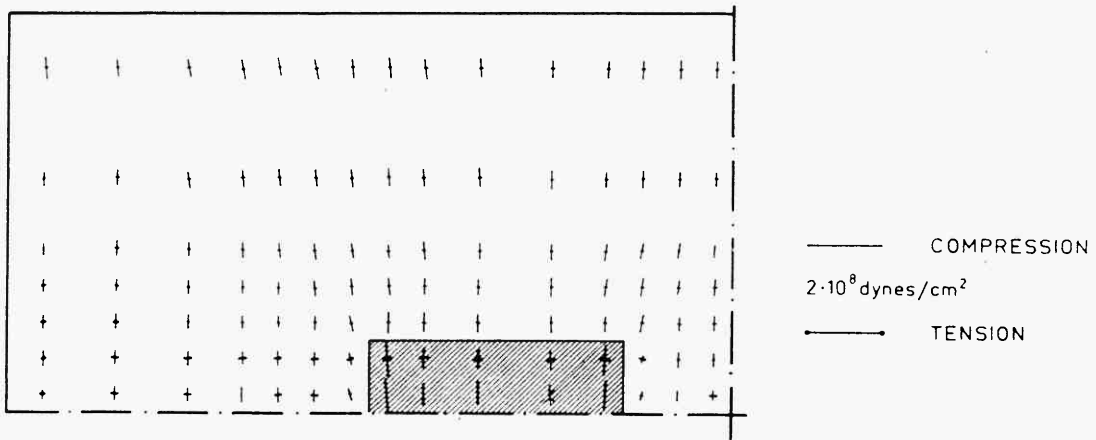


Fig. 1.37 C Principal stress distribution for one quarter of the model.

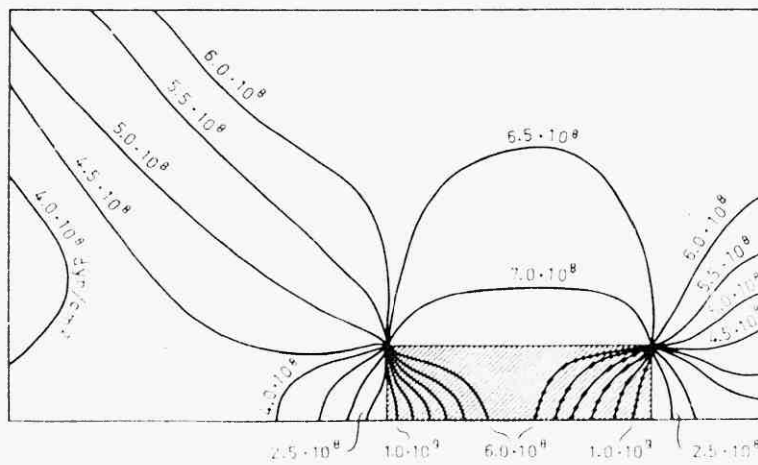


Fig. 1.37 D Mean stress distribution  $\frac{1}{3}(\sigma_1 + \sigma_2 + \sigma_3)$  for one quarter of the model.

(After Selkman, 1978)

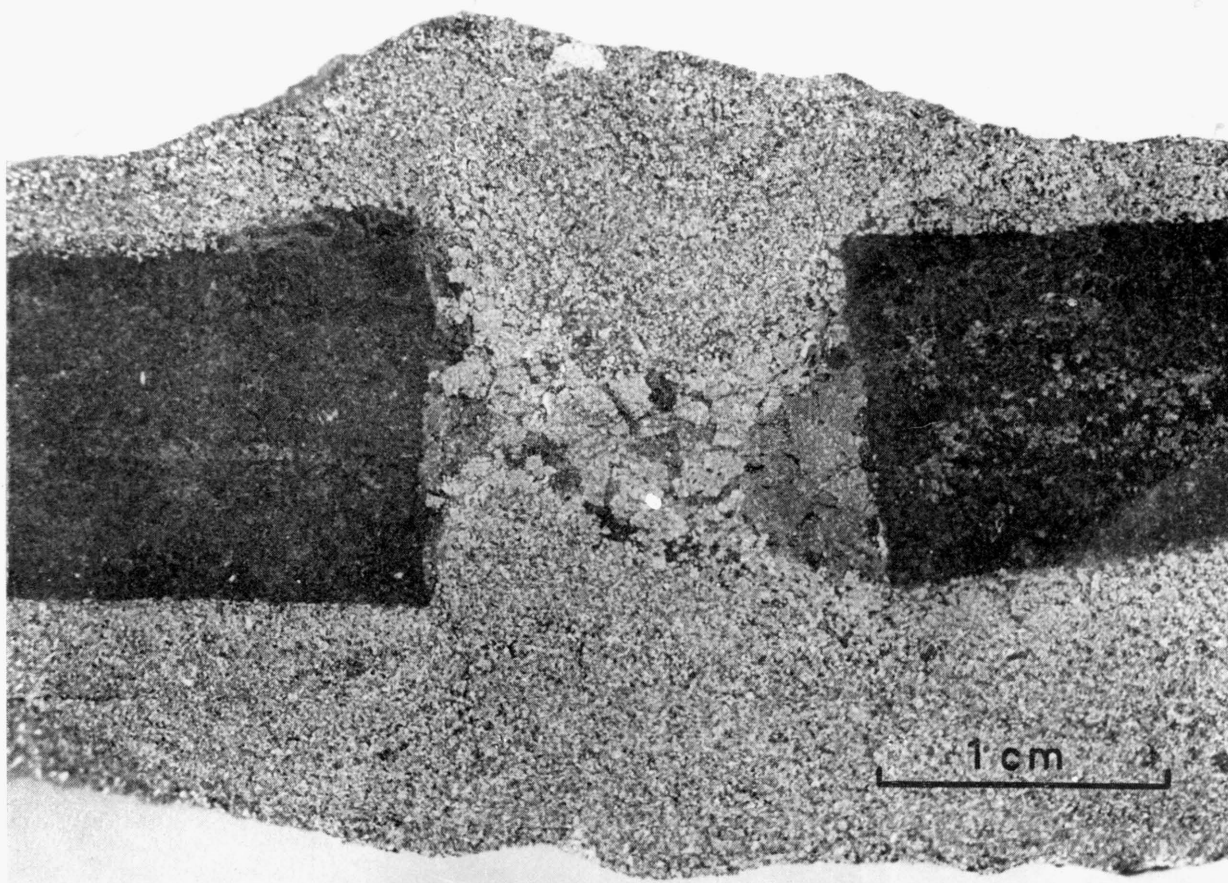


Fig. 1.38-A Amplitude boudinage investigated by Berglund and Ekstrom (1974)

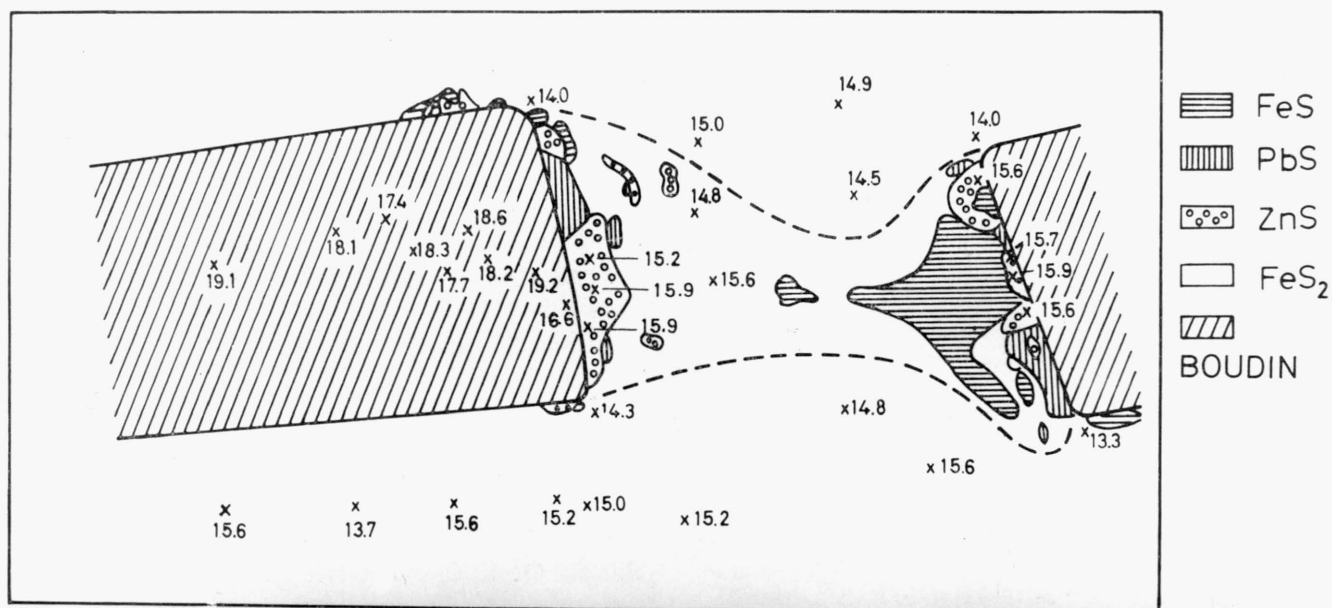


Fig. 1.38-B The distribution of large sulphide grains. The positions of analysed sphalerite grains are shown by crosses. The content of FeS in these sphalerite is also given (after Berglund and Ekstrom (1974))

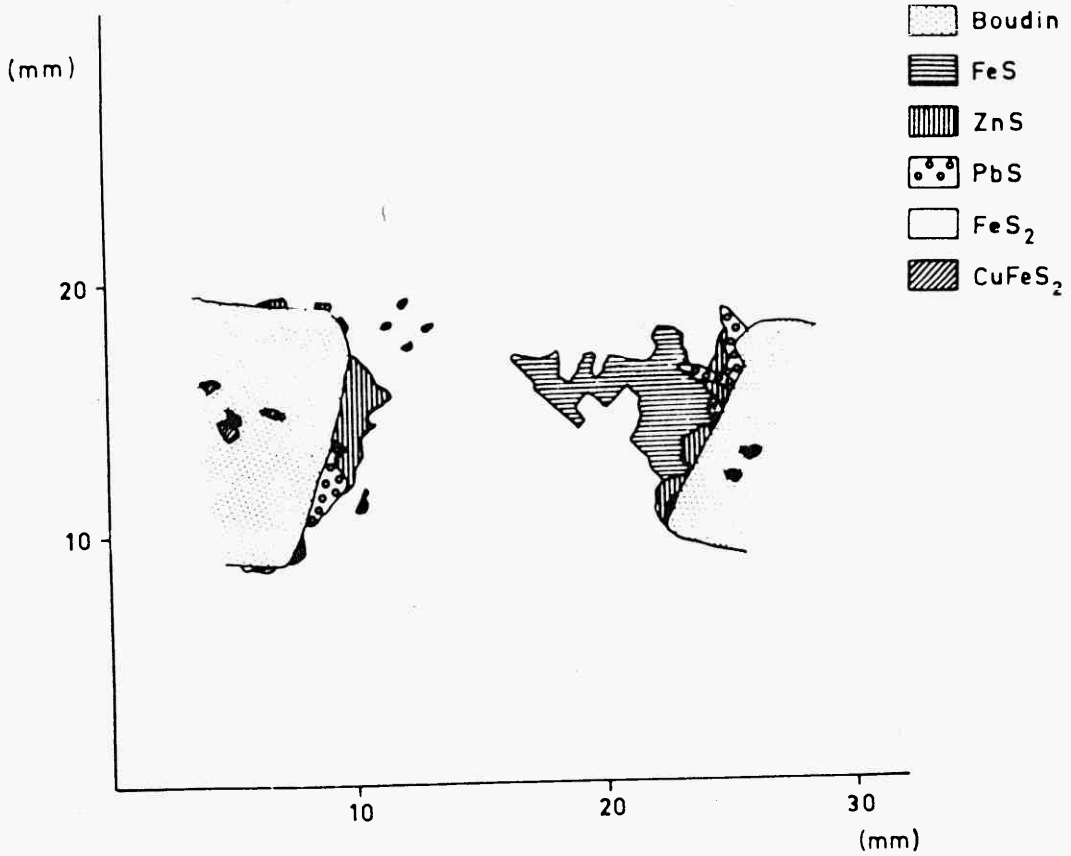


Fig. 1.39-a. Natural boudinage from the Udden Mine and its mineral distribution.

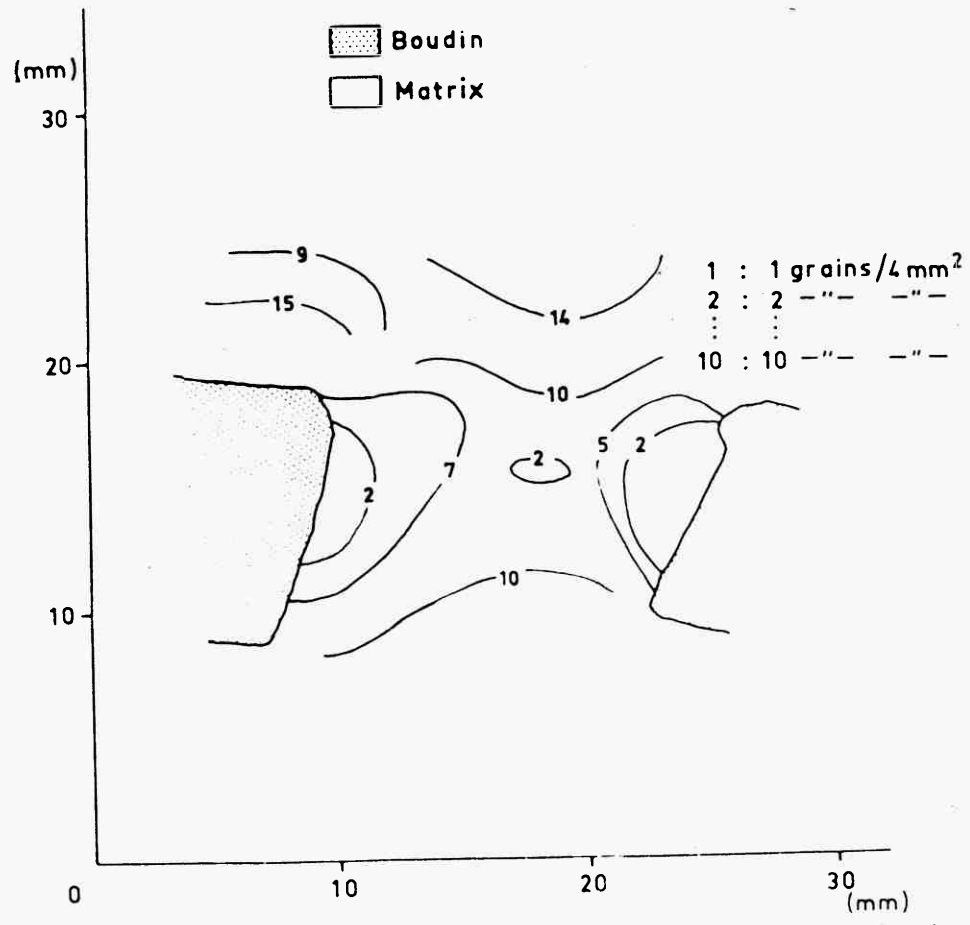
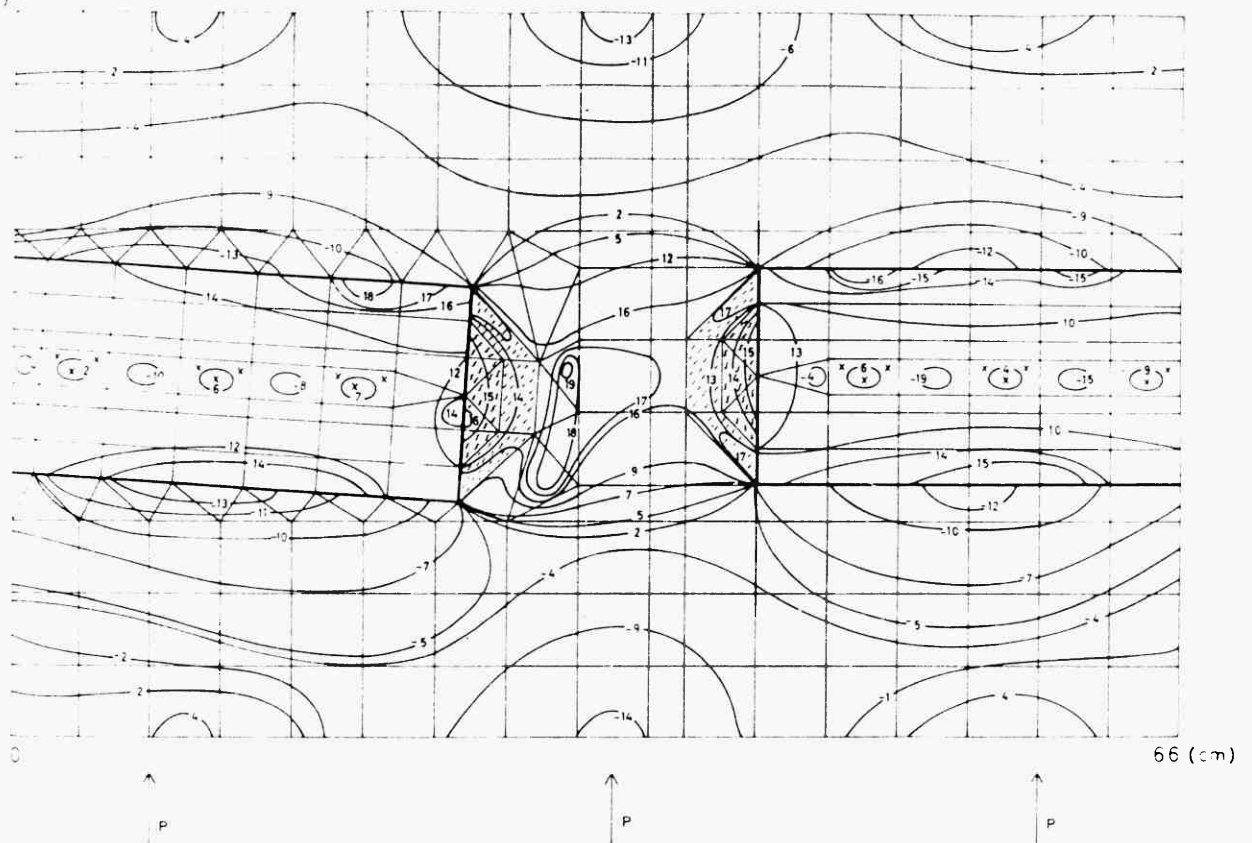


Fig. 1.39-b. Natural boudinage from the Udden Mine and its grain-size distribution. Lines are drawn between areas with equal amounts of grains. (after Selkman, 1978).



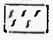


	PbS	$E = 2,0 \cdot 10^{12} \text{ dyn/cm}^2$	$\nu = 0,10$	1	$\pm (0-10) \cdot 10^7 \text{ dyn/cm}^2$	
	ZnS	$E = 3,0 \cdot 10^{12} \text{ ---}$	$\nu = 0,30$	2-3	$\pm (0-10) \cdot 10^8 \text{ ---}$	
	CuFeS <sub>2</sub>	$E = 3,0 \cdot 10^{12} \text{ ---}$	$\nu = 0,30$	4-12	$\pm (0-10) \cdot 10^9 \text{ ---}$	$P = 10^{11} \text{ dyn/cm}$
	FeS <sub>2</sub>	$E = 3,5 \cdot 10^{12} \text{ ---}$	$\nu = 0,40$	13-22	$\pm (0-10) \cdot 10^{10} \text{ ---}$	
BOUDINS		$E = 7,0 \cdot 10^{12} \text{ ---}$	$\nu = 0,45$			

Fig. 1.40 Isopachytes for the maximum-stress component of principal stress in one of Selkman's models. (after Selkman, 1978).

## 1.5 Multilayer Boudinage

Although a number of geologists have worked theoretically and experimentally on the origin and development of boudinage in single layers, very little work has been done on multilayers. Fullagar (1980) when considering single layer boudinage, considered two different incompetent layers as matrix, even so the model is still essentially a competent single layer between two different incompetent layers.

The reason multilayers have received such scant attention may be that they are too complex to be easily analysed mathematically. Alternatively, it may be that geologists consider the single layer analysis capable of explaining boudinage development in multilayers.

### 1.5.1 Theoretical

Cobbold, Cosgrove and Summers (1971) used Biot's (1965) theory of deformation of a homogeneous, anisotropic material to account for the buckling of multilayers. They considered the behaviour of a multilayer in terms of its average or bulk properties, instead of the properties of the individual layers.

They adopted Biot's (1965b) theory of deformation of a homogeneous, anisotropic material and arrived at the following equations.

A single equation for the displacement function,  $\phi$

$$\left(Q - \frac{P}{2}\right) \frac{\partial^4 \phi}{\partial x^4} + 2(2N - Q) \frac{\partial^4 \phi}{\partial^2 x^2 \partial y^2} + \left(Q + \frac{P}{2}\right) \frac{\partial^4 \phi}{\partial y^4} = 0 \quad (1.29a)$$

where  $N$  and  $Q$  are compressive and shear moduli respectively

$P = (S_{22} - S_{11})$  and  $S_{11}$  and  $S_{22}$  are the initial stresses within the material.

For an isotropic material,  $N$  and  $Q$  are equal, but for an orthotropic material  $N$  and  $Q$  are different. "The material behaves with one modulus ( $N$ ) if subjected to an increment of compression and a different modulus ( $Q$ ) if

subjected to an increment of shear. Because of this modulus difference, the material is anisotropic; but it is also homogeneous because there are no discontinuities and there is no variation in properties from point to point", noted Cobbold et al. (1971).

The initial stresses within a material affect the response to incremental applied boundary forces which are related to incremental strains within the material by the moduli M and L, given by:

$$M = N + P/4$$

$$L = Q + P/2$$

In terms of the moduli M and L, equation 1.29a becomes:

$$(L-P) \frac{\partial^4 \phi}{\partial x^4} + 2(M-L) \frac{\partial^4 \phi}{\partial x^2 \partial y^2} + L \frac{\partial^4 \phi}{\partial y^4} \quad (1.29-b)$$

The general solution of homogeneous partial differential equations such as (1.29-b) is (Green, 1951)

$$\phi = f_1(x + \xi_1 y) + f_2(x - \xi_1 y) + f_3(x + \xi_2 y) + f_4(x - \xi_2 y) \quad (1.29-c)$$

where  $\xi_1, \xi_2$  are arbitrary constants and  $f_1, f_2, f_3$  &  $f_4$  are any arbitrary functions.

Biot (1965, p. 193) shows that real values of  $\xi_1, \xi_2$  exist in the following cases:

$$\text{case 1: } M/L > \frac{1}{2}; \quad P/L > 1 \quad (1.29-d)$$

$$\text{case 2: } M/L < \frac{1}{2}; \quad 1 > P/L > 4.M/L(1-M/L)$$

$$\text{case 3: } M/L < \frac{1}{2}; \quad P/L > 1.$$

Substitution of eg. 1.29c into e.g. 1.29b gives an expression relating the critical stress difference, P, with the moduli M and L and the parameters  $\xi_1$  and  $\xi_2$ , at the onset of instability.

$$L\xi^4 + 2(2M-1)\xi^2 + (L-P) = 0 \quad (1.29-e)$$

Expression (1.29e) is shown graphically in fig. 1.41, where the

critical stress difference is plotted as the non-dimensional ratio  $P/L$  against modulus ratio  $M/L$ . Cobbold et al. (1971) called the three unstable stress fields (fig. 1.41), which correspond to the three cases of eq. 1.29-d, type 1, type 2 and type 3 instability.

It is assumed that the orthotropic material has rectangular boundaries which remain undeflected throughout the deformation and that there are no shear stresses at these boundaries. Because of these assumptions the most significant displacements occur towards the central part of an unstable body, and for this reason, the instability is internal. With the above assumptions, the conditions to be satisfied for type 1 instability are those of case 1 (1.29-d)  $M/L > \frac{1}{2}$ ;  $P/L > 1$ .

A solution of equation 1.29-b which satisfies the assumed boundary conditions and gives periodic displacements is:

$$\phi = -\frac{1}{2}C \{ \cos \ell(x-\xi y) + \cos \ell(x+\xi y) \}$$

or  $\phi = -C \cos \ell x \cdot \cos \xi \ell y$  (1.29-f)

where  $C$  and  $\ell$  are arbitrary constants.

The displacements  $u$  and  $v$  are:

$$u = \frac{\partial \phi}{\partial y} = -C \ell \xi \cos \ell x \sin \xi \ell y$$

$$v = \frac{\partial \phi}{\partial x} = C \ell \sin \ell x \cos \xi \ell y$$
 (1.29-g)

Each of the displacement vectors  $u$  and  $v$ , varies sinusoidally in magnitude, with wavelength  $W_x$  and  $W_y$ , along the coordinate directions, where:

$$W_x = \frac{2\pi}{\ell}; \quad W_y = \frac{2\pi}{\xi \ell} \text{ so that, for this displacement pattern:}$$

$$\xi = W_x / W_y$$

The displacement pattern of equation 1.29-f is that associated with the internal buckling of a homogeneous anisotropic material.



For a type 2 instability the conditions to be satisfied are (case 2, eqn. 1.29-d):

$$M/L < \frac{1}{2}; \quad 1 > P/L > 4M/L(1-M/L).$$

There is a single value for  $\xi$  at the critical value of the initial stress difference,

$$P_c = 4M/L(L-M):$$

$$\xi_c = (1-2M/L)^{\frac{1}{2}}$$

associated with this value of  $\xi$  there are characteristic directions, the angle  $\theta$  between these directions and the y-axis is given by

$$\tan \theta = \pm \xi_c$$

These characteristic directions are oblique to the y-direction, in contrast with type 1 instability, where the characteristic directions for a minimal initial stress are parallel to the y-direction. These oblique characteristic directions are considered to be associated with the development of kink-bands.

The combined effects of degree of anisotropy and orientation of compression direction on the form of finite internal structures which may develop in a statistically homogeneous rock is summarized in fig. 1.42. The theoretical forms of interlocking pinch-and-swell structures were obtained by superimposing the displacement field (eqn. 1.29-f) for type 1 instability on a set of passive marker lines, which initially were normal to the compression direction. An example of experimentally produced (by Cobbold et al., 1971) interlocking pinch-and-swell structures (internal boudins) have already been shown in fig. 1.28-a.

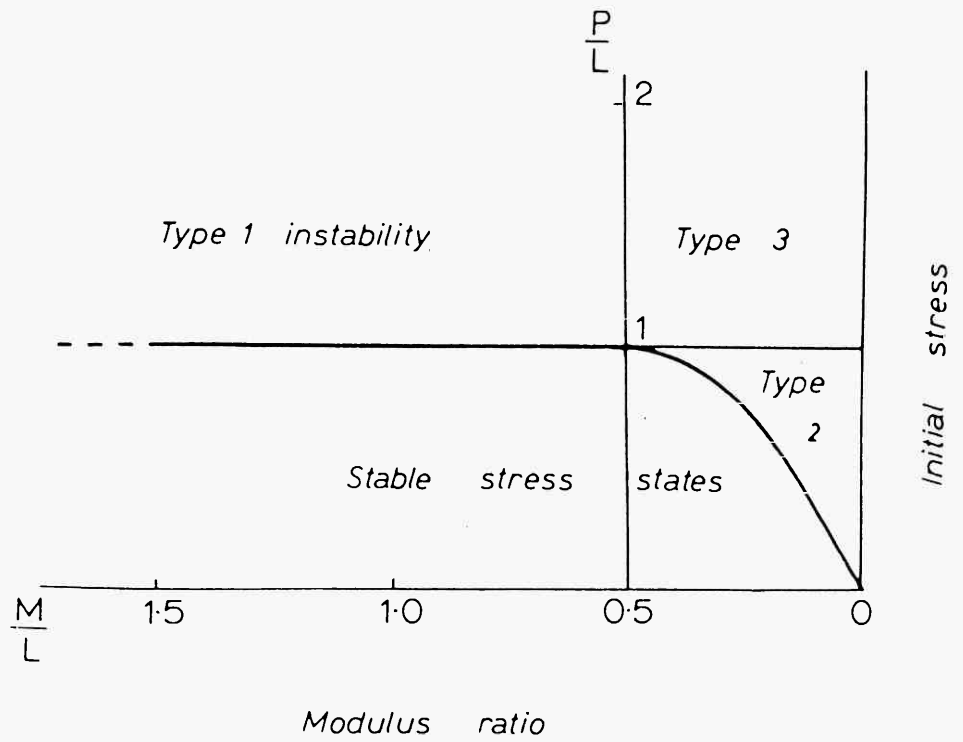


Fig.1.41. Stable and unstable values of the initial stress  $P$ , in materials with different degrees of anisotropy (expressed by modulus ratio,  $M/L$ ). The thick black line represents the critical stress  $P_c$ , of equation 1.29-c. (After Cobbold et al, 1971)

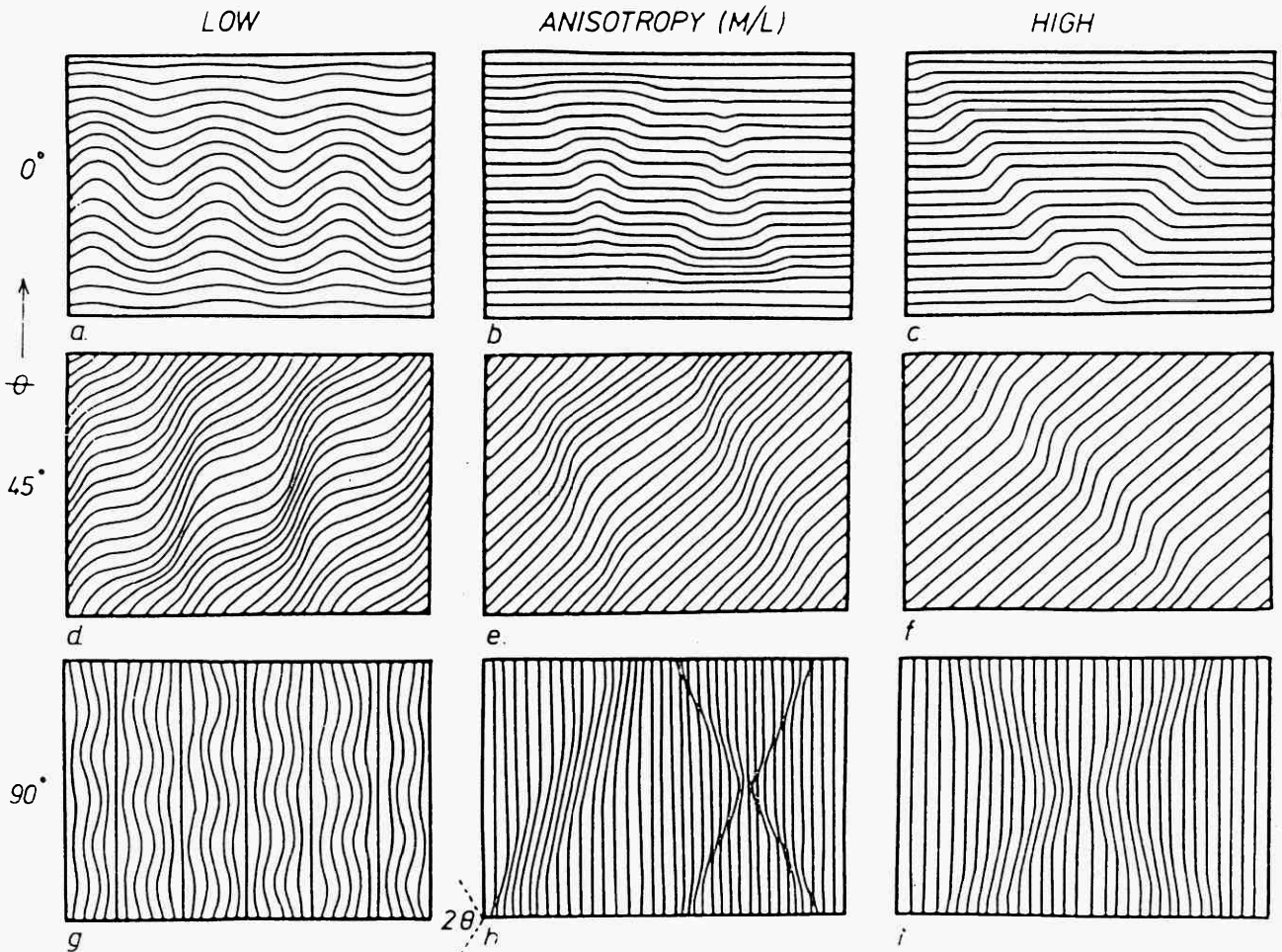


FIG.1.42. Some possible modes of expression of "buckling" instabilities in materials with different anisotropy ( $M/L$ ) and at different angles ( $\theta$ ) to the maximum compression direction. (After Cosgrove, 1976)

Stromgard (1973) is one of the few geologists to consider a multilayer boudinage model. His model takes account of the influence of viscosity contrast, thickness ratio of the layers and magnitude and orientation of external forces. All layers are viscous (or elastic) and the model is subjected to layer-parallel and layer perpendicular external stresses. Each layer is assumed to deform homogeneously until it ruptures. This assumption is valid if layer-thicknesses are small compared to the dimensions of the model. Stromgard does not take into account the effect of 'necking'.

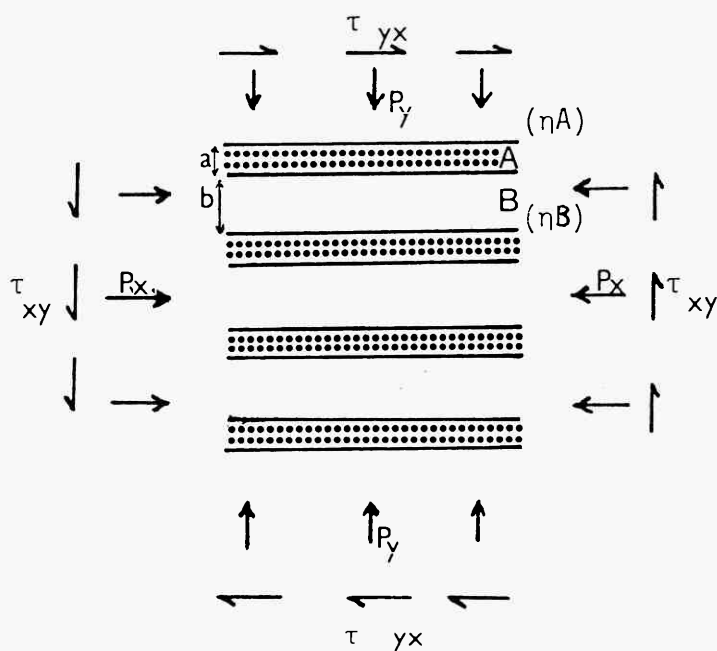


Fig. 1.43-A A loaded multilayer sequence  
(drawn from Stromgard, 1973)

The model analysed by Stromgard is shown in fig. 1.43A. It is rhythmically layered, semi-infinite and consists of linearly viscous materials, stiff A, and less stiff B with viscous tensile moduli  $\eta_A$  and  $\eta_B$ , respectively. The model is assumed to deform by plane strain. For this type of model Stromgard (1973) shows that the stress distribution in such a model is

$$\sigma_{x_A} = \frac{P_y |V_A^2 + V_A - K(V_B^2 + V_B)| + P_x K \left(\frac{a}{b} + 1\right) (1 - V_B^2)}{(1 - V_A^2) + \frac{a}{b} K(1 - V_B^2)} \quad (1.30)$$

$$\sigma_{x_B} = \frac{P_y \cdot \frac{a}{b} |K(V_B^2 + V_B) - V_A^2 - V_A| + P_x \left(1 + \frac{a}{b}\right) (1 - V_A^2)}{(1 - V_A^2) + \frac{a}{b} K(1 - V_B^2)} \quad (1.31)$$

$$\sigma_{y_A} = P_y \quad (1.32a)$$

$$\sigma_{y_B} = P_y \quad (1.32b)$$

$$\tau_{xy_A} = \tau_{yx_B} = \tau_{yx} \quad (1.33)$$

where  $V_A$  and  $V_B$  = ratios of latitudinal to longitudinal strain rates of A and B respectively.  $K = \eta_A/\eta_B$ .

Besides being valid for plane strain, eqns. 1.30 - 1.33 also hold for one special three-dimensional deformation i.e. an axisymmetrical model subjected to an applied average stress  $P_x$  in the radial direction parallel to the layers. This can be compared to 'chocolate tablet boudinage', Ramsay (1967).

According to Stromgard, in order for boudins with a rectangular shape to form, there must be an axial tension, parallel to the competent layers.

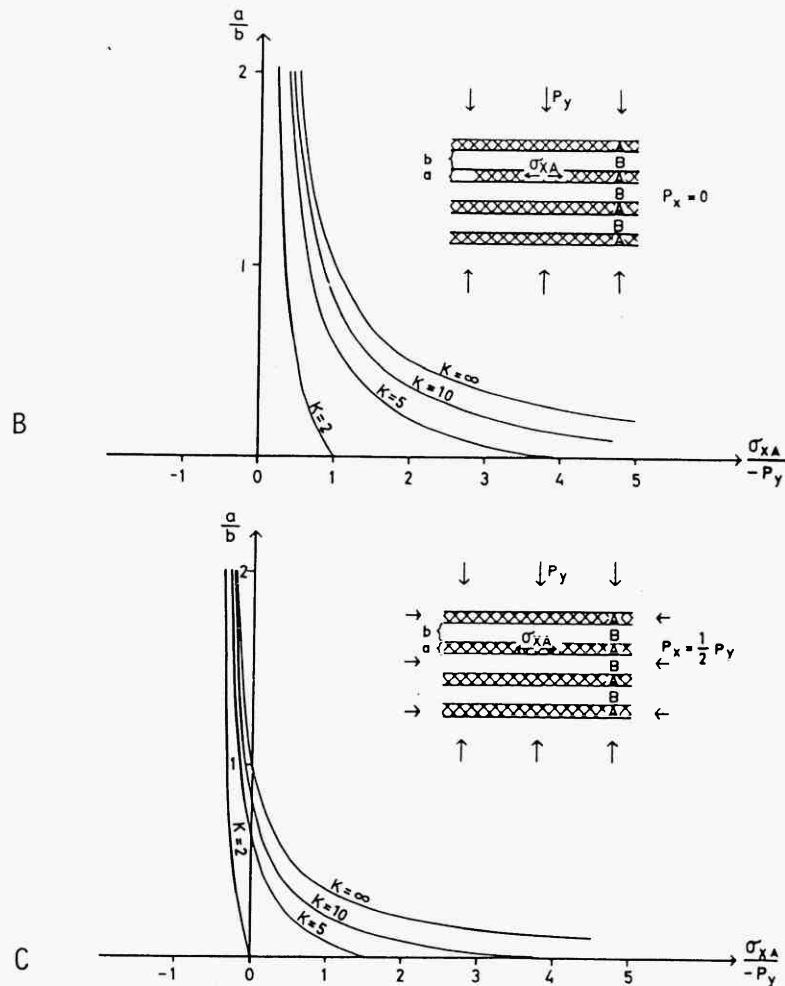


Fig. 1.43. Magnitude of longitudinal stress parallel to layering,  $\sigma_{xA}$ , in competent layers (A), for various thickness ratios  $a/b$  and viscosity ratios  $K = \eta_A/\eta_B$ ; if the applied stress  $P_y$  is compressive, stress is tensile to the right of the ordinate; B:  $P_x/P_y = 0$ ; C:  $P_x/P_y = 1/2$ .

(after Stromgard, 1973).

From his analysis, Stromgard concludes that in a multilayered rock sequence under which tension develops (as shown in the diagrams fig. 1.43-B, C) the following conditions pertain.

- In uniaxial compression (fig. 1.43-B)  $\sigma_{xA}$  is always tensile if the viscosity ratio is greater than 1 regardless of the thickness ratio.
- Tension fractures normal to bedding could develop provided the tensile strength of the competent layers was low enough.
- If  $P_x = 1/2 P_y$ , (fig. 1.43-C,)  $\sigma_{xA}$  will be tensile only for certain ratios of viscosity and thickness. If the viscosity ratio is  $< 2$  there is no possibility for tension to develop, regardless of the magnitude of  $P_y$  and of thickness ratio of the layers.
- The smaller  $a/b$ , the greater the axial tension developed in competent layers and the greater the viscosity ratio the greater the tension.

- (e) If  $\frac{P_x}{P_y} > 1/2$  boudins cannot form by fracturing and only flow occurs. If  $\frac{P_x}{P_y} < 1/2$  boudins form if the tensile stress is high enough. Thus low  $\frac{P_x}{P_y}$  ratios favour the development of boudinage structures.
- (f) If slippage between layers occurs or if the soft material is compressible the fields of fracture in fig. 1.44 will decrease.

#### Formation of Rhombohedral Boudins

Different mechanisms have been proposed for the formation of rhombohedral boudins. One assumes that failure of the competent layers occurs by shear fracturing. If  $\sigma_1$  is normal to the layering these fractures will be oblique to the layering commonly at  $60^\circ$  to it. Another method by which rhombohedral boudins can be formed is by the deformation of originally rectangular boudins. They may become rhombohedral during progressive deformation because of shear parallel to the layering.

Stromgard (1973) considered the effect of a shear stress ( $\tau_{xy}$ ) parallel to the layering in addition to  $P_x$  and  $P_y$ . In this model the principal stresses are inclined to the layering. If the materials are considered to be incompressible the orientation of the axis of maximum compression refracts across the boundaries between competent and incompetent layers according to the following equation:-

$$\tan 2\theta_A = \frac{B}{A} \tan 2\theta_B \quad (\text{fig. 1.44-A}) \quad (1.34)$$

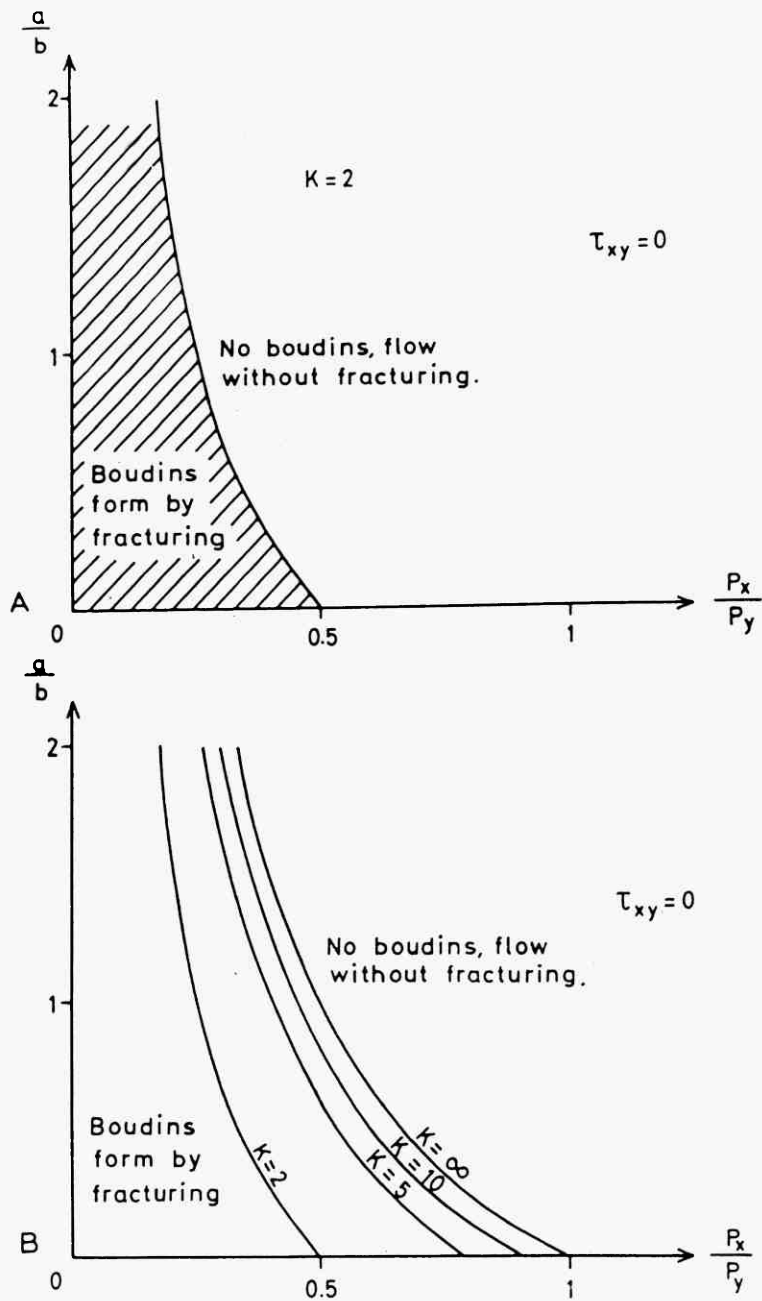


Fig. 1.44. Conditions for formation of rectangular boudins by tension cracking of competent layers of a symmetrically loaded incompressible multilayer. (after Stromgard, 1973).

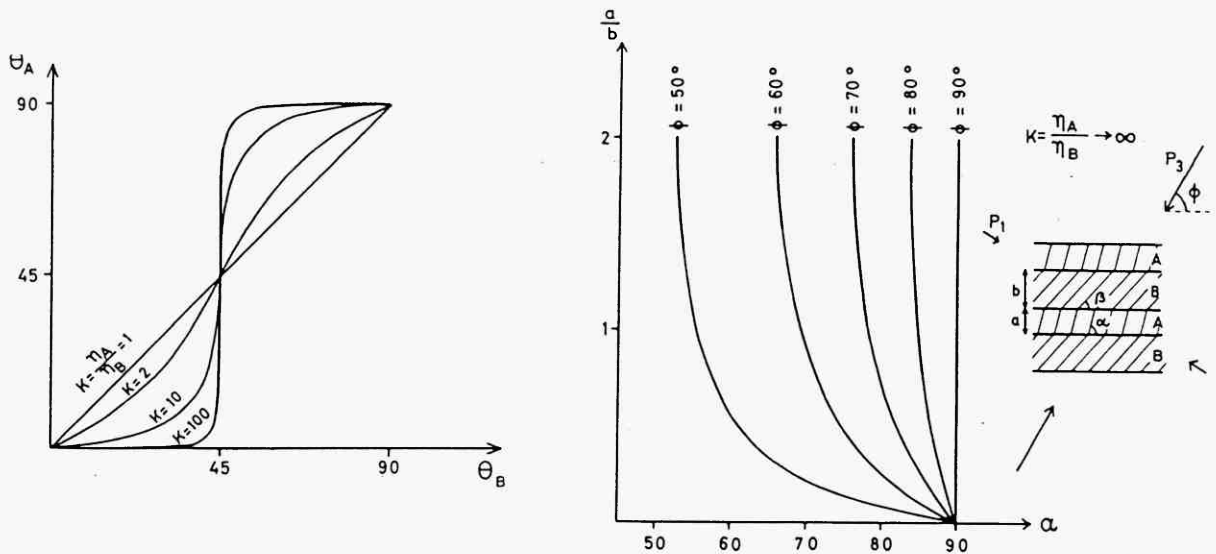


Fig. 1.45-A Relationship between orientations of principal stresses at interfaces between soft and stiff layers for various viscosity ratios  $K$ . For angles of the principal axis in the incompetent layers of less than  $45^\circ$ , the angles of the principal axis in the competent layers are greater than those in the incompetent layers. The opposite relations hold for angles in the incompetent layers of less than  $45^\circ$ .

Fig. 1.45-B Orientation  $\alpha$  of the maximum compressive stress in competent layers (A), at high competence contrast for various thickness ratios and orientations  $\phi$  of applied compression; orientation  $\beta$  of maximum compressive stress in incompetent layers (B) is constantly  $45^\circ$  except for  $\phi = 90^\circ$ .



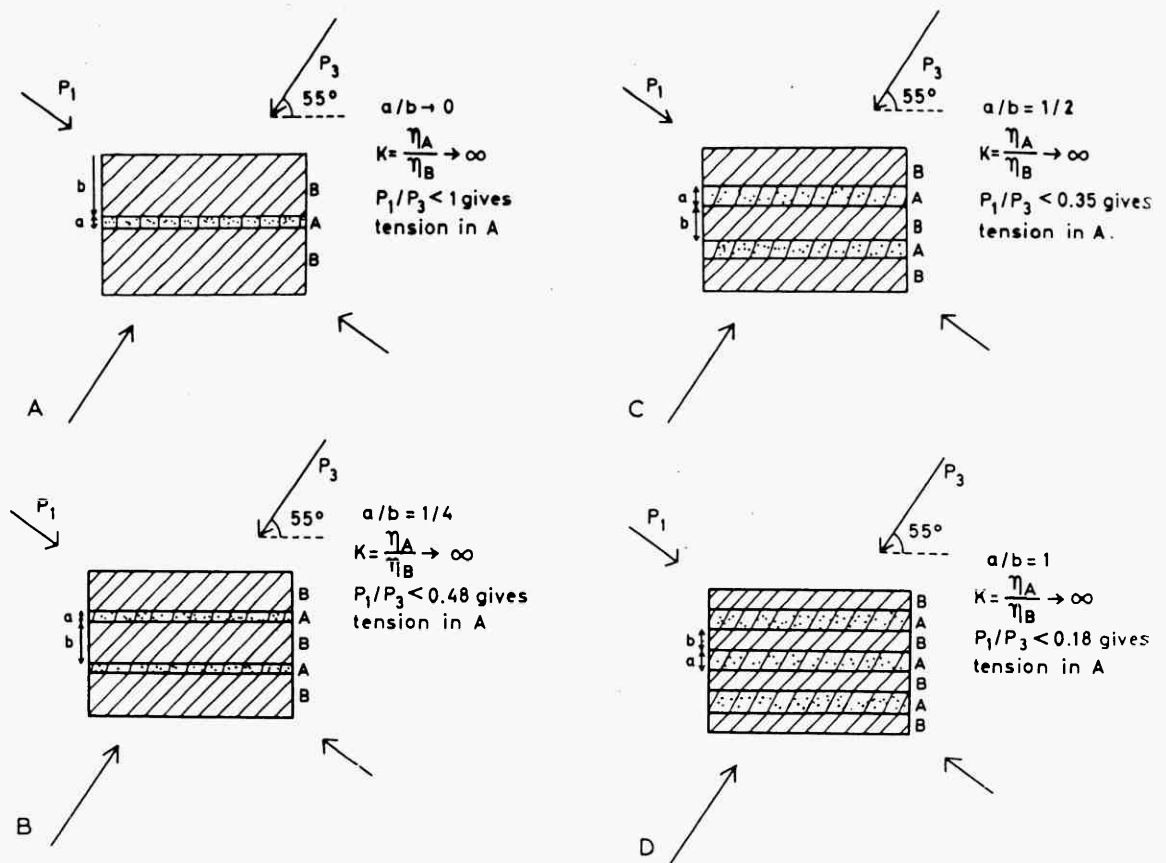


Fig. 1.46. Distribution of maximum compressive stress for four multilayers with different thickness ratios loaded in the same direction. Note that the critical ratio of  $\frac{P_1}{P_3}$  required for tension cracking, decreases as the thickness ratio increases. (after Stromgard, 1973)

The trajectories of  $P_3$  in four incompressible multilayers with a very high viscosity contrast ( $K \rightarrow \infty$ ) are shown in fig. 1.46. The orientation of the applied principal stresses  $P_1$  and  $P_3$  are the same for four models but the thickness ratio between the competent and incompetent layers is different. In the model with widely spaced competent layers, boudins which are very nearly rectangular will form (fig. 1.46-A). However, for closely spaced competent layers (for which incidentally a much lower ratio of applied stress,  $\frac{P_1}{P_3}$ , is required for stresses to be tensile in the competent layers) rhombohedral boudins may form (fig. 1.46-D).

Stromgard (1973) concludes that boudins formed by tension cracking at high confining pressure will be roughly rectangular, irrespective of the bulk orientation of compression relative to layering (fig. 1.46). According to equations (130 - 133) tension cracks markedly inclined to the normal to the

layering can develop only if  $\frac{P_1}{P_3}$  has quite a low value. If the confining pressure,  $-P_1$ , is high, differential applied stress,  $P_1-P_3$ , has to be very high for markedly rhombohedral boudins to form. The requirement of very high differential applied stress indicates that at great depth formation of markedly rhombohedral boudins by tension cracking must be rare because at great depth very high differential applied stress is not developed.

The shapes of rhombohedral boudins may also be controlled by the orientation of pre-existing planes of weakness, such as shear planes, on planes of orientation of platy minerals generated during folding (fig.1.47).

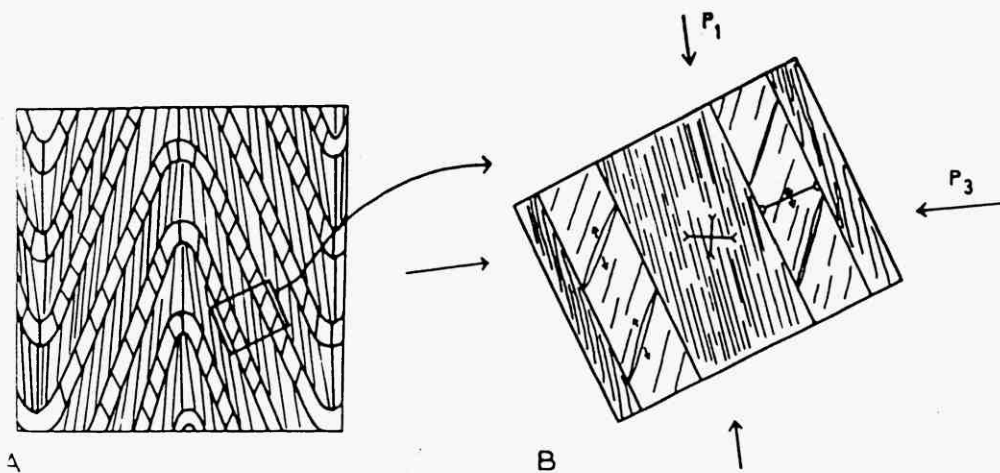


Fig. 1.47. Formation of rhomboidal boudins by separation across planes of weakness. A. Attitude of anisotropy in fold; thinner units are more competent. B. Distribution of stress in limb of fold, separation occurs across anisotropy planes. (after Stromgard, 1973).

## 1.6 Pinch-and-Swell Structures

The term 'boudinage' implies individual segments or boudins of a once continuous layer separated by fractures or veins or country rock. Pinch-and-swell structure however is the name given to the periodic thickening and thinning of a layer which remains continuous. According to many authors (e.g. Ramberg, 1955; Ramsay, 1967; Smith, 1975) most lenticular types of boudinage structures start as pinch-and-swell structures. Indeed, many (Smith, 1975) have tried to produce pinch-and-swell structures to investigate the initiation and development of boudinage. Compared to boudinage, comparatively little work has been carried out on pinch-and-swell structures.

Ramberg (1955) was probably the first to investigate the development of pinch-and-swell structures. Using clay, putty, plasticine and cheese as modelling materials, Ramberg showed that boudinage and pinch-and-swell structures develop only when a competent layer is set in an incompetent matrix and is subjected to elongation. He also observed that if the competence contrast was small, the more competent layer formed pinch-and-swell structures before rupturing, on the other hand, if the competence contrast was large rupturing occurred after only a small amount of elongation.

Ekstrom (1975) made a detailed study of pinch-and-swell from a Swedish locality. He based his investigations on field observations and measurements with special attention to the following parameters; the orientation of the dykes which contained the pinch-and-swell structures, the schistosity of the host rock, the width and thickness of the swells, the grain size, the mineral composition and the thickness or separation of the pinch zones.

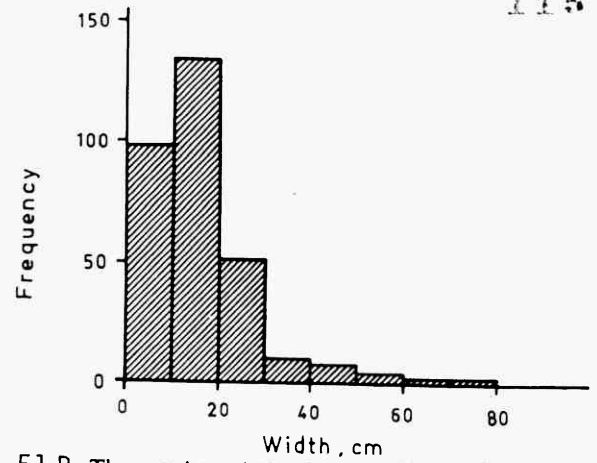
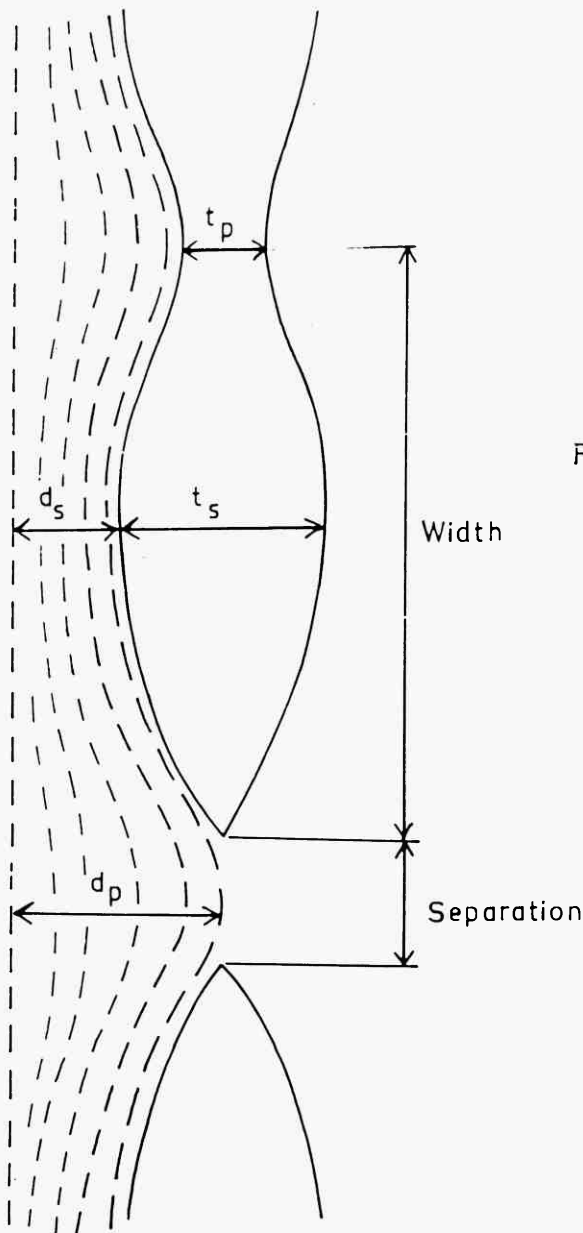


Fig. 1.51 B The varying width of the studied swells.

Fig. 1.51 B Some of the measured parameters are shown on the pinch-and-swell structure.  $t_s$  = thickness of swell,  $t_p$  = thickness of pinch,  $d_s$  = disturbed area outside the swell,  $d_p$  = disturbed area outside the pinch. (after Ekstrom, 1975).

Fig. 1.51 shows some of the measured parameters on the pinch-and-swell structure.

He presented some useful statistical analytical results and a mathematical function which describes the outer shapes of well-developed swell (fig. 1.54).

$$f(x) = \frac{1 - 2}{(e^{kx} + 1)} \quad (1.35)$$

It is suggested that a continuous flattening of the swell is a function of decreasing competence. The ratio of the average thickness of the pinch zone and the thickness of the swell is nearly constant for pinch-and-swell structures which have been deformed contemporaneously. The ratio between the width and the thickness of the swells is approximately 3:1.

There seems to be a critical thickness of layers or dykes necessary for the formation of a pinch-and-swell structure in the area. Veins less than 0.5cm thick were completely ductile during the deformation. Thick dykes behave more competently than thin ones and the number of swells increases with decreasing thickness of the dykes.

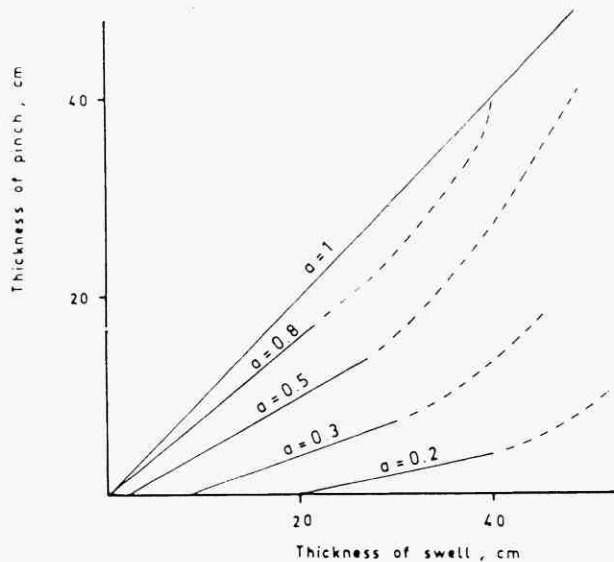


Fig. 1.52 The pinch/swell ratio as a function of increasing deformation. A low coefficient ( $a$ ) means great deformation. (after Ekstrom, 1975)

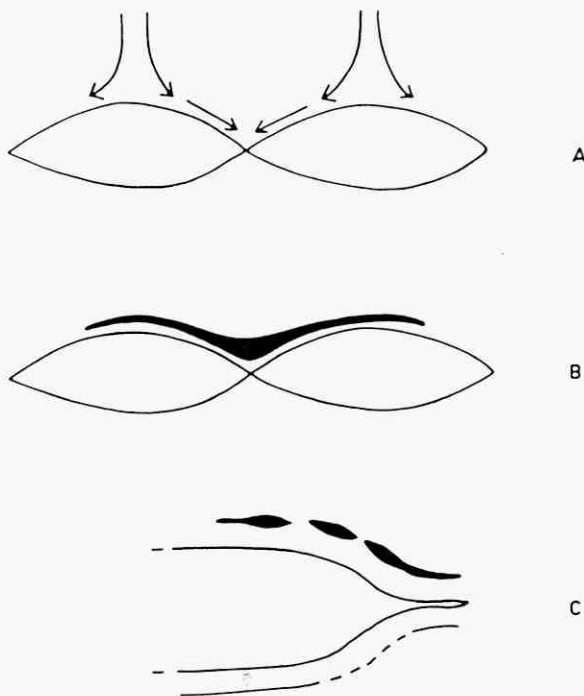


Fig. 1.53 The theoretical flow directions above a pinch-and-swell structure (A). The thinning and thickening of a vein due to 'plastic' flow (B). Small boudinage structures around a big swell (C). (after Ekstrom, 1975)

He also found that it was possible to identify pinch zones at different stages of the development of the pinch-and-swell structure.

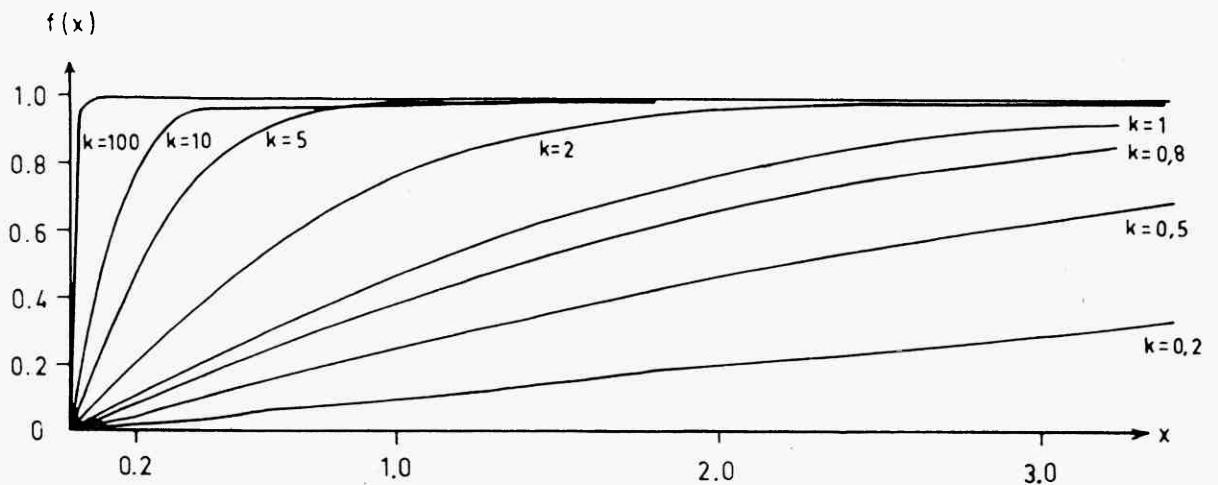


Fig. 1.54. The continuous flattening of the swells is described

$$\text{by varying } K \text{ in the function } f(x) = \frac{1 - 2}{(e^{Kx} + 1)}$$

(after Troeng, 1975).

Troeng (1975) studied one natural example of pinch-and-swell structure. He found that the deformation of individual grains of quartz and feldspar in the host rock increased towards the pinch-and-swell layer. The outer curve of the swell can be approximated by the mathematical function (1.35) (see fig. 1.54).

From his experimental model work, in which he used black and white plasticine as the competent model materials, Troeng concludes that a competence contrast less than that between putty and plasticine is needed to produce pinch-and-swell. The main mechanism of pinch-and-swell formation in the models is by sliding along shear planes.

### Deformation of Pinch-and-Swell Structures

As shown in fig. 1.55 Penge has suggested three ways the various shapes of pinch-and-swell structures can be classified.

They are:-

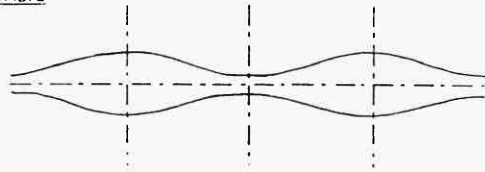
- (1) in terms of their symmetry (fig. 1.55-a).
- (2) the relationship of swell width to pinch width (fig. 1.55-b).
- (3) the ratio of swell thickness to pinch thickness (fig. 1.55-c).

Penge (1976) used plasticine models to simulate the geological process of deforming a single layer pinch-and-swell structure. He found that the maximum deformation was always concentrated within the proximity of the pinch zones. This deformation can be divided into two distinct phases, namely, the buckling of each pinch zone, which changes the original orthorhombic symmetry of the pinch-and-swell structure to triclinic (fig. 1.55-a); and the shearing of the pinch zone (fig. 1.55-b).

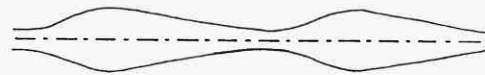
The resulting structures of the second phase (shearing) were dependent on the competence contrast and the initial angle of the layer to maximum principal compression.

The shears which often make an acute angle to the maximum principal compression, are normally en echelon. In each pinch zone either one or two parallel shears may develop. Penge also found that variation of strain rates had no significant effect on the resulting structures.

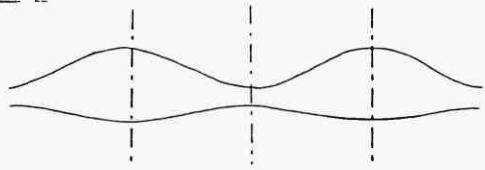
a. ORTHORHOMBIC



b. MONOCLINIC I



c. MONOCLINIC II



d. TRICLINIC

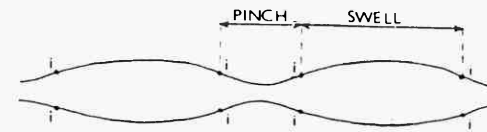


----- PLANES OF SYMMETRY

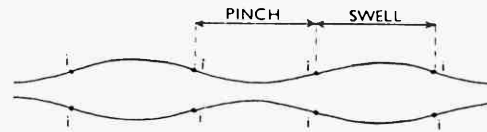
A

### CLASSIFICATION OF PINCH-AND-SWELL STRUCTURES

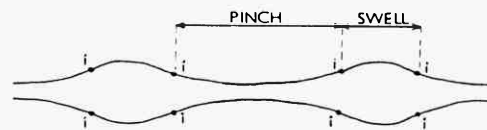
a. CLASS 1 SWELL > PINCH



b. CLASS 2 SWELL = PINCH



c. CLASS 3 SWELL < PINCH



i = INFLECTION POINTS

B

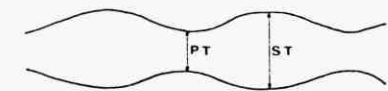
ratio of swell thickness  
to pinch thickness

1:1



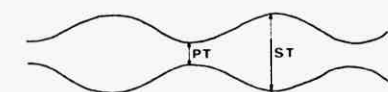
CLASS A

2:1



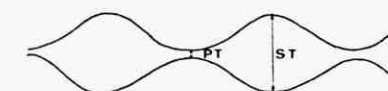
CLASS B

4:1



CLASS C

16:1



CLASS D

∞:1

ST = Swell thickness.  
PT = Pinch thickness.

C

Fig. 1.55A Fundamental types of pinch-and-swallow classes based on their symmetry.

B. Fundamental types of pinch-and-swallow classes based on the relationship of swell width to pinch width.

C. The four classes of pinch-and-swallow structures based on the ratio of swell thickness to pinch thickness.

(After Penge, 1976)



## CHAPTER 2 EXPERIMENTS

### 2.1 INTRODUCTION

In this chapter the main types of structures that develop in experiments where a multilayer is compressed normal or at high angle to the layering, are described, illustrated and analyzed.

As was discussed in Chapter 1, a number of authors have performed different types of experiments to study the development of boudinage and related structures. Ramberg (1955) used materials such as plasticine, clay and others. Strömberg (1973) & Sowers (1973) used gelatin. Apart from a few experiments by Cobbold et al. 1971, all experiments on boudinage structure have been concerned with single-layer system. Furthermore, although Cobbold (1973) and Summers (1979) have used paraffin wax multilayers to study the formation of folds, the author is not aware of any work done using paraffin wax to model boudinage structures in multilayers.

The object of the present work is to investigate the initiation and development of boudinage and related structures that develop in experiments where a multilayer is compressed normal or at high angle to the layering.

2.11 Apparatus - the apparatus used for most of the experiments is the Pure Shear Deformation rig (fig. 2.1.A.) designed and constructed by Cobbold (1973) for the scale modelling of geological structures. The models have initial dimensions of  $X = 6''$  (15 cm);  $Z = 6''$  and  $Y = 2''$  (5 cm), and are deformed under controlled conditions of strain rate and temperature. Throughout the course

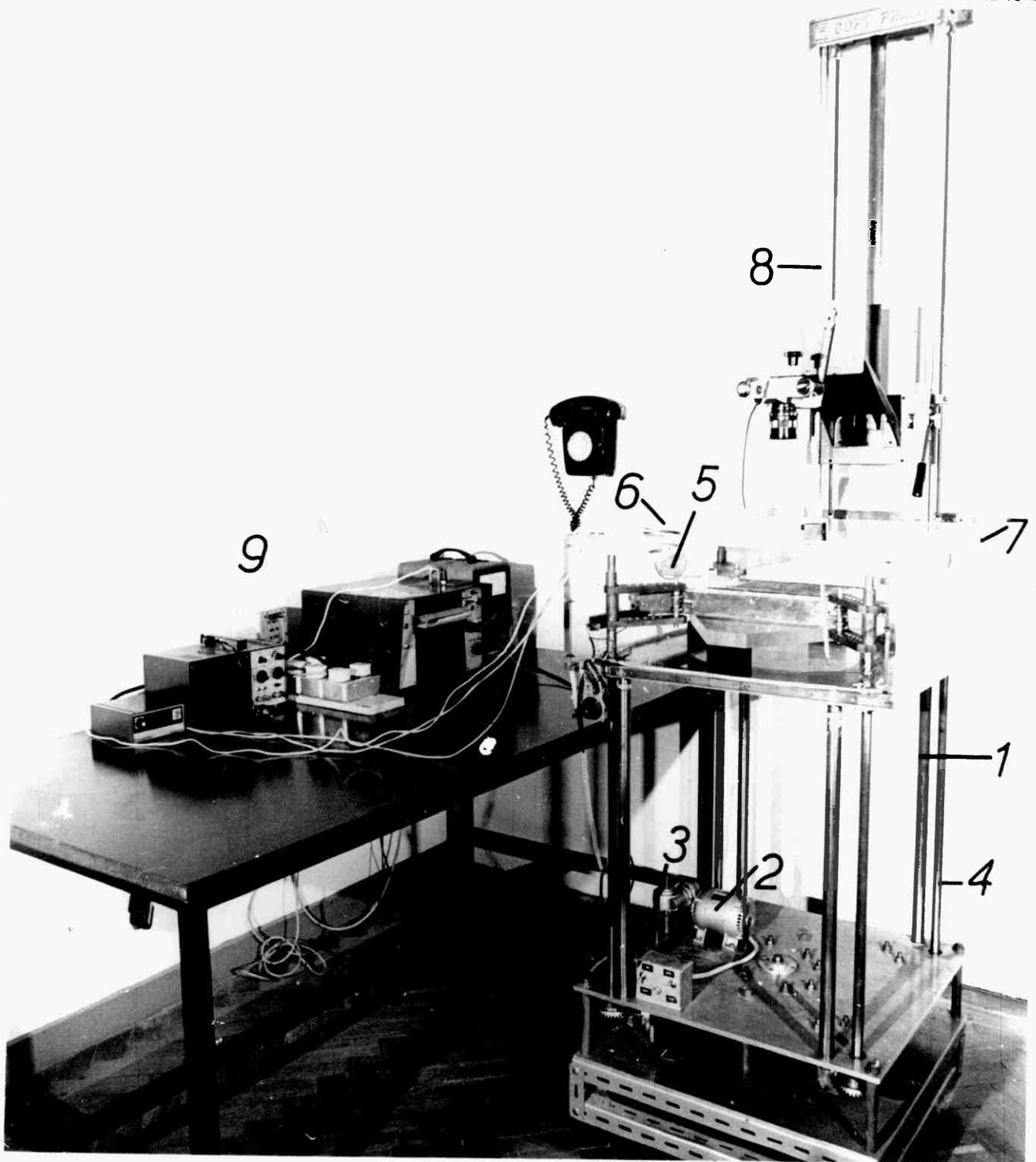


Fig.2.1.A

General view of the pure shear machine, showing the rigid frame (1), electric motor (2), gear box (3), drive-shafts (4), heating lamps (5), fan (6), deformation box (7), photographic copy-frame (8) and measurement and control systems (9). (after Cobbold,1973).

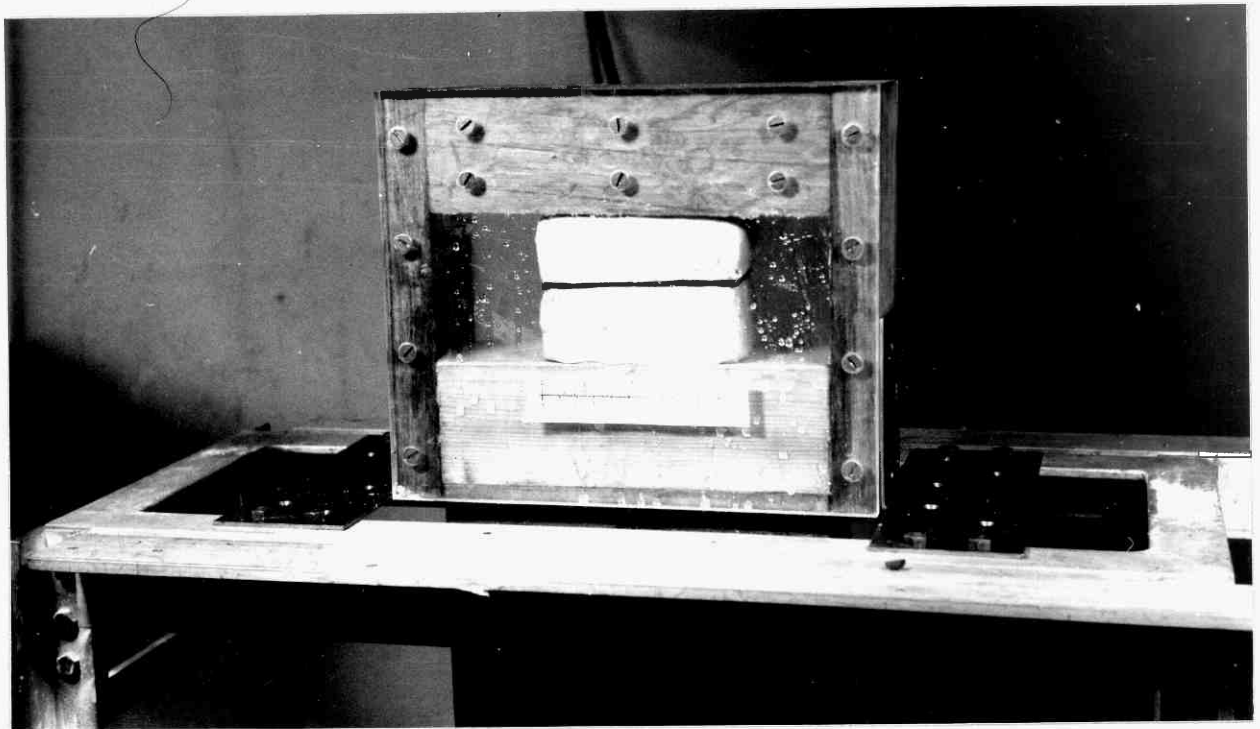
of experiment, X and Z varied, but Y was constrained to remain constant. For details see Appx. A.1.

The second apparatus used to compress single layer models of plasticine and putty (Models 11, 12, 13) was a wooden deformation box shown in fig. 2.1.B. The apparatus is described in detail in Appx. A.2.

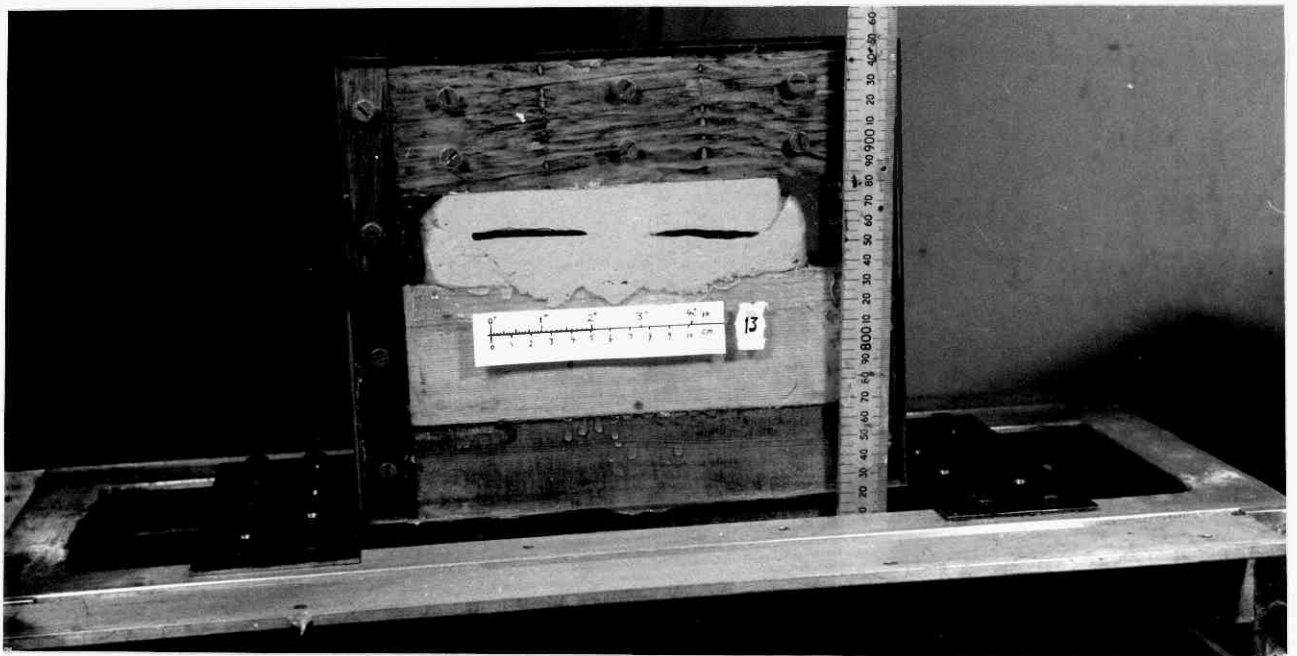
2.12 Modelling Material. Paraffin waxes with different melting points ( $50^{\circ}$ ,  $54^{\circ}$  and  $58^{\circ}\text{C}$ ) and in some experiments plasticine and putty were used as modelling materials. Paraffin wax was chosen because over the temperature and strain rate ranges that can be conveniently used in the apparatus, the rheological properties of wax vary between brittle and ductile. Paraffin wax can also undergo large deformation.

Rheological, chemical and some other properties of paraffin wax and plasticine are given in Appx. B.2. A simple method of preparing wax in the form of sheets, for use in multilayer experiments, was developed. The method, which is described fully in Appx. C.11, made use of the low specific gravity of wax by floating and cooling a thin sheet of molten wax on the surface of a water bath (Appx. C.11., fig. A.4.).

As a result of tests on the rheological properties of paraffin wax (Summers, 1979), the competence contrast of  $54^{\circ}\text{C}$  melting point paraffin wax layers ( $\sim 1\text{mm}$  thick) alternating with thin films of silicon grease can be estimated over a range of temperatures. For experiments that ran at  $36^{\circ}\text{C}$  the viscosity contrast is on average 1:500. Zalpon liquid soap can be used as



a



b

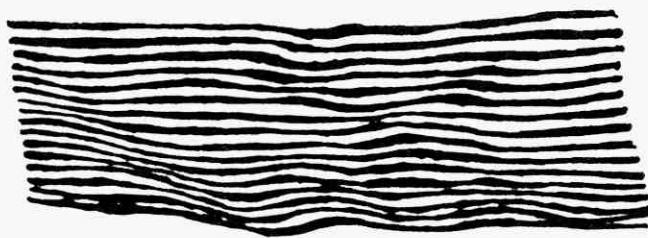
Fig. 2.1.B. The Wooden Deformation Box  
a. Before deformation  
b. At the end of deformation.

an interlayer lubricant but it is difficult to find out its viscosity because of the problem of it draining from the multi-layer during the initial clamping of a test block in the test apparatus.

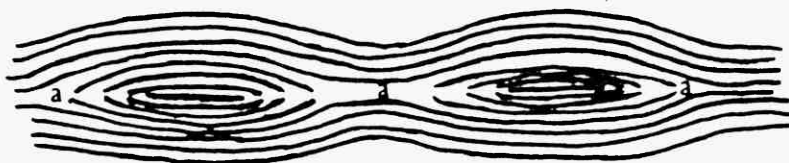
2.13 Number of Experiments. Altogether fifty-four experiments were performed. These are listed in Table 2.1. together with the major structures that developed in each model. Models 1 - 10 and models 38, 39, 40 were made up of plasticine. Three models (Mod. 11, 12, 13), which were deformed in the wooden deformation box, consisted of plasticine layer and putty or putty mixed with plasticine matrix. The remaining models were constructed using paraffin wax.

Most of the paraffin wax models had 150 layers. A few contained thicker (more than 1mm thick) layers, and these models had between 140 and 148 layers. Models 47 - 51 had between 138 - 148 layers.

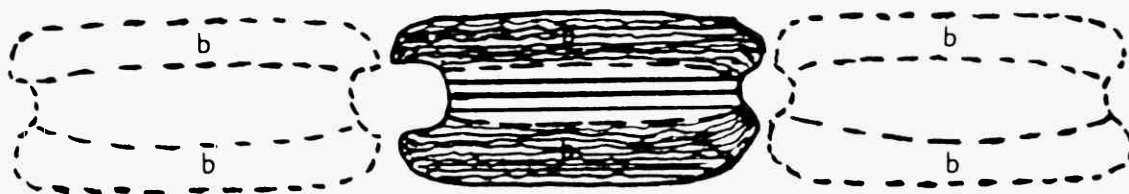
In the following sections of this chapter the different types of structures (fig.2.2) that were recognised in the deformed models will be discussed in turn together with the description of relevant selected models which best illustrate these structures.



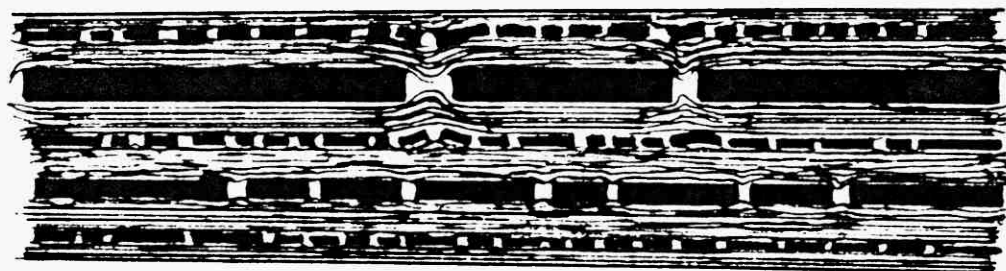
Type A. - Interlocked pinch-and-swell (or Internal boudins) structures



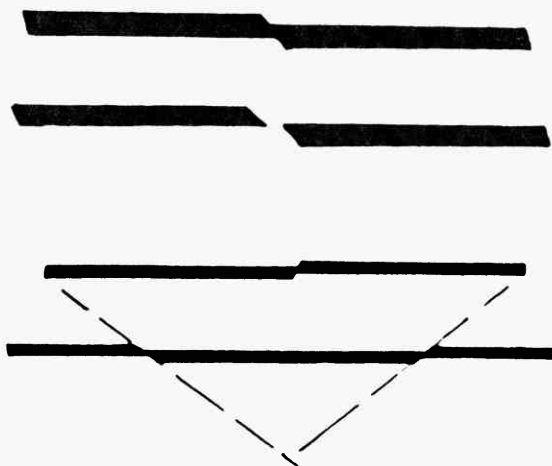
Type B-I. - Boudins initiated by in-built cross-shaped holes, (a) representing tension fractures.



Type B-II. - Boudinage generated by the formation of relatively incompetent (strain softened) bands, b, b.



Type C. - Classical Boudins formed in competent layers sandwiched by incompetent layers.



Type D - "Boudins" generated by shear fractures.

Table 2.1.a.

Model No.	Model Construction (Plasticine)	Temperature °C.	Strain Rate Sec <sup>-1</sup>	% Finite Bulk Shortening	Structures
1	Single layer 1cm thick Black Standard plasticine, matrix soft pink plasticine.	Room temp. 24-25°C	2.05 x 10 <sup>-4</sup>	37.3	Boudinage initiated by shear fractures (Type D)
2	Same as above	"	2.05 x 10 <sup>-4</sup>	37.3	D
3	Same as above, except layer .5cm thick.	"	2.05 x 10 <sup>-4</sup>	34	D
4	Same as above, except layer 2cm thick	"	2.05 x 10 <sup>-4</sup>	37	D
5	Same as above, except layer 1.5cm thick.	"	2.05 x 10 <sup>-4</sup>	34.8	D
6	Same as Model 1 except layer inclined at 45°.	"	2.05 x 10 <sup>-4</sup>	36	No boudins
7	Same as above, except layer inclined at 65° to p. stress direction.	"	2.05 x 10 <sup>-4</sup>		D
8	Same as above, except layer .5cm thick inclined at 60° to p.s.d.	"	2.05 x 10 <sup>-4</sup>	36.6	D
9	Same as Model 3, except layers are two separated by matrix.	"	2.05 x 10 <sup>-4</sup>	27.6	D
10	Same as above, except layers 1cm thick each	"	2.05 x 10 <sup>-4</sup>	30	D
11	Single layer .5cm thick in putty matrix	"	Models 11, 12, 13 Shortened at 3.5 x 10 <sup>3</sup> cm per sec.	47.5	D and C with necking.
12	Single layer .5cm thick black standard plasticine in soft pink & putty mix matrix	"		48	D
13	Same as above except layer .2cm thick	"		48.8	D

Table 2.1.b.

Model No.	Model Construction (Wax).	Temperature °C	Strain Rate Sec <sup>-1</sup>	% Finite Bulk Shortening	Structures
14	Multilayer of 54 <sup>0</sup> C Melting Point wax of 1mm thick each, lubricated by silicon grease.	36	$2.05 \times 10^{-4}$	40	A (good) B-II (good) D
15	Same as in 14	41	$2.05 \times 10^{-4}$	32	Homogeneous Flattening
16	Same as in 14	36	$2.05 \times 10^{-4}$	30	A (good) B-I, B-II, D
17	Same as in 14	36	$2.05 \times 10^{-4}$	36	A, B-I, B-II, D
18	Same as in 14 with 2 fractured layers in the middle	36	$2.05 \times 10^{-4}$	33	A, B-I, B-II, D.
19	Same as in 14 but multilayer (94mm thick) sandwiched between 2 isotropic blocks of weaker wax (28&30mm thick)	36	$2.05 \times 10^{-4}$	33	A and B-II
20	Same as in 19 with fractured layers in the middle of model.	36	$2.05 \times 10^{-4}$	31.5	A and B-I
21	Same as in 14 with 3 cross-shaped holes, 12 x 12mm in the middle of model	36	$2.05 \times 10^{-4}$	35	A and B-I (good)
22	Same as in 21 but with smaller holes.	36	$2.05 \times 10^{-4}$	31.5	B-I (good)
23	Same as in 21	36	$2.05 \times 10^{-4}$	40	A (good), B-I (good)
24	Same as in 18	40	$2.05 \times 10^{-4}$	30.5	Homogeneous Flattening
25	Same as in 14 but colouring 1 black layer every 5 yellow.	36	$2.05 \times 10^{-4}$	38	A, B-II(good) D.
26	Same as in 25 with liquid soap lubricant	36.5	$2.05 \times 10^{-4}$	38	A(good), B-II, D
27	Same as in 25 without lubricant	36.2	$2.05 \times 10^{-4}$	38	B-II (good), C, D.



Table 2.1.c.

Model No.	Model Construction (Wax)	Temperature °C	Strain Rate Sec <sup>-1</sup>	% Finite Bulk Shortening	Structures
28	Same as in 25 but black layers more competent (58°C M.pt wax) than yellow layers. No lubricant.	36	$2.05 \times 10^{-4}$	31	A, B-II (good) C, D.
29	Same as in 28 with liquid soap lubricant	36	$2.05 \times 10^{-4}$	31	A, C, D.
30	Single layer (10mm thick 58°C M.pt. wax) in multilayer matrix as 14 but all yellow	36	$2.05 \times 10^{-4}$	39	A, the layer slightly bent.
31	Two (5mm thick each) 58°C layers in a multilayer matrix as in 30.	36	$2.05 \times 10^{-4}$	Abandoned	due to technical failure.
32	Same as in 31	36	$2.05 \times 10^{-4}$	38.5	A(poor), B-I (poor), C,D.
33	Same as in 31 but competent layers are 3mm thick each.	36	$2.05 \times 10^{-4}$	40.5	A(good) B-I, B-II and minor folds on ends.
34	Single 58°C M.Pt. layer in an isotropic 54°C M.Pt. wax block	36	$2.05 \times 10^{-4}$	35	C (initiated by necking)
35	Same as in 34 but 2mm thick competent layer	37.5	$2.05 \times 10^{-4}$	33	Flow of matrix and homogeneous flattening of layer.
36	Same as in 14	36	$2.05 \times 10^{-4}$	34	A and homogeneous flattening.
37	Multilayer of 54°C M.Pt P. wax (101mm total thickness) embedded by 25mm thick 50°C M.Pt. p.wax on each end.	36.5	$2.05 \times 10^{-4}$	32.6	A, B-II.

Table 2.1.d

Model No.	Model Construction and materials	Temperature °C	Strain Rate Sec <sup>-1</sup>	% Finite Bulk Shortening.	Structures
38	Pinch-and-swell (4.5mm - 9mm thick) of standard white in an isotropic standard black plasticine matrix.	24-25°C	$2.05 \times 10^{-4}$	33	Shortening of pinch-and-swell layer by slip along shear faults
39	Same as in 38 but pinch to swell 3.5:6.5 thickness ratio.	24-25°C	$2.05 \times 10^{-4}$	31.5	Pinch-and-swell shortened by slip along shear faults
40	Black standard pinch-and-swell in special soft pink plasticine (2mm and 6mm thick) vaseline lubricant	24-25°C	$2.05 \times 10^{-4}$	34.6	Shortening of pinch-and-swell by slip along shear faults
41	58°C M.Pt. wax pinch-and-swell layer in 50°C isotropic matrix, vaseline lubricant	43.5 °C	$2.05 \times 10^{-4}$	31.5	Shortening by assymetric folding. Void formation and cusp-like structures at matrix interfaces.
42	Same as in 41	39 °C	$2.05 \times 10^{-4}$	31.5	Shortening by assymetric folding. Void formation and cusp-like structures at matrix interfaces.
43	Same as in 42 but pinch to swell 1.4:6.0	39 °C	$2.05 \times 10^{-4}$	30.5	Shortening by tight assymetric folding.
44	Same as in 43	35°C	$4.1 \times 10^{-5}$	32	Folded pinch-and-swell layer and tight assymetric folds in pinches.

Table 2.1.e.

Model No.	Model Construction (Wax)	Temperature °C	Strain Rate Sec <sup>-1</sup>	% Finite Bulk Shortening.	Structures
45	Same as in 44 but the pinch to swell width ratio is 2:1	34	$2.05 \times 10^{-4}$	28.6	Shortening by asymmetric folding
46	Same as in 45	38.3	$2.05 \times 10^{-4}$	33	Shortening by asymmetric folding
47	Multilayer of 3mm, 2mm, 1mm thick black (2,3,6 layers respectively, 54°C M.Pt. wax) competent layers in a layered (50°C M.Pt. orange 1mm thick each) matrix.	28.3	$2.05 \times 10^{-4}$	36	TYPE C structures, boudins initiated by tension fractures, later shear faults (zones) formed joining many of the tension fractures.
48	Same as in 47 but slower strain rate	28.3	$4.11 \times 10^{-5}$	36.3	C as in 47
49	Same as in 47	30	$2.05 \times 10^{-4}$	37	C as in 47
50	Same as in 47	32	$2.05 \times 10^{-4}$	37.3	Mostly homogeneous flattening.
51	Same as in 47 but the incompetent layers coloured white	28	$2.05 \times 10^{-4}$	36	C as in 47
52	Same as in 14	36	$2.05 \times 10^{-4}$	37	A
53	Same as in 23 but orange instead of yellow	36	$2.05 \times 10^{-4}$	36.4	A and B-I
54	Same as in 23		$2.05 \times 10^{-4}$	35.6	B-I

2.2 TYPE A STRUCTURES - INTERLOCKING PINCH-AND-SWELL (OR  
INTERNAL BOUDINS) STRUCTURES

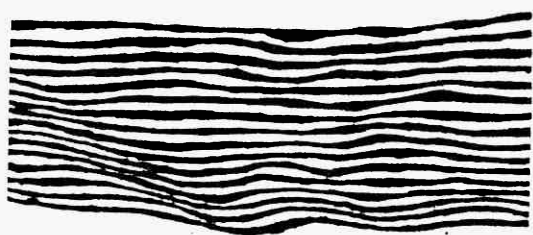


Fig. 2.3.A.



Fig. 2.3.B.

The type A structure is a combination of a network of conjugate normal kink bands and interlocking pinch-and-swell structures. When viewed closely (fig. 2.3.B.) the individual layers are seen to be deformed into triclinic pinch-and-swell structures. In some experiments the early interlocked pinch-and-swell structures seem to be symmetric, but they immediately change into triclinic as deformation proceeds. The alignment of the pinches in adjacent layers gives rise to the line (plane in 3D) which define the normal kink band (or shear zone). These kink bands may form in conjugate sets and initially form at around  $60^\circ$  to the principal compression direction ( $\sigma_1$ ).

#### Model 14

Model 14 consists of alternating black and yellow  $54^\circ\text{C}$  melting point paraffin wax layers each approximately 1mm thick (fig.2.4.A). Each layer was smeared with a thin (about  $1.6 \times 10^{-3}$  mm thick) film of silicon grease (supplied by N.V. Dowcorning S.A., Seneffee, Belgium) to allow frictionless slip between the layers.

Five minutes after the start of compression, individual layers near the "top"\* and "bottom"\* of the model started forming pinch-and-swell structures. After another minute certain pinches (necks) in the various layers deflected in such a way as to form a shear zone inclined at  $30^\circ$  to the layering. Each individual pinch-and-swell layer interferes with the adjacent layers, the swells of one layer favouring the development of a neck in the adjacent layer. A swell in one layer is often seen to cause a deflection of a neck in an adjacent layer. Photographs in fig. 2.4.B, C show Model 14 at 27% and 40% bulk shortening, respectively.

\* "top" and "bottom" refer to photographic face.

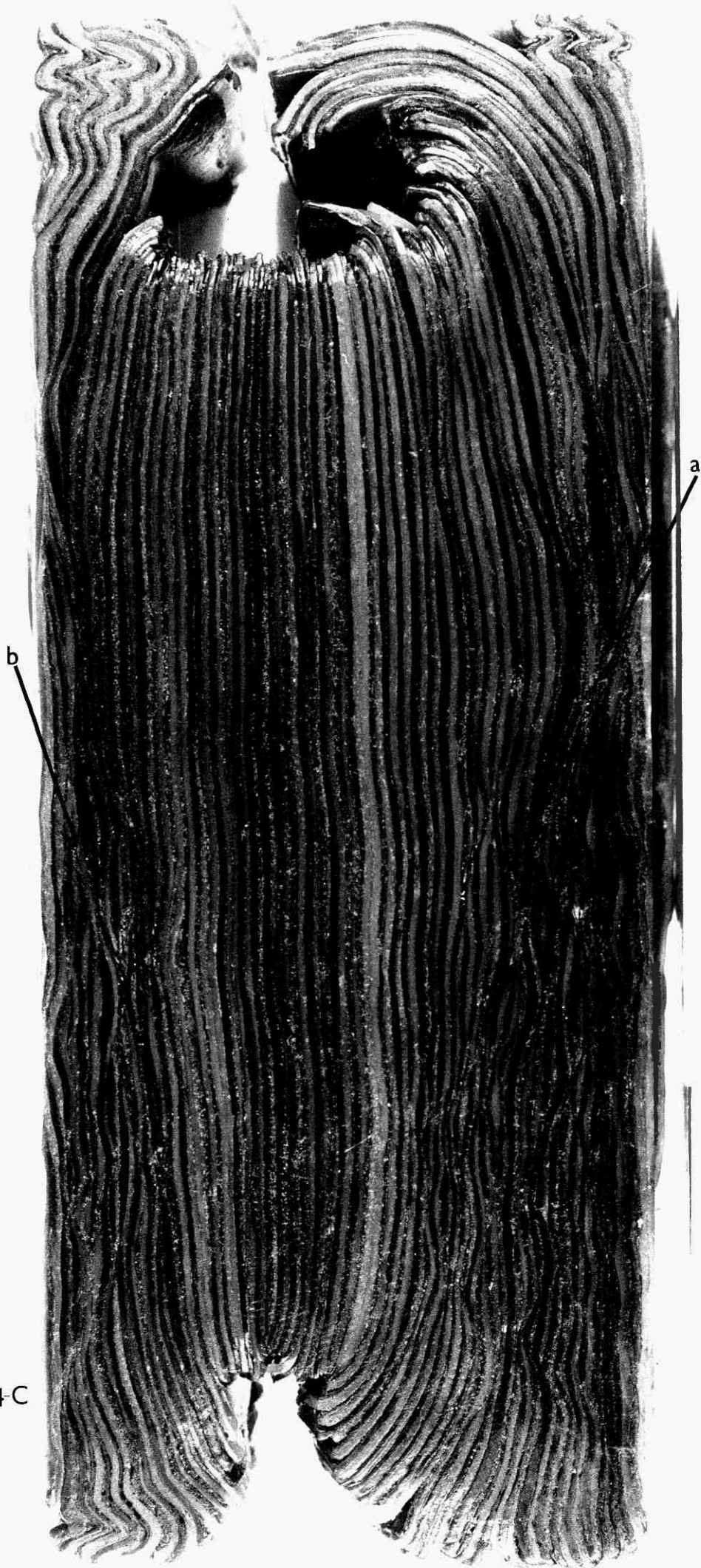
Fig. 2.4. Three stages in the progressive deformation of  
Model 14.

A - 0.0%

B - 27% (% bulk shortening)

C - 40%





*[Faint, illegible handwritten text, possibly bleed-through from the reverse side of the page.]*

Fig.24 C

.4.C



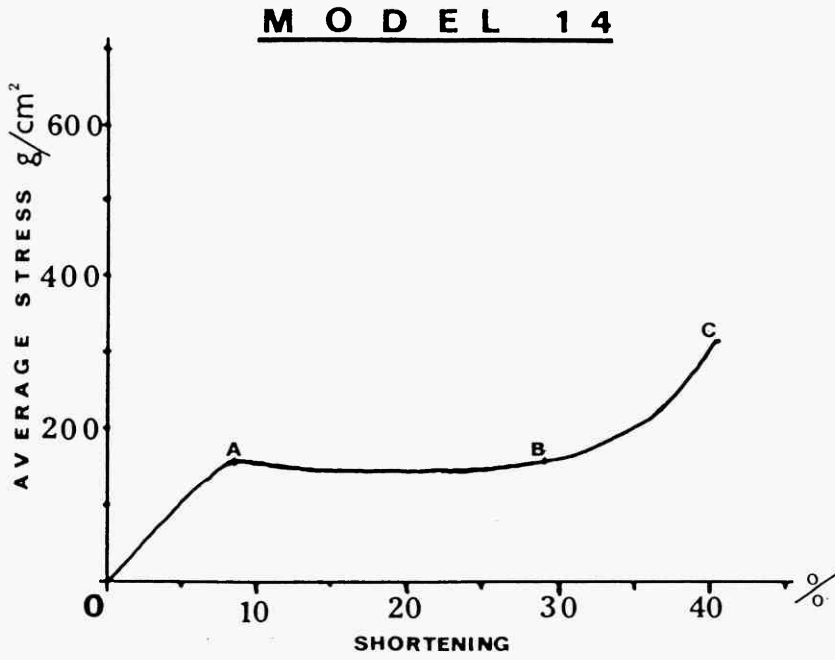


Fig. 2.4.D

Fig. 2.4.D. Plot of the average bulk shortening against the average stress in the progressive deformation of Model 14. A-C correspond to the three photographs in fig. 2.4 A-C.

The major shear zone (fig. 2.4.C.a) is at  $25^{\circ}$  to the layering when bulk shortening reached an average of 27% and at  $22^{\circ}$  to the layering at the end of the experiment after an average bulk shortening of 40%. The obtuse angle between conjugate shear zones was  $127^{\circ}$  when the shortening was 27% and  $132^{\circ}$  when the shortening reached 40%.

The area in the central part of the model (fig. 2.4.C) is less deformed than the margins. This relatively undeformed region is 26mm thick after 40% bulk shortening. This area which flattened homogeneously acted as a relatively competent band between two strain softened incompetent bands in which pinch-and-swell structures and normal kink bands developed. The relatively incompetent bands flowed around the competent bands, as shown in figures 2.4.B. and 2.4.C.

Local shortening within the model can differ considerably from the bulk shortening. For example, at 27% bulk shortening the "top" 25 layers (fig.2.4.B) had shortened by 33% and the "bottom" 20 layers by 31%. Similarly at 31.5% bulk shortening, the "top" 25 layers have undergone 36.7% shortening and the bottom 20 layers 34% shortening. At the end of the experiment the bulk shortening was 40%. However, the upper 25 layers had shortened by 45.5% and the less deformed area in the central part shortened by only 25%.

Fig. 2.4.D shows the plot of the average bulk shortening against the average stress during the progressive deformation of Model 14. The stress is seen to increase until the appearance of the first pinch-and-swell structures (fig. 2.4.D.a). It then drops

slightly and the deformation continues at an approximately constant stress until about 30% (fig. 2.4.D.b) shortening has occurred when the 'locking up' processes start. These 'locking up' processes are mainly caused by restraints imposed by the experimental rig, for example, the confining barriers begin to resist the flow of the less competent bands of the model. As a result minor folds form and the incompetent material is deflected in such a way as to make it difficult for the more competent band to flow. The result is that the stress must be increased to maintain a constant strain rate.

#### Model 23

Model 23 consists of black and yellow 54°C melting point paraffin wax layers, each ~1mm thick. Three cross-like holes were cut in the central part of the model (fig. 2.5.A). After a bulk shortening of 5% ( $\dot{\epsilon} = 1 \times 10^{-4}$ ), the layers adjacent to the holes began to flow to fill the gaps (fig. 2.5.B, C), and as deformation continued the gaps were gradually filled. Infilling was complete after 14% shortening. During the deflection of the layers towards the gaps lubricant also flowed towards the gaps.

After a bulk shortening of 8% pinch-and-swell structures developed in the individual layers at the bottom of the model (fig.2.5.C). As in Model 14, these structures first developed near the edge of the piston-face and then propagated towards the central part of the model. Because of the irregularities, that is, gaps built into the model and therefore the formation of the type B-1 structure in the central region of the model, type A structures were able to develop almost everywhere in the model (fig.2.5.F.G).

Fig. 2.5. Six stages in the progressive deformation of Model 23.

A - 0.0%

B - 5%

C - 8% (% bulk shortening)

D - 10%

E - 16%

F - 40%

G (Overleaf) - enlargement of the whole model at 40% finite  
bulk shortening.

H (page 142) - enlargement of the upper central part of fig. 2.5.G.

N.B. not all the model is shown in fig. 2.5A-F

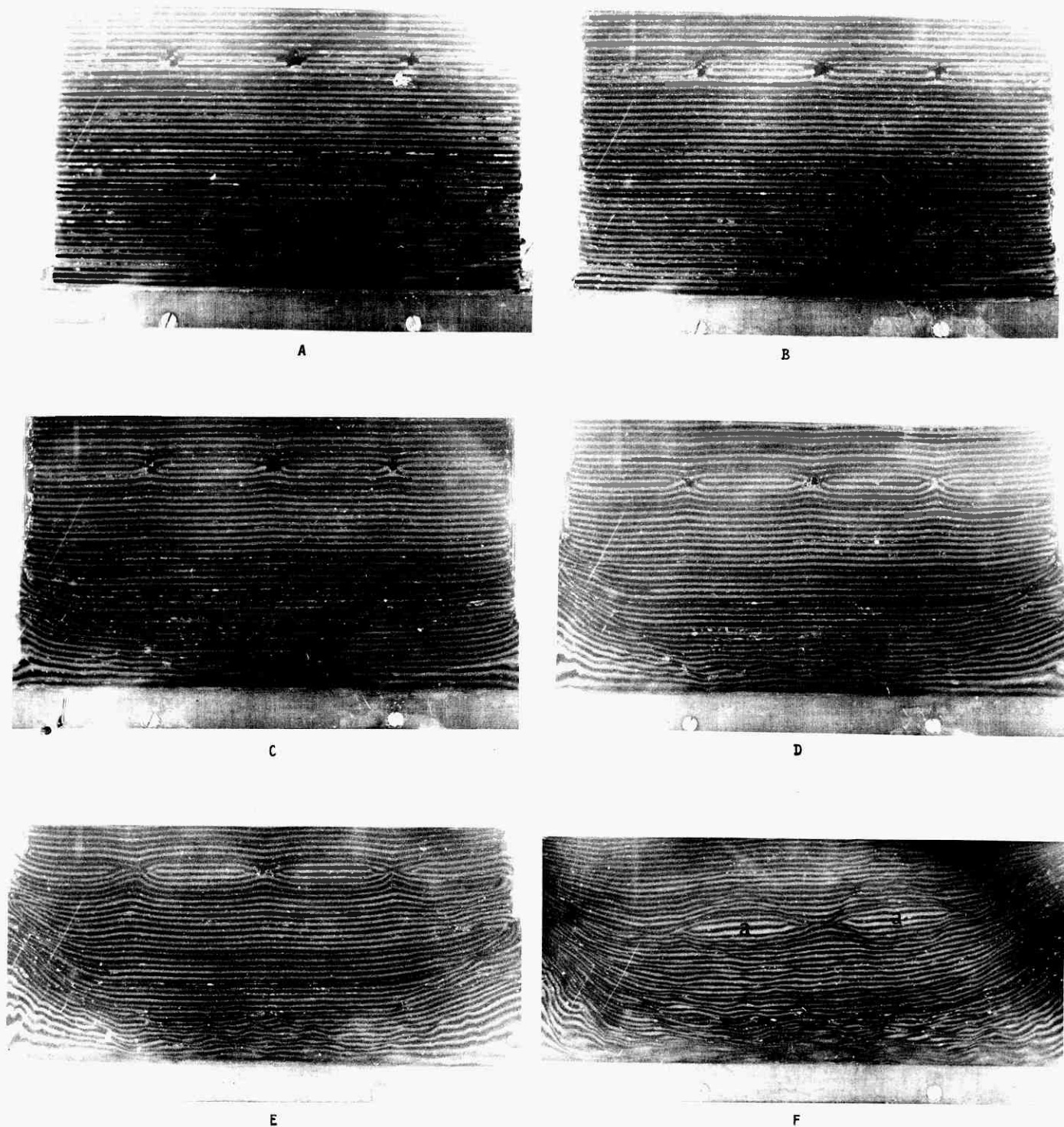
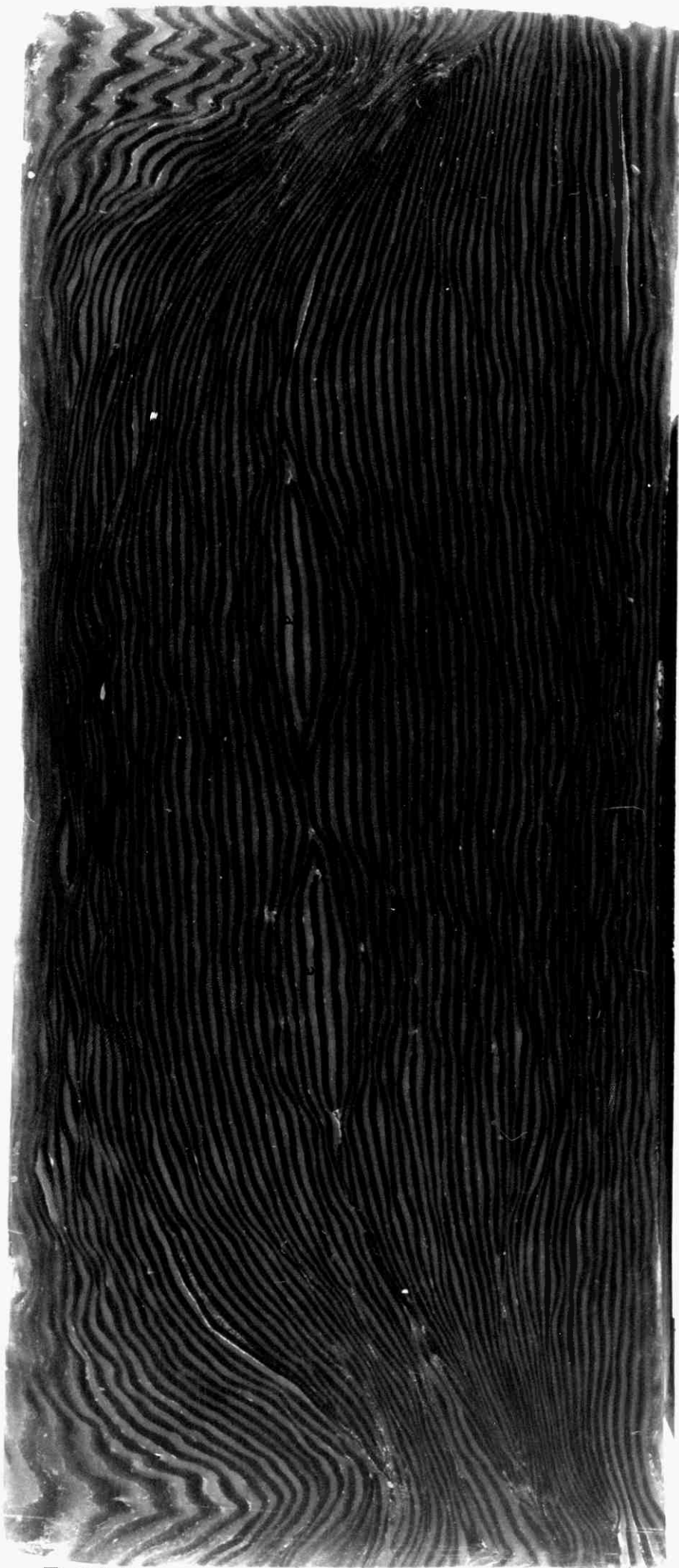


**FIG. 2.5** SIX STAGES IN THE PROGRESSIVE DEFORMATION OF MODEL 23. THE % SHOWN IS BULK SHORTENING.



23

Fig 2.5-G

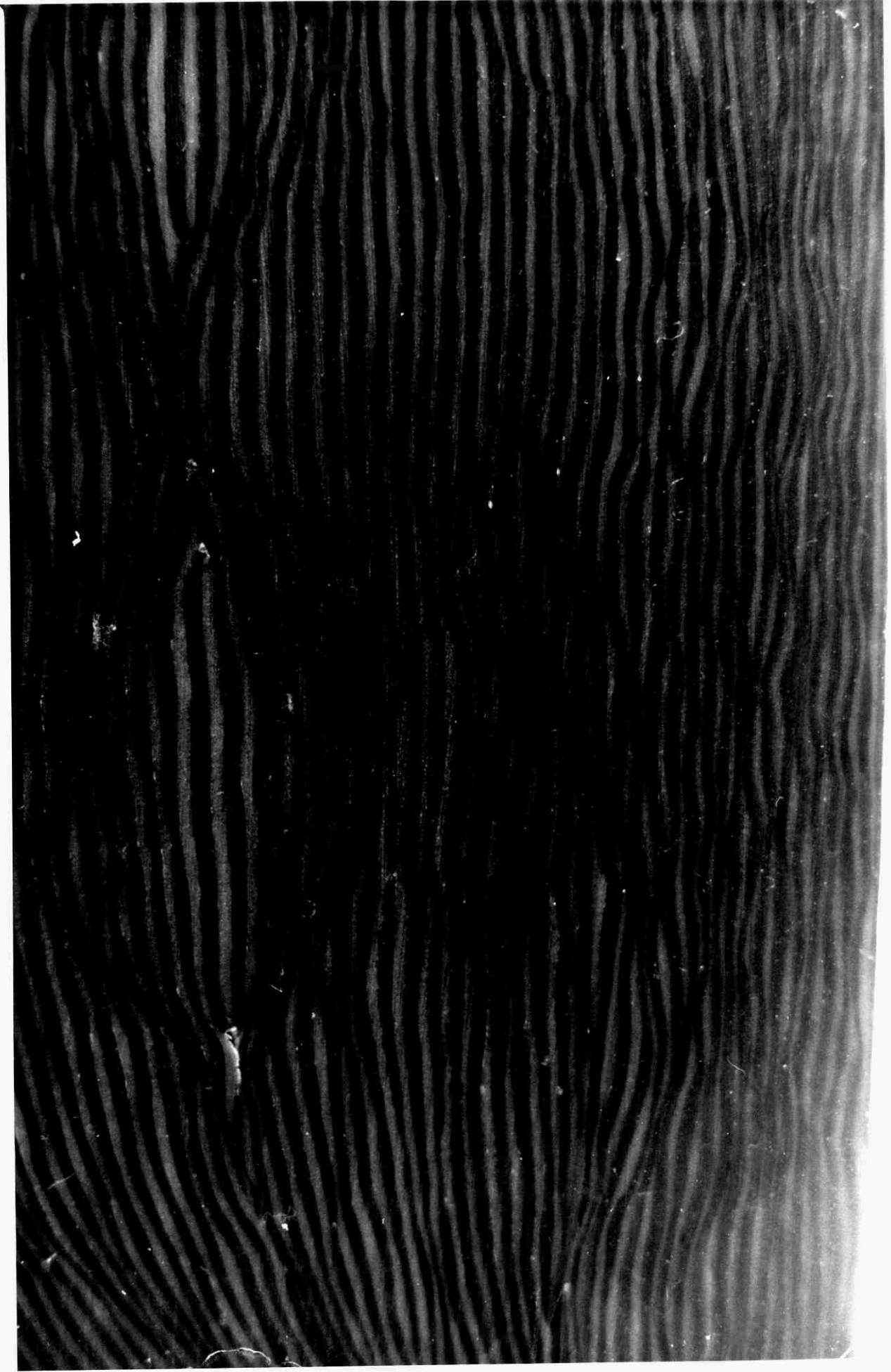


Fig.2-5-H

•  
G  
G  
•

At 40% bulk shortening only a small area of the model remained unaffected by one or other of type A and B1 structures.

The type B1 boudins were extended at both free ends of the model and eventually reached the barriers which caused the structures to fold (fig. 2.5.D-F).

The angle of alignment of the deflected pinches (i.e. shear zone) at 10% bulk shortening (21.5% local shortening) was between  $25^{\circ}$  and  $28^{\circ}$  to the layering ( $65^{\circ}$  -  $62^{\circ}$  to  $\sigma_1$ ) (fig. 2.5.D). This angle rotated towards the layering by about  $10^{\circ}$  to  $20^{\circ}$  as the shortening increased.

The gaps between type B1 boudins acted as zones of initiation from which normal kink bands (shear zones) initiated. These normal kink bands, which appeared at 26% bulk shortening, range in orientation between  $40^{\circ}$  -  $46^{\circ}$  to the layering. By the time the gaps were closed the zone at the "bottom" of the model, where type A boudins were forming, had reached a shortening of an average of 28%, twice the bulk strain. At the end of the experiment (46% bulk shortening) this zone had been shortened by 51%.

### 2.3 TYPE B-1 STRUCTURES

The second most important structures to develop in the experiments are called type B-1 structures. They were mentioned briefly in the description of Model 23 and are lenticular or lozenge-shaped boudins generated at a specific locality by building into a model neck region (gaps). The introduction into the model of a band of layers which are cut to create voids 1.2cm long (fig. 2.5.A)



caused the adjacent layers in the matrix to flow into the gap when the model was deformed.

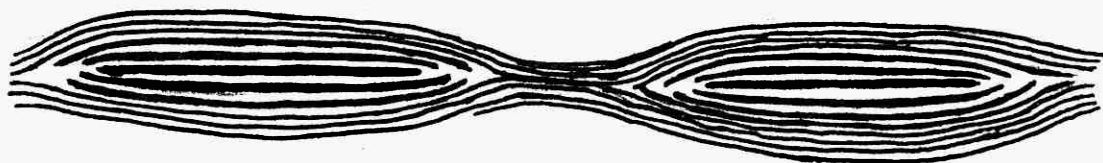


Fig. 2.6.A

As can be seen in fig. 2.6.A the layers inside the "boudins" are thicker than the outer layers. It is thought that these layers remained thicker, that is relatively unstretched (1mm thick), because the layers that flowed into the gap acted as a barrier preventing the "boudin" extending.



Fig. 2.6.B

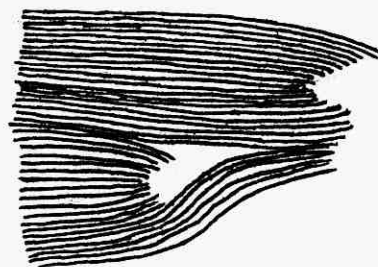


Fig.2.6.C

Type B-1 structures also developed in models in which no gaps were introduced (fig. 2.6.C). These structures were formed because a small gap was created during the experiment as a result of different rates of stretching in different bands of layers. The layers

adjacent to this gap are deflected into it creating a type B-1 'boudin'. Breaks in individual layers may also cause type B-1 boudins to form as shown in fig.2.6.B.

### Model 21

This model is identical to Model 23 in construction. They both had 3 cross-shaped holes and were deformed at the same temperature and strain rate. However, Model 21 was deformed until the bulk shortening reached an average of 35% whereas in Model 23 it reached 40%. Model 21 has all the major structures that are in Model 23 except the micro-folds. Because of this the B-1 type structures have not been obliterated and remnants of the original gaps can still be seen (fig. 2.7).

The layer of B-1 boudins is bent. The bending started at  $\approx 6\%$  shortening when an area at the centre of the bottom edge of the model began to develop type A structures. It was this localised zone of strain softening that caused the central part of the model to be deflected. After  $\approx 9\%$  bulk shortening type B-1 structures started to appear at positions 1 and 3 of the model (fig. 2.7). A zone of type A structures initiated by the separation of the two central type B-1 boudins formed at an angle of  $\approx 45^\circ$  to the layering at positions 2 fig. 2.7. The type A structure (shear zone) mentioned above and another shear zone at a lower angle to the layering form the boundary of type B-1 structure of the second kind (fig. 2.7(3)).

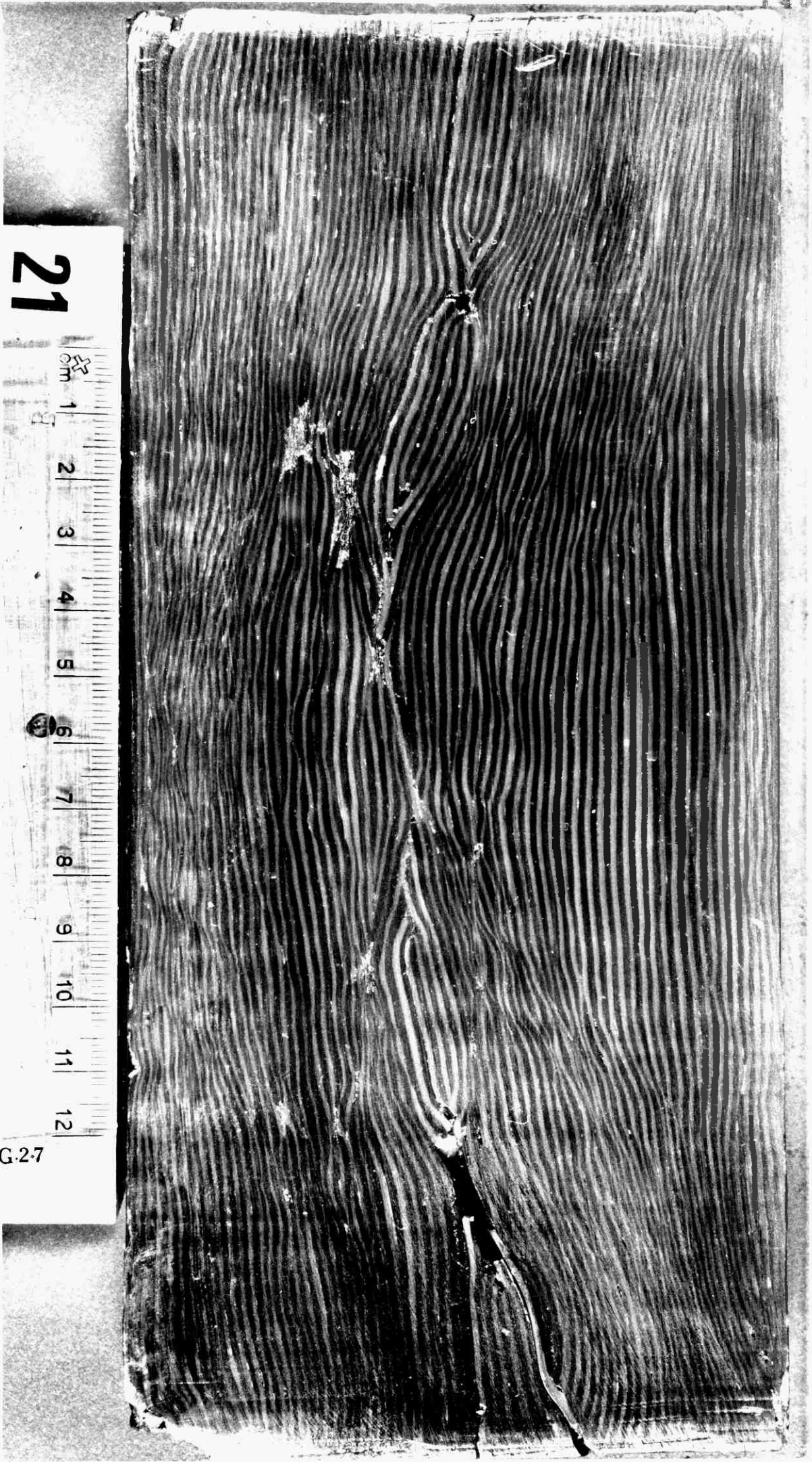
Some areas of the model deformed homogeneously (fig.2.7(4)).



21

cm 1 2 3 4 5 6 7 8 9 10 11 12

FIG.27



21

cm

1

2

3

4

5

6

7

8

9

10

11

12

FIG. 27

However, type A structures would most probably have formed here had the deformation continued (c.f. experiment 23).

During the deformation lubricant from between the layers and between the top plate and the model filled the gaps. However, the lubricant was squeezed out and displaced towards the ends of the model as the matrix flowed in.

#### 2.4 TYPE B-II STRUCTURES

The boudin structures that form when a relatively undeformed area is isolated in a model in which there is no competence contrast between the layers as in Model 14, are referred to as type B-II.

These structures result from the localisation of type A structures in specific horizons within the model. Once the type A structures have developed the horizons containing them deform more easily than horizons in which they do not occur. The model becomes essentially one containing relatively competent and relatively incompetent horizons and boudins may develop (fig.2.8) in the relatively competent horizon in the same way as they do in a competent single layer.

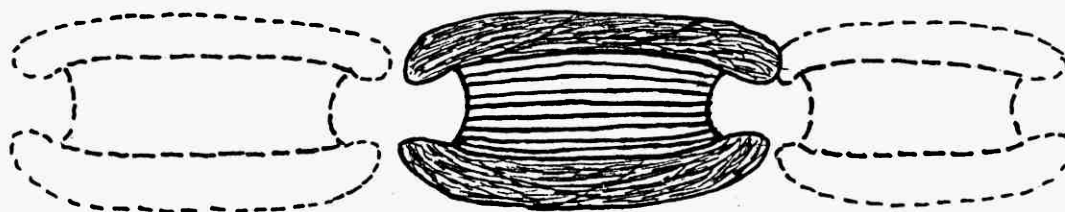


Fig. 2.8



The boudins are barrel-shaped and are often in the central part of the models (fig.2.4.C, 2.9). Type B-II structure also develops in models made up of alternating competent and incompetent layers of the same thickness, for example, Models 27, 28 and 29. Fig.2.9 shows the progressive development of B-II type boudins in such a model.

#### Model 28

The model was made up of alternating yellow layers of 54°C melting point paraffin wax with alternating black and plain (colourless) layers of 58°C melting point paraffin wax, all the layers having the same thickness, 1.0 - 1.1mm.

After 16 minutes a competent layer near the piston developed embryonic necks and broke. As deformation continued more and more competent layers near the 'top' and 'bottom' of the model necked and separated. The incompetent matrix layers flowed into the gaps between the competent layer and deflected the boudins (fig.2.9G). There is a very significant, relatively undeformed area in the central part of the model. After an average bulk shortening of 38.3%, the incompetent layers in the relatively undeformed area had elongated to 168mm (from 152mm), an increase of 10%, while the unbroken competent layers had elongated to 157mm, an increase of only 3%. This area covers ~45% of the whole deformed model at 38.3% bulk shortening. Different stages of necking and fracturing of the competent layers can be observed in this relatively undeformed area (fig. 2.9.C). The resistance offered by the confining plates to extension of the two strain softening zones that developed near

Fig. 2.9. Seven stages in the progressive deformation of  
Model 28.

A - 0.0%

B - 10%

C - 13.5%

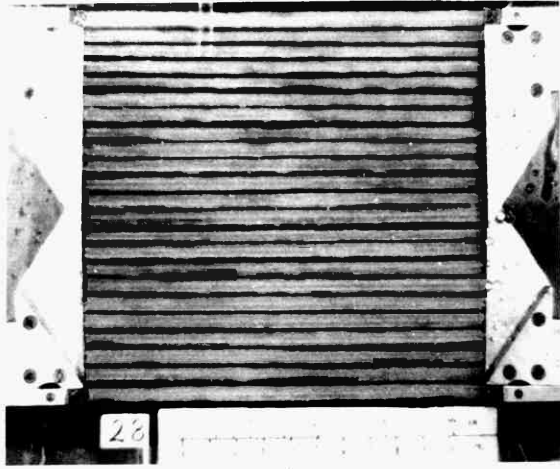
D - 17.6% (% bulk shortening)

E - 25%

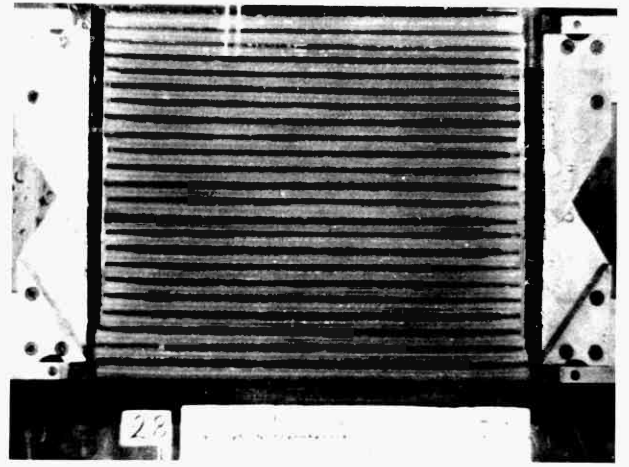
F - 31.3%

G - 37.5%

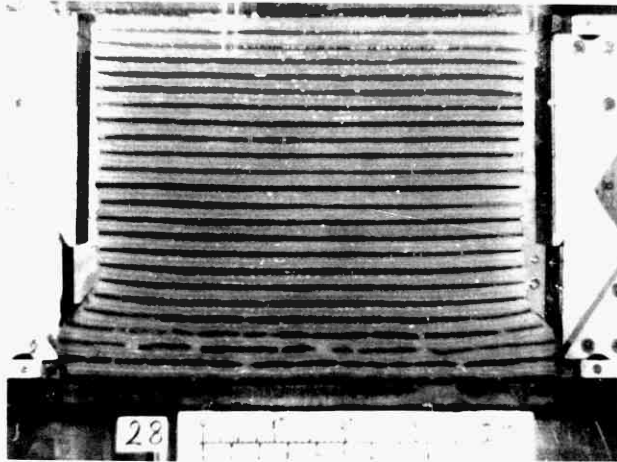
H (Overleaf) - an enlargement of fig. 2.9.G



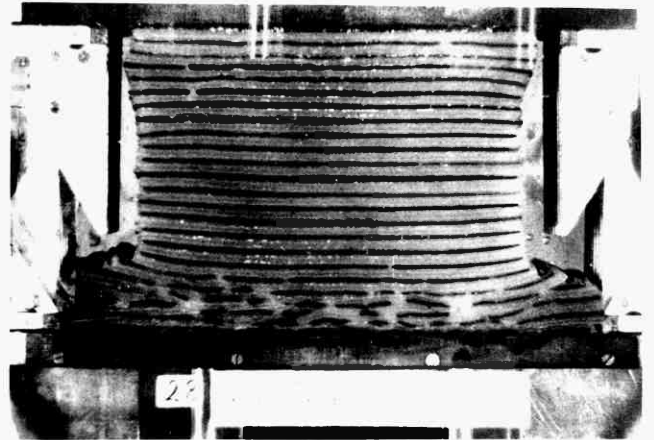
A



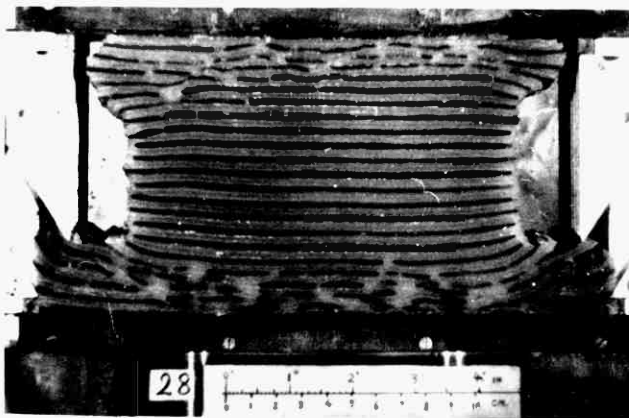
B



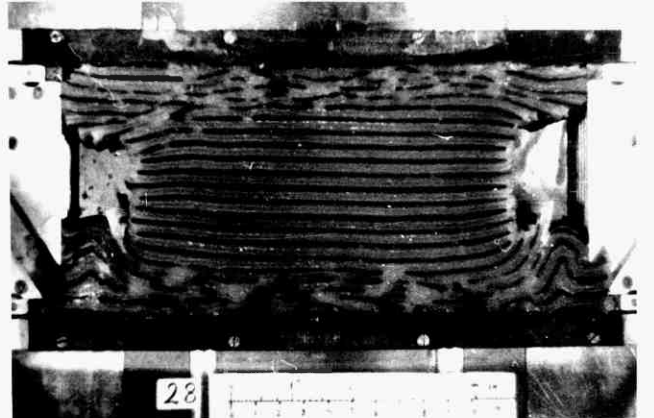
C



D



E



F

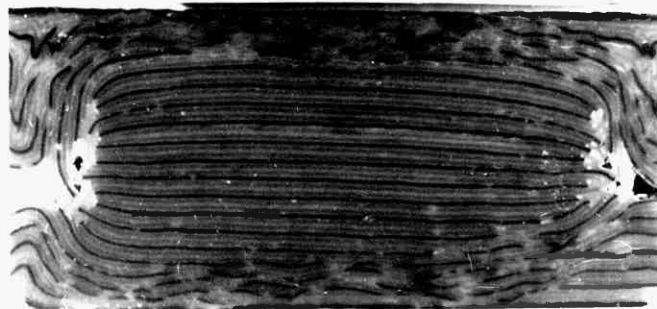
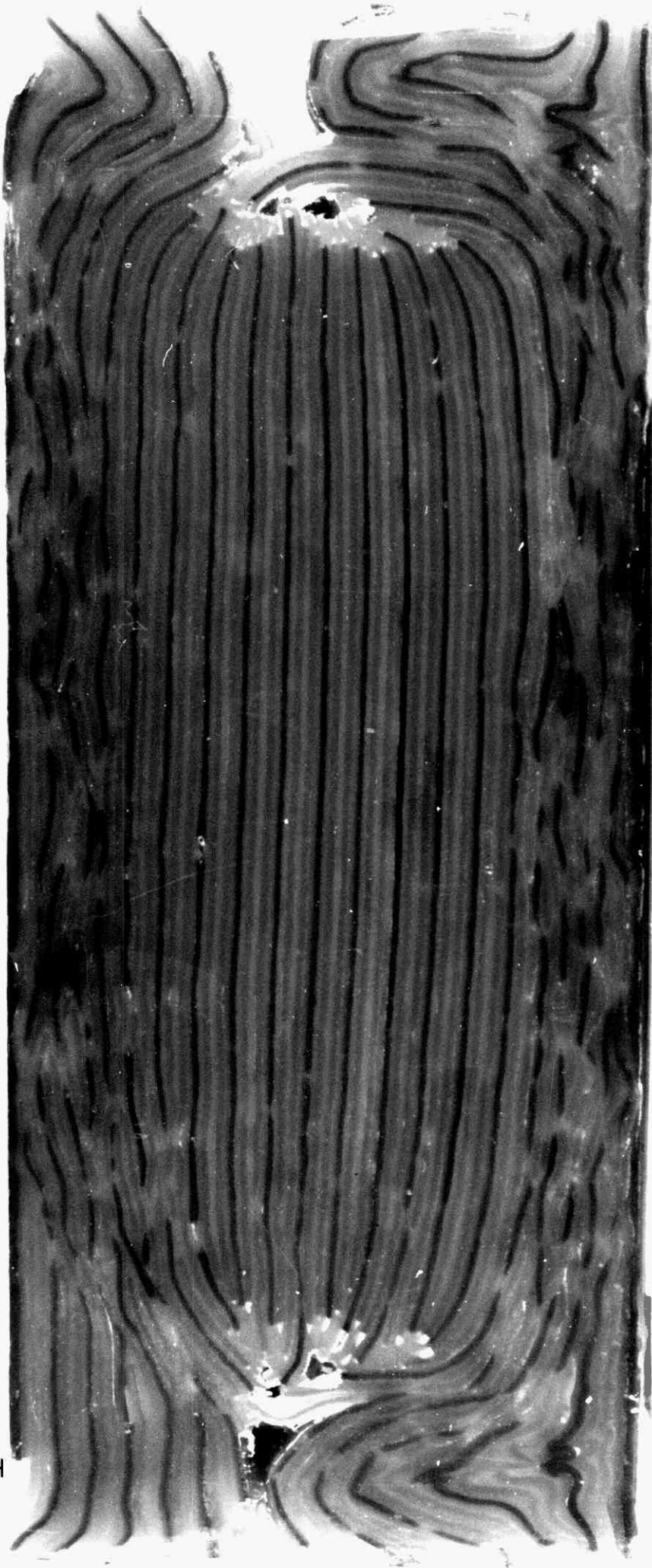


Fig.29

G





H-62

Handwritten text, possibly a title or description, oriented vertically on the right side of the page. The text is faint and difficult to read, but appears to contain several lines of characters.

2.8

FIG. 29-H

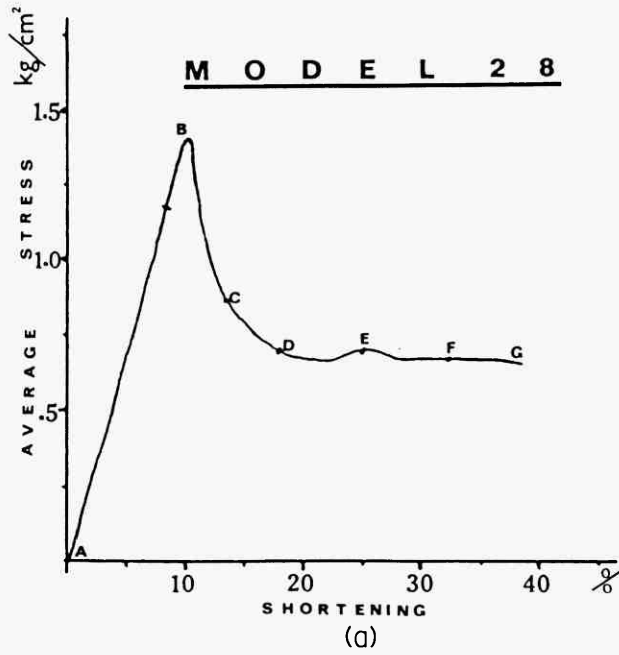
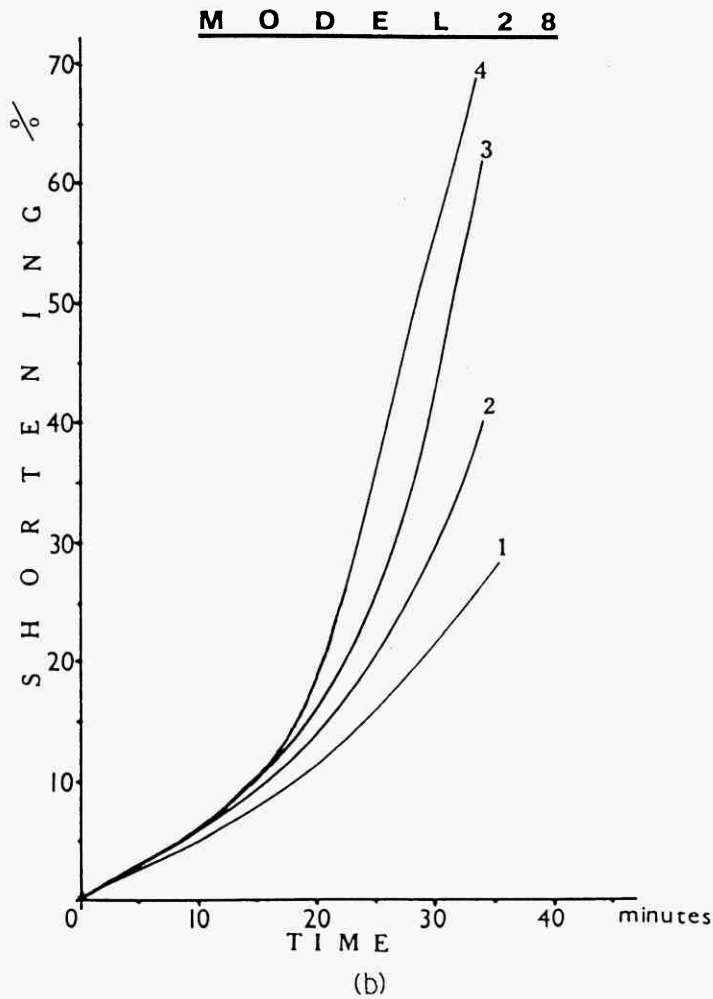


Fig. 2.10 (a) Plot of the average stress against the bulk shortening in the progressive deformation of Model 28. A-F correspond to the photographs in fig. 2.9 A-F. (b) Plot of percent shortening against time of deformation. Curves 1-4 show the variation of strain in different parts of the model during the deformation.



the piston caused microfolds to develop at the ends of these zones (fig. 2.9. F,G).

The strain in the strain softened areas is much higher than the bulk shortening. Fig. 2.9 shows seven stages in the progressive deformation of Model 28. The variation of average stress during this progressive deformation is shown in fig. 2.10.A., where the seven stages (A-G) in fig. 2.9 are also indicated. On this graph (fig. 2.10.A.) bulk shortening has been plotted against average stress. The stress increased steadily until one of the competent layers failed (point B in fig. 2.10.A.), as can be seen in fig. 2.9.B. Fig. 2.10.B shows the variation of strain in the 'upper' and 'lower' 25 layers with the bulk shortening of Model 28. The variation in strain between the upper and lower 25 layers is not very much, for example, after 10 minutes the bulk shortening was 13.5% (curve 2) while the lower 25 layers shortened by 18.3% (curve 4) and the upper by 17.5% (curve 3). Curve 1 shows the strain in the relatively undeformed area. At a bulk shortening of 37.5% the lower 25 layers shortened by 67.8% and the upper 25 layers by 59.8% while the central part of the model shortened only by ~24%.

## 2.5 TYPE C STRUCTURES

Type C is the well-known boudinage structure that is formed in models where a relatively competent layer is sandwiched between layers that are relatively incompetent. In the multi-layer experiments where the competent layers were thicker or as thick as the incompetent layers, the competent layers fracture and the incompetent layers flow into the gap formed between the separating boudin blocks.

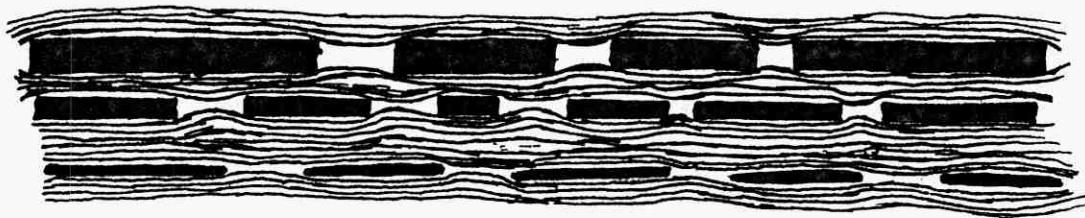


Fig.2.11.A.

As shown in fig. 2.11.A. the boudins that form in a multilayer can either be rectangular or lenticular (as in Model 28 (fig.2.9)). The corners of the former have not been affected by the inflow of the incompetent matrix into the gaps. Lenticular boudins may be formed from rectangular boudins as the inflow of matrix deforms the ends of the rectangular block (see fig. 2.13.H) or they may result from the separation of original pinch-and-swell structures (fig. 2.9-H).

#### Model 47

Model 47 is a multilayer made up of layers of relatively competent, 54°C M.pt.p.\* wax of different thickness coloured black or brown (dark), separated from each other by 4, 1mm thick 50°C m.pt.p. wax coloured orange (light). The thickness of the competent layers starting from the bottom is four 1mm (one black and three brown), one 3mm, three 1mm (one black and two brown), one 2mm, three 1mm (one black and two brown), one 2mm, three 1mm (one black and two brown), one 2mm, three 1mm (one black and two brown), one 3mm and three 1mm (one black and two brown).

In this relatively faster strain rate ( $2.05 \times 10^{-4}$ ) experiment, it took 27 minutes before tension fractures in the competent layers developed (7.3% bulk shortening). The tension fractures at this stage appeared in most of the 1mm thick competent

\* M.pt.p. - melting point paraffin

layers. Tension fractures appeared in 2mm and 3mm layers immediately after the 1mm layer fractured (between 7.5% - 8% shortening). Fractures were more closely spaced in the thinner layers than thicker layers. As deformation continued the number of fractures increased in all the competent layers (fig.2.12.B). The incompetent matrix flowed into the space created by the separating of boudins. During the filling of the gap between boudins in the 3mm and 2mm layers, the 1mm competent layers bent towards the gaps following the matrix. The gaps in the 2mm and 3mm layers seemed to affect the spacing (breaking) pattern of 1mm layers and the familiar ellipse-shaped cross section view of boudinage developed. (fig. 2.11.B and 2.12.C).

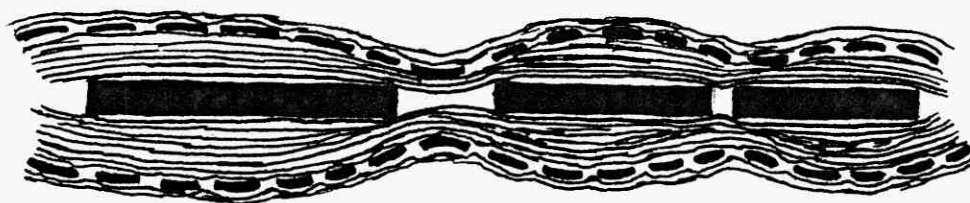


Fig. 2.11.B.

The gaps also controlled the initiation of shear zones that follow the deflection of 1mm boudins and the alignment of tension fractures in the thicker layers. The shear zones initiated at  $\sim 45^\circ$  to the layering and soon rotated towards the layering as deformation continued. Because of the shear some 1mm boudins became inclined at  $45^\circ$  to the layering. The shear zones also displaced and fractured various segments of the 1mm layers.

Five stages in the progressive deformation of Model 47

Fig. 2.12. Five stages in the progressive deformation of  
Model 47.

A - 0.0%

B - 8.3%

C - 16.1% (% bulk shortening)

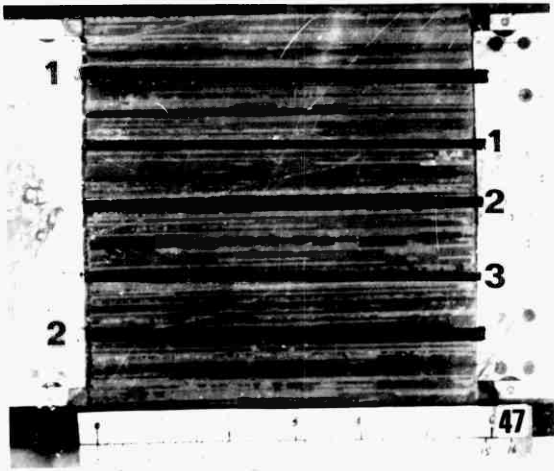
D - 28.7%

E - 36.1%

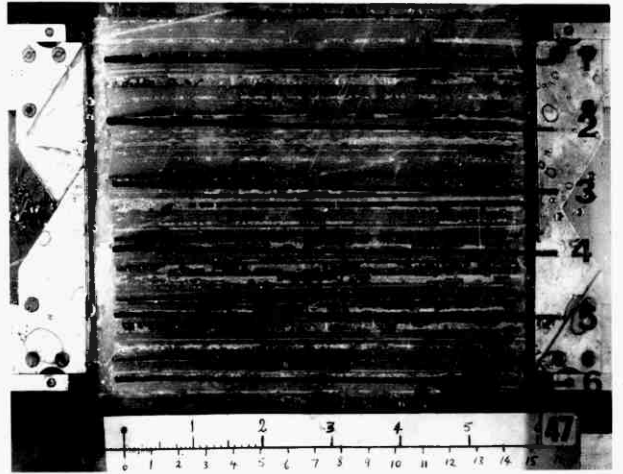
F - Enlargement of the central part of fig. 2.12.E

G (Overleaf) - Enlargement of fig. 2.12.E.

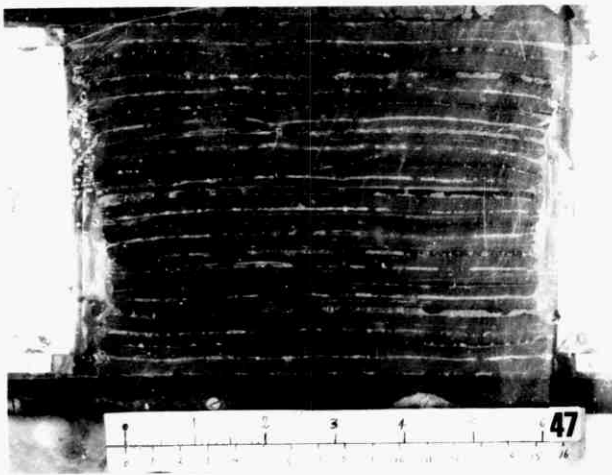
H (see page 157b) - Enlargement of the central part of  
fig. 2.12.G.



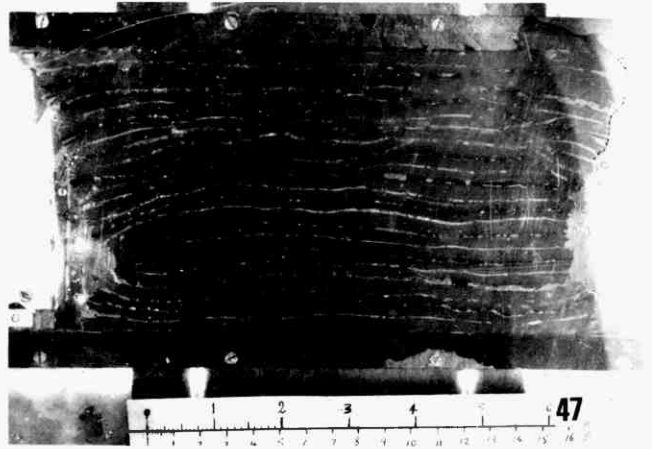
A



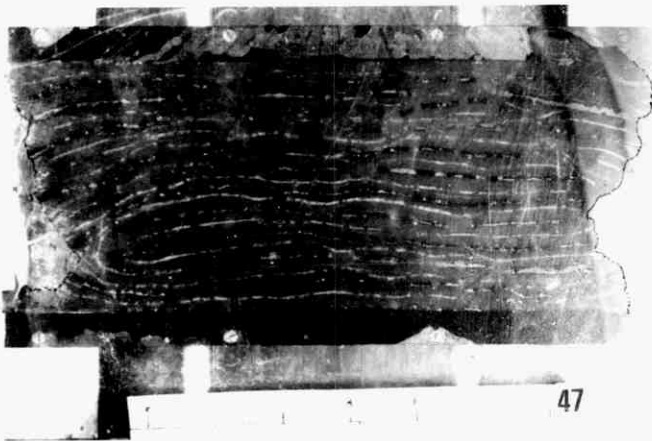
B



C



D

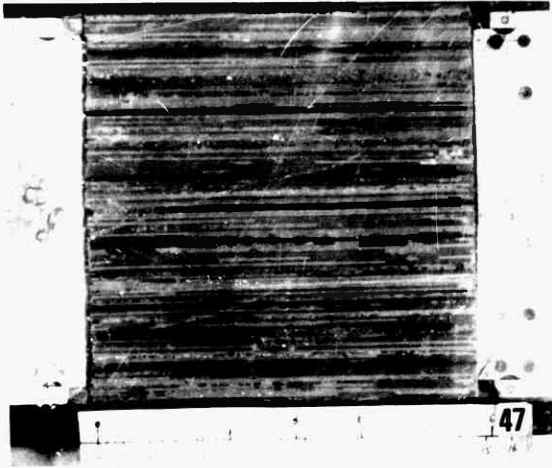


E

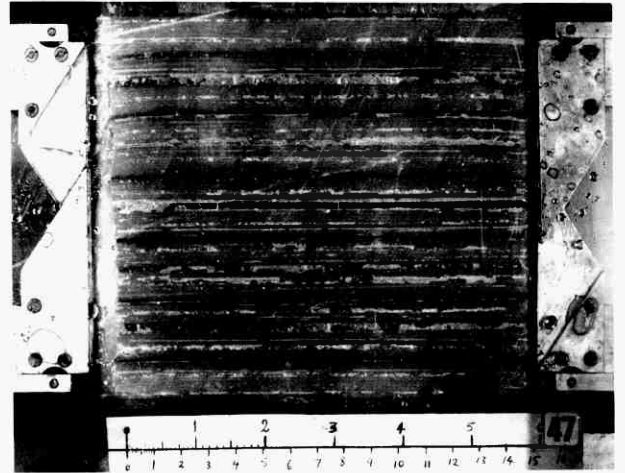


F

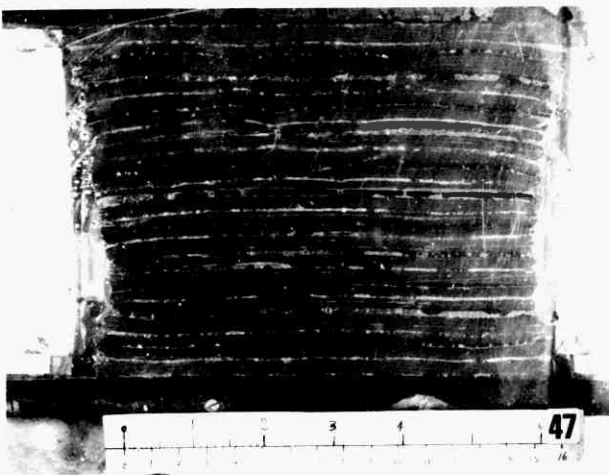
Fig. 2.12



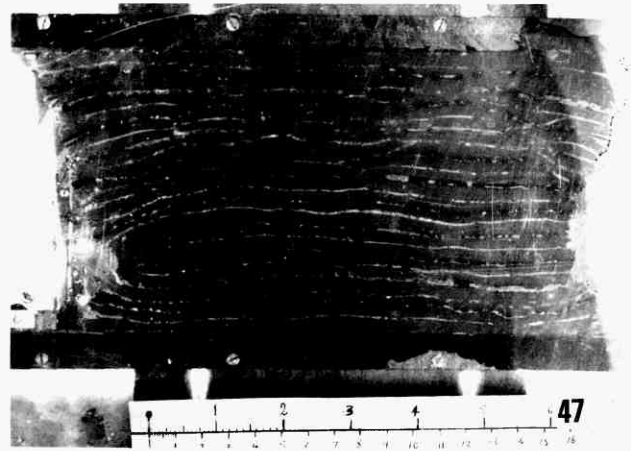
A



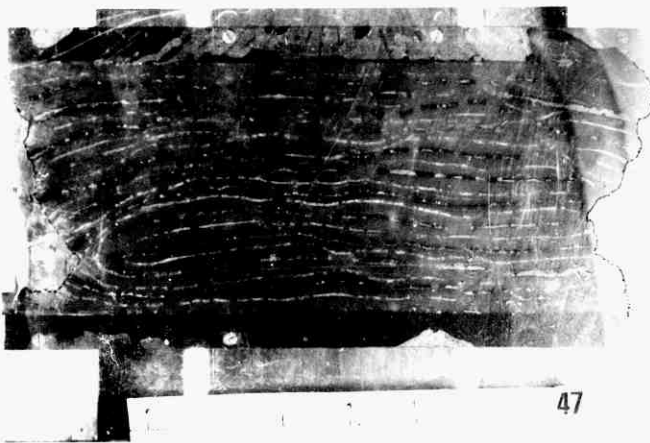
B



C



D



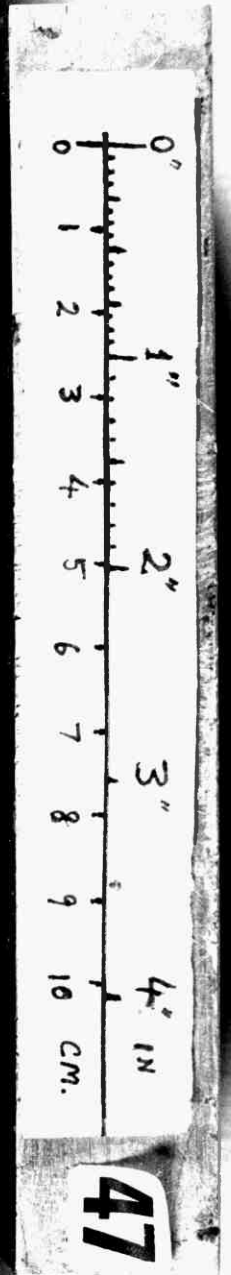
E



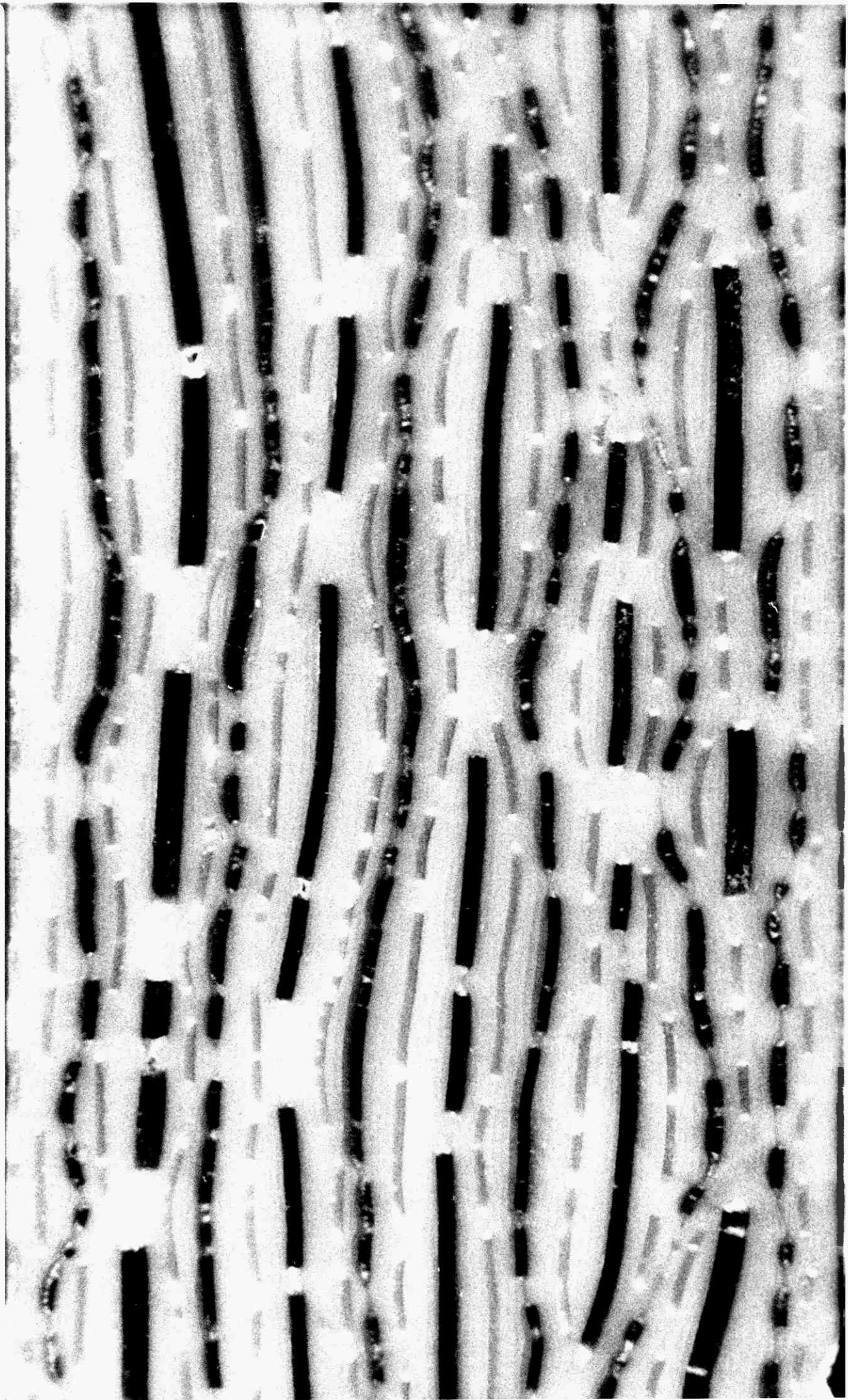
F

Fig. 2.12





5



H

are shown in fig. 2.12. The shortening shown as a percentage is the bulk shortening during the progressive deformation.

There is a relatively less deformed area near the 'bottom' left of the model and the black 1mm competent layer inside this area has fewer fractures than the 1mm black competent layers outside the region.

#### Model 51

Model 51 was identical to Model 47 except that the relatively incompetent layer of 50°C m.pt.p. wax were coloured white using fine artists powder paint ( $\approx 1.5$ cc to 1300 ml of molten wax). The strain rate at which the experiment ran was the same as that used in experiment 47, that is,  $2.05 \times 10^{-4}$ /sec.

At 8% bulk strain (21 minutes) tension fractures appeared in four 1mm black layers (layers 1, 2, 5, 6)(fig.2.13.B). Some of the fractures did not cut completely through the layer. As deformation continued, although fractures appeared in the brown 1mm layers, the number of fractures in 1mm black layers did not increase. At  $\sim 10\%$  strain a few 'half-developed' tension fractures initiated in 2mm layers (layers 1 and 2), but were very weakly developed. Some fractures also appeared in layers 3 and 4 (1mm black layers). At 12% strain all the competent layers except the 3mm layers had fractured (fig.2.13.C). The average width of the boudins or segments decreased as deformation continued. The number of tension fractures was found to be inversely proportional to the thickness of the layers.

After 13-14% shortening tensile fractures occurred in

the lower 3mm competent layer. This initiated the development of a shear zone which exploited conveniently positioned tension fractures in the adjacent layers. The orientation of the shear zone was initially  $\approx 45^\circ$  to the layering and a conjugate zone also at  $45^\circ$  to the layering developed. At 24% shortening (fig. 2.13.E) the shear zone had rotated to  $36^\circ$  to the layering and the angle between the conjugate set was  $\sim 100^\circ$ . New shear zones (fig. 2.13.E) appeared at 24% shortening and were initially at  $45^\circ$  to the layering. With increasing bulk strain the shear zones rotated until at a finite strain of  $\sim 36\%$  shortening, the first set of shear zones were inclined at  $30^\circ$  and the second set at  $35^\circ$  to the layering (fig. 2.13.F). Fig. 2.13.I. shows the plot of the average stress against the bulk shortening in the progressive deformation of Model 51. The various stages described above (fig.2.13.A-F) have been indicated on the graph with same notation (A-F).

2.13. Six stages in the progressive deformation of Model 51.

A - 0.0%

B - 8.4%

C - 12.5% (% bulk shortening)

D - 15.9%

E - 24%

F - 36%

G (overleaf) Enlargement of fig. 2.13.F

H (on page 163) Enlargement of the central part of fig. 2.13.G

(Note how the negative print made the flow of the matrix stand out markedly)

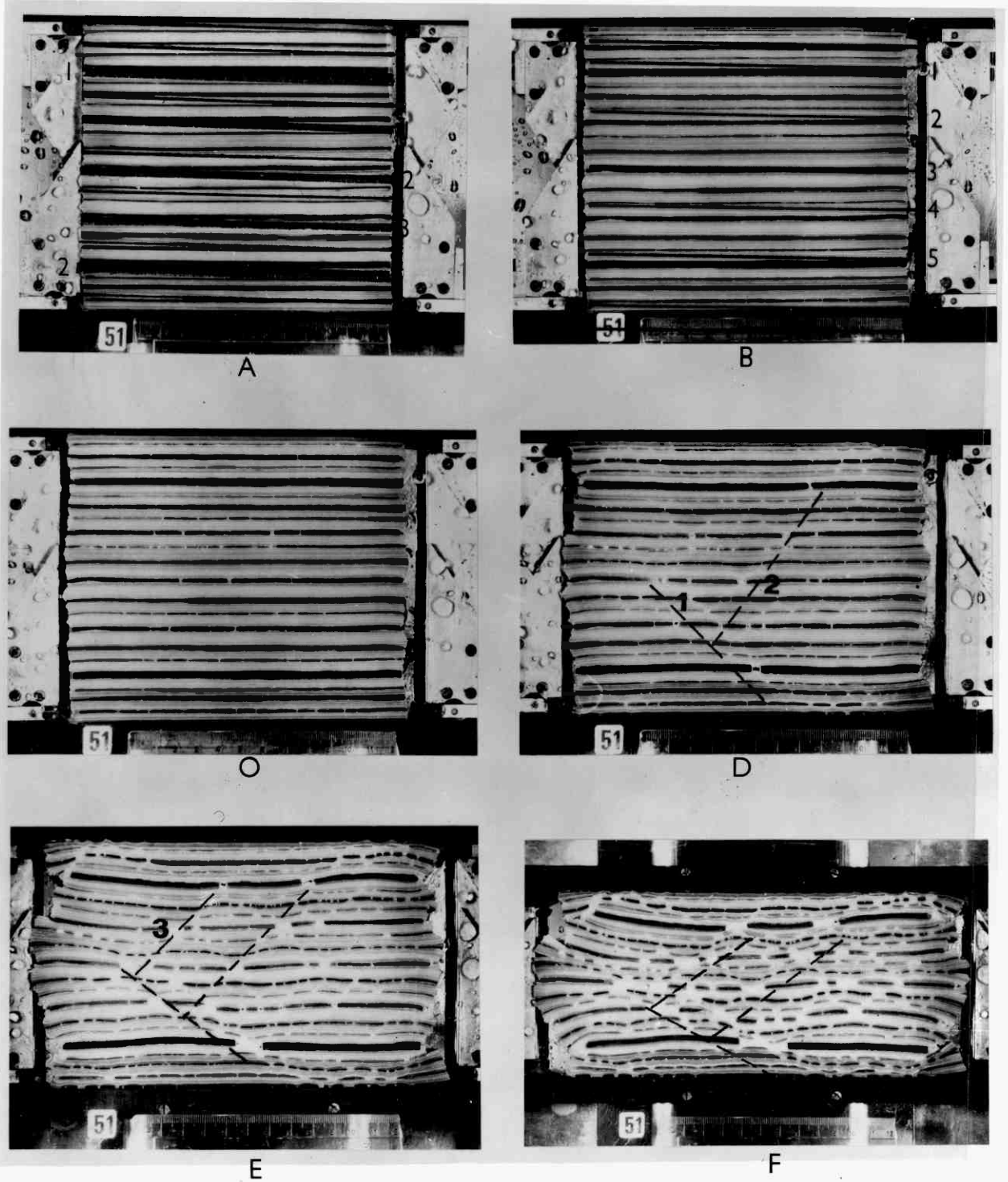


FIG. 2-13



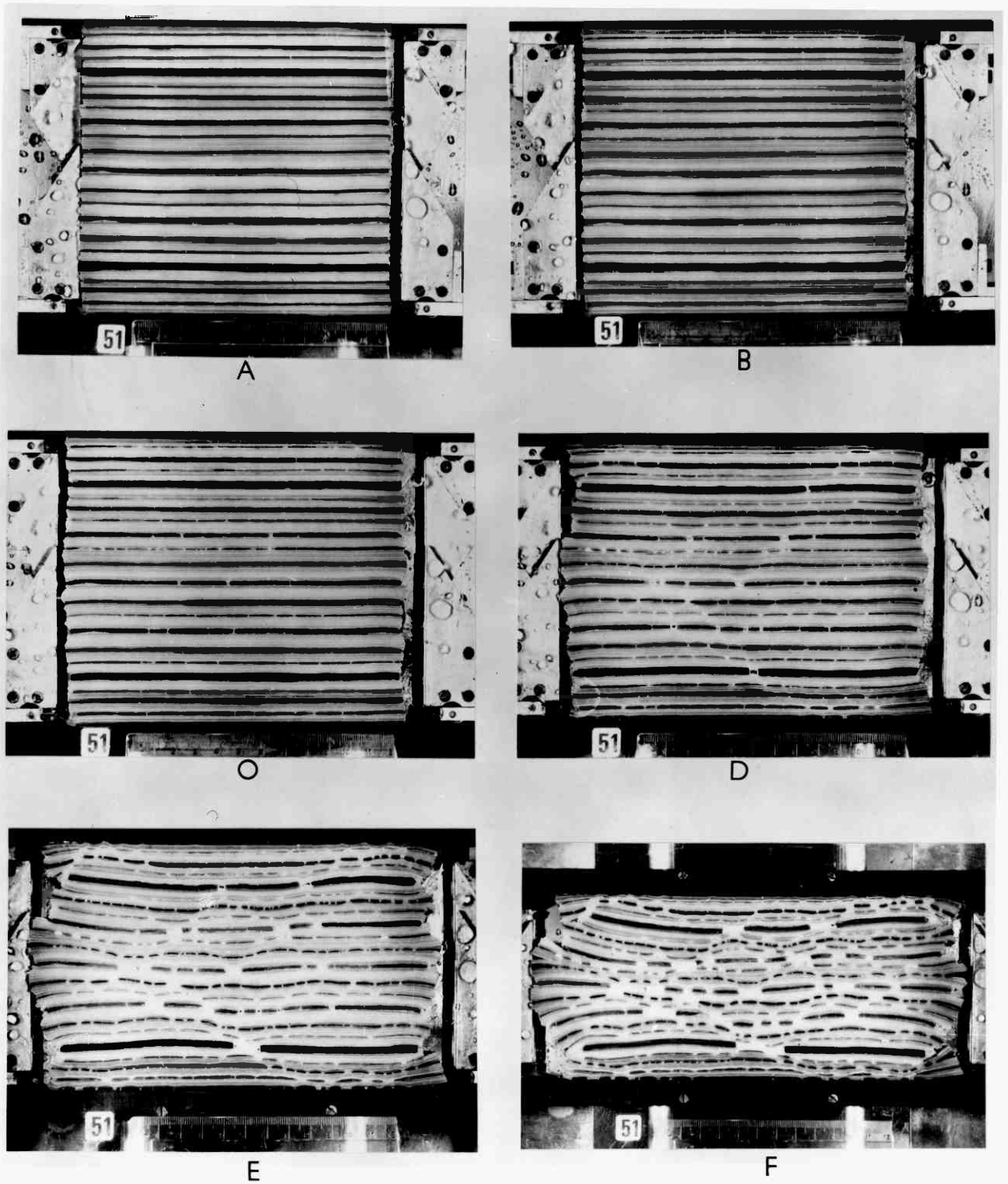
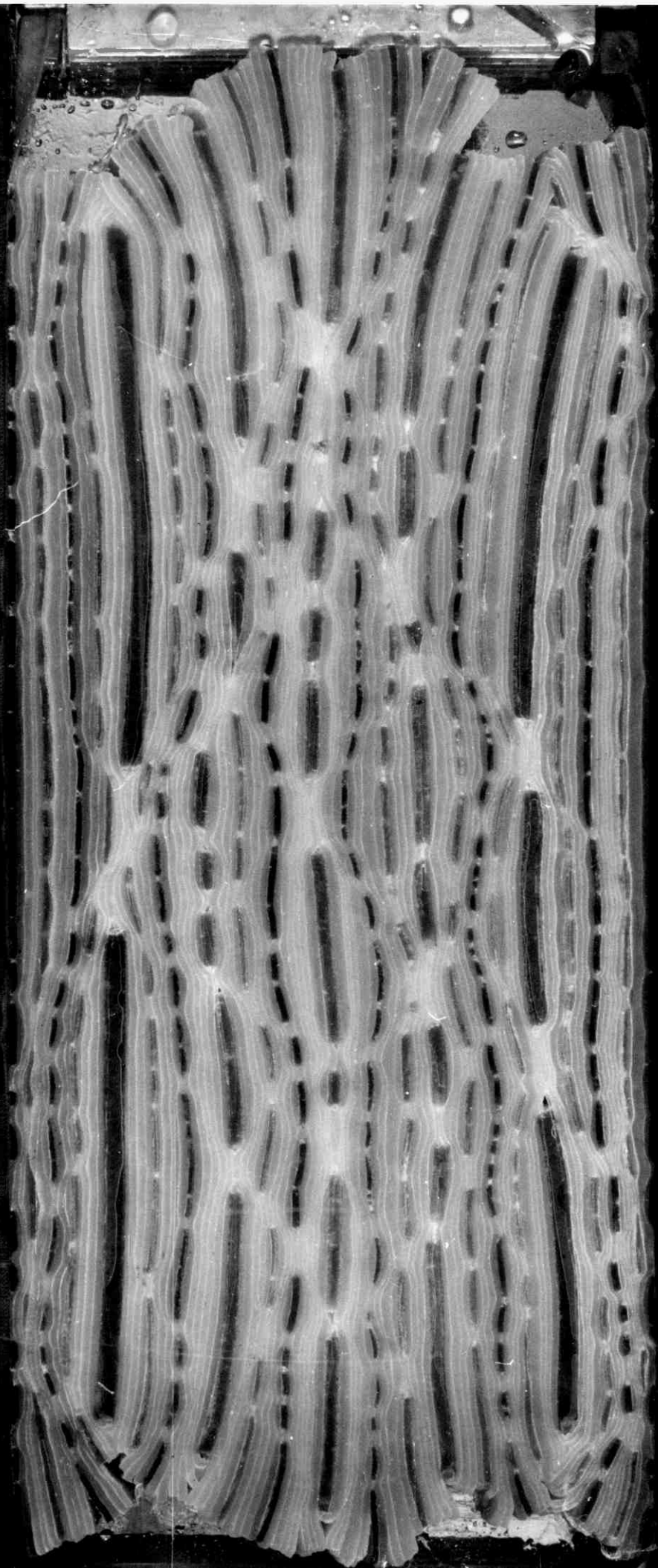


FIG. 2-13

51



G







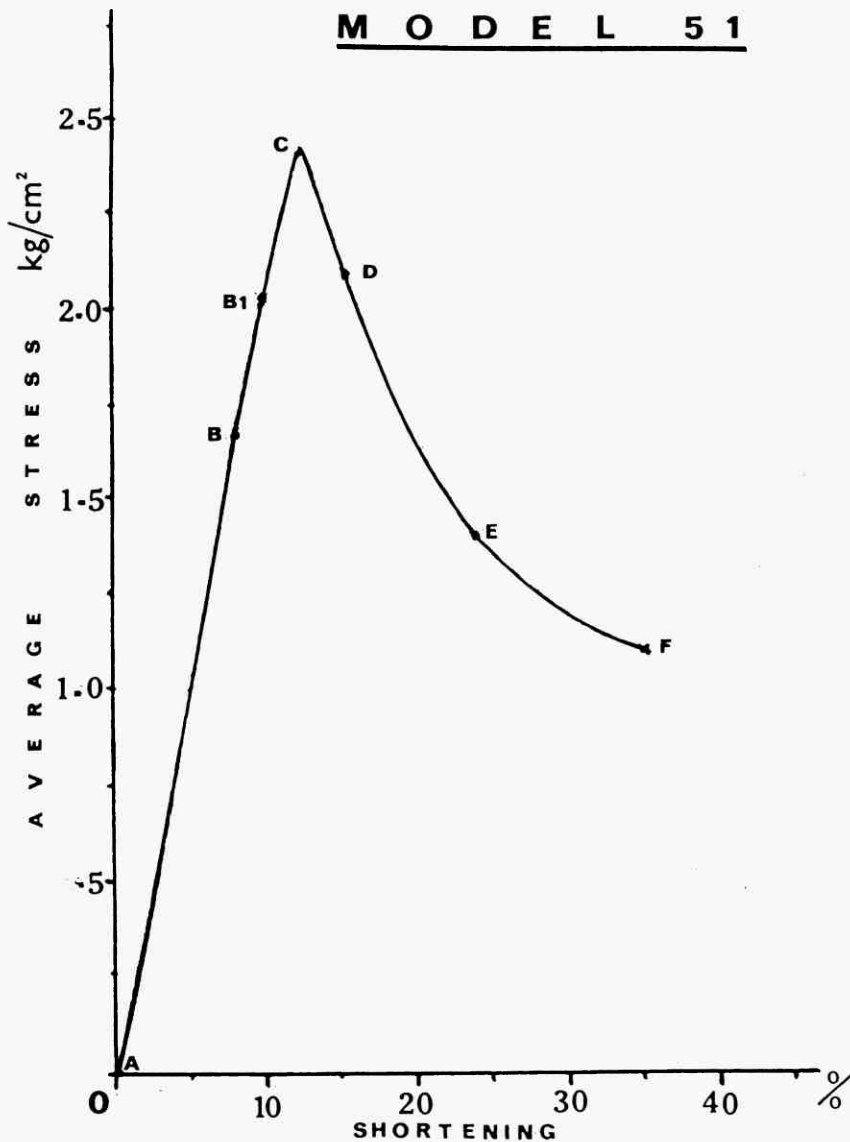


Fig. 2.13.I. Plot of the average stress against bulk shortening in the progressive deformation of Model 51. A. Undeformed. B. 8.5% shortening - tension fractures appear in 1mm thick layers. B-1. Fractures in 2mm thick layers. C. Stress drops just after the initiation of tension fractures in 3mm thick layers. D-F. Stress drops gradually as shear zones are formed (D) by exploiting the suitably positioned tension fractures and as more boudins break further and separate.

## 2.6 Type D Structures

### Boudins generated by Shear Failure

Type D structures formed in the models made of plasticine (experiments 2, 3, 4, 5, 6, 7, 8, 9 and 10). The experiments were carried out at room temperature. In both the single layer and double layer experiments (experiments 9 and 10) the matrix was unlayered, special soft pink plasticine and the layers were standard black plasticine. The details of the preparation of the models and the properties of the plasticine are in Appendix C.2.

The boudins were initiated and formed by shear fractures in the competent layers and the subsequent development of conjugate shear fractures in the matrix caused additional movement along the shear planes that separated the boudins.

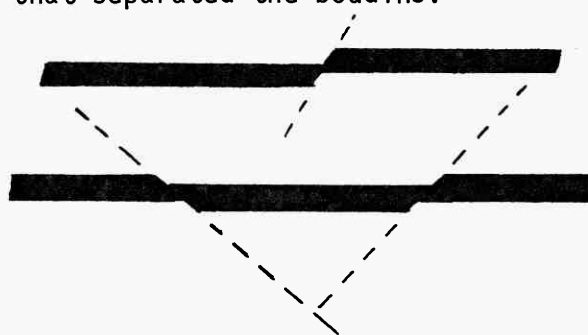


Fig. 2.14

It is rather difficult to detect how the failure of thinner competent layers was initiated. In some models it was initiated by pinching which was then followed by tensile failure. In others layer failure initiated by shear followed by the separation of the layer segments. There were none that initiated by clean brittle tensile failure.

All the models described in the following section were deformed in the Pure Shear Deformation machine and the average size of the models was 150mm by 50 by 150mm.

### 2.6.1. Single Layer Experiments

Model 2 (fig. 2.15.E.H.) consisted of a single 10mm thick layer of black standard plasticine in a matrix of special pink soft plasticine. After 25 minutes (at a strain rate of  $\sim 1.2 \times 10^{-4}$ ) shear planes appeared in the matrix as it flowed towards both ends of the competent layer.

At  $\approx 23\%$  bulk shortening a shear fault developed in the competent layer (fig.2.15.F) at  $40^\circ$  to  $\sigma_1$ . At 26% shortening while layer separation was occurring at the first fault another fault initiated in the longer segment of the competent layer at  $\sim 40^\circ$  to  $\sigma_1$ . At this stage of the experiment the faults in the matrix had rotated from  $\approx 40^\circ$  to  $50^\circ$  to  $\sigma_1$ . Neither faults in the competent layer was the continuation of the faults in the matrix. They were however at  $90^\circ$  to some of the faults in the matrix.

At 29% shortening (fig. 2.15.G), the segments on either side of the first fracture in the layer had completely separated and the segment between the two shear fractures became more visible. It had a thickness to width ratio of 1:5 at the end of the experiment, at 33% finite strain, (fig.2.15.H) the first and second shear planes in the layer had rotated to  $47^\circ$  and  $46^\circ$  to  $\sigma_1$  respectively.

### Model 3 (fig. 2.15. A.D)

Model 3 is very similar to Model 2 except that the thick-

Fig. 2.15. A-D. Four stages in the progressive deformation of Model 3.

A - 0.0%

B - 23% (% bulk shortening)

C - 30%

D - 37%

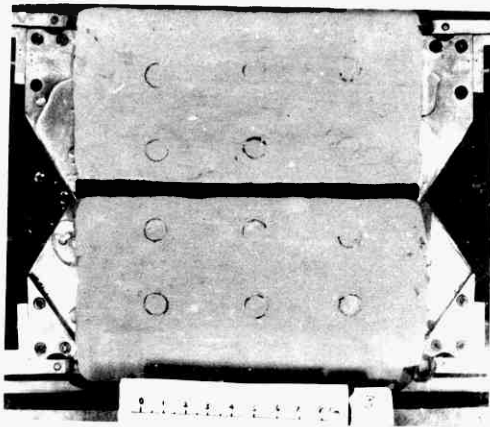
Fig. 2.15. E-H. Four stages in the progressive deformation of Model 2.

E - 0.0%

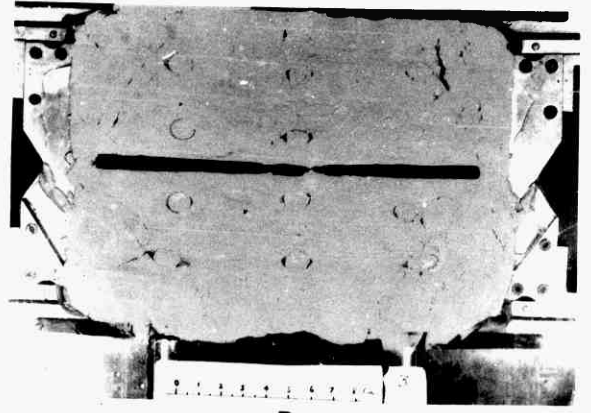
F - 23% (% bulk shortening)

G - 29%

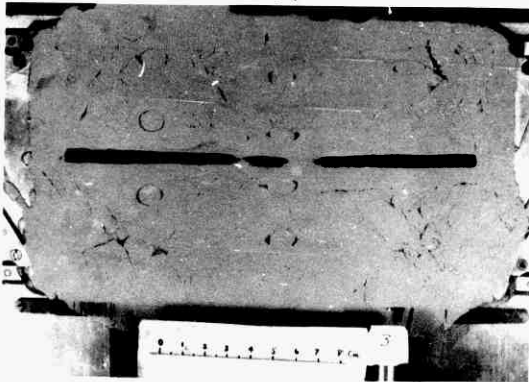
H - 33%



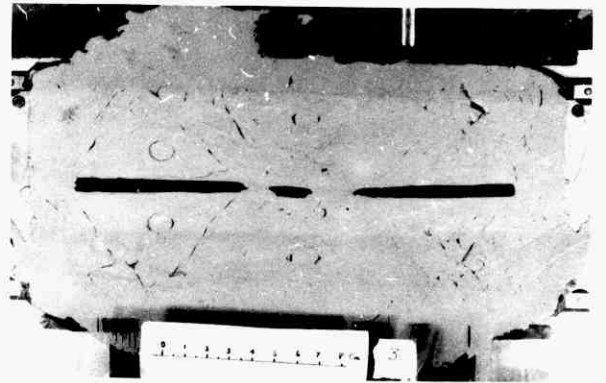
A



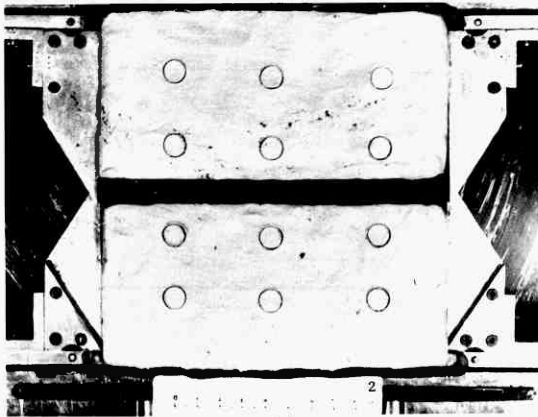
B



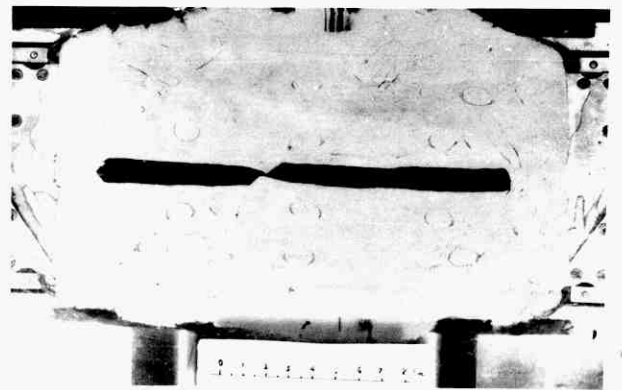
C



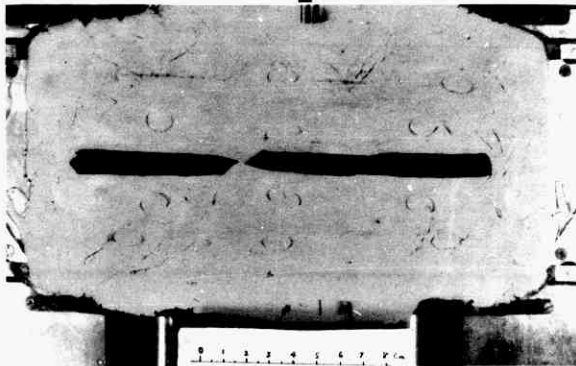
D



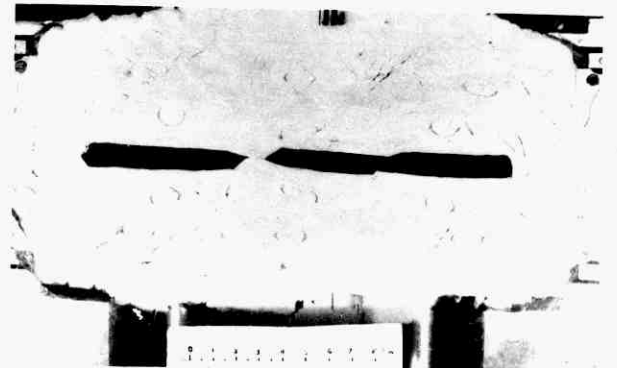
E



F



G



H

FIG.2:15

ness of the layer was 5mm.

As in Model 2, shear faults appeared in the matrix as it started to flow towards the ends of the competent layer. The first shear fault in the competent layer was coupled with necking (stretching) and appeared at 21% shortening (after 28 minutes) and was inclined at  $\approx 45^\circ$  to the principal compression. The second fault, also coupled with pinching, developed after 23% bulk shortening (fig.2.15.B). These two shear faults in the layer formed a conjugate set with the faults in the matrix. The stretching of the layer and the flow of the matrix into the gap between boudins obscured the rotation of the fault direction. More conjugate sets of faults appeared in the matrix as the gap between the boudins widened. The finite bulk strain was 37% shortening (fig.2.15.D).

## 2.62 Inclined Single Layer Experiments

### Model 7 (fig.2.16.A.D.)

This model is the same as Model 2 except that the layer was inclined at  $65^\circ$  to  $\sigma_1$ . As in the previous models shear faults appeared in the matrix as it flowed towards the ends of the layer. As deformation proceeded the layer rotated to a higher angle to  $\sigma_1$  and at 20% shortening a shear fault appeared in the layer. The fault is not the continuation of any fault in the matrix although its orientation ( $33^\circ$  to  $\sigma_1$ ) was at  $90^\circ$  to the faults in the matrix. At 25% shortening the layer had rotated to  $73^\circ$  to  $\sigma_1$ , and the shear fracture had rotated to  $45^\circ$  to  $\sigma_1$ .

After 33% shortening the layer had rotated to  $78^\circ$  to  $\sigma_1$  and the shear direction rotated to  $53^\circ$  to  $\sigma_1$ , that is  $7^\circ$  rotation in 8% bulk strain.

Fig. 2.16 A-D. Four stages in the progressive deformation  
of Model 7.

A - 0.0%

B - 20% (% bulk shortening)

C - 25%

D - 33%

Fig. 2.16. E-H. Four stages in the progressive deformation  
of Model 8.

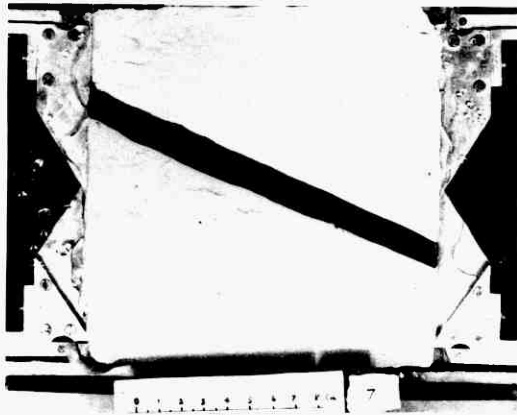
E - 0.0%

F - 23% (% bulk shortening)

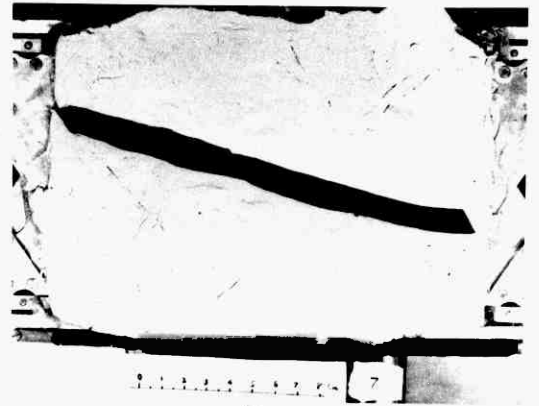
G - 31%

H - 36%





A



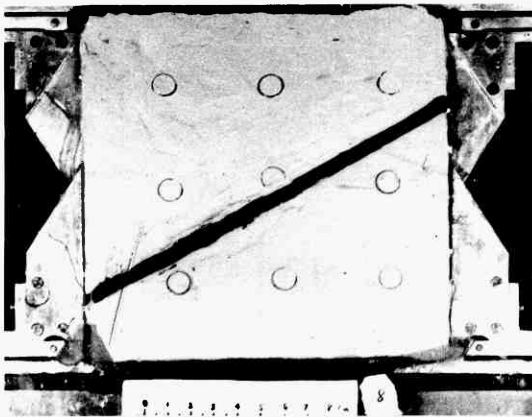
B



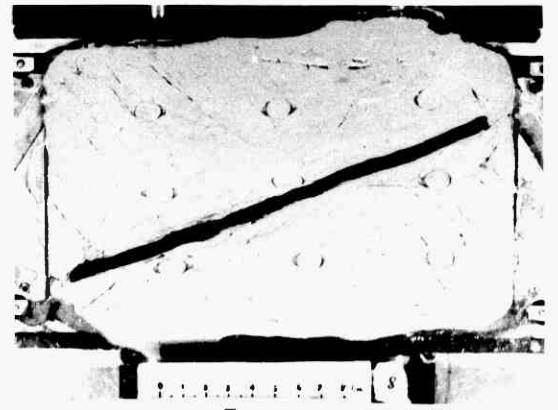
C



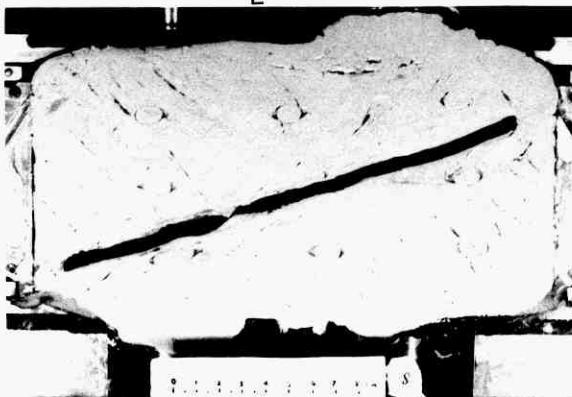
E



E



F



G



H

FIG216

Model 8 (fig. 2.16.E.H.)

The layer in this model is 5mm thick and was originally inclined at  $63^{\circ}$  to  $\sigma_1$ . As in all the previous plasticine models shear faults first developed in the matrix as it flowed towards the ends of the competent layer. It took 35 minutes and a bulk strain of 23% shortening before the initiation of a shear fault in the competent layer. The fault made an angle of  $26^{\circ}$  to  $\sigma_1$ . By then the layer had rotated to  $70^{\circ}$  to  $\sigma_1$ , a rotation of  $8^{\circ}$ . Both the layer and the shear orientation continued to rotate as the bulk strain increased. As shown in fig. 2.16.H. at the finite strain of 36% shortening the layer had rotated to  $77^{\circ}$  to  $\sigma_1$  (i.e.  $15^{\circ}$  rotation) and the shear fault to  $55^{\circ}$  to  $\sigma_1$  (i.e.  $29^{\circ}$  rotation).

2.63 Double Layer ExperimentsModel 9 (fig.2.17.A.D.)

Two 5mm thick layers separated by homogeneous special soft pink plasticine matrix (fig.2.17.A) were compressed at  $90^{\circ}$  to the layering. As in the single layer experiments, shear faults first appeared in the matrix as it flowed towards the ends of the layers. After 14% bulk shortening (fig. 2.17.B-1) a shear fault (fault 1) appeared in layer II and this had rotated to an angle of  $47^{\circ}$  to  $\sigma_1$  at 19% shortening, before a shear fault inclined at  $42^{\circ}$  to  $\sigma_1$  appeared in layer I (fig.2.17.G-2). This fault (fault 2) in layer I is normal to the first fault in layer II and both faults can be seen to have extended into the matrix. At the same time a

Fig. 2.17 A-D. Four stages in the progressive deformation of Model 9.

A - 0.0%  
B - 14%  
C - 19%  
D - 29%

(% bulk shortening)

Fig. 2.17 E-H. Four stages in the progressive deformation of Model 10.

E - 0.0%  
F - 12%  
G - 20%  
H - 30%

(% bulk shortening)

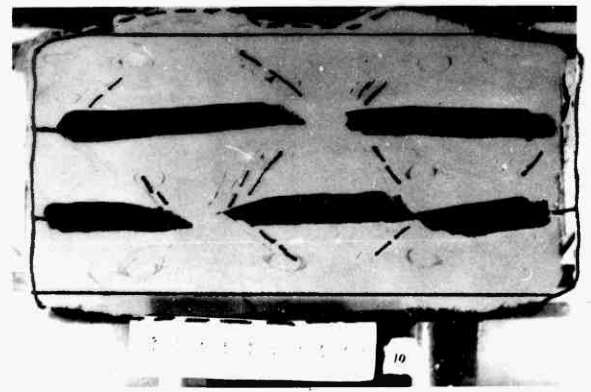
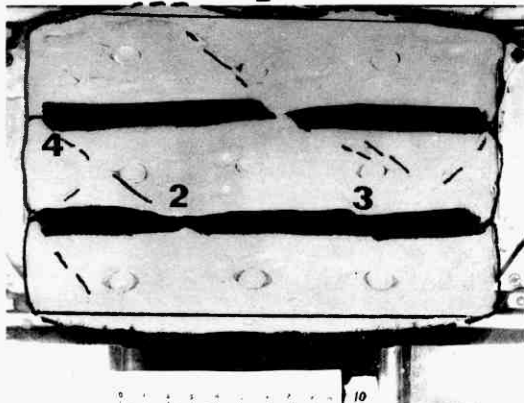
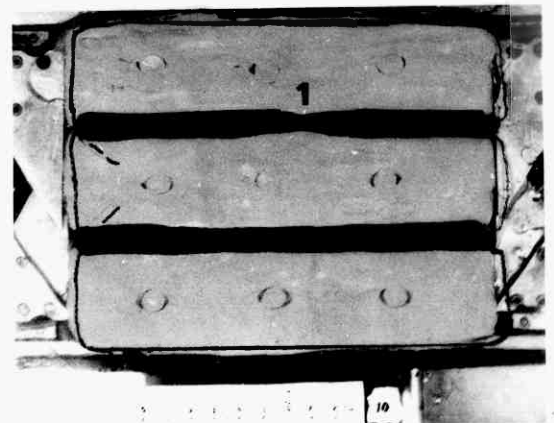
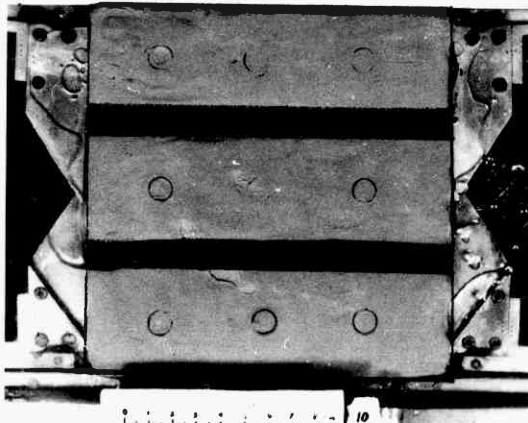
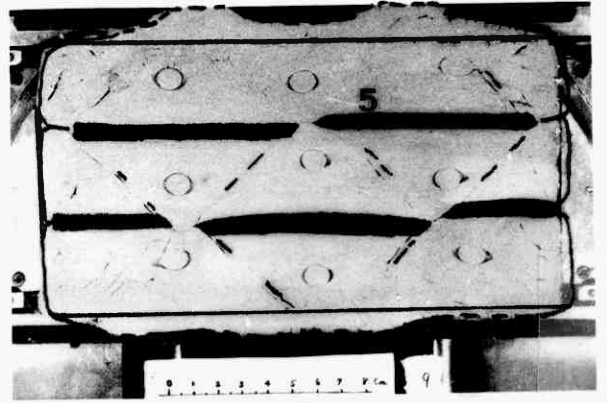
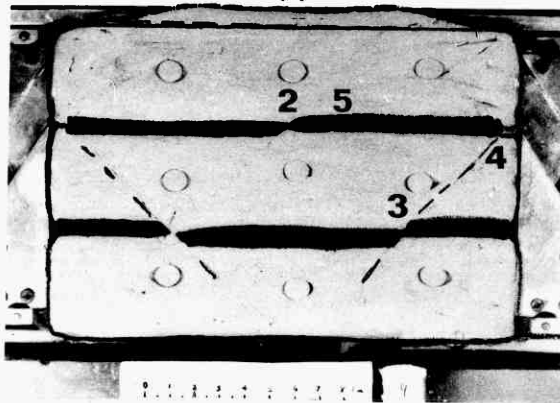
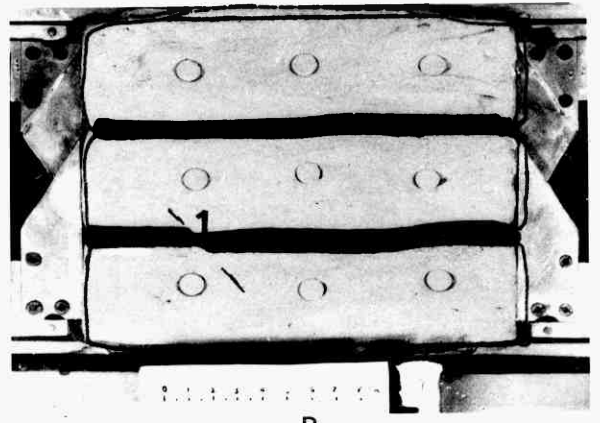
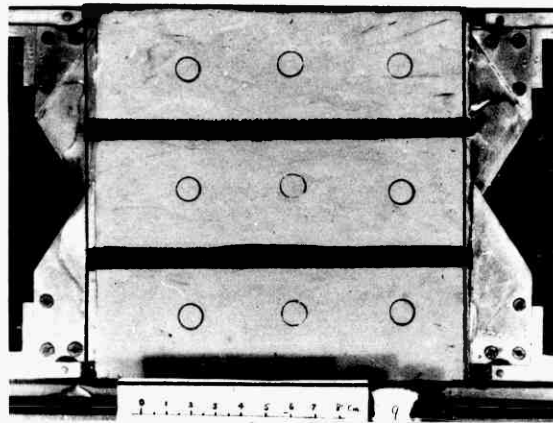


FIG. 2.17

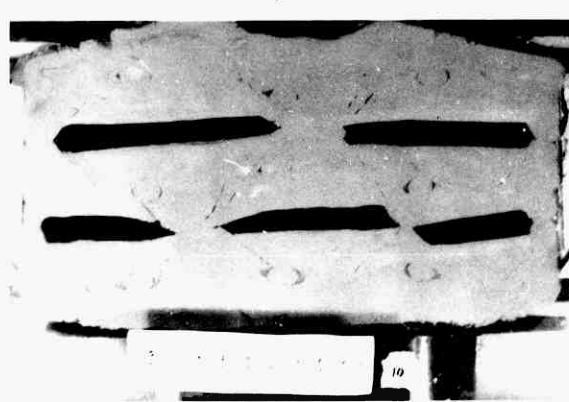
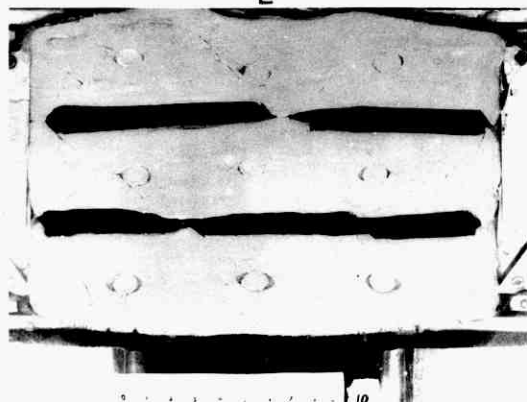
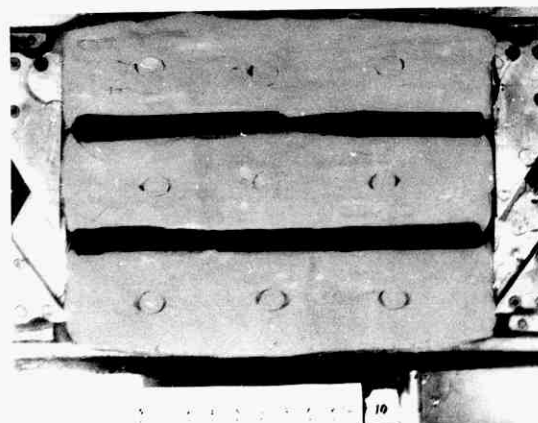
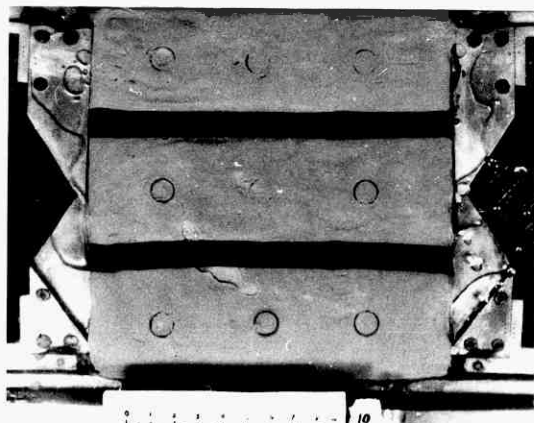
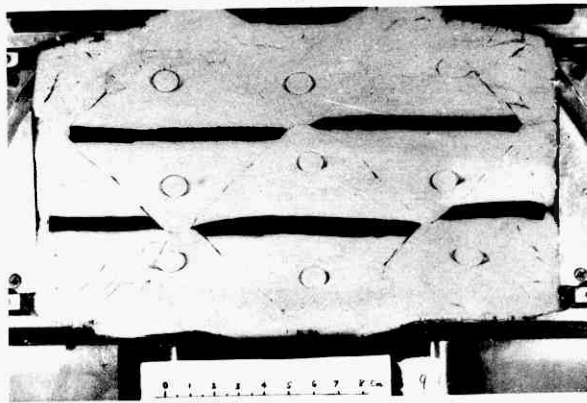
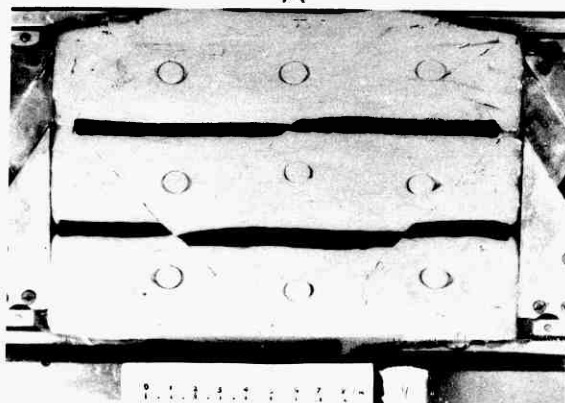
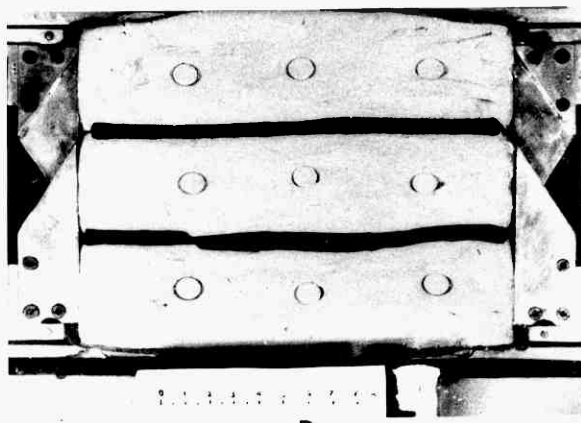
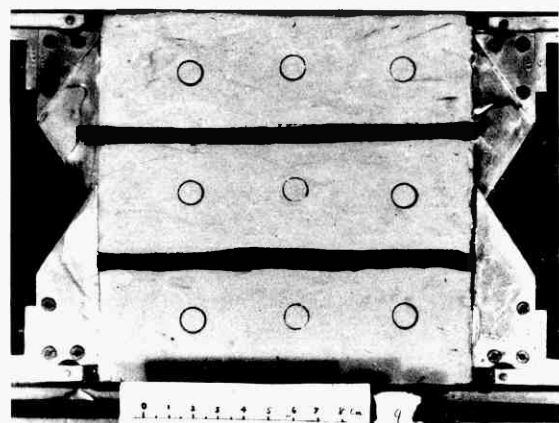


FIG. 2.17

third shear fault (at  $42^{\circ}$  to  $\sigma_1$ ) developed in layer II on the right side of the model (fig.2.17.C-3). This fault (fault 3) was instigated by a fault in the matrix which started at the right end of layer I (fig.2.17.C-4). The two faults in layer II form a conjugate and are at  $90^{\circ}$  to each other. The fault in layer I, which divided the layer into 2 equal widths, was followed by two 'less developed' faults on the right boudin (fig. 2.17.C-5). At this stage because of movement on one of the shear fractures, layer I looked like a pinched layer with slightly displaced segments.

The amount of rotation of the faults increased as deformation continued. By the end of the experiment (29% shortening), the first shear fault in layer II was rotated to  $50^{\circ}$  to  $\sigma_1$  ( $\theta = 50^{\circ}$ ), a rotation of  $8^{\circ}$  during  $\approx 15\%$  strain. The next two faults in layer I and II have been reorientated to  $46^{\circ}$  to  $\sigma_1$ , a rotation of  $4^{\circ}$  in  $\approx 10\%$  strain. The layers have been displaced and separated by these three shear faults (fig.2.17.D)

#### Model 10 (fig.2.17.E.H)

Model 10 was the same as Model 9 except that the two competent layers were 10mm thick each. After 12% shortening a shear fault appeared in layer I at  $40^{\circ}$  to  $\sigma_1$  (fig.2.17.F-1). This divided the layer into two equal widths. The next fault appeared in layer II (fig.2.17.G-2) at  $\theta = 40^{\circ}$  to  $\sigma_1$ . At 20% shortening a third fault developed in layer II at  $40^{\circ}$  to  $\sigma_1$  (fig.2.17.G-3) and the first two faults rotated to  $\theta = 45^{\circ}$ . The second fault was instigated by faults that developed in the matrix (fig.2.17.G-4).

By the end of the experiment (a shortening of 30%) the

first two faults had rotated to  $50^\circ$  to  $\sigma_1$ , a rotation of  $10^\circ$  (in about 18% shortening) and the third fault rotated to  $46^\circ$  to  $\sigma_1$ .

## 2.7 DEFORMATION OF PINCH-AND-SWELL STRUCTURES

Nine (three plasticine and six wax) experiments were carried out to investigate the deformation of a layer containing pinch-and-swell structure. The layer was cast in a plaster-of-paris mould, which itself was cast in a specially made steel box (see fig 2.18.A.B)

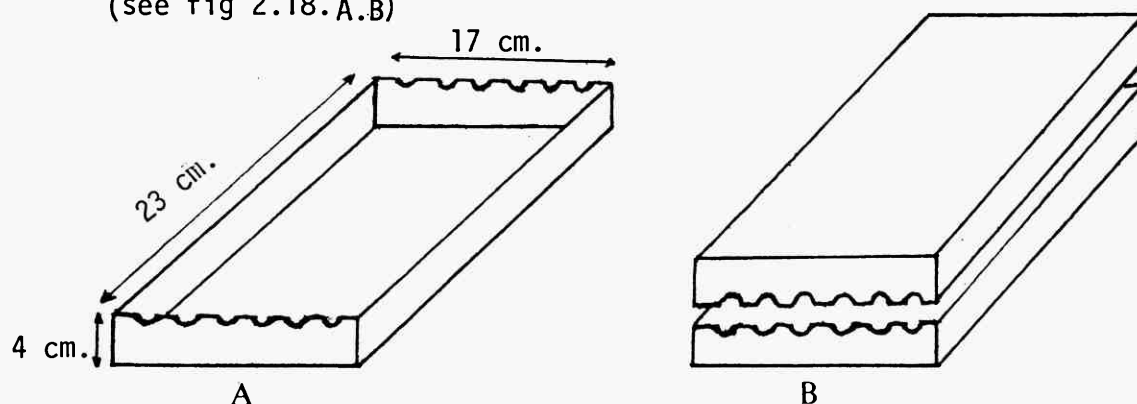


Fig.2.18. A. Steel box for casting the plaster-of-paris mould.  
B. The two halves of plaster-of-paris mould for casting the pinch-and-swell structures.

All the experiments had only a single layer containing pinch-and-swell structure but the average thickness of the layer was different in different experiments. In the plasticine models the layer shortened by shear failure which occurred in the pinch regions. The shear fault was a continuation of the shear faults that appeared initially in the matrix.

In the wax models the pinch-and-swell layer shortened by buckling although the voids, which formed because of separation of the matrix and the layer during heating up and during running

of the experiments, have obscured the regularity of the folds which are all asymmetric. Some of these models (40, 44, 45, 46) will now be described. Note the numbering of pinches or swells 1, 2, 3..... is from left to right.

Model 40 (fig. 2.19., 2.20-A, 2.22.A)

The model consists of a single pinch-and-swell layer (thickness: pinch = 2mm and swell = 6mm) of black standard plasticine in a matrix of special soft pink plasticine. A grid of spot strain markers was painted on the top of the model.

Voids, between the matrix and the layer appeared at about 6.8% shortening generally in the pinch regions. At  $\approx 12\%$  shortening, incipient buckling initiated at pinch regions 3 and 5. Shear faults developed in the layer at the folded pinched regions when the strain approached 18%. The shears were at  $\sim 30^\circ$  to  $\sigma_1$ . The matrix deformed homogeneously until about 16% shortening, when conjugate sets of shear faults were initiated slowly at  $90^\circ$  or less to each other, ( $2\theta < 90^\circ$ ). As deformation proceeded shortening of the layer occurred by sliding on the shear faults and of the matrix by homogeneous flattening and the formation of shear faults.

At the end of the experiment (36% shortening) the original pinch-and-swell shape was transformed into a layer of segments with 'imbricate' shape separated by four shear planes each at  $\sim 30^\circ$  to  $\sigma_1$  (fig. 2.22.A)

Model 44 (fig. 2.21., 2.20.B., 2.22.B.)

The model consists of black  $58^\circ\text{C}$  m.pt. paraffin wax layer painted white after deformation for identification (pinch thickness = 1.4mm, swell = 6.0mm) in a matrix of  $54^\circ\text{C}$  m.pt. paraffin wax. The



MODEL 40

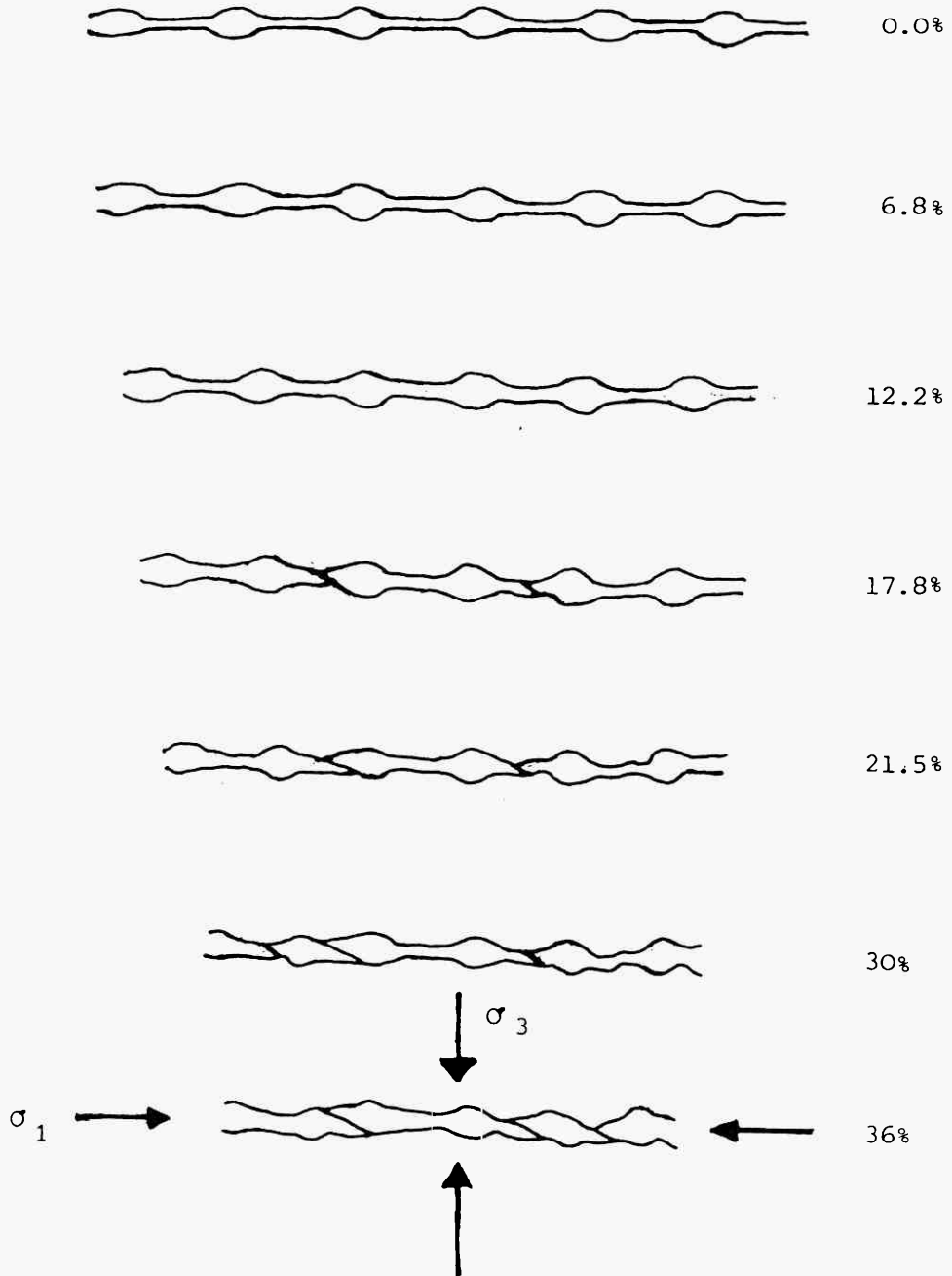


Fig. 2,19 Seven stages in the progressive deformation of Model 40

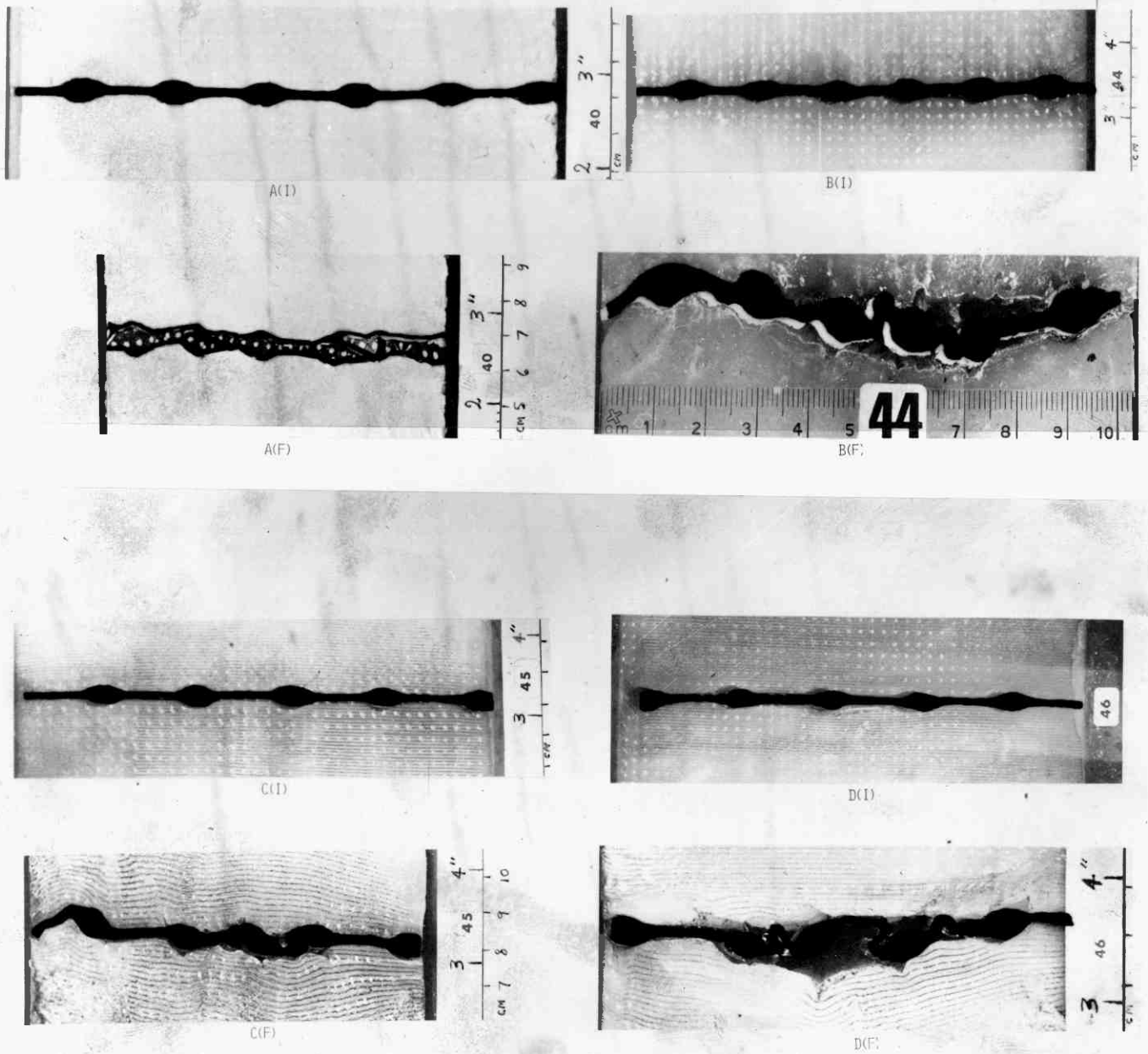


Fig. 2.20. INITIAL (I) AND FINAL (F) STAGES IN THE PROGRESSIVE DEFORMATION OF MODELS 40(A), 44(B), 45(C) AND 46(D)

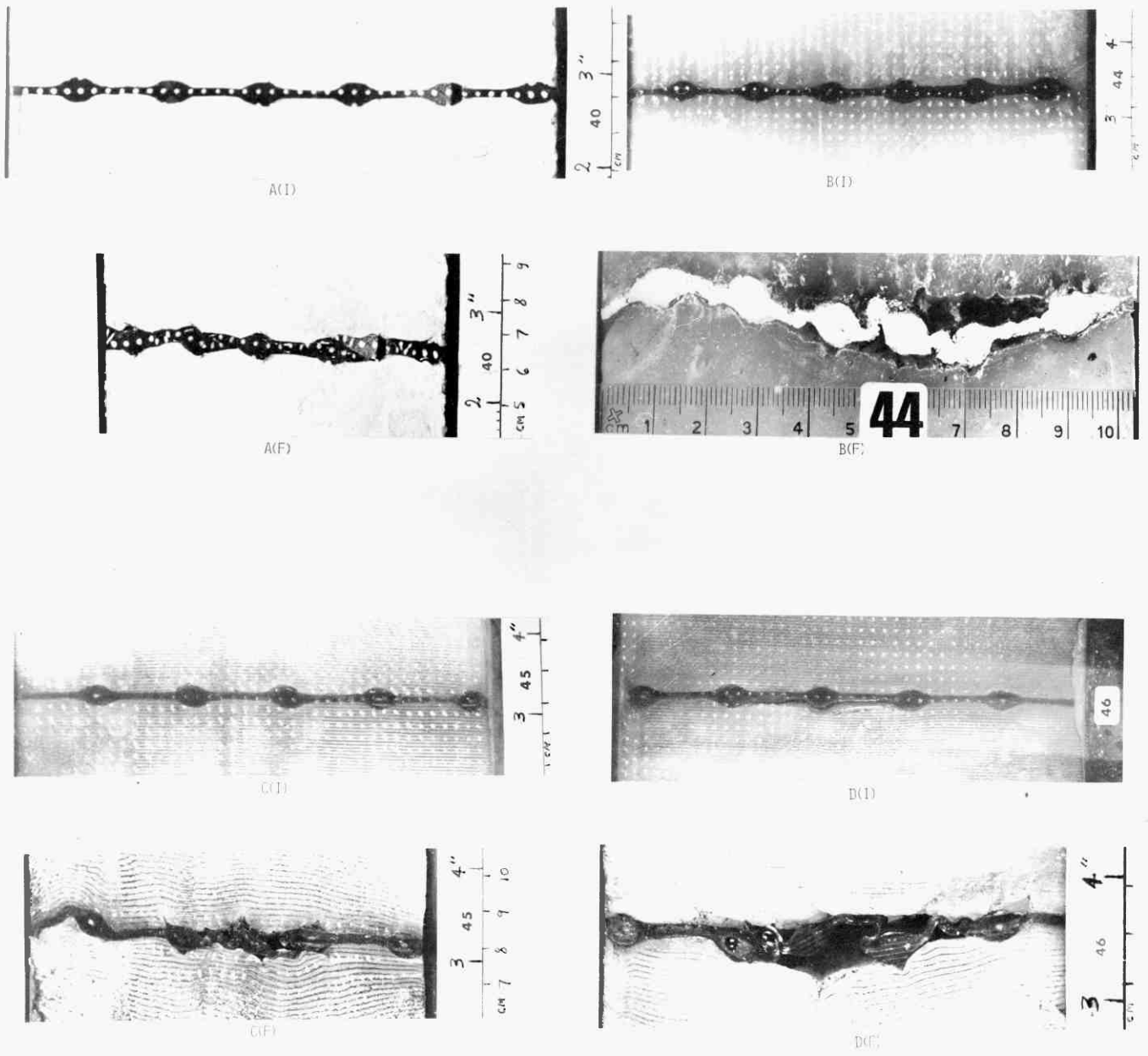


Fig. 2.20. INITIAL (I) AND FINAL (F) STAGES IN THE PROGRESSIVE DEFORMATION OF MODELS 40(A), 44(B), 45(C) AND 46(D)

experiment was run at 35°C and strain rate of  $4.11 \times 10^{-5}$ . Voids appeared between the layer and matrix (fig.2.20.B(f), 2.22.B) during the heating up of the experiment from room temperature to 35°C. The layer as a whole also started to buckle with a much larger wavelength during the early stages of the deformation. As deformation progressed pinch 5 buckled at about 18% shortening. The smaller buckles amplified and the folding of the layer as a whole became more significant. Both the larger and the smaller buckles are asymmetric. The second pinch started folding at about 27-28% shortening and by the end of the experiment, which took 3½ hours with a shortening of 36%, all the pinches were folded, some into very tight asymmetric folds (2.22.B).

Model 45 (fig.2.20.C., 2.22.C., 2.23)

Like Model 44, Model 45 consists of a black 58°C m.pt. p. wax pinch-and-swell layer in a clear 54°C m.pt. p.wax matrix. The pinches are 1.5mm thick and 20mm wide and the swells are 6mm thick and 10mm wide.

Voids appeared during the heating up and during the deformation as in Model 44. At 8% shortening a slight bending occurred at pinches 1 and 5, but no significant buckling occurred until a shortening of 13%. At this stage a buckle developed at pinch 4. This fold amplified and tightened making the nearest swell (4) one of its limbs, and another fold formed at about 21.0% shortening at pinch 3. This second fold also had one of its limbs made up of a swell (swell 3) and the other limb a pinch (pinch 3).

## MODEL 44

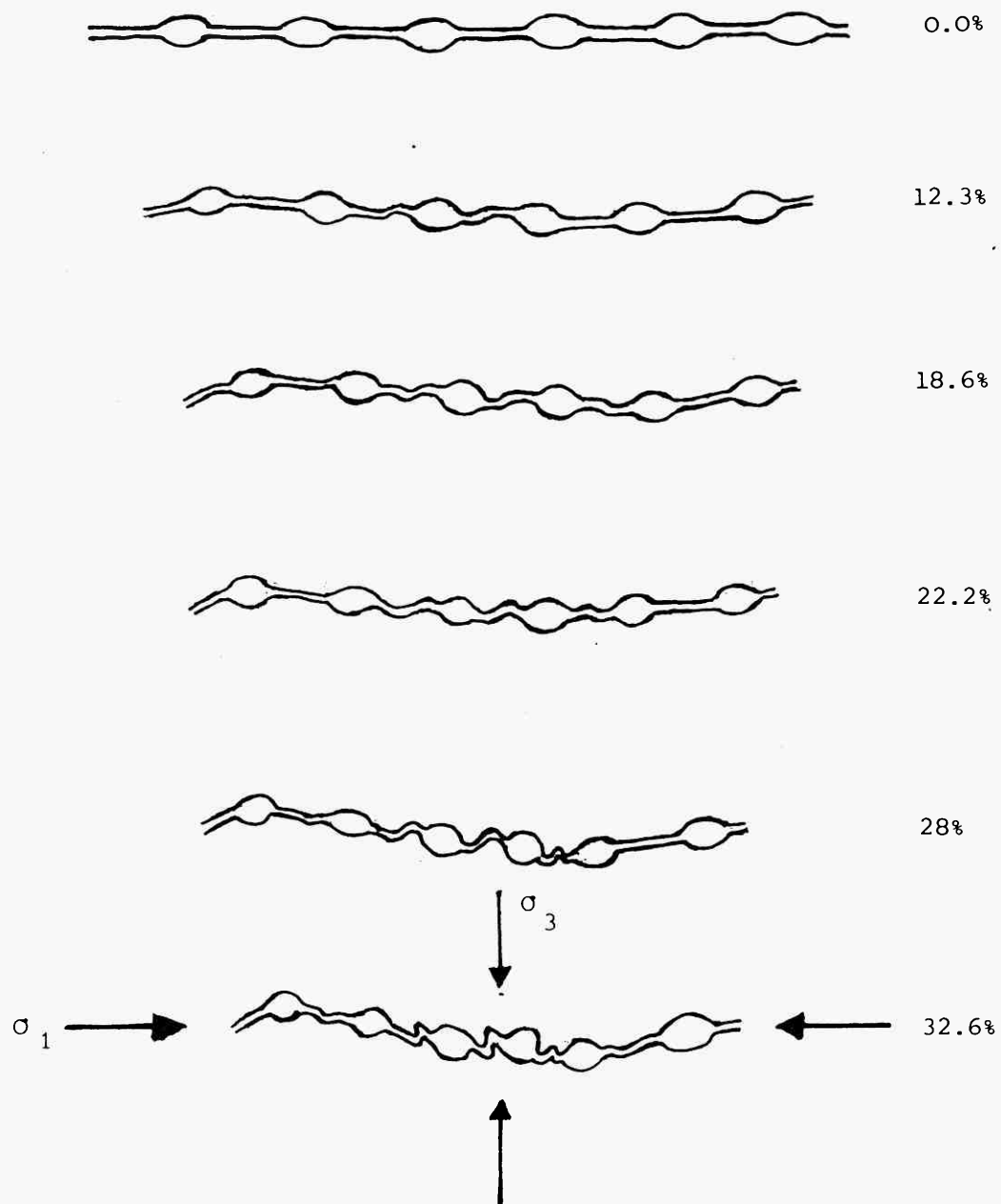


Fig. 2.21 Six stages in the progressive deformation of Model 44

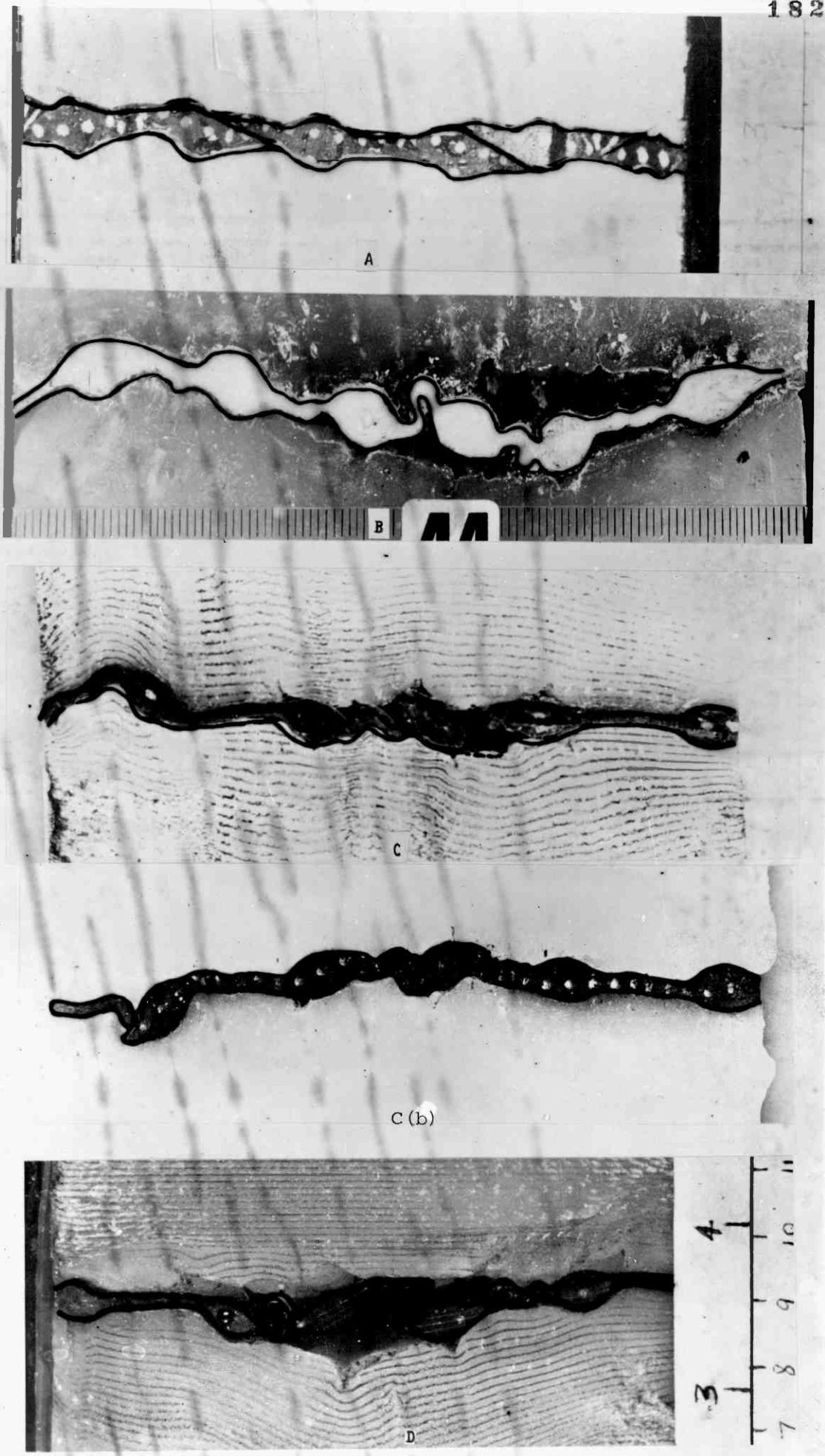


FIG. 2.22. ENLARGEMENTS OF THE FINAL DEFORMATION OF THE MODELS SHOWN IN FIG. 2.20  
C(b) IS THE BACK SIDE OF MODEL 45.

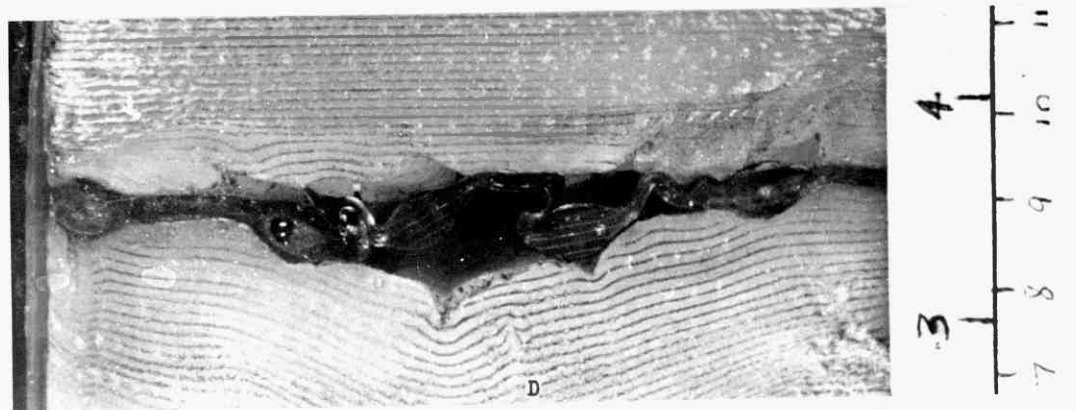
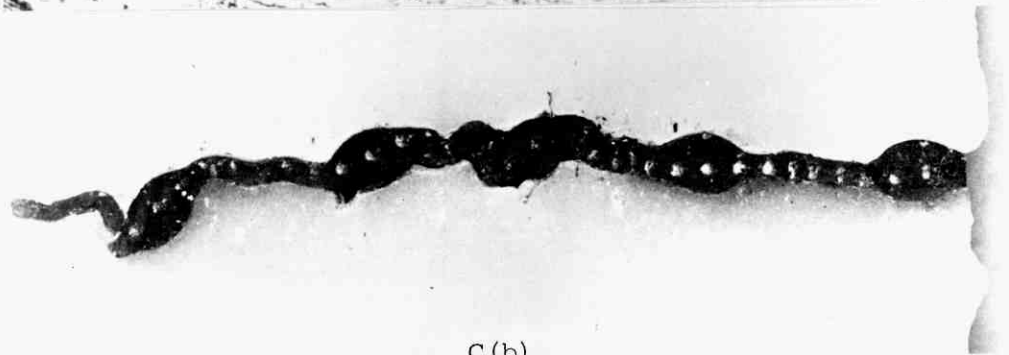
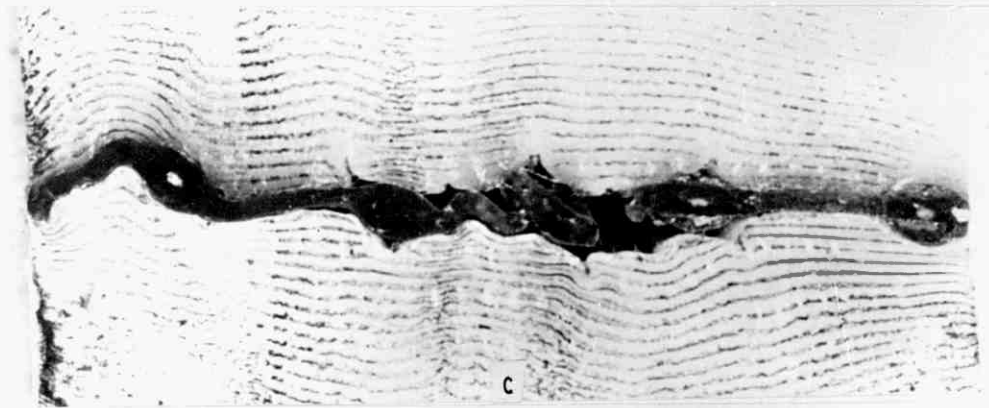
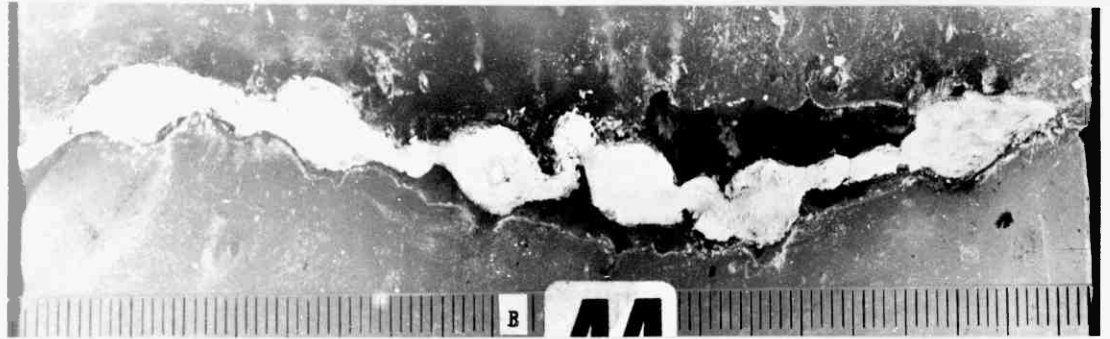
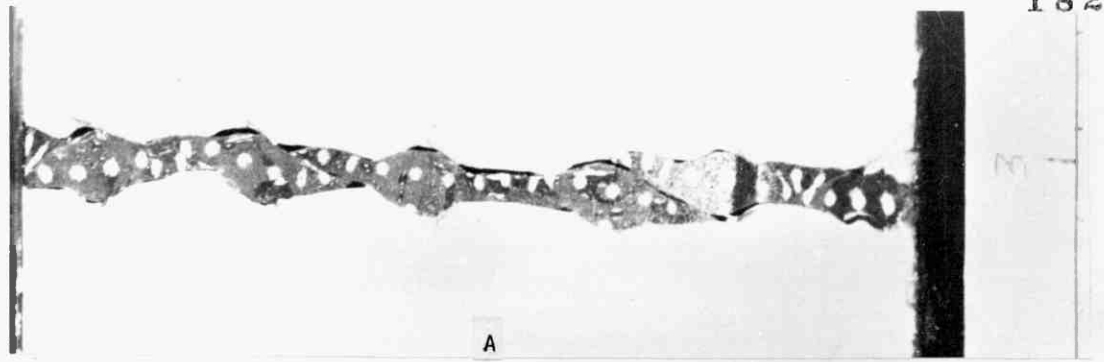


FIG. 2.22. ENLARGEMENTS OF THE FINAL DEFORMATION OF THE MODELS SHOWN IN FIG. 2.20  
C(b) IS THE BACK SIDE OF MODEL 45.

## MODEL 45

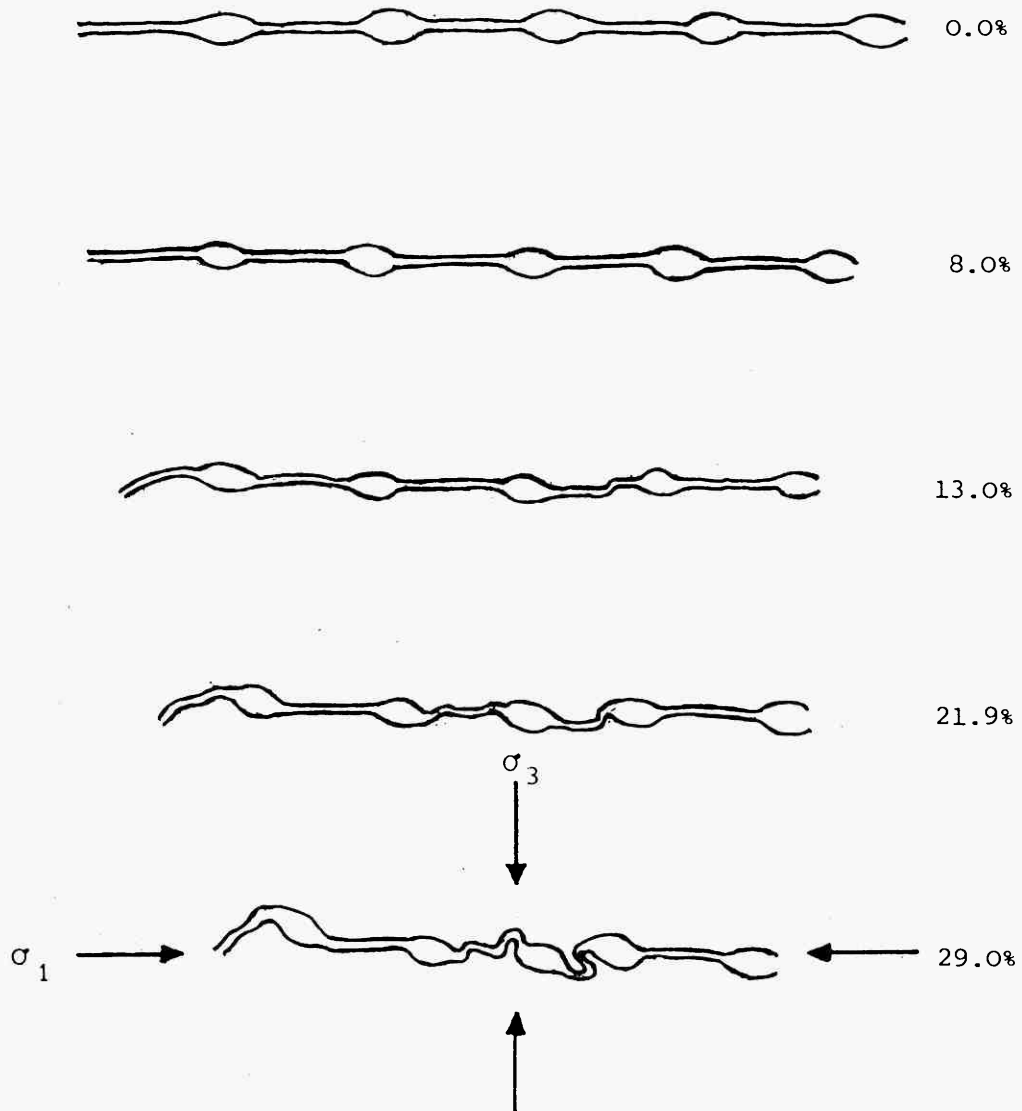


Fig. 2.23 Five stages in the progressive deformation of Model 45



The slight bending that occurred at pinch 5 did not amplify but the bending at pinch 1 did to form a fold with a larger wavelength than the buckles which developed at pinches 3 and 4. At the end of the experiment (finite shortening of 29%) pinches 2 and 5 had only slight deflection while very tight asymmetric folds formed at pinches 1, 3 and 4 (fig. 2.20.C., 2.22.C., C (b) and 2.23).

Model 46 (fig. 2.20.D., 2.22.D. and 2.24)

This model is the same as model 45, but was run at 38.3°C at the faster strain rate of  $2.05 \times 10^{-4}$ .

As in the three models previously described, voids appeared between the layer and the matrix during the heating up and during the deformation.

The first fold was initiated at 12% shortening at pinch 2. This fold developed within the relatively wide void and did not deflect the matrix. The second fold was initiated at pinch 3 near swell 4 at 16.0% shortening. A sinusoidal fold also initiated at pinch 4 at this stage. The development of the folds in this model occurred more readily than in the previous experiments because of the large voids that developed at the layer/matrix junction. This void effectively removed the resistance to buckling offered by the matrix in the other experiments. This large void also affected the style of folding, for example, the first fold to form developed into a kind of 'mushroom' fold while the folds in most of the other models were inclined isoclinal folds.

## MODEL 46

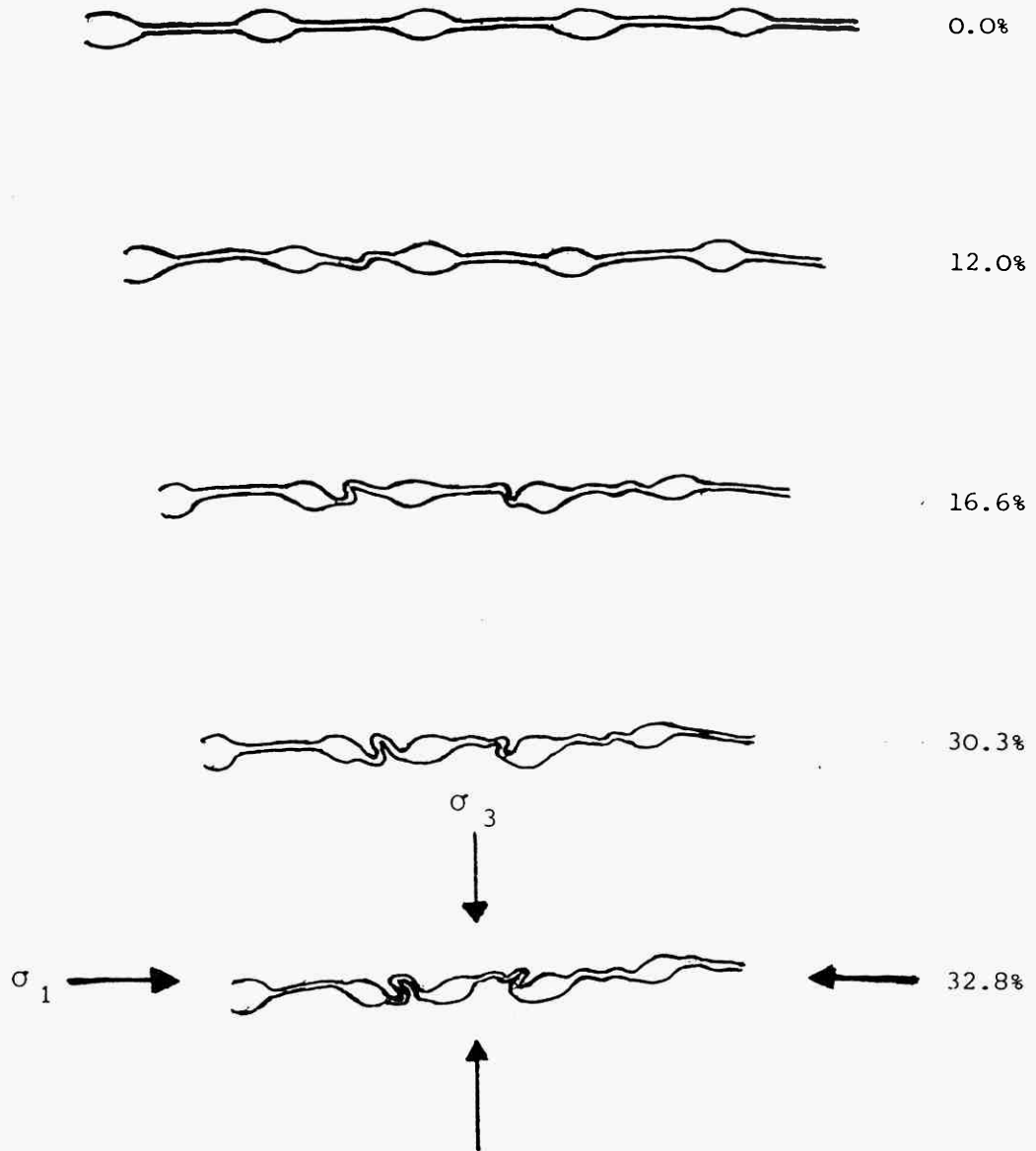


Fig.2.24 Five stages in the progressive deformation of Model 46

## 2.8 Experimental Problems

### 2.8.1. Volume change

1. The Pure Shear Deformation rig (fig. 2.1.A) was designed to achieve deformation without volume change. However volume changes do occur. The variation in model area with deformation is shown in the graph in fig. 2.25. Since the width of the model is kept constant (5cm) it is the area change that accounts for volume change. For details see Cobbold (1973).

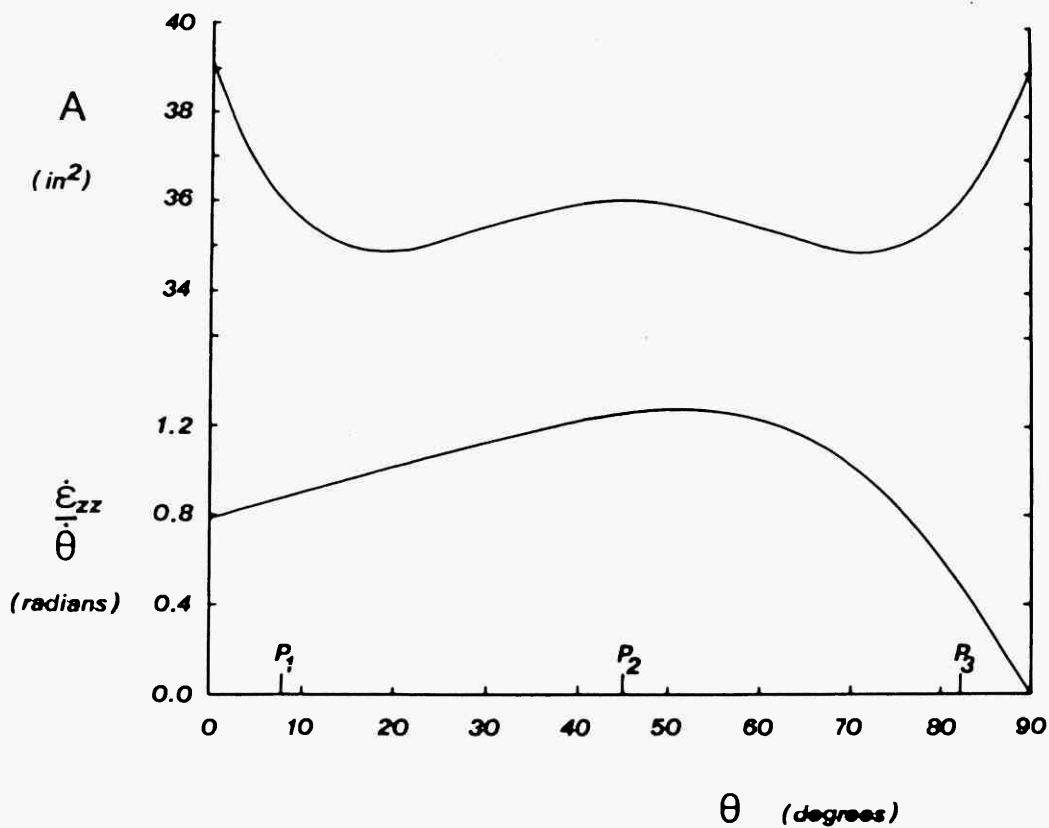


Fig. 2.25. Variation in model area ( $A$ ) and ratio of strain-rate and angular velocity ( $\dot{\epsilon}_{zz} / \dot{\theta}$ ) with the angle,  $\theta$ , of the rotors (see fig. A.1.5) (after Cobbold, 1973).

2. In wax experiments after the model has been placed in the deformation rig volume change occurs during the heating up of the model from room temperature to the temperature at which the experiment is to be run. The volume change is particularly significant ( $\approx 5\%$  maximum) in models using low melting point paraffin wax and in experiments run at high temperatures ( $38^{\circ} - 41^{\circ}\text{C}$ ). The main reason why it is significant in low melting point paraffin wax running at high temperatures is probably because the oily constituents of the less competent wax escape during the early stages of the experiments. This does not, however, seem to affect the structures formed by compression normal to the layering. However in the experiments involving the deformation of pinch-and-swell structures where the compression was parallel to the layering the effect of the draining of the lubricants from the upper part of the model on the style of folding that develops is significant. In experiment 46 (fig. 2.20D, 2.24) for example, the folds with large volume change (or large voids) developed into a kind of 'mushroom' (or 'box') fold while in most of the other models the folds were inclined isoclinal folds.

3. The matrix in the plasticine models contains air trapped during the preparation. Rolling helps to remove this but does not remove it all. As a consequence there is some volume change as air escapes during the deformation.

#### 2.8.2. LUBRICANTS

The lubricants used were silicon grease, vaseline, liquid soap and glycerol (see Cobbold, 1973, for details of rheological behaviour). The performance of liquid soap is excellent but it has a tendency to

dry and must be kept wet during the heating up of the model. This is achieved by placing beakers of water in the deformation box (fig. 2.1.A.7). During the heating up of the model, the liquid soap tends to drain to the bottom of the model. This depletion in lubricant at the top of the model may result in the smearing of the top of the model against the retaining plates partially obscuring the structures as they develop and making photography difficult. The best way to avoid this effect is by cutting the top surface of the model as smooth as possible and spreading the lubricant very evenly over the model. The best lubricants were found to be liquid soap and glycerol. Low temperature experiments ( $28^{\circ}$  -  $30^{\circ}\text{C}$ ) had fewer lubrication problems than high temperature experiments.

### 2.8.3. Different batches of paraffin waxes

There were slight differences in rheological behaviour of different batches of commercially 'identical' waxes. These differences were found to affect the behaviour of some models, in particular models run at  $36^{\circ}\text{C}$  using  $54^{\circ}\text{C}$  m.pt. wax. For example, Model 52 was made up of commercially 'identical' waxes ( $54^{\circ}\text{C}$  m.pt.) and run at  $36^{\circ}\text{C}$ , as was Model 14; type A structures in Model 52 were almost non-existent compared to the type A structures that developed in Model 14. It is therefore important to make some rheological checks before using paraffin from different batches.

In this chapter the various types of structures which developed experimentally in multilayers and single layers compressed at a high angle to the layering are discussed. These structures were described and classified in chapter 2. In the discussion that follows the four classes of structures recognised in chapter 2 are considered and an attempt is made to relate them to the structures predicted by various theories discussed in chapter 1. Natural examples which resemble the structures are also given.

### 3.1 Type A - Interlocking Pinch-and-Swell Structures (Internal Boudins)

These extensional structures (fig. 2.4.B.C) were described by Coe (1959) as boudinage structures which developed in a series of siltstones within which there was no obvious lithological variation (i.e. no competence contrast), but which possessed a marked mechanical anisotropy (fig.1.9). Biot (1965) has investigated the deformation of such a material and considered the structures (internal buckles) that would develop if it were compressed parallel to the planar fabric. Cobbold et al (1971) and Cosgrove (1976) using Biot's theory described structures that might develop in an anisotropic material compressed normal to the planar fabric. They argue that when a material with a relatively low mechanical anisotropy is compressed normal to the planar fabric interlocking pinch-and-swell structures (internal boudins) will develop (fig.3.1.). They demonstrated this using multilayers of identical plasticine layers (i.e. no competence contrast) but with low cohesion between the layers. Interlocking pinch-and-swell structures developed when the multilayer was compressed normal to the layering (fig.1.28a).

Interlocking pinch-and-swell structures may develop in a variety of materials, for example, a planar or linear fabric or a layered media.

If a finely foliated media is compressed at a high angle to the foliation, interlocking pinch-and-swell structures may develop as shown in fig. 3.1.A.

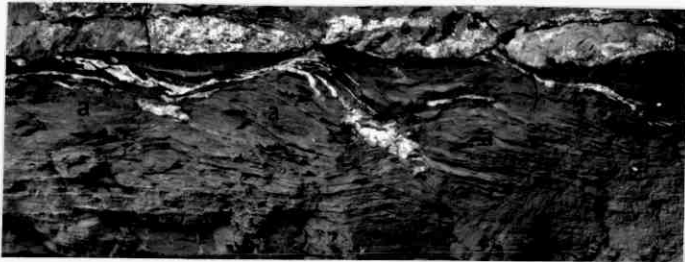


fig. 3.1.A.

Fig. 3.1.A. interlocking pinch-and-swell structures in a finely foliated media (shale) compressed at a high angle to the foliation. (after Cobbold et al., 1971)

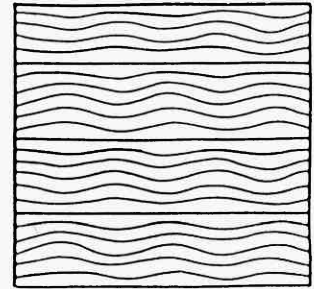


fig. 3.1.B

Fig. 3.1.B. The effect of type 1 displacement pattern (sec. 1.5, pages 103-105) on marker lines originally at  $90^\circ$  to  $\sigma_1$ .

Cobbold et al. (1971) have shown that if the mechanical anisotropy of a material is high then normal kink bands rather than interlocking pinch-and-swell structures may form when compression is at a high angle to the fabric (fig. 3.1.C). It is interesting to compare the geometry of interlocking pinch-and-swell structures (fig. 3.1.A and B) with that of the normal kink bands (fig. 3.D). The interlocking pinch-and-swell structures are geometrically indistinguishable from a regular array of intersecting conjugate kink bands (cf. fig. 3.1.A and D).

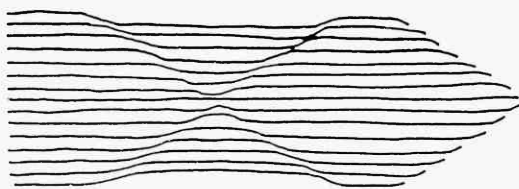


fig.3.1.C

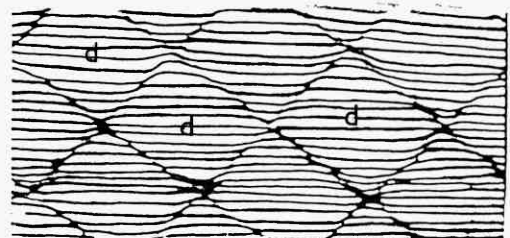


fig.3.1.D

If an anisotropic material is distinctly layered as opposed to having a more pervasive fabric, then there are two possible ways in which interlocking pinch-and-swell structures may develop when the multi-layer is compressed at a high angle to the layering.

The first is the development of interlocking pinch-and-swell structures in which each individual layer develops pinch-and-swell structures as shown in fig. 3.2.A.

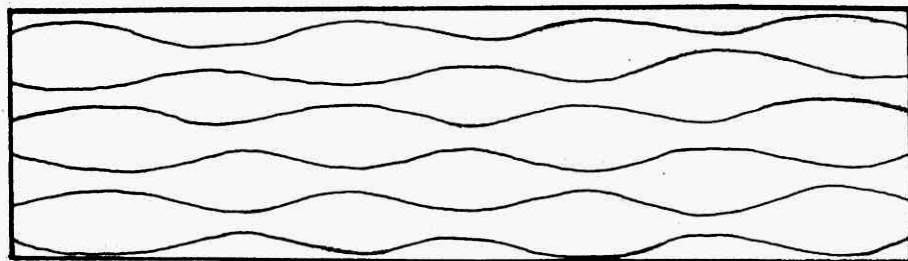


fig.3.2.A

Alternatively, the unit in which pinch-and-swell structures are developed contain several layers (8 in the example shown in fig. 3.2.B). The limits of the pinch-and-swell structure units are shown by a thicker line in fig. 3.2.B.

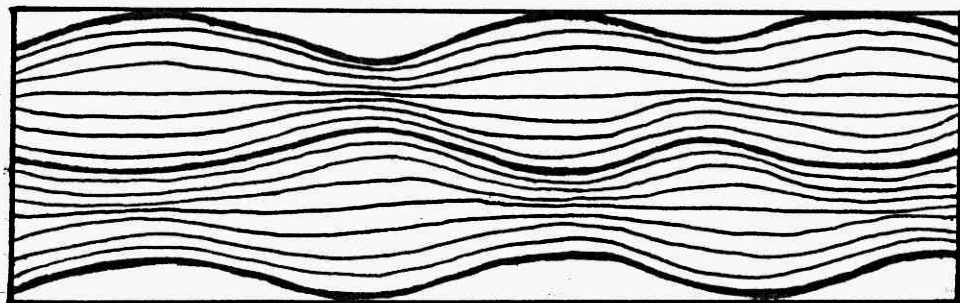


fig.3.2.B

The present author has investigated the initiation and development of interlocking pinch-and-swell structures using paraffin wax as a modelling material. From these experiments (fig. 2.4 and 2.5) it was observed that once a particular layer necked and formed a pinch-and-swell structure, the swell of that layer produced a pinch in the adjacent layer. The process continued forming an interlocking pinch-and-swell structure



geometry similar to those shown in fig. 3.1.A and 3.1.B.

The geometry that results from the oblique alignment of pinched zones (fig. 3.2.A and fig. 2.4.C) is indistinguishable from that of a normal kink band. Similarly interlocking pinch-and-swell structures may be geometrically indistinguishable from a regular array of intersecting normal kink bands.

In the experiments (No. 14 and 23) it was observed that the thinning that occurred at the pinches formed by the pulling apart of individual layers or band of layers, and were therefore tensile instabilities. They did not form as a result of the intersection of conjugate shear zones (i.e. were not shear instability). However, as mentioned above the pinch zones are often aligned in such a way as to constitute normal kink bands at  $60^{\circ}$  to  $65^{\circ}$  to  $\sigma_1$  as soon as the pinches are initiated.

The interesting problem poses itself as to whether "shear failure" occurs by the en echelon arrangement of local tensile failure. The close relationship between the internal instability associated with interlocking pinch-and-swell structures and normal kink bands will be apparent from the above discussion. However, although structures with identical geometry could result by two different mechanisms, that is, the development of interlocking pinch-and-swell structures or of intersecting normal kink band array (c.f. fig. 3.1.D and 3.1.A), it may be possible to differentiate between these two possibilities in the field if the spacing between the normal kink-bands in the arrays is large enough for the lozenge shaped zones (fig.3.1.D.d) to contain relatively undeformed foliation (c.f. 3.1.A.a and 3.1.D.d).

From experiments such as Experiment 14 (fig. 2.4) it can be inferred

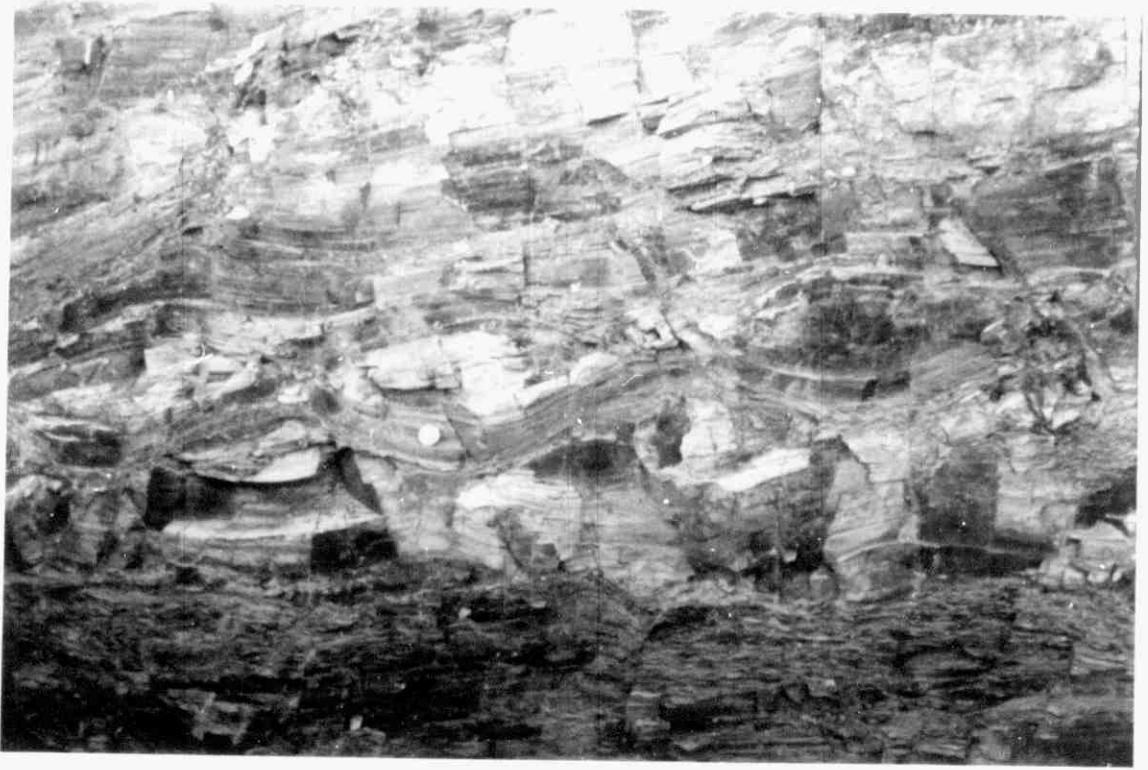


Fig. 3.3 Complex of multilayer boudins. La Carolina, near Ciudad Real, Spain. (Lower photograph is magnified view of one boudin). (after Cobbold, 1973)







Fig. 3.4 A. Interlocking pinch-and-swell structures and incipient shears in metasediments - below Glarus Nappe, near Flimms, Swiss Alps, (after J. Cosgrove).

B. Interlocking pinch-and-swell structures and "incipient" shears (normal kink bands) in a rock consisting of alternating quartz-rich and mica-rich layers from near Torcross, N. Devon, England, (after J. Cosgrove).

that when pinch-and-swell structures are concentrated in a particular horizon (e.g. next to the pistons in the experiments) (fig. 2.2-b.b), the horizon is strained-softened. The initiation of pinches and swells seems to initiate local rheological change perhaps as a result of the change in orientation of the plane of anisotropy in the perturbed domain. The localisation of pinch-and-swell structures in particular horizons is discussed more fully in section 3.3.

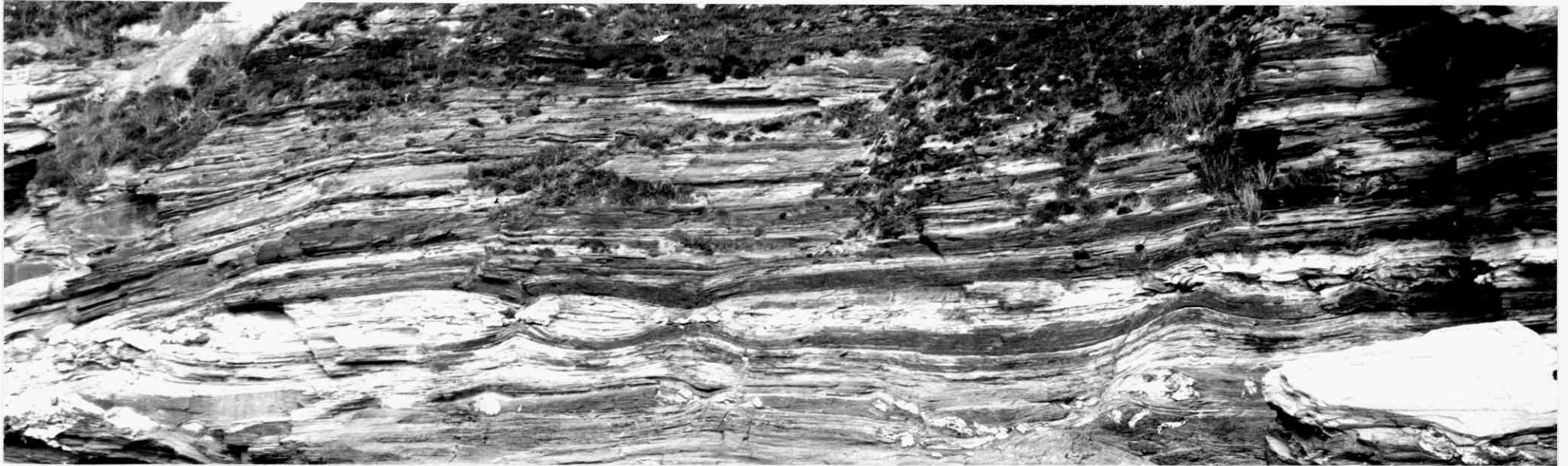
Fig. 3.3 shows an example of interlocking pinch-and-swell structures in multilayers from La Carolina, near Ciudad Real, Spain.

Another natural example of internal boudinage structure of triclinic cross-section shape is shown in fig. 3.4.A This is strikingly similar to the type A structures formed in Models 14 and 23 (fig. 2.4 and 2.5).

Note the similarity of the interlocking pinch-and-swell geometry between those of natural examples in metasediments (fig. 3.3) and foliated rocks (fig. 3.1.A and 3.5).

An example of both interlocking pinch-and-swell structures and boudins which developed as a result of breaking at the pinch regions is shown in fig. 3.6. These lenticular boudins are similar to those produced in experiments (No. 28, fig. 2.9).





0 5 m

Fig. 3.5 Large-scale interlocking pinch-and-swell structures (internal boudins) in metavolcanics from Trebarwith Strand, Tintagel, N. Cornwall, England.

NB. The volcanic pile has a pervasive mechanical anisotropy but also has layers of different properties. It is apparent that these layers determine where pinch-and-swell structures develop.

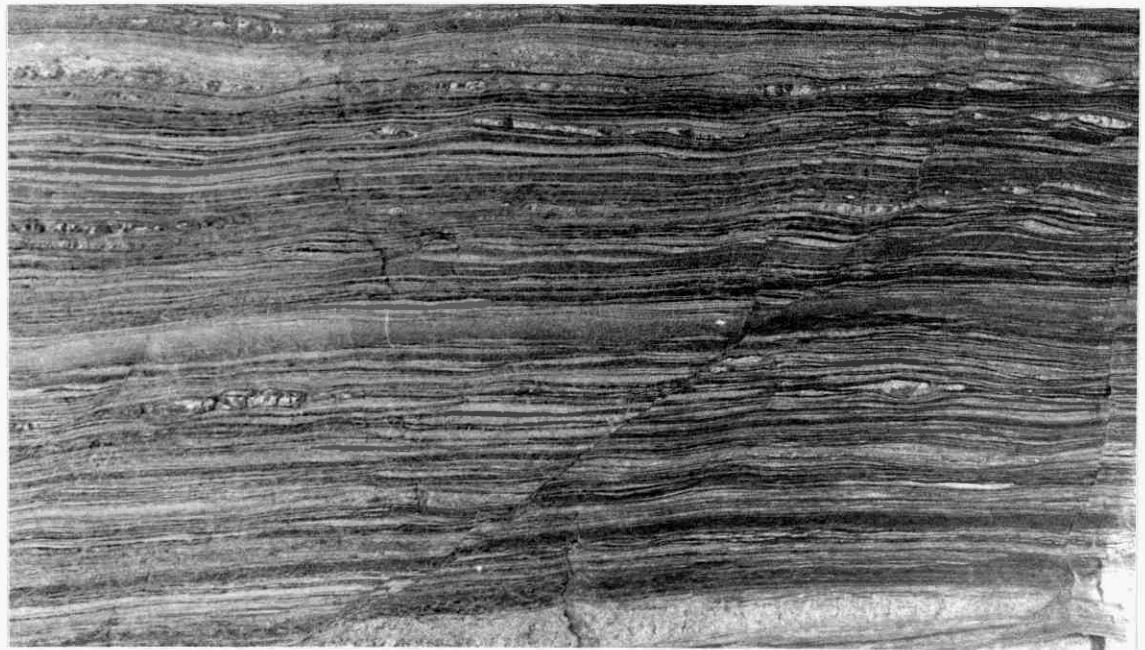


Fig. 3.6 Interlocking pinch-and-swell structures in metasediments (quartzite/phyllite) from Castañeras Beach, Oviedo, N.Spain.

A. Note the incipient shear initiated from the pinch region of the thick layer.

B. Enlargement of part of photograph A.

### 3.2 Type B-1 structures

A horizon of tension gashes in an apparently uniform planar fabric as shown in fig. 3.7.A. is often seen in nature. A number of experiments (21, 22, 23) were performed to investigate the effect that these tension gashes might have if deformation had continued after their formation.

The development of tensile fractures in a particular horizon may occur, for example by hydraulic fractures if the horizon has a slightly lower permeability than the rest of the multilayer. During deformation these fractures may open and the adjacent layers may be deflected into the fracture. Alternatively the voids may be filled by mobile minerals such as quartz or calcite that migrate to areas of relatively low pressure. In experiments 21-23 lubricating fluid squeezed out from the multilayers during the deformation and filled the voids.

This type of boudinage structures has been identified and described by Platt and Vissers (fig. 3.8). The examples they describe are from Waroga shear zone, Western Australia. They believe the boudins are controlled by a pre-existing foliation and suggest that the presence of a strong foliation limits the rate of ductile extension parallel to foliation (S). Extensional fractures form normal to S (fig. 3.9) and open out along S. The open fractures and the adjacent foliation are then pinched in by shortening normal to S. This implies the finite pinch-and-swell geometry was caused by brittle failure. In the experiments, however, (fig. 2.4) it is difficult to form extension fractures in thinly layered media. They usually produce interlocked pinch-and-swell structures (sometimes however individual pinched layers break and form local type B-1 structures). In order to study the development of B-1 structures it was found necessary to introduce fractures into the models.

The results of experiments 21 and 23 show that a distinct class of

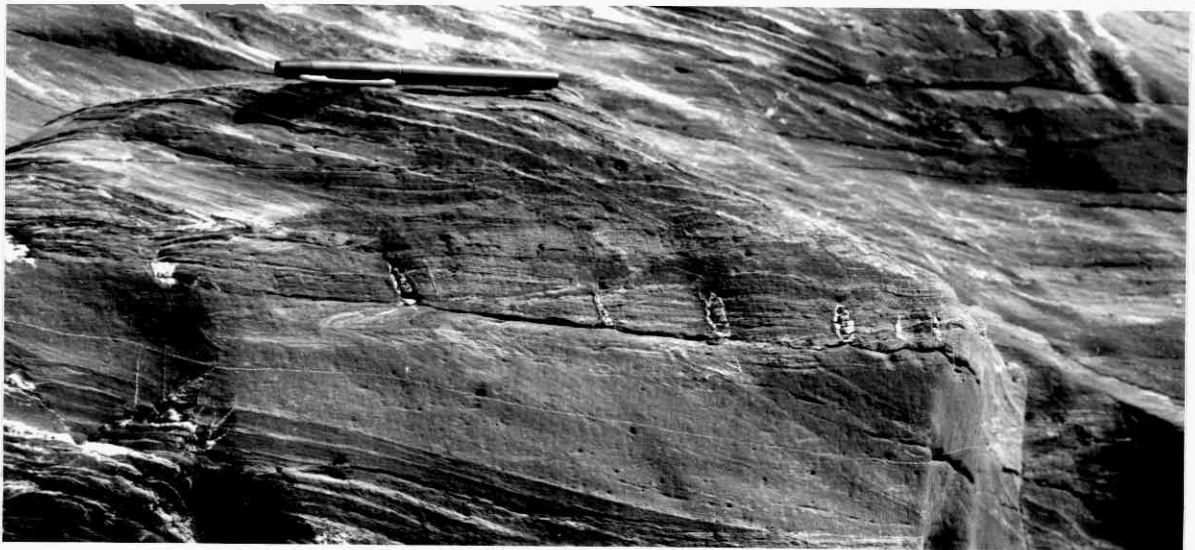


Fig. 3.7 A. A horizon of tension gashes in an apparently uniform planar fabric from Porthleven, S. Cornwall, England.

B. Enlargement of fig. 3.7.A.



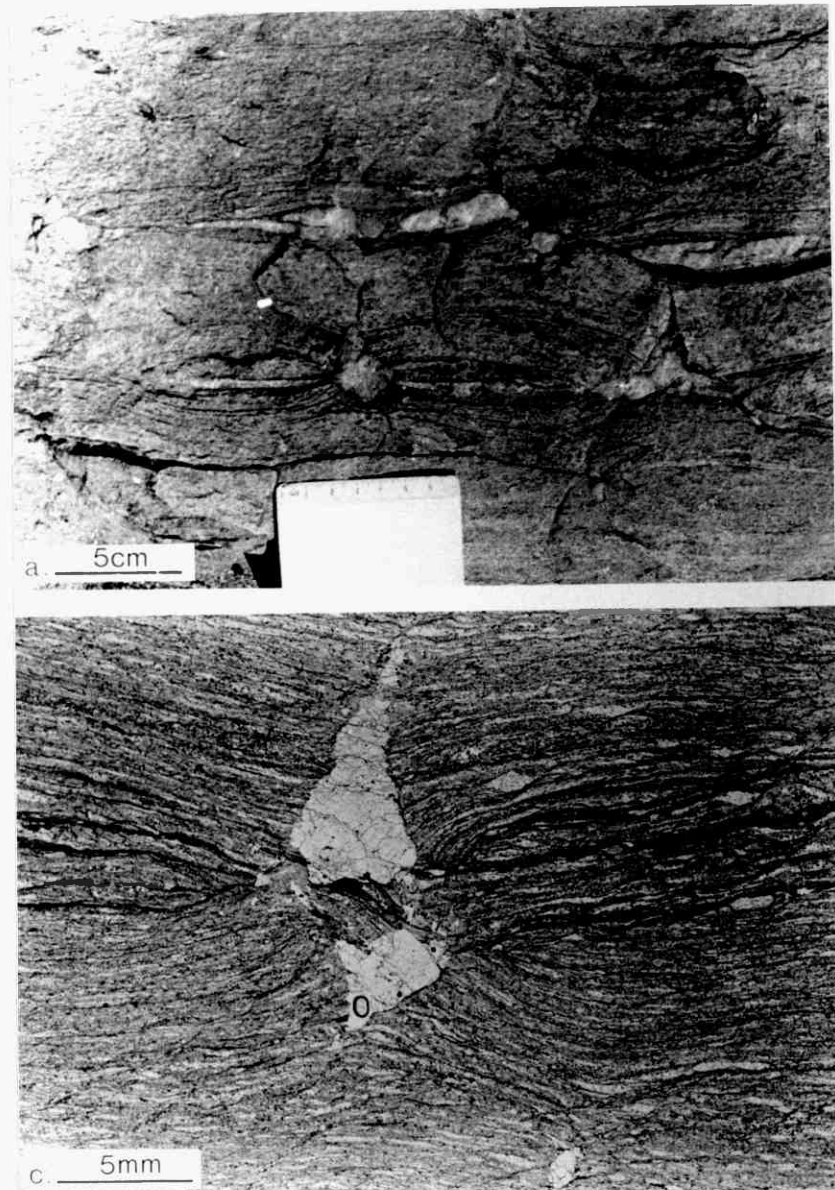


Fig. 3.8 Natural examples (schists) of type B-I structures from Waronga shear zone, Western Australia. (a) Field example, (b) Photomicrograph of a similar rock as (a), (after Platt and Vissers, 1980)

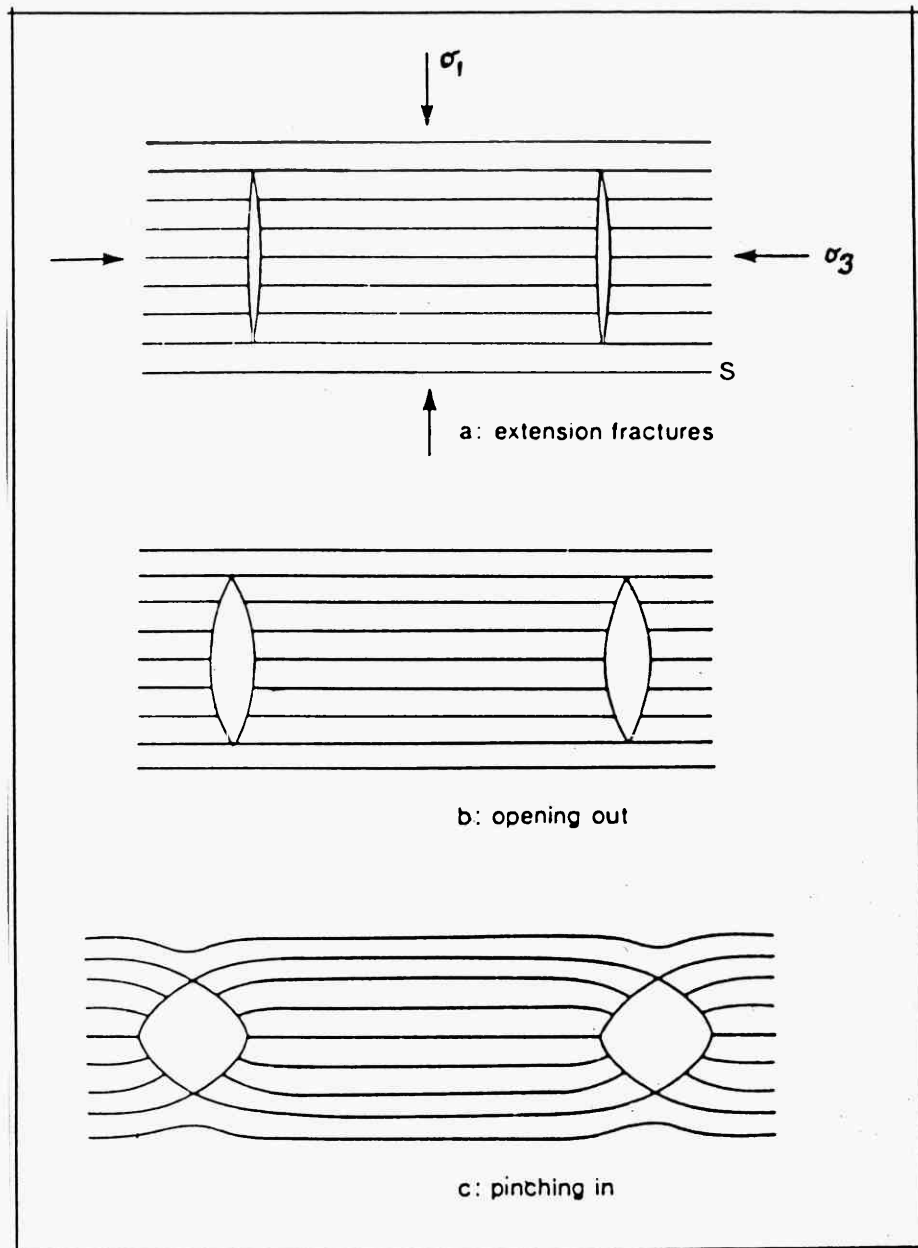


Fig. 3.9 Conceptual model of the development of type B-I structures (after Platt and Vissers, 1980).

boudinage structure is formed by the introduction of a gap (void) into the model. These voids act as a widened tensile fracture cutting a band of the multilayers. Apart from containing the 'fractures' the band is identical to the unfractured multilayer on either side of it. It has already been noted that a multilayer of identical layers compressed normal to the layering may develop interlocked pinch-and-swell structures. However it is found experimentally that the presence of voids (fractures) in such a multilayer favours the formation of a structure rather like the classical boudinage that forms in multilayers and single layers in which a high competence contrast exists between the layers or the layer and matrix.

Like type A structures, type B-1 structures occur in both multilayers and foliated rocks such as phyllites. However the initiation of type B-1 structures requires a local tension fracture in an individual layer or band of layers.

### 3.3 Type B-II structures

As was described in section 2.4 and mentioned in section 3.1, type B-II structures (fig. 2.2, 2.8) are lenticular 'boudins' which develop in a thinly layered media. They are similar to type B-I structures (fig. 2.2, 2.6) but are of horizons in which strain softening occurs sandwiching an horizon where no strain softening occurs. In the experiments the softening developed near the deformation plates and the central region of the model in which no strain softening was developed acted as a relatively competent horizon. Interlocking pinch-and-swell structures formed in the strain softened horizon whilst the central, relatively undeformed region deformed by homogeneous flattening.

The similarity between types B-I and B-II becomes apparent when the B-II structures developed in the experiments are viewed as individual boudins (fig. 2.4C, 2.9F), the re-entrants formed at the end of the models as the central horizon fails to extend as much as the surrounding strain softened horizons represent the neck region between boudins. At the end of experiment 14 the relatively undeformed central region had been shortened by 25% while the bulk shortening was 40%. The relatively undeformed central region of experiment 14 can be compared with the central part, a, of the type B-I boudins in Model 23 (fig. 2.5.F.a,a) which was shortened by 26% after 40% bulk shortening.

The initiation and development of type B-II structures confirms the idea that the properties of the individual layers making up a multilayer are not the only factors that determines the resistance to deformation. The deformation process also plays an important role, especially in thinly layered media. It was observed in experiment 14 that at a particular temperature ( $35^{\circ}\text{C}$ - $36^{\circ}\text{C}$  for  $54^{\circ}\text{C}$  m.pt.p.wax) strain softening of the multilayer occurred near the deformation plates. It was these softened bands which effectively

became the incompetent bands while the relatively undeformed central region became the competent band. Thus an original uniform multilayer in which no competence contrast existed between the layers is converted by the development of strain softened horizons into a material with bands that are relatively easily deformed (incompetent) and bands that are not so easily deformed (competent).

These effectively competent and incompetent bands which contain several individual layers, may also develop in multilayers containing layers with different competencies (experiment 28, fig. 2.9).

#### 3.4 TYPE C STRUCTURES

Type C boudins discussed in section 2.5, are the classical boudins named and described by Lohest (1909). They include rectangular and barrel-shaped boudins.

Experiments such as 47 and 51 (fig. 2.12 and 2.13) demonstrate clearly that the tensile fracture spacing in the relatively competent layers of a multilayer is governed by the layer thickness. The development of tension fractures in multilayers made up of alternating competent and relatively incompetent layers is discussed in detail below.

##### Effect of Temperature on Fracture separation (boudin width)

In the paraffin wax models the temperature proved to be the major factor that determined whether the layers behaved in a brittle or ductile manner. In the low temperature experiments (28°C for Models 47 and 51) rectangular boudins formed in the higher melting point (54°C) wax layers which behaved as a brittle competent material. In the higher temperature experiments (36°C for Model 28) lenticular boudins formed in the 54°C m.pt. p.wax layers which necked before separating. In Model 28, a relatively high

temperature experiment (fig. 2.9), the average width of boudins in the 1mm thick competent layers is more than in Models 47 and 51, relatively low temperature experiments. It is interesting to note that models used in experiments 49 and 50 were identical to those used in experiments 47 and 51. However experiments 49 and 50 were run at the relatively higher temperatures of 30<sup>o</sup> and 32<sup>o</sup>C respectively. Many of the structures that formed in the relatively competent layer were similar to those formed in experiment 28. The width of the boudins in experiments 49, 50 and 28, i.e. in the relatively high temperature experiments is greater than the width in experiments 47 and 51 (the relatively low temperature experiments). The reason for this is that extension of the relatively competent layer in the high temperature experiments is achieved by a combination of ductile flow and brittle fracture whereas in the relatively low temperature experiments the extension is achieved predominantly by brittle failure.

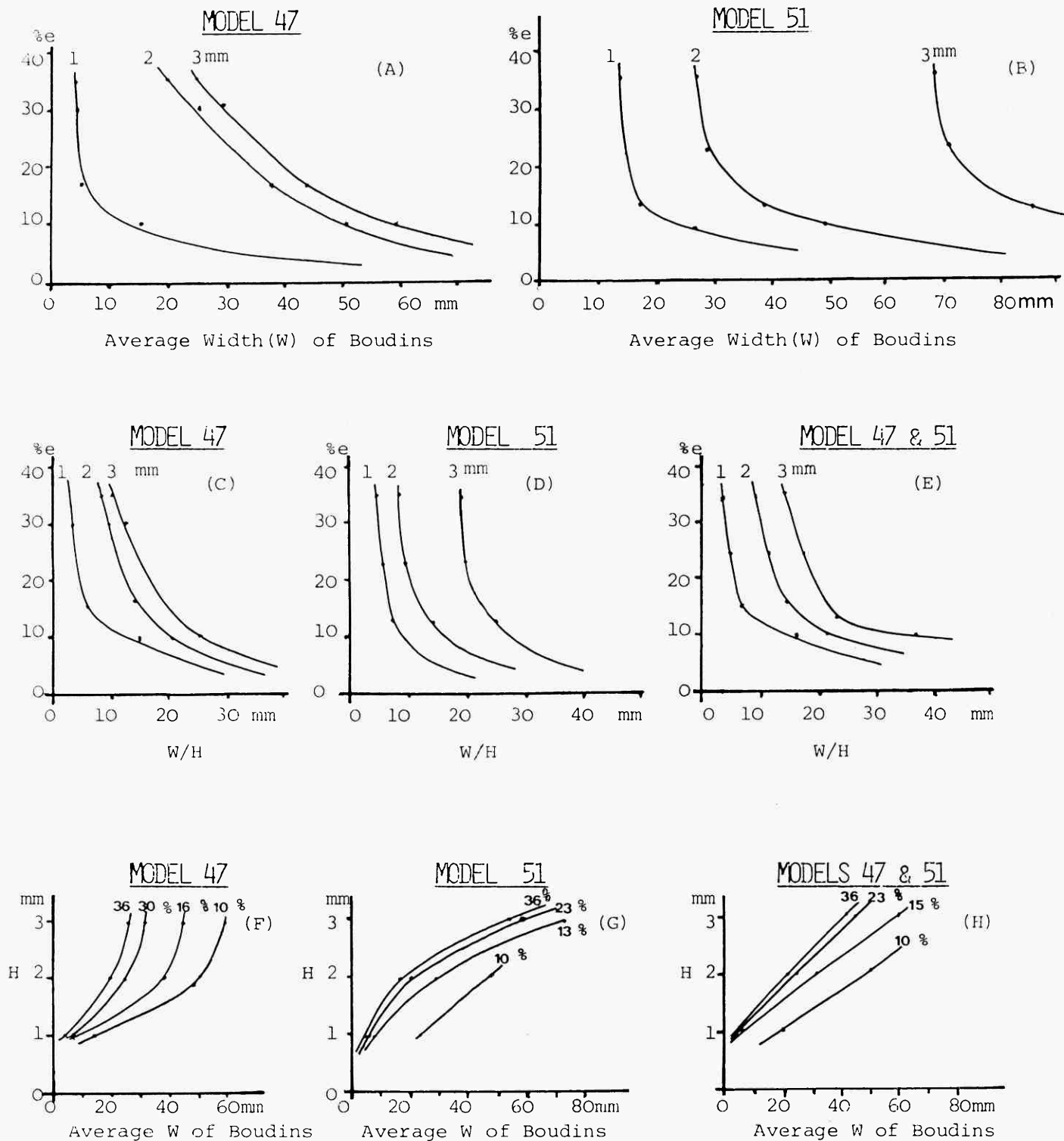
#### The effect of thickness on fracture spacing

Several experiments (28, 47, 48, 49, 50, 51) were performed to investigate the relationship between fracture spacing and layer thickness. The results of some of these experiments are summarised in the graphs and histograms of figs. 3.10, 3.11 and 3.12.

In the initial stages of the experiments the first formed tension fractures break the competent layers into boudins with relatively large width (fig. 2.13 B,C).

Graphs A-E (fig. 3.10) show the plots of the average width of boudins for the competent layers 1, 2 and 3mm thick against the percent strain (shortening) for Models 47 and 51. It is clear from the graphs that the width of the boudins decreases as strain increases.

The plot of the average width/thickness ratio of boudins against percent strain for the 1, 2 and 3mm thick competent layers of Models 47



%e is percent bulk shortening

H is the thickness of competent layers

W/H is the ratio of the average width of boudins to layer thickness.

Fig. 3.10 See text for explanation.

and 51 are shown in fig. 3.10.C, D & E.

The forms of graphs A to E (fig. 3.10) can be conveniently described by the hyperbolic function

$$y = \frac{k}{x} \quad (3.1)$$

where  $y$  = percent bulk strain

$x$  = average width of boudin

$k$  is a constant, which depends on layer thickness.

It can be seen from the graphs (fig. 3.10.A to E) that the fracture spacing in a particular layer varies in a non-linear way during the progressive deformation.

The set of graphs in fig. 3.10 F to H show the plot of layer thickness against the average width of boudins. Each curve represents a different stage in the bulk shortening of Models 47 and 51.

The curves are straighter in fig. 3.10.H, which is a graph of combination of graphs F and G (fig. 3.10), than in fig. 3.10 and G.

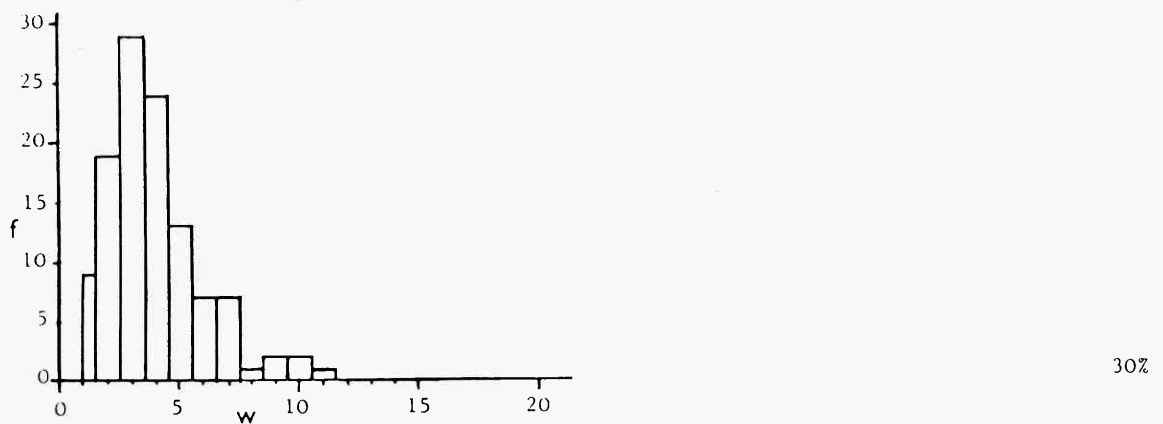
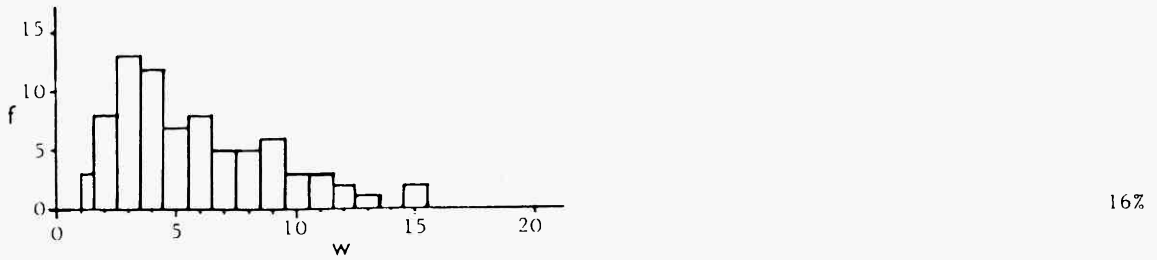
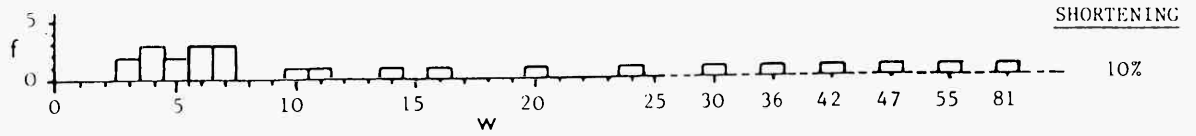
This suggests that statistically the relationship between the thickness and width of the boudins developed at a particular stage of deformation would be linear or nearly linear.

The histograms of the width of boudins at various stages in the progressive deformation of Models 47 and 51 are shown in fig. 3.11 and 3.12. It is apparent from these histograms that with progressive deformation the relatively wide boudins break down to form narrower boudins and that this breaking down occurs until an optimum width of boudins is obtained.

Although the experiments indicate that fracture spacing (boudin width) depends on both the layer thickness and the amount of deformation, it can be seen from the histograms of fig. 3.11, that the dominant width of boudins associated with a particular layer becomes apparent even after only a relatively



## MODEL 47



## MODEL 51

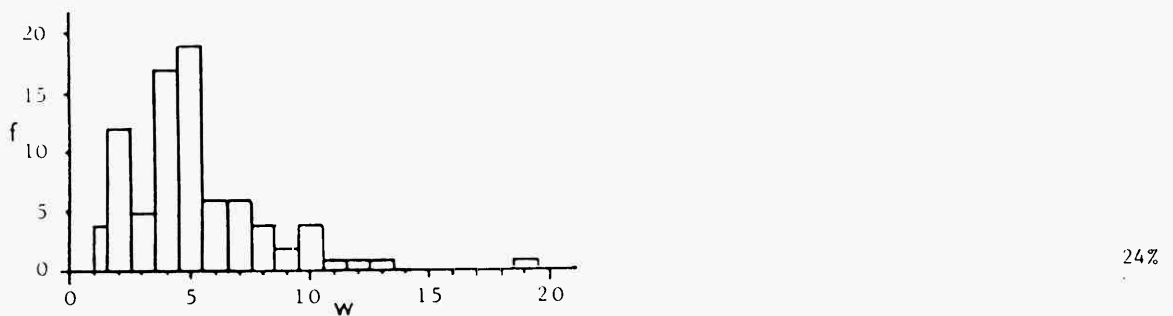
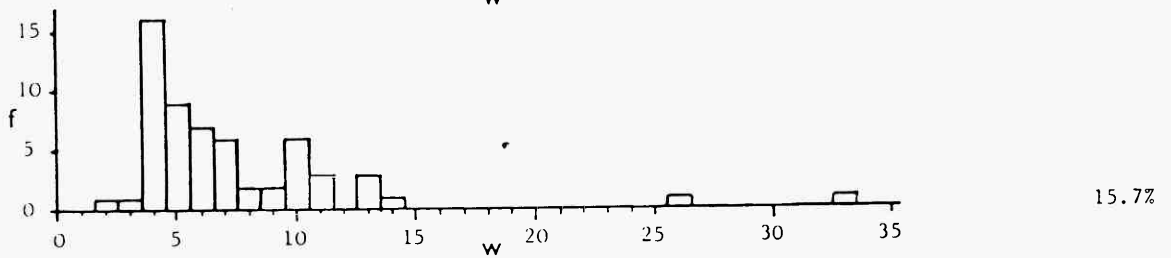
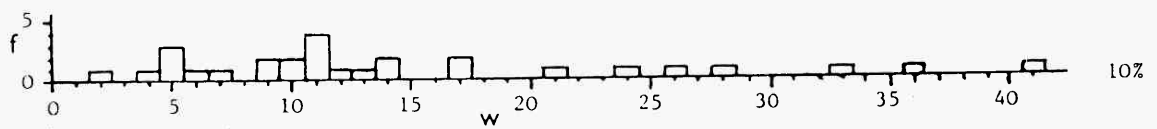


Fig.3.11 Histograms showing width( $w$ ) in mm, of the 1mm thick boudins of various stages in the progressive deformation of Models 47 and 51.

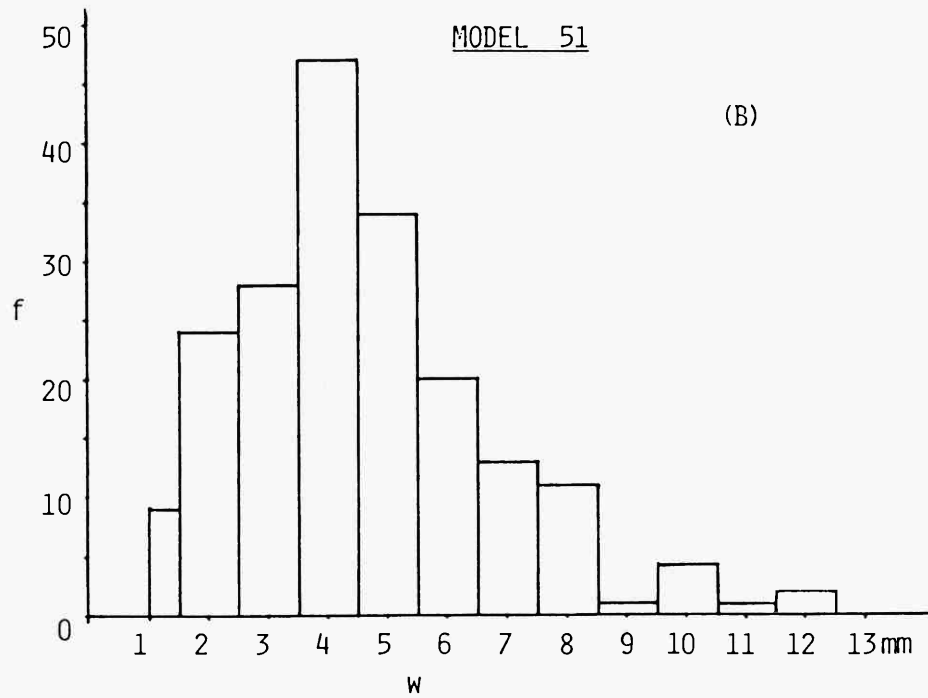
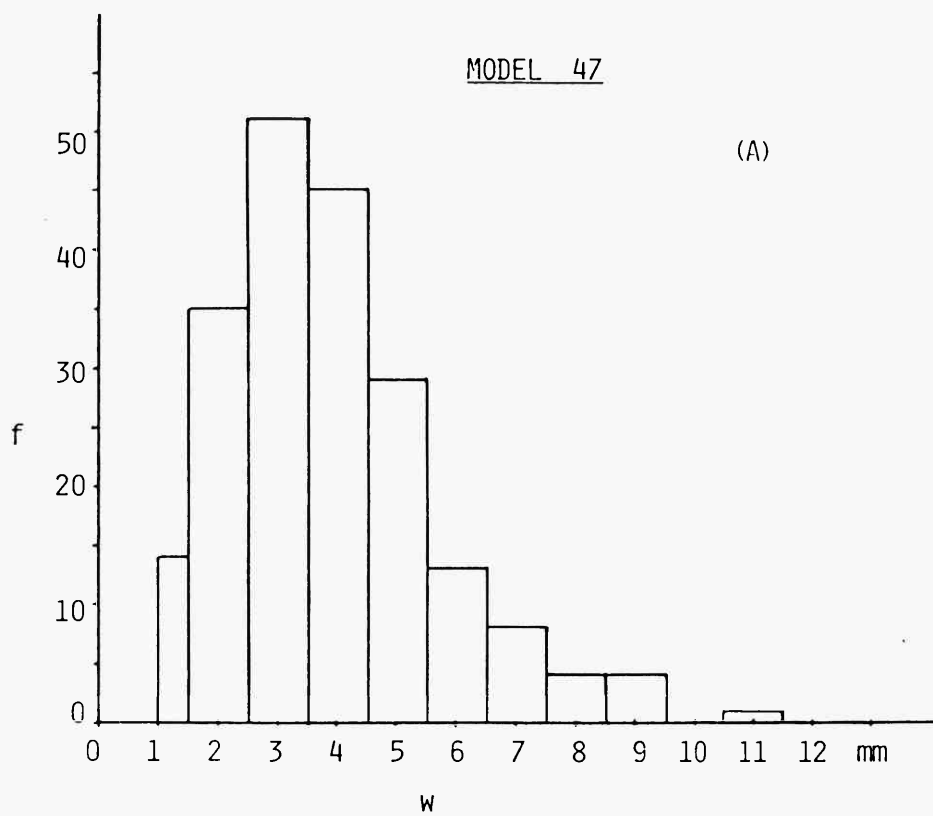


Fig.3.12 Histograms showing the width( $w$ ) in mm, of the 1mm thick boudins in the finite strain of Models 47 and 51 at 36% bulk shortening.

small amount of deformation. In experiment 47, for example, the optimum boudin width ( $\approx 4\text{mm}$ ) that developed in the 1mm competent layer can be clearly seen from the histograms after only 16% shortening (fig. 3.11).

In natural examples of boudins a fairly constant boudin width is generally observed to occur in a particular layer. However sometimes boudin widths are observed to vary considerably within a layer (fig. 3.13). This may be due to the fact that the total strain is relatively small and the optimum boudin width has not yet developed.

The examples shown in fig. 3.13. a, b, c are all from the region of Monte Ferone near Bazena, Bréno, Province of Brescia, N. Italy.



Fig. 3.13 (a)

Fig. 3.13 (a) Section view of competent pelite (grey-brown) boudinaged layers in a matrix of limestone (blue-grey). (after F. Peel).



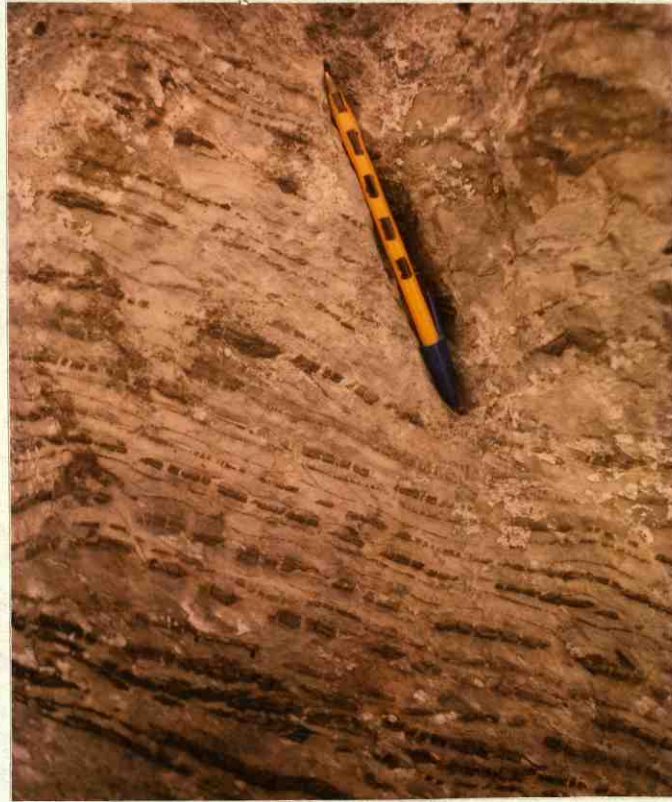


Fig. 3.13 (b)

Fig. 3.13 (b) Section view of a multilayer of competent pelite (dark) boudinaged layers containing various thicknesses in a matrix of limestone. Note the difference of boudin width in the various thicknesses.



Fig. 3.13 (c)

Fig. 3.13 (c) Close up view of the boudins shown in fig. 3.13(b) the section is however at a slightly different angle (after F. Peel).

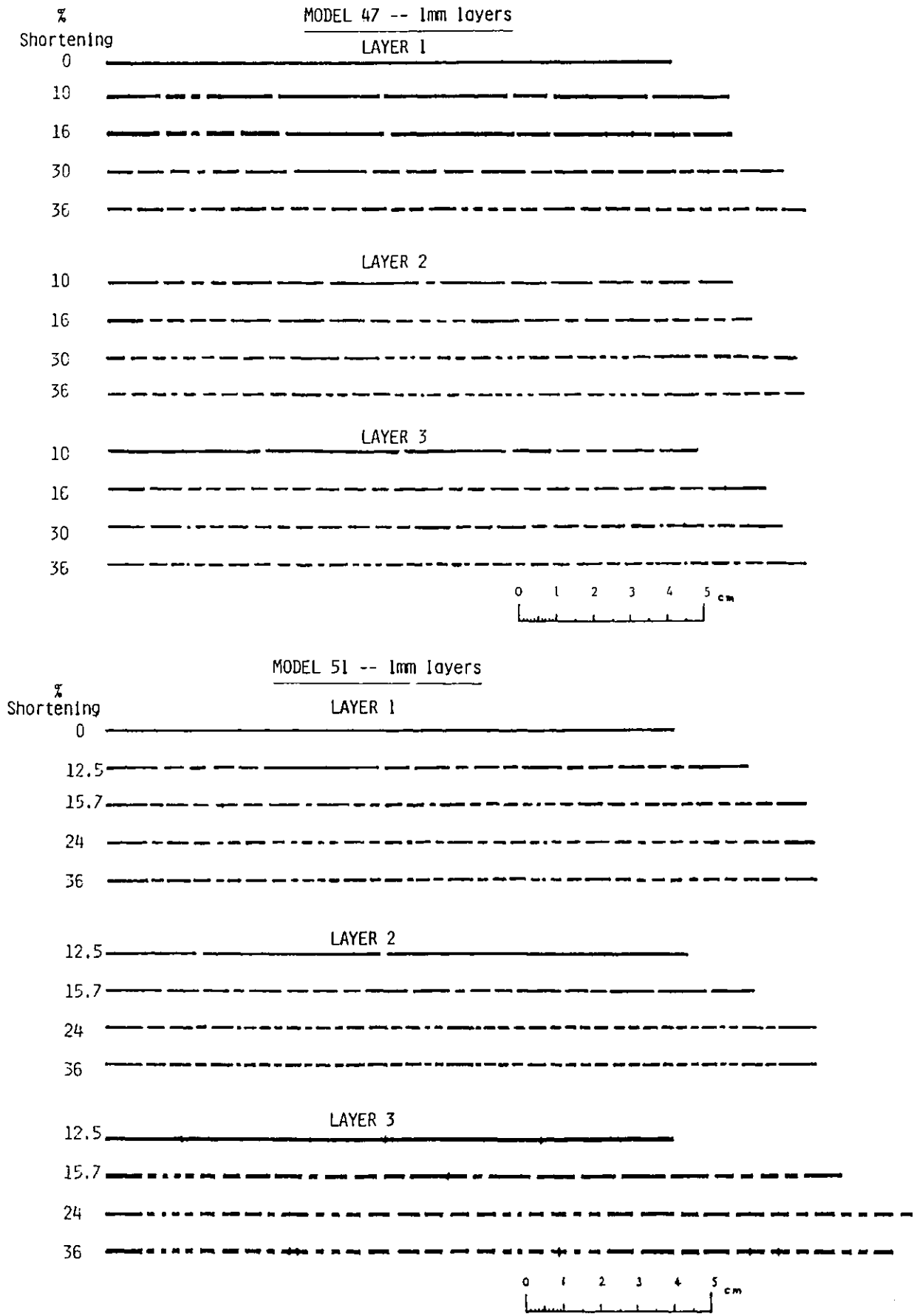
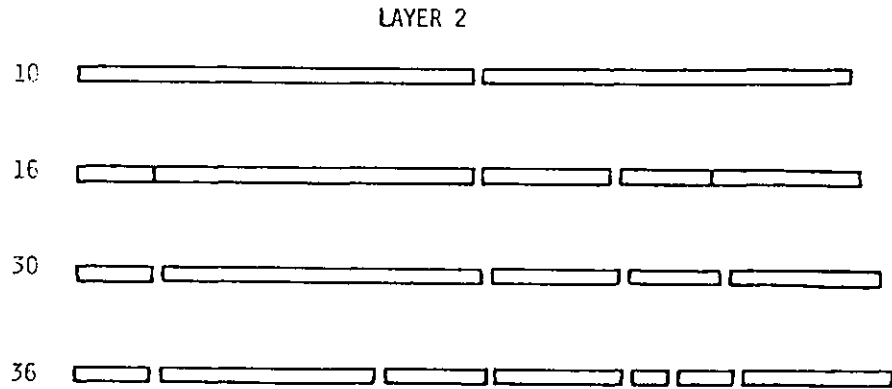
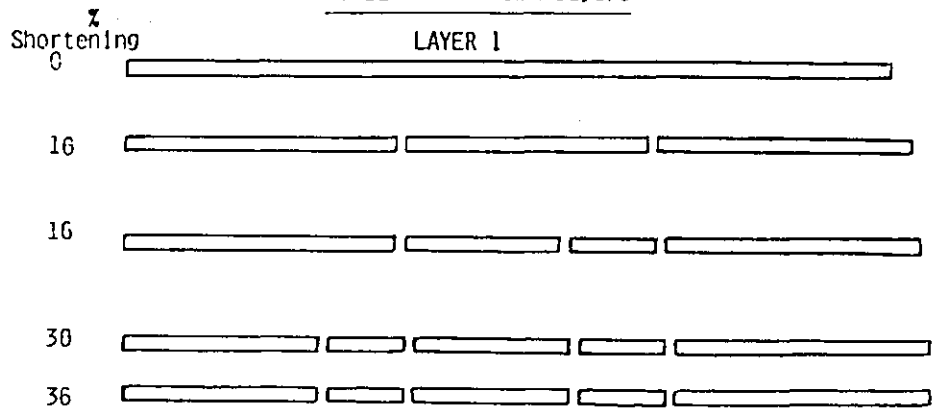


Fig. 3.14 Schematic representation to show the progressive fracturing of some of the relatively competent 1mm layers in Models 47 and 51.



MODEL 47 -- 2mm layers

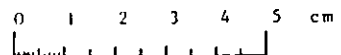
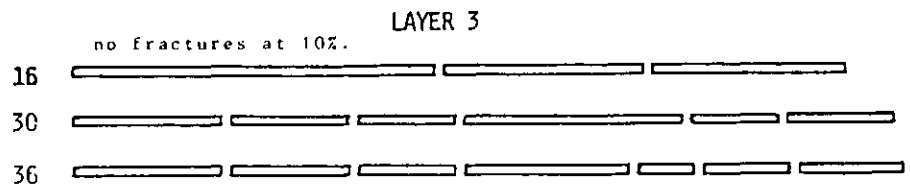
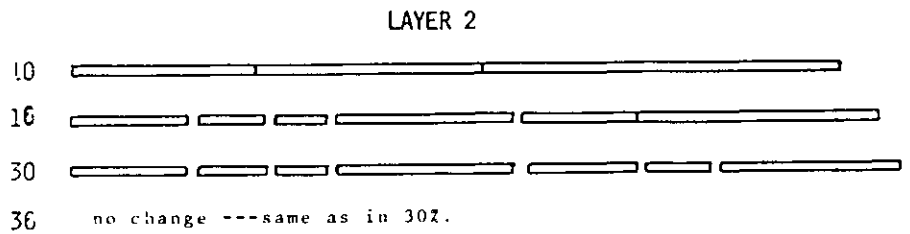
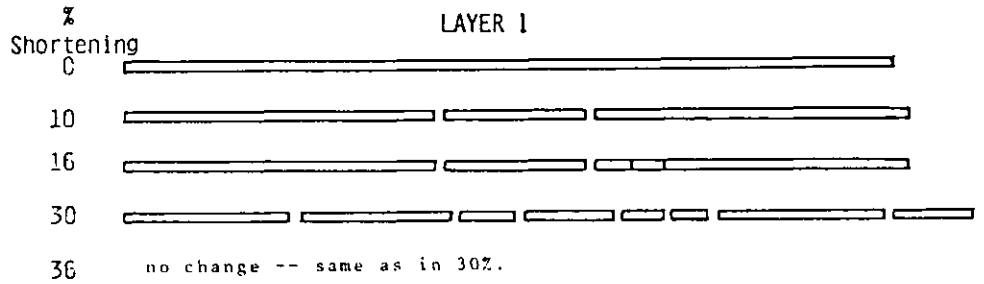


Fig. 3.15 Schematic representation to show the progressive fracturing of some of the relatively competent 2mm and 3mm layers in Model 47.

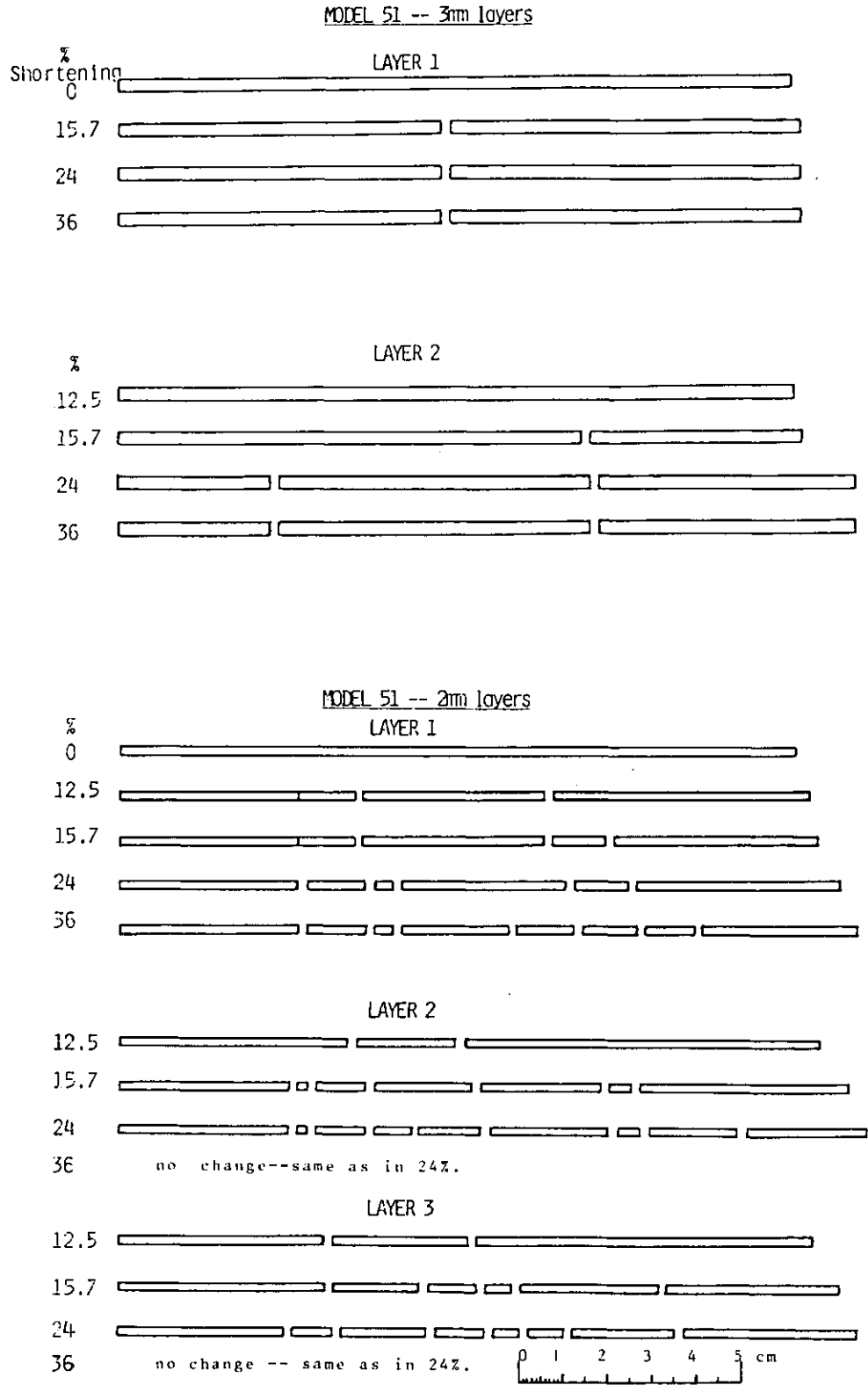


Fig. 3.16 Schematic representation to show the progressive fracturing of some of the relatively competent 2mm and 3mm layers in Model 51.

Six 1 mm thick layers (three from Model 47 and three from Model 51) at various stages of deformation are represented schematically in fig. 3.14. After 36% bulk shortening the average number of boudins for the three layers of Model 47 is 37 and for those of Model 51 is 36.

In fig. 3.15 and 3.16 six 2mm and six 3mm layers are represented schematically at various stages in the progressive deformation of Model 47 and 51. At 36% bulk shortening the average number of boudins in the 2mm layers is 8, in both models. At 36% bulk shortening the average number of boudins in each 3mm layer is 4. Thus the ratio of the number of boudins of 1mm to 2mm to 3mm thick layers is 9:2:1.

The relationship between the number of boudins and layer thickness determined from the experiments is, therefore, slightly non-linear. It is difficult to say whether this indicates a real non-linearity or whether the non-linearity is due to an incorrect value for the boudin width in the relatively thick layers. This value, based on relatively few boudins does not have same statistical confidence as the average boudin width for the thinner layers.

#### THE BREAKING OF BOUDINS DURING PROGRESSIVE DEFORMATION

In the early stages of an experiment the initially continuous competent layers are cut by only one or two tension fractures. These often divide the layer into boudins of considerably different widths. These boudins are then broken down into smaller boudins during the progressive deformation by the development of new tension fractures. The position of these new tension fractures has been studied and the ratio of the width of the two boudins formed from a larger boudin by the development of a tension fracture recorded for experiments 47 and 51. The results are shown by the histograms in fig. 3.17.



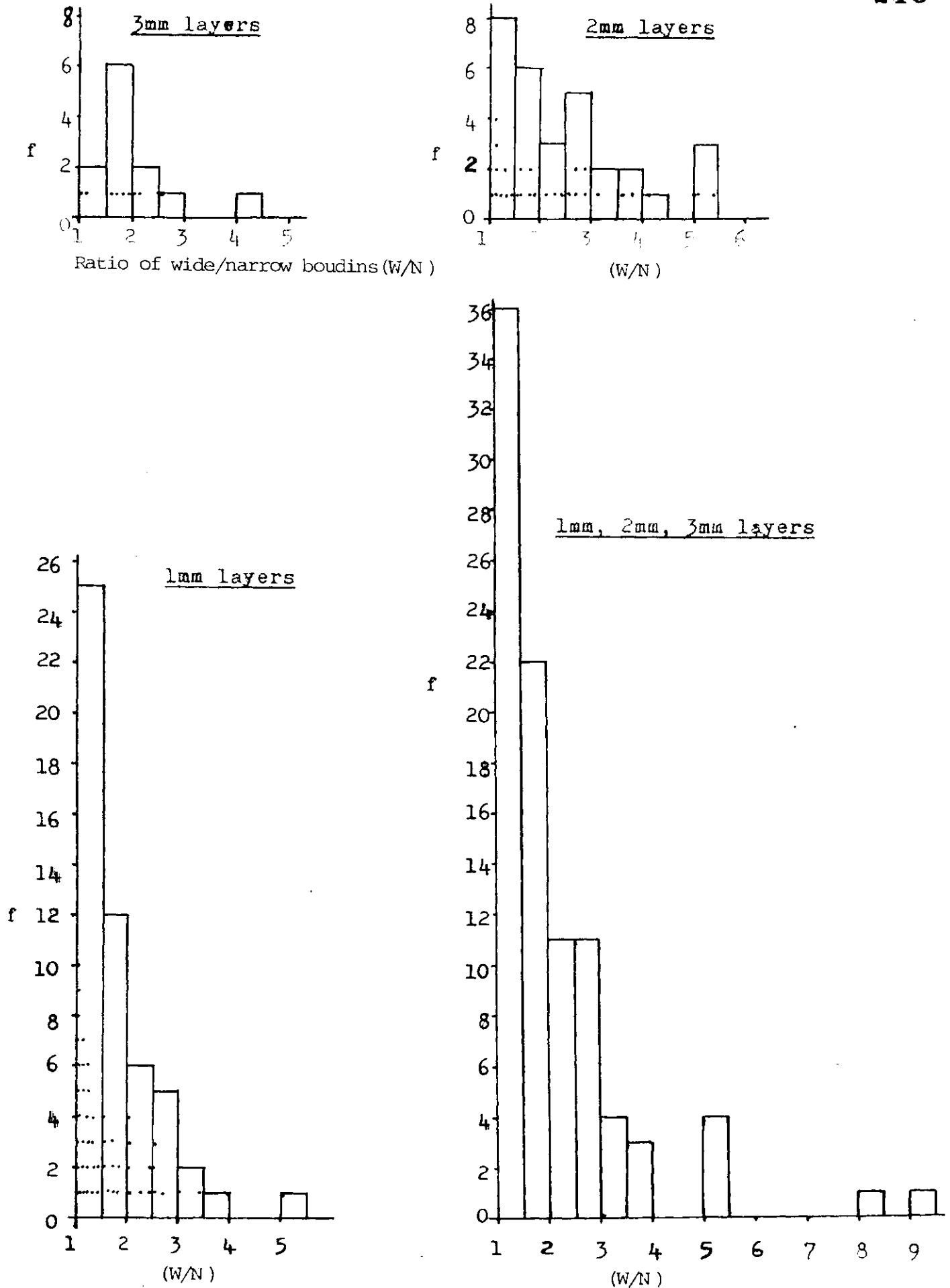


Fig. 3.17 Histograms of the ratio of wide to narrow boudins (or segments) as layers fracture during the progressive deformation of Models 47 and 51.

From these histograms (particularly C and D) it can be seen that statistically each boudin breaks into two smaller boudins of equal width as the theories of fibre loading (Ramberg 1955) and fracture spacing predict. However the spread of the histograms indicates that this does not always occur and that splitting in the ratios 1:2, 1:3 or 1:4 may occur. This is seen in the experiments, for example in Models 47 and 51 (fig. 3.17).

The splitting into ratios other than 1:1 may be a consequence of the experimental boundary conditions. However it is interesting to note that many geological examples (fig. 3.13) show boudins divided in ratios other than 1:1.

Fig. 3.18.a is a photograph taken looking down on a 1mm competent layer in Model 49. The neck regions between the boudins in the layer are the light areas.

The photograph, fig. 3.18.b, is taken looking down on a pelite (grey brown) layer and neck regions (blue-grey) of limestone from Monte Frerone, Breno, Brescia, N. Italy. It is interesting to note the similarity between the experimentally produced boudins (fig. 3.18.a) and the natural boudins (fig. 3.18.b).

The deflections of the layered matrix and the relatively thin competent layers towards the gaps (necked regions) between the relatively thick boudins produces fold-like structures as shown in fig. 2.11.b and 2.13.b. Watkinson (1981) pointed out that there is evidence that indicates some folding may have been influenced or initiated as a result of nucleation by large-scale boudins.

In both the experiments and in nature it is found that shear zones are commonly generated following the deflections of the matrix into the gaps between the relatively thick boudins. The zones, often conjugate pairs, propagate from the neck region at about  $45^{\circ}$  to the layering. In the experi-

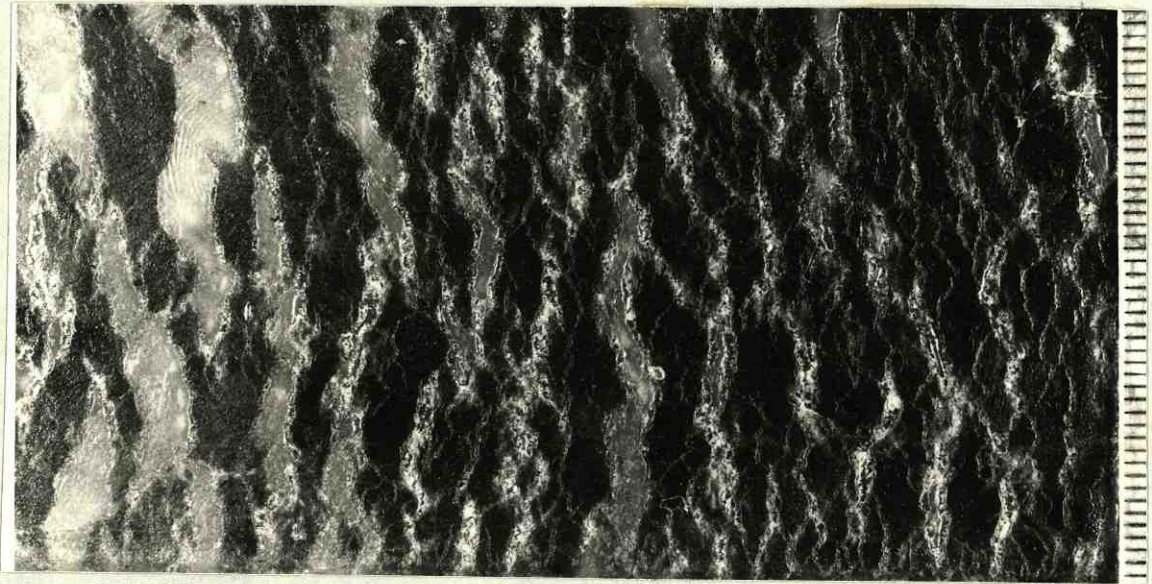


Fig. 3.18.a.



Fig. 3.18.b.

Fig. 3.18 Length (i.e. plan) view of experimentally produced boudins (a) and natural examples of boudins (b). See text for explanation. (b)(after F. Peel).

ments (e.g. experiment 51) it was found that the zones incorporated suitably situated tension fractures in the thinner competent beds.

Shear zones (fig. 3.18.c) which initiate from a local perturbation such as the neck region between two regions may occur in conjugate sets (see fig. 2.13 D,E). It is interesting to compare these (shear zones) with those associated with interlocking pinch-and-swell structures. In the latter example (fig.3.18.d) the regular array of perturbations (thinning and thickening of layers) produce regular array of conjugate normal kink bands (shear zones) as compared to the isolated structures, fig. 2.13.D,E, associated with local perturbation of a boudin neck.

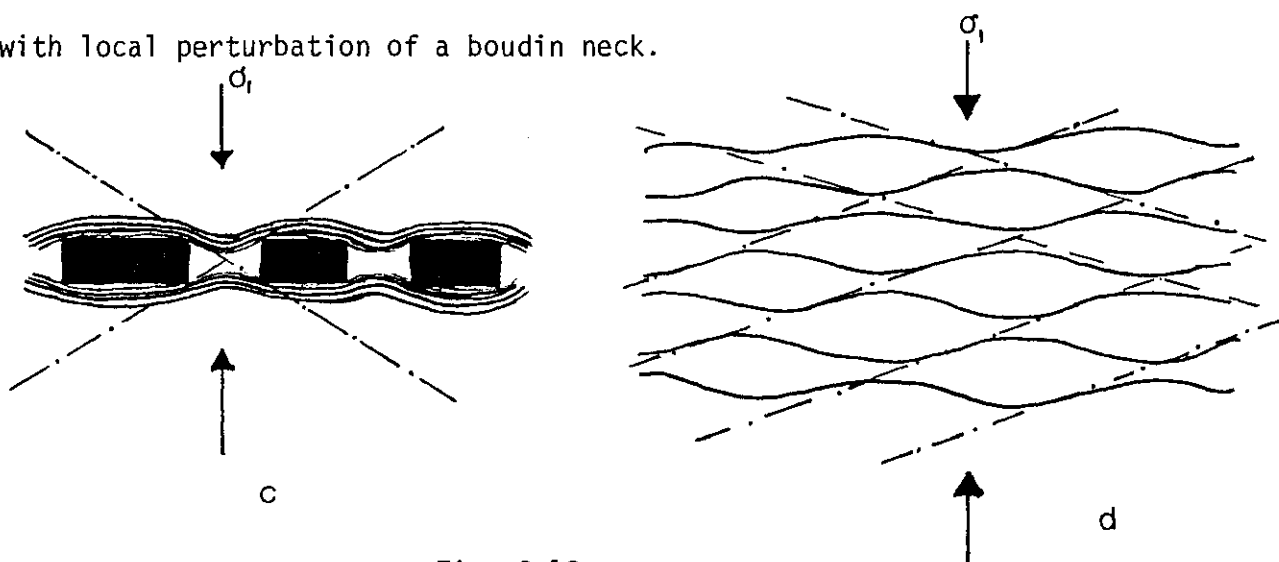


Fig. 3.18.

### 3.5 TYPE D STRUCTURES

In experiments in which multilayers and single layers were compressed at a high angle to the layering, structures were often formed in association with the development of discrete shear planes.

Shear failure planes often broke the competent layers into rhomboidal shaped blocks (fig. 2.14, 2.15, 2.17). Such blocks have been termed type D structures. It is interesting to note that discrete shear planes developed only in the plasticine and/or putty models. In the paraffin wax

models, although shear zones were produced they developed only after tension fractures (or pinch-and-swell structure in individual layers in the case of multilayers with identical layers) had formed in the relatively competent layers. The shear zones then incorporated suitably positioned tension fractures or pinched regions as they passed through the individual layers (see section 2.6, page 165 and fig. 2.13).

In the experiments involving a single layer of relatively competent plasticine set in a matrix of less competent plasticine it was observed that shear failure generally occurred initially in the competent layer. Later shear faults formed in the matrix and the orientation of the shears in the matrix was often such as to form the conjugate shear to that formed in the layer. Less frequently shear failure occurred in the matrix first. Sometimes the matrix shears propagated through the competent layer and at other times a shear, conjugate to the mature shear developed independently in the competent layer.

In multilayers consisting of identical plasticine layers, discrete shear faults initiated randomly throughout the model and were usually at  $45^{\circ}$  to  $\sigma_1$  (see section 1.22, fig. 1.28b and c).

In the single layer experiments discussed above the boudins are separated from each other by shear planes. During subsequent deformation displacement may occur along these planes. Consequently type D boudins are likely to be offset from each other (fig. 3.19).

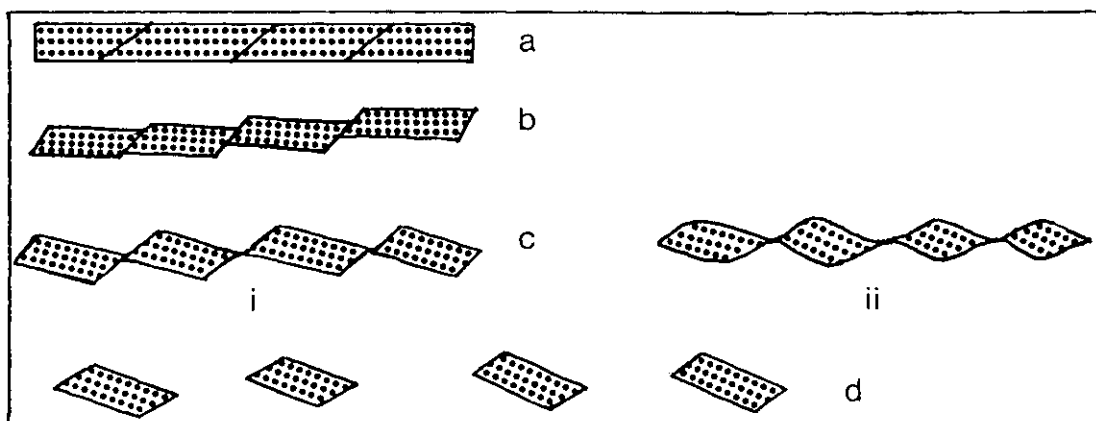


Fig. 3.19





e



f

Fig. 3.19 (e,f) Two natural examples of type D structures, multilayers of quartzite (competent) and phyllite from Castañeras Beach, Oviedo, N. Spain ((f) after J. Cosgrove).

As deformation proceeds slip occurs on the shear planes and the shear planes, originally at  $\approx 45^\circ$  to  $\sigma_1$ , rotate to a higher angle to  $\sigma_1$ . This process of rotation and slipping may continue until the individual boudins separate (fig. 3.19.c.ii and d). At this stage they may be indistinguishable from pinch-and-swell structures especially if an element of ductile deformation has occurred and the corners of the rhombohedral block have become rounded (fig. 3.19.c.ii and ii).

Ideally then, unless the deformation has progressed to stage d (fig. 3.19), it should be relatively easy to differentiate between type C and type D structures in the field.

Fig. 3.19(e) shows an excellent natural example of rhombohedral boudins initiated by shear failure. The multilayers consist of competent quartzite and incompetent thinner layers of phyllites.

The natural example of rhombohedral boudins shown in fig. 3.19(f) may also have been initiated by shear failure.

Type C are rectangular and not offset. Type D are rhombohedral and may be offset (fig. 3.20a.b).

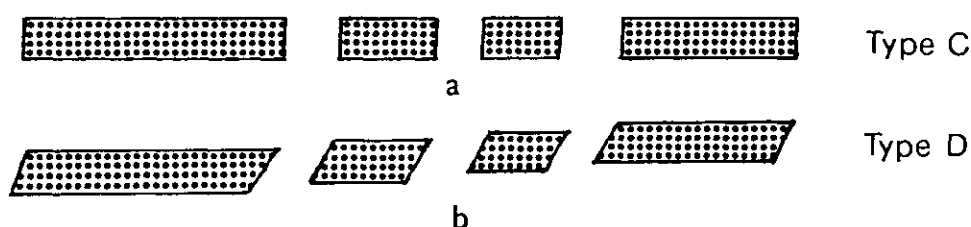


Fig. 3.20

However, there are several reasons why it is often difficult to distinguish between the two types in the field. Apart from the shear initiated rhombohedral boudins, there are three other ways in which rhombohedral boudins can be formed.

1. If the boudinaged layer was originally inclined to  $\sigma_1$ , then there

is a 'double' rotation effect, i.e. rotation of the individual boudins and of the inclined layer as a whole as it rotates away from  $\sigma_1$ . It was observed experimentally by both Ramsay (1967) and Hossain (1979) that the individual segments (or boudins) rotate more slowly than the layer as a whole. This results in the 'en echelon' arrangement of boudins shown in fig. 1.16.d.

In such a layer even rectangular boudins which initiate by tension fractures, will be offset (fig. 3.22.b). Shear parallel to boudin edges may during this rotation change the profile of individual boudins from rectangular to rhombohedral (fig. 3.22.c). The natural example shown in fig. 3.21 was probably formed in this way.

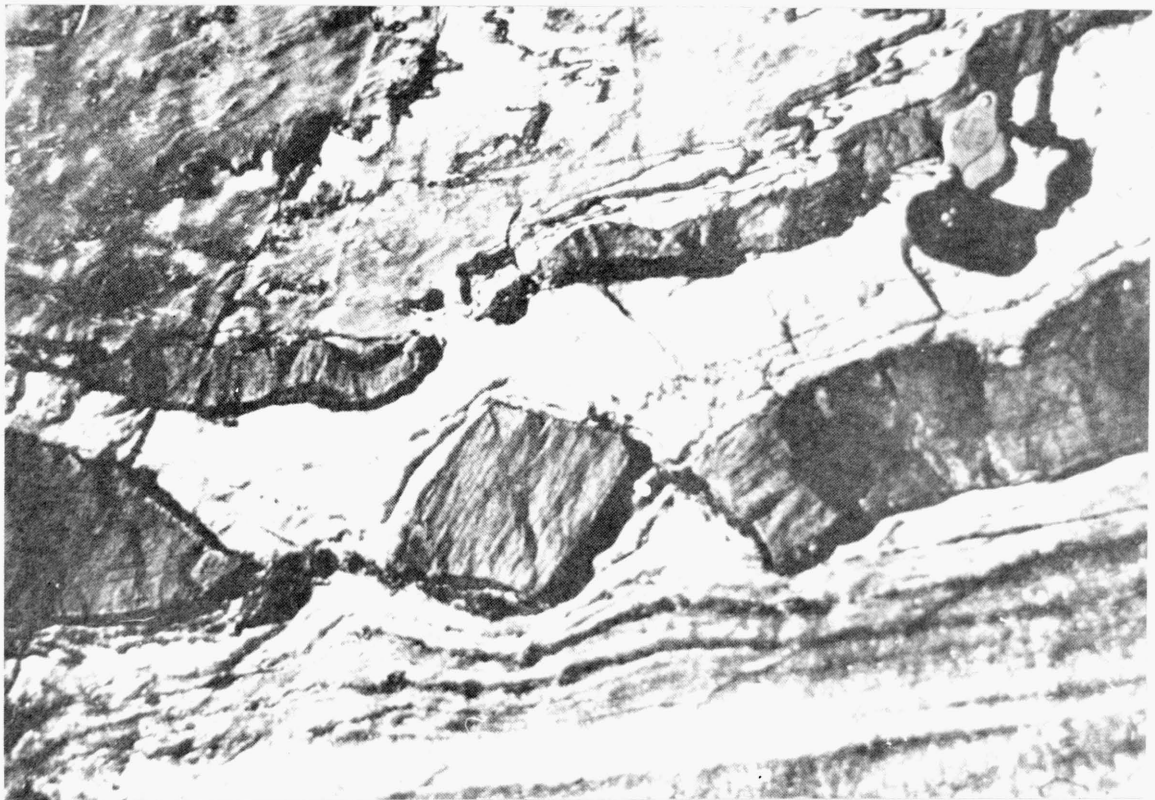


Fig. 3.21. Apparent rotation of a boudin relative to the banding in the surrounding strata, Kahn Gorge, Namibia (S.W.A.) (after Ramsay, 1967).



It is interesting to note that the boudins are offset in opposite sense to that of the rhombohedral boudins shown in fig. 3.20 (i.e. those which initiated by shear failure). It may, therefore, be possible to differentiate between the two reasonably easily in the field.

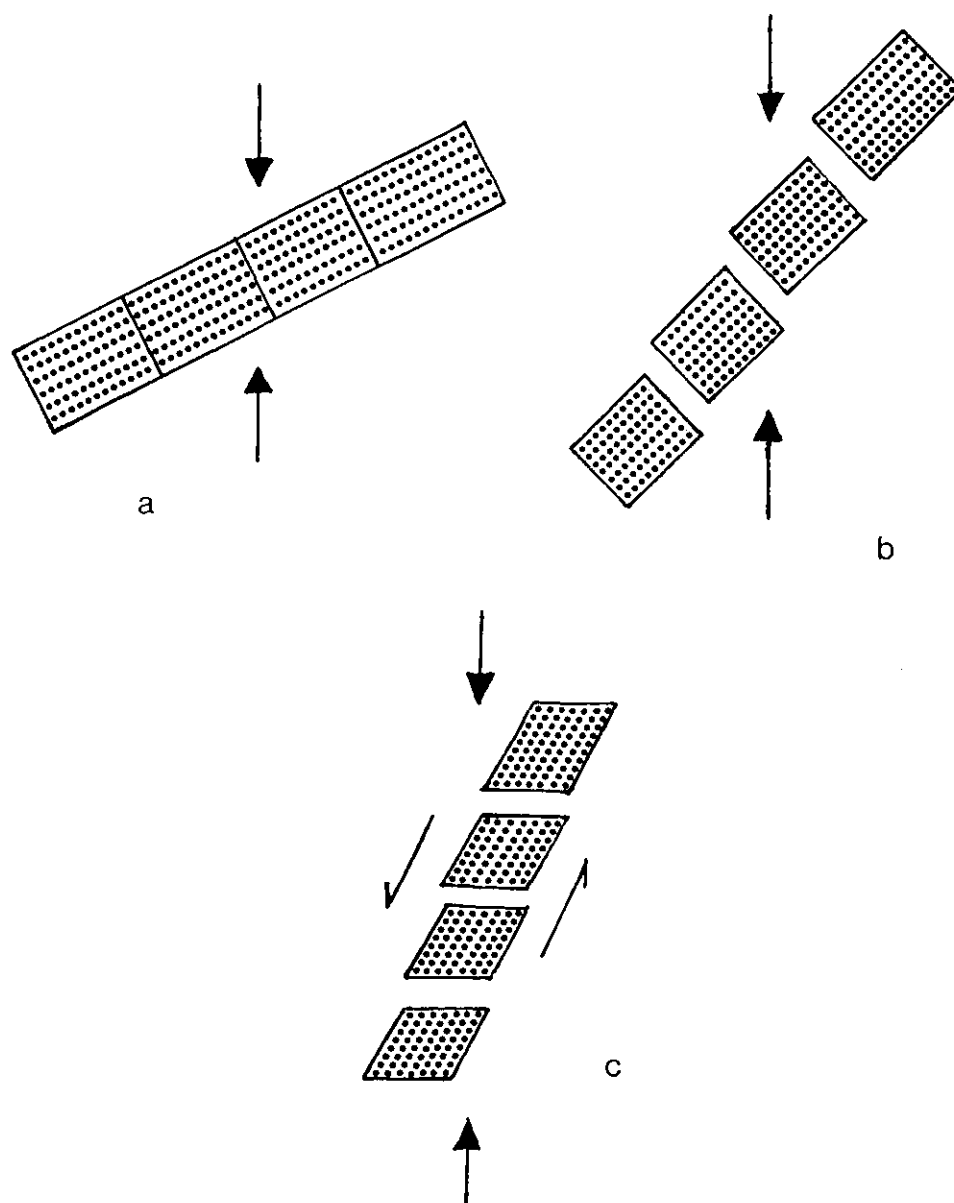


Fig. 3.22

2. Stromgard (1973) pointed out that under certain conditions (see section 1, pages 109-113) when the principal compression is not perpendicular to the competent layer, tensile failure may occur at an angle less than  $90^{\circ}$  to the layering boundary. Thus rhombohedral boudins can be generated by tensile failure (see section 1.5, fig. 1.4b).

From his theoretical considerations Stromgard also noted that boudins formed by tension cracking at high confining pressure will be roughly rectangular regardless of the bulk orientation of compression relative to the layering. He argued that the occurrence of rectangular boudins in high grade metamorphic rocks (i.e. high confining pressure) supports this idea.

3. Another way in which rhombohedral boudins may be formed is by the exploitation of existing planes of weakness such as cleavage in a competent layer. Cleavage is thought to develop parallel or subparallel to the AB plane of the finite strain ellipsoid and except at the hinge of a fold cleavage is generally not at  $90^{\circ}$  to bedding.

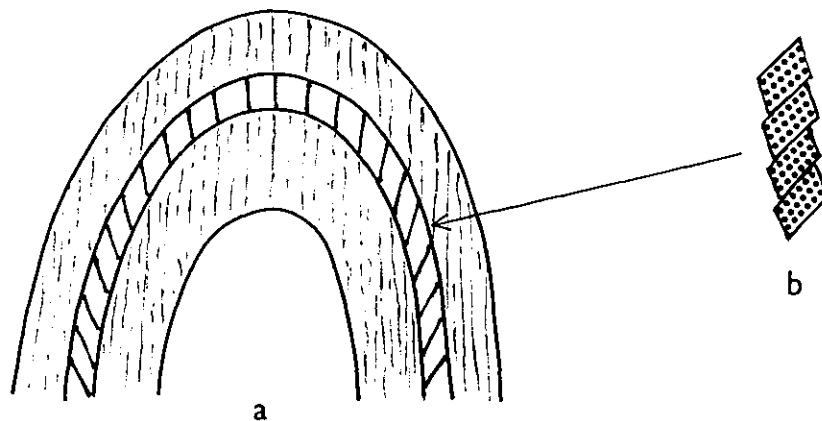


Fig. 3.23

The cleavage pattern characteristic of a relatively competent bed in a tight fold is shown in fig. 3.23 (a) and fig. 1.47. Once the cleavage planes are well developed, the blocks between these cleavage planes (the microlithons) may rotate at different rates to the rotation of the fold limb during the progressive deformation of the fold (in the manner described previously and summarised in figs. 3.19 & 3.21). This rotation and the slip along the cleavage planes in the competent layer may produce structures indistinguishable from offset rhombohedral boudins.

### 3.6 DEFORMED PINCH-AND-SWELL STRUCTURES

Pinch-and-swell structures are sometimes found deformed in the field. The deformation is most apparent when the original compression associated with the deformation of the pinch-and-swell structures is approximately parallel to the layer containing the structures.

Turton (1975) investigated deformed pinch-and-swell structures from Hele Bay, North Devon and Penge (1976) deformed pinch-and-swell structures experimentally, as mentioned in section 1.61. He deformed orthorhombic class 2 and class B type pinch-and-swell structures (fig. 1.55) and from his experimental results and field observations concluded that pinch-and-swell structures may undergo two modes of deformation. These are buckling in the proximity of the pinch zone and/or shearing along the same zone. One or other or both of these modes of deformation occurred in all the models regardless of the competent contrast or whether the layers were oblique or parallel to  $\sigma_1$ .

Cosgrove (1980) has shown that many of the quartzite layers in the South Stack Formation in the Rhoscolyn anticline (Rhoscolyn area of Anglesey, North Wales) developed pinch-and-swell structures during the first deformation and that these structures often control the wavelength of the folds which develop during the second deformation. Field observations in this area and experimental work (Penge 1976) on the folding of a layer containing pinch-and-swell structures indicate that buckles form such that one limb contains the 'pinch' portion and the other limb the 'swell' portion of the pinch-and-swell structures (fig. 3.24).

The present author attempted to investigate the effect of the class of a pinch-and-swell structure on its deformation. The result of the plasticine experiments (fig. 2.20a, 2.22a) show that both shear and buckling

4.1 Experimental

From the experimental results it is possible to identify four types of boudinage and related structures which developed where multilayers and/or single layers are compressed normal or at a high angle to the layering.

(1) Type A structures - interlocking pinch-and-swell structures (or internal boudins). These developed in multilayers made up of identical layers with a lubricant between the layers (i.e. low cohesion). Experiments in which such a multilayer was deformed confirm the prediction regarding the formation of internal boudins made by Cobbold et al. (1971) (see section 3.1).

These structures may form in fabrics as well as in discretely layered media. In both materials a similar geometry of interlocking pinch-and-swell structures develops either as a result of intersecting normal kink bands or as a result of the periodic necking of a layer or packet of layers or of the fabric. The geometries of the structures produced in these two ways are often identical.

(2) (a) Type B-I Structures is the name given to lenticular boudins which develop when a multilayer with pre-existing fractures (e.g. tension gashes) is compressed at a high angle to the layering or foliation. In experiments (23, 21, fig. 2.5 & 2.7) the unfractured multilayer on either side of the band containing the pre-existing fracture were deflected into the opening fractures giving rise to a neck region similar to that often found associated with "classical" boudinage (Type C)(fig. 2.5 C -E). Fluids squeezed out from the multilayers during the deformation and filled the gaps. In natural examples (fig. 3.8) the voids (tension openings) are usually filled with quartz.

(b) Type B-II Structures, like type B-I are lenticular boudins which develop in finely layered media but are formed as a result of the development of strain softened (relatively incompetent) horizons within a multilayer. Horizons within the multilayer which are not strain softened are relatively competent. Boudins may develop in these competent horizons in much the same way as they do in relatively competent single layers. However, in single layer boudinage, competence contrast is an intrinsic property of the system whereas type B-II structures develop as the result of an induced competence contrast.

(3) Type C structures are the classical boudins named and described by Lohest (1909). In the paraffin wax experiments the temperature proved to be the major factor in determining whether the layers behaved in a brittle or ductile manner, which in turn influenced the fracture spacing (i.e. width of boudins), the ductile necking instability having a different spacing than the brittle failure instability. However, the major factor influencing the width of boudins was found to be the thickness of the relatively competent layer. It was also noted that the width of the boudins in any particular layer decreased with progressive deformation during which the relatively wide boudins subdivided until an optimum width of boudin was obtained (fig. 3.11). It was observed, for example, that the optimum width of boudins in the 1mm thick competent layers in experiment 47 was  $\approx 4$ mm after 36% bulk shortening. For any particular stage in the progressive deformation it was found that the optimum boudin width increases with the thickness of the competent layer.

(4) Type D structures are 'boudins' which are generated by shear failure planes, a single competent layer is broken into boudins by approximately regularly spaced shear planes. The boudins are rhombohedral in profile section and adjacent 'boudins' may be offset. There are three other mechanisms by which rhombohedral boudins can be formed (see section 3.5) and it is often difficult to distinguish between them in the field.

### Deformed pinch-and-swell structures

From experiments it was found that when a layer or layers containing pinch-and-swell structures is compressed parallel to the layering, layer shortening occurs by either buckling or shearing (fig. 2.20a and 2.20 b-d). In both mechanisms the pinch-and-swell structures govern the style of structures which form. The buckles are asymmetric, one limb containing the 'pinch' and the other the 'swell'. When layer shortening occurs by shearing, the shear planes usually cut through pinch regions and the swells, separated from each other by shear planes, rotate to form an imbricate arrangement.

#### 4.2 Theoretical

It is concluded that the theories at present available are adequate to explain the initiation and development of boudinage and pinch-and-swell structures. Ramberg's (1955) theoretical analysis of boudin formation, when aided by field measurements and some knowledge of viscosity ratios of the rocks concerned, provides a way of estimating pressure gradients and rates of flowage associated with the formation of boudins.

The theory developed by Cobbold et al. (1971), based on Biot's (1965) theory of internal buckling, gives a good explanation of interlocking pinch-and-swell structures and normal kink bands which often develop in multilayers or anisotropic materials compressed normal or at high angle to the layering. Sowers (1973) reviews Biot's (1965) theory of internal buckling in anisotropic materials and uses the theory to predict the spacing of brittle failure in such a material. Sowers used the strain energy methods to calculate the critical tension necessary for the initiation of tensile fracture.

Smith's (1975, 1977, 1978) theories predict that pinch-and-swell

structures (which Smith calls boudinage structures) develop only if the competent layer in which the structures form has non-linear rheological properties. For example, if the layer is a linear viscous material he concludes that the amplification rate of the pinch-and-swell instability is too small to allow any instability to amplify into a finite structure.

Stromgard's (1973) theoretical analysis of a multilayer made up of welded, rhythmically layered units with different viscosities, is an important contribution to the understanding of the formation of boudins in multilayers. He considers the theoretical stress distribution in such a multilayer deformed in plane strain and concludes:

(a) boudinage is favoured by high competence contrast, low compressibility, great thickness of the incompetent layers and low ratio of applied stress  $P_1/P_3$  (fig. 1.46).

(b) boudins formed by tension cracking at high confining pressure will be roughly rectangular, irrespective of the bulk orientation of compression relative to layering.

(c) the width of boudins by tension cracking will be in the range of 2 - 4 times the thickness of the competent layer.

Stephansson and Berner (1971) and Stromgard (1973) worked on photoelastic and finite element models of boudinage. They determined the stress distribution in and around boudins during their formation and demonstrated how the mineral redistribution observed in the field around boudins is compatible with the stress distribution predicted from both the finite element and photoelastic models.

In contrast to the theory of fibre loading (halving of segments or boudins) both Sowers and the present author observed in their

respective experiments that a number of tensile fractures develop in competent layer at the same time. However, once these fractures are formed the next tensile fractures which form tend to divide the segments formed by the initial tensile failure into halves, thus behaving in the manner predicted by the theory of fibre loading.

#### 4.2 Future work on Boudinage and related structures

The following paragraphs attempt to indicate the possible direction future research into the formation of boudinage and related structures might take. The suggestions relate to the three main areas of research namely experimental, theoretical and field work.

Smith (1977,1979) has shown that non-linear behaviour of materials is important in the development of pinch-and-swell structures in single layer system and Latham(1982) has incorporated both bending resistance and non-linearity in his instability theory of an anisotropic system compressed parallel to the layering or fabric. It would therefore be very instructive to extend this theory and to determine the effect of compression at a high angle to the layering or fabric.

Having determined the effects that compression at a high angle to the layering or fabric would have on a non-linear anisotropic material it would be instructive to test the theoretical prediction by performing suitable experiments. Such experiments might involve materials such as metals with well known non-linear rheological properties.



One of the limitations of the experiments outlined in section 2.5 was that the size of the models was too small to enable the thickness to width ratio of all but the thinnest competent layer to be determined accurately. Experiments on larger models would enable the ratio of width/thickness to be determined for a large range of competent layer thickness and thus enable the relationship between the two parameters (width and thickness) to be determined.

It is possible to record the stress history of an experiment. The relationship of the stress values to the initiation of structure, their amplification and their locking up could provide an interesting insight into the problems of 'instability'.

Close study of natural examples of structures developed in multilayers and fabric that have been compressed at a high angle to the layering or fabric would undoubtedly shed considerable light on the relationship between these various structures, that is, boudins, pinch-and-swell, reverse kink bands and faults.

## APPENDIX

### Appendix A APPARATUS

#### A.1 PURE SHEAR DEFORMATION RIG

The deformation apparatus used for most of the experiments described in this thesis was the Pure Shear Deformation Rig (fig.2.1, A.1) designed and constructed by Cobbold (1973) for (1) deforming geological scale models (152mm x 152mm x 50mm) under controlled conditions of strain rates and temperature; and (2) measuring the rheological properties of model materials such as waxes, plasticine, gelatine, clays and putty. A detailed description of the apparatus is given by Cobbold (1973, 1975) and a brief account of its main features is given below.

The rig is made up of three main units

(1) A rigid framework mounted on wheels for the convenience of mobility, incorporating an electric motor, a gear box, five bevel gears and four drive shafts.

(2) A deformation box which is situated on top of the rigid frame which accommodates the model and its boundary plates.

(3) Several measurement and control systems.

The loads which cause the deformation are transmitted through rigid plates to the boundaries of the model. The required condition of the planar frictionless boundaries is achieved to a close approximation by lubricating the boundary plates. The models y-boundary (x-z plane)(fig.A.2) can be photographed at any stage of deformation through the thick perspex plate cover.

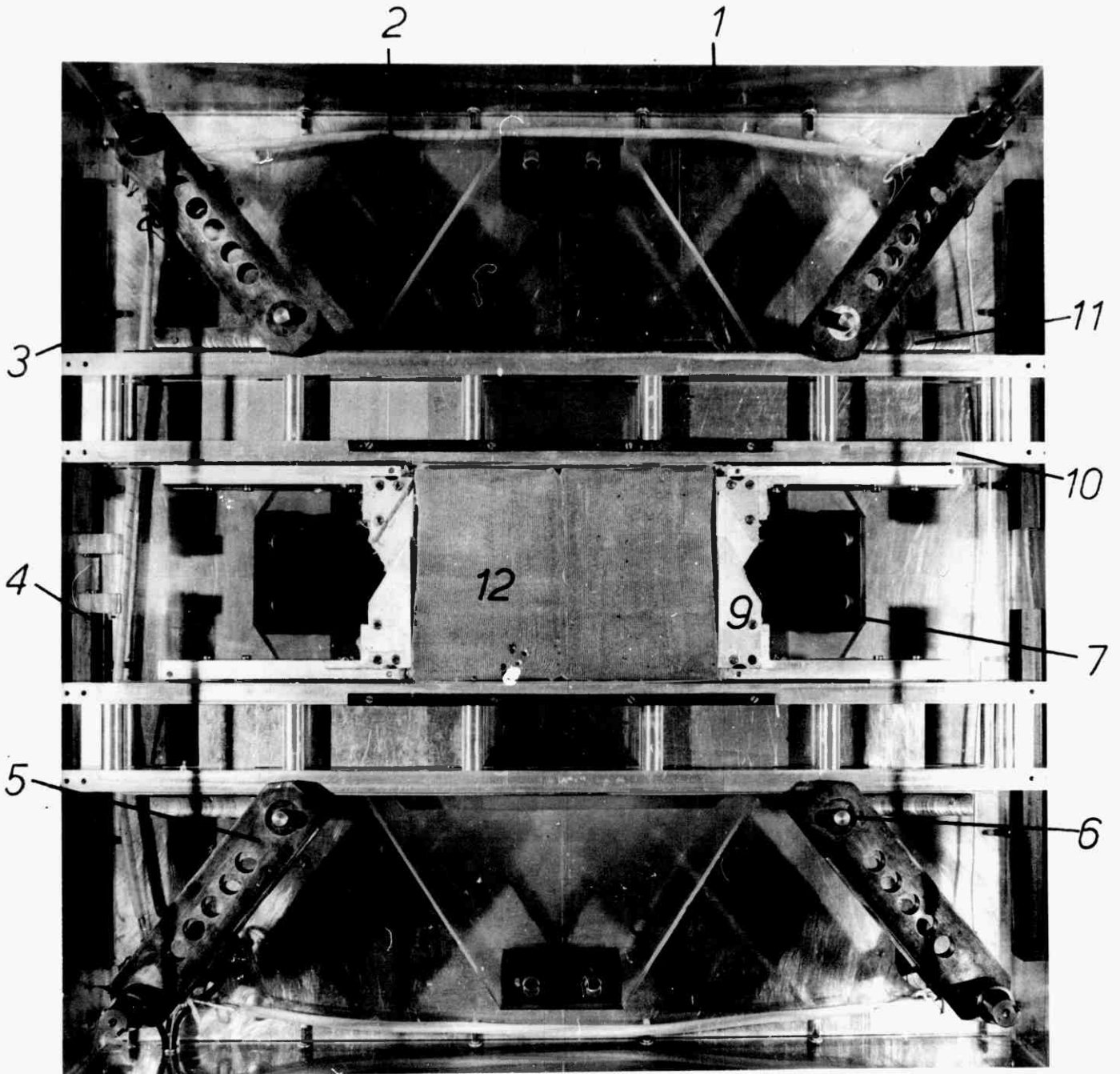


Fig.A.1. Deformation box, viewed from above, showing side-walls (1), window (2), rails (3), displacement gauge (4), rotors (5), bearings (6), blocks (7), lower y-plate (8), x-plates (9), z-plates (10), bogies (11) and a model (12).

(after Cobbold, 1973)

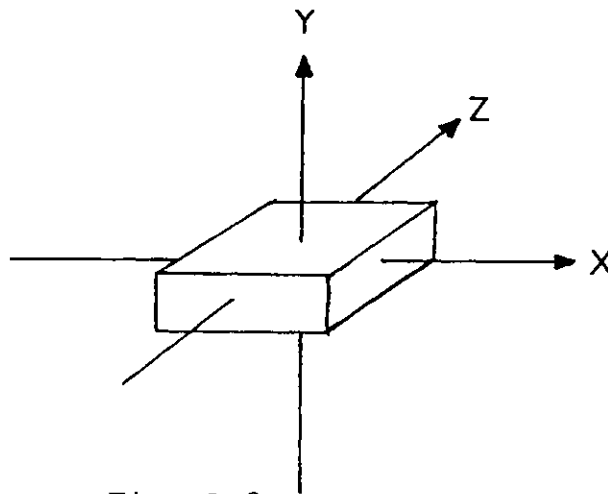


Fig. A.2

## A.2 WOODEN DEFORMATION BOX

Models 11, 12 and 13 were deformed in a wooden deformation box shown in Fig. A.3.

The rectangular model is compressed between two wooden blocks (Fig. A3-A,B) which are driven towards each other by a vertical piston (Y direction). Extension in the Z direction (Fig.A.3a) is prevented by two perspex plates and the model is allowed to extend in the X direction until it eventually reaches the two wooden blocks (C and D in Fig. A.3.). Both the perspex plates can be unscrewed for loading and removing the model.

## Appendix B MODELLING MATERIALS

### B.1 PARAFFIN WAXES

Paraffin waxes are mixtures of crystalline and amorphous hydrocarbons. They are the result of fractional crystallization of melts, each grade of wax consolidating over a range of temperature (its melting point range). Commercial manufacturers use cleansing and filtering techniques to produce refined waxes suitable, for example, for use in histology. These waxes have narrow melting ranges (e.g. 55<sup>o</sup> - 57<sup>o</sup>C) and are classified by their nominal melting-point (e.g. 56<sup>o</sup>C). The physical properties of refined wax are reasonably consistent from batch to batch.

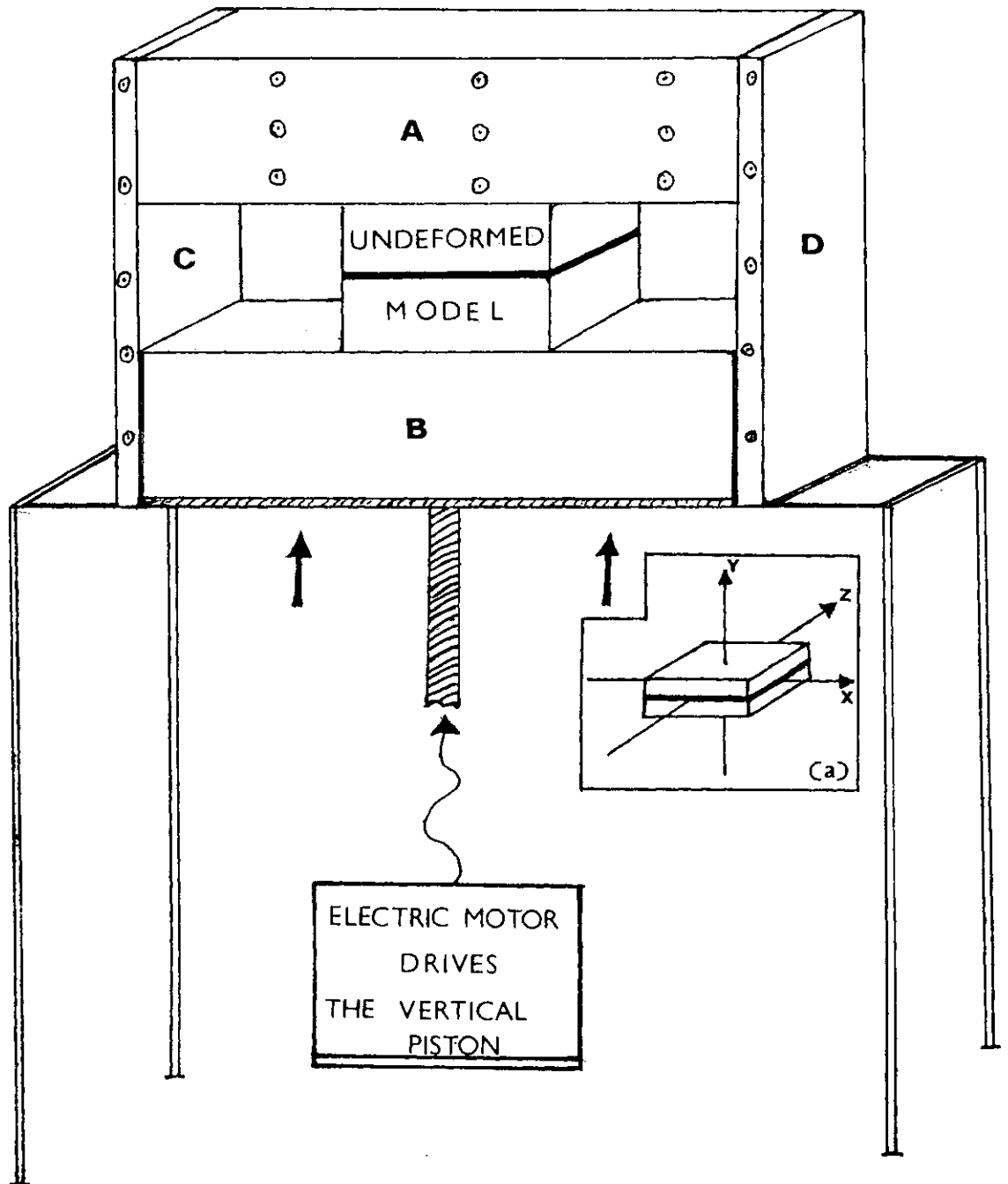


Fig. A.3. The Wooden Deformation Box

Paraffin waxes have been used to simulate the plastic flow of metals. Patterns of deformation in wax produced experimentally are similar to those derived theoretically from the flow laws of an ideal plastic solid according to the work of Halling and Mitchell (1965). The waxes are convenient to work with because they are clean and chemically inert. Other advantages are that one can construct models using a different grade of wax for each component. Different grades have different properties, which can be scaled so that their relative contrasts are equivalent to the contrasts that exist in heterogeneous rocks. The waxes also have rheological properties which are proportional to those obtained in laboratory experiments on rock, consequently the waxes are excellent rock analogues. A list of more detailed advantages and some disadvantages is given by Cobbold (1973).

#### B.1.1. Physical and Chemical Constitution of Paraffin Wax.

The following brief account of the chemical and physical constitution of paraffin wax has been taken mainly from Mazee (1962).

A solid paraffin wax is a polycrystalline aggregate of various hydrocarbon species, containing oil or non-crystalline material at crystal interfaces. The properties of the aggregate therefore depend on the properties of the crystalline constituents as well as on those of the oil.

The major constituents are normal alkane hydrocarbons of several different molecular weights, together with small quantities of iso- and cyclo-alkanes. The exact composition of a given grade of wax depends on its origin and the methods used in its manufacture.

Crystalline alkanes belong to various crystal systems (triclinic to orthorhombic) and have transition points in the solid phase. The phase-change, from  $\beta$  to  $\alpha$ -modification is accompanied by changes in crystal

habit, refractive index, specific gravity and elastic modulus. For an alkane with a melting point of  $51^{\circ}\text{C}$ , for example, the transition temperature is  $48.1^{\circ}\text{C}$ .

Commercially manufactured waxes contain unspecified amounts of unknown constituents, belonging to several different crystal systems. This is because they are formed by fractional crystallization of liquid melts, probably in the same way as many igneous rocks. The range of constituents of a commercial wax can be limited by solvent-cleansing and filtering, but a certain amount of oil usually adheres to the crystal interfaces. The yielding properties of the wax depend significantly on the amount of oil present, as well as on the temperature. Some crystalline constituents may undergo temperature-dependent phase changes in the solid state; others may undergo total or partial melting, especially if the temperature approaches the nominal melting point of the wax.

#### B.1.2. Frictional Properties of wax surfaces

According to Cobbold (1973) the coefficient of friction of a flat machined surface of paraffin wax, in contact with a flat surface of perspex, metal or glass, is low (about 0.1), probably because of (i) the softness of wax and (ii) the lubricating action of its non-crystalline components. Many other lubricants (e.g. petroleum jelly or silicon grease) adhere easily to a wax surface and do not squeeze out under pressure. These lubricants reduce the coefficient of friction to values as low as 0.01. This is a good approximation of a frictionless surface, a condition which may be necessary for rheological tests.

#### B.2 PLASTICINE AND PUTTY

Authors such as Green (1951), Durney (1968), Bever (1971), Mendum (1972), Treagus (1972), Troeg (1975), Woldekidan (1975) and others

have used plasticine\* and painters putty as model materials to simulate geological deformations. McClay (1973) examined previous rheological work on plasticine and carried out further tests.

As shown in Table 2.1. most of the models described in this thesis were made of paraffin wax. However, most of the models containing a single competent layer were made of plasticine. In some of these single layer experiments painters putty was used as a matrix.

#### B.2.1 Composition of Putty and Plasticine

Plasticine and putty have similar compositions: both are the mixtures of mineral fillers, oils and waxes. Putty is mainly a mixture of linseed oil and chalk. On storing or at high strains putty separates into its constituents. Large deformations generate strong grain fabrics. These two rheological behaviours limit its use as a model material in deformation experiments.

Plasticine consists of linseed oil and chalk like putty but also contains significant amounts of paraffin waxes which stabilize the material so there is little change of properties over periods of weeks. Both materials are therefore aggregates of chalk (mainly calcite grains), oils and waxes (only in plasticine) - thus making mechanisms of deformation complex. Platy carbonate fragments in both materials will tend to produce a grain fabric with deformation.

#### B.2.2 Mechanism of Deformation and rheology of Plasticine

From his rheological tests McClay found out that the rheology of plasticine was complex. At 25°C and at low strains it has initially the behaviour of a Newtonian liquid. Then as the mineral grains come into contact, grain boundary sliding and small shears occur. As deformation continues platy mineral fragments develop a preferred orientation

\* Plasticine is the registered trade name, made by Harbut Plasticine Ltd., Bath, England.



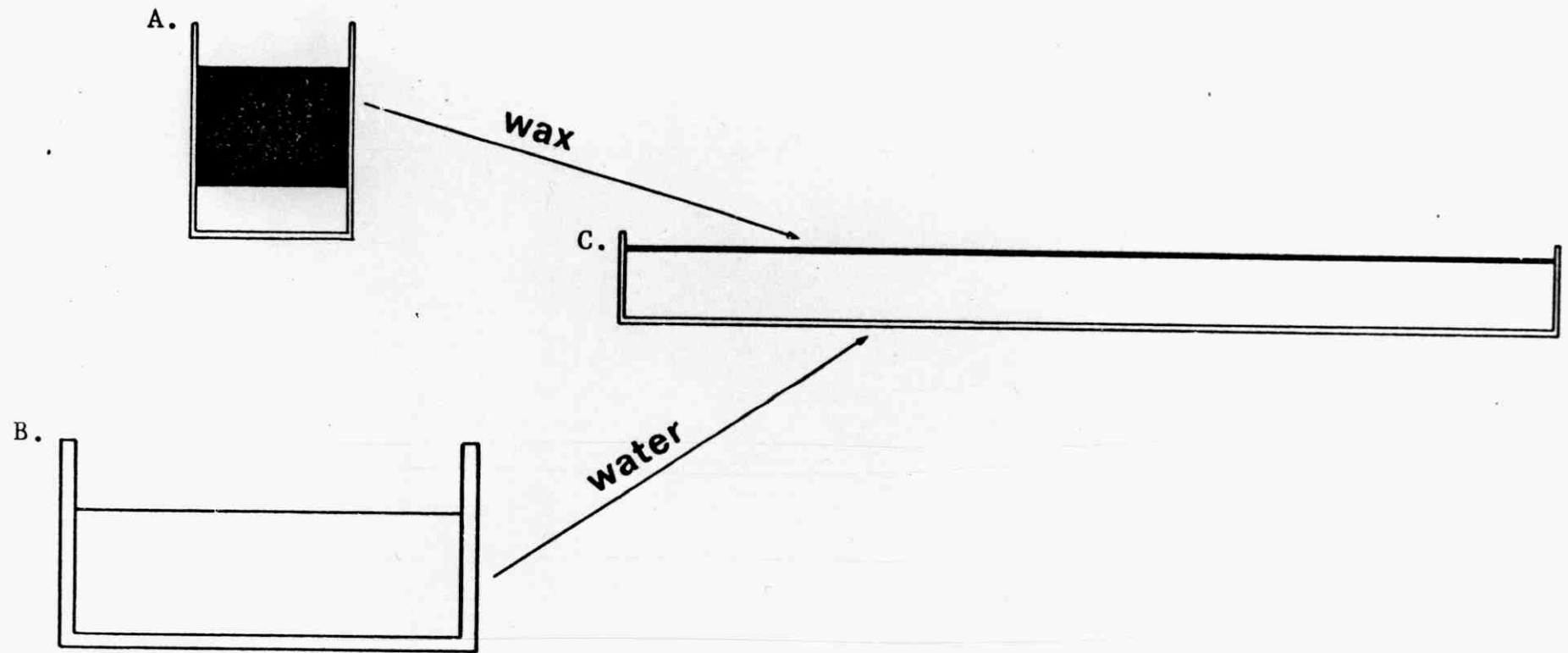


Fig. A.4. Method of preparation of thin wax sheet. (after Summers, 1979)

and this anisotropy allows instabilities to develop and propagate. At high strain rate in pure shear deformation instabilities develop and propagate in the period of accumulating permanent strain before steady state flow occurs. In effect the plasticine is strain softened at high strain rates before steady state flow occurs. As minute shears propagate throughout the material steady state flow occurs and then work hardening begins as conjugate shears develop and interact with existing shears. The work hardening may be attributed to the squeezing out of pore fluids as the deformation proceeds.

## Appendix C. MODEL CONSTRUCTION

### C.1 WAX MODELS

#### C.1.1. Layered Models

A simple method of preparing wax in the form of thin sheets for use in multilayer experiments, was developed by Summers (1979). This method made use of the low specific gravity of wax by floating and cooling a thin sheet of molten wax on the surface of a water bath (Fig.A.4).

(a) A large quantity of water was heated separately in an electric water bath to a temperature approximately  $25^{\circ}$  -  $30^{\circ}\text{C}$  above the melting temperature of the wax, (Fig.A.4).

A known quantity of granular or tablet wax (determined by the thickness of layer to be produced) was added to a large beaker approximately one-fifth full of water. The wax floats on the water and the water prevents the wax from becoming overheated. The contents of the beaker were heated to a temperature approximately  $15^{\circ}\text{C}$  above the melting temperature of the wax of known volume. A dye\* was added to the wax at this stage. The dye was put in a small (100ml) beaker and some molten

\* The dye was supplied by Farbwerke Hoechst A.G. Votmals Meister & Brüning, W.Germany.

wax was poured into the beaker. After mixing the wax and the dye thoroughly, the mix was poured into the main beaker and again stirred thoroughly.

(c) The large quantity of heated water (Fig. A.4B) was transferred to a shallow plastic tank measuring approximately 200 by 75 by 5cm and then the hot wax and water were poured from the beaker (Fig. A.4A) onto the water surface of the tank to form a thin sheet of floating wax. The thickness of this sheet was controlled by the volume of wax used. The contents of the tank were then allowed to cool to room temperature producing a thin sheet of solidified wax of constant thickness. A large quantity of sheet wax with a controlled thickness which varies by less than 5% over the total area of the sheet can be obtained. If this method is used to produce a sheet of wax 1mm thick or less it is found that the effects of surface tension in the molten wax cause significant local thickness variations.

(d) The solidified wax sheet can be cut into convenient size strips which can then be machined to the dimensions required in a particular experiment. Because of the high strength of the material at room temperature, sheets with a thickness as low as 1mm could be handled easily. It is possible to store wax in sheet form indefinitely and this is one of the main advantages of wax over materials such as plasticine.

#### C.1.2. Single layered

In single layer models in which wax was used as the matrix, the matrix was made by pouring molten wax into a rectangular perspex mould. The solidified blocks of wax were machined to the required size and the two blocks and the single layer assembled. If lubrication was required between the layer and the matrix, vaseline, silicon grease or

liquid soap (Zalpon) was applied before the model was assembled.

### C.1.3. Construction of Pinch-and-swell models

To produce the required pinch-and-swell layer, a steel box containing half the profile of a series of pinch-and-swell structure was constructed (Fig.A.5.)

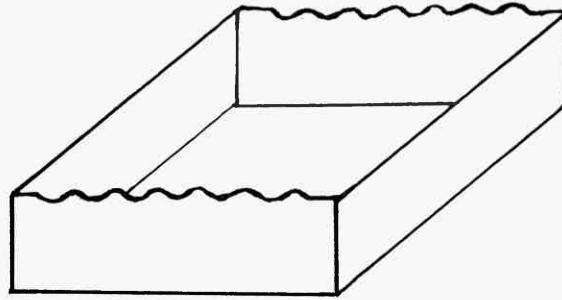
Two moulds of plaster-of-paris (Fig.A.5.) were cast in this box. These moulds were arranged so that the half profiles faced each other and the pinch-and-swell layer was then cast between them. The pinch-to-swell thickness ratio could be varied to some extent by varying the separation of the two moulds. In order to cast the matrix with a side that fits the pinch-and-swell layer exactly, a second mould (plaster-of-paris) which produced a 'reverse' pinch-and-swell side in the matrix was cast from one of the plaster-of-paris moulds. The matrix block was then cast using the 'reverse' mould in a perspex box. All the sides of the moulds were painted and then lubricated with glycerol or vaseline to prevent the wax or plasticine from sticking to the plaster-of-paris moulds.

### C.2. PLASTICINE MODEL CONSTRUCTION

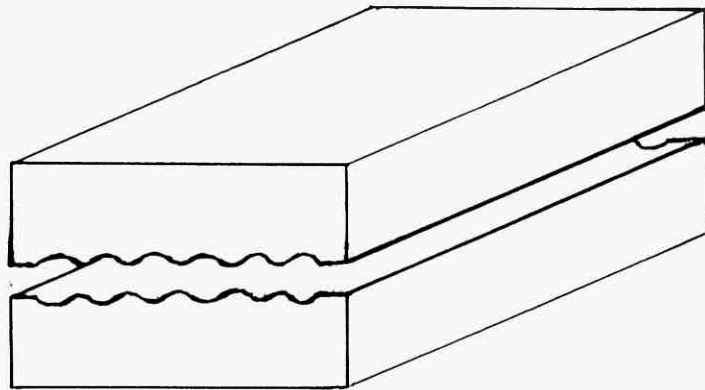
Each of the competent layers was prepared from a block of plasticine by rolling and flattening to the required thickness. The layer was then cut to the required size by a rectangular metal cutter.

The matrix was prepared in the same way as the layers except that the cutting to the required size was done using a knife. The layer was placed between two blocks of matrix and stuck together by thin films of vaseline. The assembled mould was then cut, with great care, to fit into the appropriate deformation rig.

In the Pure Shear deformation rig the base and sides of the model



A



B

Fig. A.5. A. Steel box for casting one of the plaster-of-Paris moulds shown in B.  
B. The two halves of plaster-of-Paris mould for casting pinch-and-swell structure

were lubricated with vaseline and the interface between the top of the model and the perspex plate lubricated by glycerol or liquid soap (trade name Zalpon).

After fitting and clamping the model inside the deformation box, a photograph of the undeformed model was taken. A series of photographs were taken as the model deformed. Before starting the machine, the gearing was arranged to give the required strain rate.

BIBLIOGRAPHY

- Aderca, B.M. 1957. Un cas de "boudinage" à grande échelle; la mine de Rutongo au Rwanda. *Annals Soc. Geol. Belg.* 80B:279-285.
- Akaad, M.K. 1956. The Ardara Granitic diapir of County Donegal, Ireland. *Geol. Soc. London* 112:263-288.
- Allison, I. and Latour, I.B. 1977. Brittle deformation of hornblende in a mylonite. *Can Jour. Earth Sci.* 14:1953-58.
- Bain, G.W. 1933. Wall-rock mineralization along Ontario gold deposits. *Econ. Geol.* 28:705-743.
- Balk, R. 1927. Die primäre Struktur des Nortmassivs von Peekskill am Hudson, Nordlich New York, *Neues Jahrb. Beil. Bd.* 57, Abt. B. 249-303.
- Belousov, V.V. 1952. Spacing of Fracture in Rocks. *Akad. Nauk. SSSR Trad. Geofiz Inst.* 17:144.
- Belousov, V.V. 1960. Tectonophysical Investigations. *Geol. Soc. Am. Bull.* 71:1255-1270.
- Belousov, V.V. 1964. Basic Problems in Geotectonics. McGraw Hill, New York, 809p.
- Berglund, S. and Ekstrom, T.K. 1974. Sphalerite Composition in Relation to the Stress Distribution of Boudinage. *Lithos* 7:1-6.
- Berthelsen, 1957. The structural evolution of an ultra and poly-metamorphic gneiss complex, West Greenland. *Geol. Rdsch.* 46:173-85.
- Bever, K. 1971. Deformation of angular discordances: angular conformities. Unpubl. M.Sc. thesis, Imperial College.
- Biot, M.A. 1937. Bending of an infinite beam of an elastic foundation. *ASME Appl. Mec. Div. Trans.* A1-A6.
- Biot, M.A. 1965. Mechanics of incremental deformation. John Wiley and Son Inc. New York. 505p.
- Bogdanov, A.A. 1947. The intensity of cleavage as related to bedding thickness. *Soviet Geology*, 16:147.
- Bridgman, P. 1952. Large Plastic flow and fracture. McGraw Hill, New York, 375p.

- Bruhl, H. 1969. Boudinage als Ergebnis der inneren Deformation, Geol. Mitt. 8:263-308.
- Chertkova, E.I. 1950 Some results of the Modelling of tectonic faults: Akad. Nauk. SSSR Izv. Ser. Geol. 14:5 42-44.
- Christie, A.M. 1953. Gold fields Martin Lake map area, Saskatchewan. Mem. Geol. Surv. Berch Can. 269:1-126.
- Cloos, E. and Hietanen, A. 1941 Geology of the 'Martic Overthrust' and the Blenarm series in Pennsylvania and Maryland, Geol. Soc. Am., Spec. paper 35:207.
- Cloos, E. 1946. Lineation, a critical review and annotated bibliography, Geol. Soc. Am., Mem. 18:122.
- Cloos, E. 1947. Boudinage. Trans. Am. Geoph. Union 28:4:626-632.
- Cobbold, P.R. Cosgrove, J. and Summers, J. 1971 Development of internal structures in deformed anisotropic rocks. Tectophysics, 12:23-53
- Cobbold, P.R. 1973. Initiation and development of folds in rocks. Unpubl.Ph.D. thesis, Univ. of London.
- Cobbold, P.R. 1975. A biaxial press for model deformation and rheological tests. Tectonophysics 26:T1-T5.
- Cobbold, P.R. 1976. Unified theory of the onset of folding, boudinage and mullion structure. (Discussion on Smith's 1975 paper, reply by R.B. Smith in the same page) Geol. Soc. Am. Bull. 87:1663.
- Coe, K. 1959. Boudinage structure in West Cork, Ireland. Geol. Mag. 96:191-200.
- Corin, F. 1932. A propos du boudinage en Ardenne. Soc. Belg. Geol. 42:101-117.
- Cosgrove, J. 1976. The formation of crenulation cleavage. Jour. Geol. London. 132:155-178.
- Cosgrove, J. 1980. The tectonic implications of some small scale structures in the Mona Complex of Holy Isle, North Wales. Jour. Struct. Geol. 2:4:383-396.
- Currie, J.B. 1966. Experimental Structural Geology. Earth Sc. Rev. 1:51-57.



- De Sitter, L.U. 1958 Boudins and Parasitic folds in relation to cleavage and folding. *Geologie En Mijnbouw* 20:277-286.
- Dunnet, D. and Siddans, A.W.B. 1971 Non-Random Sedimentary Fabrics and their Modifications by Strain. *Tectonophysics* 12:307-325.
- Durney, D.W. 1968. Some Experimental work on putty and plasticine. Unpubl. M.Sc. thesis, Imperial College, London.
- Ekstrom, T.K. 1975. Pinch-and-swell structures from a Swedish locality. *Geol. Foren. Stockh. Forh.* 97:180-187.
- Flinn, D. 1962. On folding during three dimensional progressive deformation. *Quart. Jour. Geol. Soc.* 118:385-433.
- Friedman, M. 1964. Petrographic techniques for the determination of principal stress state of stress in the earth's crust. Elsevier Publishing Co., New York.
- Frocht, M.M. 1966. Photoelasticity. Wiley, New York.
- Fullagar, K. 1980. A description of nucleation of folds and boudins in terms of vorticity. *Tectonophysics* 65:39-55.
- Fyson, W.K. 1962. Tectonic structures of Devonian rocks near Plymouth, Devon. *Geol. Mag.* 99:206-26.
- Gay, N. C. and Jaeger, J.C. 1975. Cataclastic deformation of geologic materials in matrices of differing composition II Boudinage. *Tectonophysics* 27:323-331.
- Gault, H.R., 1945. Petrography, structures and petrofabrics of the Pinckneyville quartz diorite, Alabama. *Geol. Soc. Am.* 56:181-246.
- Gindy, A.R. 1953. The plutonic history of the district around Trawenagh Bay, County Doengal. *Q. Jour. Geol. Soc. Lond.* 108:377-411.
- Goguel, J. 1946. Introduction à l'étude mécanique des déformations de l'écorce terrestre (2nd. ed.): Paris, France Service Carte Geol. Mem. 182-197.
- Green, B.A. 1951. The use of plasticine to simulate the plastic flow of metals. *Phil. Mag. Series* 7:42:365-373.
- Griggs, D.T. and Handin, J. 1960. Observations on fracture and a hypothesis of earthquakes. D.T. Griggs and J. Handin (editors) Rock Deformation (A Symposium) *Geol. Soc. Am. Mem.* 79:347-365.

- Gzovsky, M.V. 1959. The use of scale models in tectonophysics. *Internat. Geol. Rev.* k:4:31-47.
- Halling, J. and Michell, 1965. An experimental study of symmetrical extrusion using paraffin wax as a model material. *Proc. 5th. Int'l. Mech. Tool design Res. Conf.*, Birmingham, UK. 353-390.
- Harker, A. 1889. On the local thickening of dikes and beds by folding. *Geol. Mag. New Ser.* 6:69-70.
- Heim, A. 1921. *Geologie der Schweiz*, Chr. Herm. Tauchnitz. Leipzig 2:1:47.
- Hill, R. 1950. *The mathematical theory of Plasticity*. Oxford Univ. Press, Oxford, UK.
- Hobbs, B.E., Means, W.D. and Williams, P.F. 1976. *An Outline of Structural Geology*. Wiley, New York.
- Hobbs, D.W. 1967. The formation of tension joints in sedimentary: an explanation. *Geol. Mag.* 104:550-556.
- Holmquist, 1931. On the relations of the boudinage structure. *Geol. Foren. Stockholm*, 34:193-208.
- Hossain, K.M. 1970. Experimental work on Boudinage. Unpubl. M.Sc. thesis, Imperial College, London.
- Hossain, K.M. 1979. Determination of strain from stretched belmenites. *Tectonophysics*, 60:279-288.
- Hubbert, M.K. 1937. Theory of scale models as applied to the study of geological structures. *Geol. Soc. Am. Bull.*, 48:1459-1520.
- Hambrey, M.J. and Milnes, A.G. 1975. Boudinage in Glacier ice -- some examples. *Jour. Glaciol.*, 14:72:383-393.
- Jaeger, J.C. 1965. *Elasticity, fracture and flow*. Methun, London, 268p.
- Jones, A.G. 1959. Vernon Map-area, British Columbia. *Mem Geol. Surv. Byrch. Can.* 296:1:86.
- Johnson, A.M. 1977. *Styles of Folding*. *Developments in Geotectonics II* Elsevier, Amsterdam, Netherlands, 405p.
- Kirillova, I.V. 1949. Problems of the mechanics of folding: Akad. Nauk. SSSR Trad. Geofiz. Inst. 6, p27. (in Russian).
- Latham, J.P. 1982. The influence of mechanical anisotropy on the development of geological structures. Unpubl. Ph.D. thesis (in preparation) Univ. of London.

- Lohest, M. 1909. Del origine des veines et de geodes des terraines primaries de Belgique. Soc. Geol. Belg. Ann. 36B:275-282.
- Ladeira, F.L. and Price, N.J. 1981. Relationship between fracture spacing and bed thickness. Jour. Struct. Geol. 3:2:179-183.
- Lloyd, G.E. and Ferguson, C.C. 1981. Boudinage structure: some interpretations based on elastic-plastic finite element simulations. Jour Struct. Geol. 3:2:117-128.
- Mazee, W.M. 1962. Petroleum waxes. E.B. Evans (editor). Modern Petroleum Technology. Inst of Petroleum (Gt. Britain). 873p.
- McClay, K.R. 1973. The Rheology of Plasticine and Putty applied to asymmetric fold development. Unpubl. M.Sc. thesis, Imperial College, London.
- McClay, K.R. 1976. The rheology of Plasticine. Tectonophysics, 33:T7-T15.
- McIntyre, D.B. 1950B. Note on lineation, boudinage and recumbent folds near Dalnacardoch, Perthshire. Geol. Mag. 87:422-32.
- McQuillan, H. 1973. Small-scale fracture density in the Asmari Formation of Southwest Iran and its relation to bed thickness and structural setting. Bull. Am. Assoc. Petrol. Geol. 57:3267-2385.
- Mendum, 1972. An experimental study of conglomerate deformation. Unpubl. M.Sc. thesis. Imperial College, London.
- Nadai, A. 1950. Theory of flow and fracture of solids: McGraw-Hill, New York, 1269p.
- Paterson, M.S. and Weiss, L.E. 1968. Folding and Boudinage of quartz-rich layers in experimentally deformed phyllite. Geol. Soc. Am. Bull. 79:795-812.
- Penge, J. 1976. Experimental deformation of pinch-and-swell structures. Unpubl. M.Sc. thesis, Imperial College, London.
- Platt, J.P. and Vissers, R.L.M. 1980. Extensional structures in anisotropic rocks. Jour of struct. Geol. 2:4:397-410.
- Price, N.J. 1966. Fault and Joint development in Brittle and semi-Brittle Rock. Pergamon Press.
- Quirke, T.T. 1923. Boudinage an unusual Phenomenon. Geol. Soc. Am. Bull. 34:649-660.

- Ramberg, H. 1955. Natural and Experimental Boudinage and Pinch-and-swell structures. *Jour. Geol.* 63:512-526.
- Ramberg, H. 1959. Evolution of pygmic folding. *Norsk. Geol. Tidsskr.* 39:99-152.
- Ramberg, H. 1964. Selective buckling of composite layers with contrasted rheological properties, a theory for simultaneous formation of several orders of folds. *Tectonophysics*, 1:4:307-41.
- Ramberg, H. 1970. Folding of laterally compressed multilayers in the field of gravity. Part I and II. *Phys. Earth Planet. Inter.* 2:203-33.
- Ramsay, A.C. 1886. The Geology of N. Wales. *Mem. Geol. Surv. Gt. Britain* III 1-381.
- Ramsay, J. 1967. Folding and fracturing of Rocks. McGraw-Hill, New York.
- Ramsay, J. 1980. Shear Zone Geometry: a Review. *Jour. Struct. Geol.* 2:1/2:83-99.
- Rast, N. 1956. The origin and significance of boudinage. *Geol. Mag.* 93:401-408.
- Read, H.H. 1934. On the segregation of quartz-chlorite pyrite masses in Shetland igneous rocks during dislocation metamorphism with a note on an occurrence of boudinage structure. *Proc. Liverpool Geol. Soc.* 16:134-38.
- Reid, R.R. 1957. Bedrock geology of the north end of the Tobacco Root Mountains, Madison County, Montana. *Mem. Mont. St. Bur. Mines Geol.*, 36:1-27.
- Renard, 1909. Referred to by Lohest, *ibid.*
- Reyer, ED. 1892. *Geologische und geographische Experimente*, Engelmann, Leipzig, 55pp.
- Sanderson, D.J. 1974. Patterns of Boudinage and Apparent stretching lineation developed in folded rocks. *Jour. Geol.* 82:651-661.
- Sanderson, D.J. and Meneilly, A.W. 1981. Analysis of 3-D strain modified uniform distributions: Andalusite fabrics from a granite aureole. *Jour. Struct. Geol.* 3:2:117-128.
- Sederholm, J.J. 1911. *Geol. Ofversiktskarta. Sekt. B2, Tammerfors, Geol. Komm, Finlande.*

- Scheuman, K.H. 1956. Boudinagen und Microboudinage im metagabbrischen Plagiokles-Amphibolit von Rosswein (Sachs, Granulit-gebirge) Abh. Sachs. Akad Wiss. Math-Phys. KI 45:1-18.
- Selkman, S. 1978. Stress and Displacement analysis of Boudinage by finite-element method. *Tectonophysics*, 44:115-139.
- Sen, R. and Mukherjee, A.D. 1975. Comparison of experimental and natural Boudinage. *Geol. Mag.* 112:2:191-196.
- Smith, R.B. 1975. Unified theory of the Onset of folding, boudinage and mullion structure. *Geol. Soc. Am. Bull.* 86:10:1601-1609.
- Smith, R.B. 1977. Formation of folds, boudinage and mullions in non-Newtonian materials. *Geol. Soc. Am. Bull.* 88:2:312-320.
- Smith, R.B. 1979. The folding of a strongly non-Newtonian layer. *American Jour. Sc.* 279:3:272-287.
- Sowers, G.M. 1973. Theory of Spacing of extension fracture. *Geol. Soc. Am. Bull. Engineering Case History*, Number 9.
- Stainer, H. 1907. Sur le mode de gisement et l'origine des roches metamorphiques de la region de Bastogne (Belgique). *Mem. Acad. Roy. Belgique*, Ser. 2.
- Stephansson, O. and Berner, H. 1971. The finite element method in Tectonic Processes. *Phys. Earth Planet. Inter.* 4:301-321.
- Stromgard, K.E. 1973. Stress Distribution during formation of Boudinage and Pressure Shadow. *Tectonophysics*, 16:215-248.
- Summers, J. 1979. An Experimental and theoretical investigation of multilayer fold development. Unpubl. Ph.D. thesis, Univ. of London.
- Timoshenko, S.P. and Goodier, J.N. 1970. *Theory of elasticity* (3rd. ed.) McGraw-Hill, New York, 525-.
- Treagus, 1972. Processes in fold development. Unpubl. Ph.D. thesis Univ. of Manchester.
- Troeng, B. 1975. One natural and some experimental pinch-and-swell structures. *Geol. Foreh. Stockh. Forh.* 97:383-386.
- Turton, R. 1975. An examination of folds exposed in the rocks of Hale Bay. Unpubl. M. Sc. thesis. Imperial College, London.

- Uemura, T. 1965. Tectonic analysis of the boudin structure in the Muro Group Kii Peninsula, S.W. Japan. Jour. Earth Sci. Nagoya Univ. 13:99-114.
- Voight, B. 1965. Plane flow of viscous matrix with an interned layer compressed between two rectangular parallel rigid plates: A geologic applicaton and a potential viscosimeter in distorted rocks. Geol. Soc. Am Bull. Abstract spec. papers. No. 87.
- Waters, A.C. and Krauskopf, K. 1941. Protoclastic border of the Colville batholith. Geol. Soc. Am. Bull. 52:1355-1418.
- Walls, R. 1937. A New record of boudinage structure from Scotland. Geol. Mag. 74:325-32.
- Wegmann, C.E. 1932. Note sur le boudinage. Soc. Géol. France Compte Renda. 5:2:477-489.
- White, S., Burrows, S., Carreras, J., Shaw, N. and Humphreys, F. 1980. On mylonites in ductile shear zones. Jour. Struct. Geol. 2:1/2:175-187.
- Whitten, E.H.T. 1951. Cataclastic pegmatites and calc-silicate skarns near Bunbeg, County Donegal. Mineralog. Mag. 29:737-356.
- Whitten, E.H.T. 1966. Structural Geology of Folded Rocks. Rand McNally, Chicago, Ill.
- Wilson, G. 1951. The tectonics of the Tintagel Area, N. Cornwall. Q. Jour. Geol Soc. London 106:393-432.
- Wilson, G. 1953. Mullion and rodding structures in the Moine series of Scotland. Proc. Geol. Ass. 64:118-151.
- Wilson, G. 1961. The tectonic significance of small scale structures, and their importance to the geologist in the field. Annals Soc. Géol. Belg. 84:423-548.
- Woldekidan, T. 1975. Internal structures in multilayers compressed normal to the layering. Unpubl. M.Sc. thesis, Imperial College, London.
- Winter, D.A. 1980. The initiation and sequential development of boudinage. Unpubl. M.Sc. thesis, Imperial College, London.
- Wunderlich, H.G. 1959. Zur Entstehung von Boudins und Parasitarfalten Neues. Jb. Geol. Palaout. Mh. 132-137.
- Wunderlich, H.G. 1962. Faltenstereometrie und Gesteinsverformung. Geol. Rdsch. 52:417-426.